



# **Subsurface Reservoir Evaluation and Image Log Analysis of the Shaly-Sand Lower Acacus Reservoir, Block-114, Northern Ghadames Basin**

**By**

**Abraheem Ahmed Hasan Elmasli**

**Supervisor**

**Prof. Mohamed B. Abdelmalik**

**This Thesis Was Submitted as a Partial Fulfillment of the  
Requirements for Master's Degree in Earth Sciences**

**University of Benghazi**

**Faculty of Science**

**April 2018**

Copyright © 2018. All rights are reserved, no part of this thesis may be reproduced in any form, electronic or mechanical, including photocopy, recording scanning, or any information, without the permission in writing from the author or the directorate of graduate studies and training of Benghazi University.

حقوق الطبع 2018 محفوظة. لا يسمح اخذ اى معلومة من اى جزء من هذه الرسالة على هيئة نسخة الكترونية او ميكانيكية بطريقة التصوير او التسجيل او المسح من دون الحصول على إذن كتابي من المؤلف أو إدارة الدارسات العليا والتدريب جامعة بنغازي.



**Student Name:** Abraheem Ahmed Hasan Elmasli

**Faculty:** Faculty of Science

**Title of Thesis:** Subsurface Reservoir Evaluation and Image Log Analysis of the Shaly-Sand Lower Acacus Reservoir, Bolck-114, Northern Ghadames Basin.

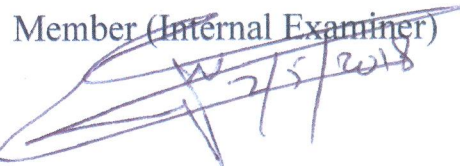
Defended and Approved date: 28 / 04 / 2018

**Examination Committee Signature:**

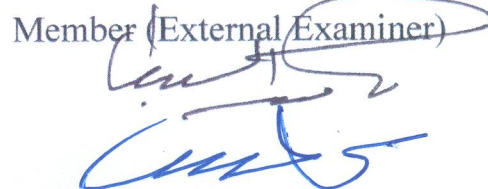
Dr. Mohamed Abdelmalik (Supervisor),  
Professor of Geophysics

  
3/5/2018  
Chairman

Dr. Saad El-Shari  
Professor of Geophysics

Member (Internal Examiner)  
  
2/5/2018

Dr. Belgasim El-Saiti  
Professor of Geophysics

Member (External Examiner)  


Hussein Elbarasi  
(Dean of Faculty)



**Prof. Mohamed Saleh Buamud**  
(Director of Graduate studies and training)



## ACKNOWLEDGEMENTS

*First and foremost, I would like to thank ALLAH for all that I have been given.*

I wish to devote this page to express my deep appreciation to the individuals who contributed to the achievement of this study.

Firstly, I am deeply indebted to my supervisor Dr. Mohamed Abdelmalik, Professor of Geophysicist, Department of the Earth Sciences, Benghazi University, for his invaluable help in determining the point of research, advices during the work and constructive guidance during the preparation and revision of this work.

Special thanks also extend to the staff members of the Exploration Division of the Arabian Gulf Oil Company (AGOCO); especially Mr. Khalifa Alshomi, for his comment and revision on some parts of the thesis.

I am very grateful to the staff members in the Department of Earth Sciences, Benghazi University for their cooperation and assistance during the whole period of my study. Special thanks must go to Mr. Abdelgader Kernaf and Mr. Walid Baragati for helping with the occasional challenges I have faced while interpreting the image log.

Last, but not least, I would like to express my deepest gratitude to my family, for unconditional support and encouragement to pursue my thesis work, to my friends and colleagues for their help and sincere wishes for the successful completion of this project.

Abraheem Elmasli

## TABLE OF CONTENTS

Title	Page
Copyright © 2018.....	ii
Examination Committee.....	iii
Acknowledgments.....	iv
Table of Contents.....	v
List of Tables.....	viii
List of Figures.....	ix
List of Abbreviation.....	xii
Abstract.....	xiii
<b>CHAPTER ONE</b>	
Introduction.....	1
1.1 Introduction.....	1
1.2 Location of Study Area.....	1
1.3 Pervious Work.....	1
1.4 Methodology .....	3
1.5 Data Base.....	4
1.6 Objective of the Study.....	5
1.7 Observations and Scientific Problem.....	5
<b>CHAPTER TWO</b>	
Regional Geological Setting.....	7
2.1 Introduction.....	7
2.2 Geological Setting.....	7
2.3 Petroleum System of Ghadames Basin.....	11
2.3.1 Source Rock.....	11
2.3.2 Reservoir Rock.....	11
2.3.3 Seal Rock.....	12
2.3.4 Trap Style.....	13
2.4 Oil and Gas Generation and Migration.....	14
<b>CHAPTER THREE</b>	

Petrophysical Analysis.....	16
3.1 Introduction.....	16
3.2 Well logs used in the study.....	17
3.2.1 Mechanical log (Caliper log).....	17
3.2.2 Natural radiation log (Gamma ray log).....	17
3.2.3 Electrical log (resistivity logs).....	18
3.2.4 Acoustic log (sonic log).....	19
3.2.5 Neutron log.....	19
3.2.6 Density log.....	20
3.3 Logs interpretation and work flow.....	20
3.3.1 Shale Volume Calculation.....	21
3.3.3 Formation Water Resistivity.....	21
3.3.3 Neutron-Density Combination.....	22
3.3.4 Neutron-Density Cross Plot.....	23
3.3.5 Total Porosity ( $\varphi$ ) and effective porosity ( $\varphi_e$ ).....	23
3.3.6 Water saturation.....	24
3.4 Petrophysical Interpretation.....	25
3.4.1 Net reservoir and Netpay Cutoffs.....	26
3.5 Petrophysical Evaluation of well M1-114.....	27
3.6 Petrophysical Evaluation of well N1-114.....	38
3.7 Petrophysical Evaluation of well X1-114.....	46
3.8 Petrophysical Evaluation of well Y1-114.....	53
3.9 Petrophysical Evaluation of well Z1-114.....	61
<b>CHAPTER FOUR</b>	
Subsurface Mapping and Cross-sections.....	68
4.1 Introduction.....	68
4.2 Maps.....	73
4.2.1 Sand/shale ratio map.....	73
4.2.2 Isopach maps.....	75
4.3 Cross sections.....	79
4.3.1 Stratigraphic cross section.....	79
4.3.2 Structural cross section.....	80
<b>CHAPTER FIVE</b>	
Subsurface Facies Analysis.....	86

5.1 Introduction.....	86
5.2 Imaging Tool.....	87
5.3 Schlumberger Fullbore MicroImager (FMI).....	87
5.4 Signal processing.....	87
5.5 Geological classification of image features.....	89
5.6 Image integration using core data.....	89
5.7 FMI Interpretation.....	94
5.7.1 FMI Analysis of well N1-114 well.....	94
5.7.2 FMI Analysis of well X1-114 well.....	107
5.7.3 FMI Analysis of well Y1-114 well.....	121
5.8 Stratigraphic cross-section and lateral facies continuity.....	133
5.8.1. Lateral facies change of Unit A1 &A2.....	133
5.8.2. Lateral facies change of Unit A3 &A4.....	133
5.8.3. Lateral facies change of Unit B1 &B2.....	136
5.8.4. Lateral facies change of Unit B3 &B4.....	136
5.8.5. Lateral facies change of Unit C.....	136
5.9. Considerations and discussions.....	140
Conclusions.....	142
Recommendations.....	144
References.....	145
Abstract in Arabic Language.....	151

## LIST OF TABLES

No.	Title	Page
1.1	Data list of the wells in Block-114.....	5
1.2	Production Test of well X1-114 and Y1-114 in the study area.....	6
3.1	Log Types in the studied wells.....	16
3.2	Average Formation Water Resistivity in the study area.....	22
3.3	The selected net reservoir and net pay cut-offs.....	26
3.4	Production Test summary of M1-114 well.....	27
3.5	Reservoir and Pay summary of well M1-114.....	29
3.6	Production Test summary of N1-114 well.....	38
3.7	Reservoir and Pay summary of well N1-114.....	39
3.8	Production Test summary of X1-114 well.....	46
3.9	Reservoir and Pay summary of well X1-114.....	47
3.10	Production Test summary of Y1-114 well.....	53
3.11	Reservoir and Pay summary of well Y1-114.....	54
3.12	Reservoir and Pay summary of well Z1-114.....	61
4.1	Sand-Shale Ratio of the wells in the study area.....	73
4.2	Net reservoir and net pay of the wells in the study area.....	75
4.3	Determined subunits in the studied wells.....	79
5.1	Symbols of geological features on the image log.....	89



## LIST OF FIGURES

No.	Title	Page
1.1	Location of Ghadames Basin and location of Block-114 in Libya.....	2
1.2	Depth structure maps of wells Y1-114 and X1-114 in the study area.....	6
1.3	Tectonic Elements of Ghadames Basin.....	7
1.4	Section shows the progressive truncation of the Palaeozoic strata.....	8
2.1	Paleozoic stratigraphy of Ghadames Basin.....	10
2.2	Petroleum systems event chart for the Ghadames Basin.....	15
3.1	Cross section among the studied wells.....	30
3.2	M1-114 petrophysical results of Unit A.....	32
3.3a	Density-Neutron cross plot of Unit A in M1-114.....	33
3.3b	Pota-Thor cross plot of Unit A in M1-114.....	33
3.4	M1-114 petrophysical results of Unit B.....	34
3.5a	Density-Neutron cross plot of Unit B in M1-114.....	34
3.5b	Pota-Thor cross plot of Unit B in M1-114.....	35
3.6	M1-114 petrophysical results of Unit C.....	36
3.7a	Density-Neutron cross plot of Unit C in M1-114.....	37
3.7b	Pota-Thor cross plot of Unit C in M1-114.....	37
3.8	N1-114 petrophysical results of Unit A.....	40
3.9	N1-114 Density-Neutron cross plot of Unit A.....	41
3.10	N1-114 petrophysical results of Unit B.....	42
3.11	N1-114 Density-Neutron cross plot of Unit B.....	43
3.12	N1-114 petrophysical results of Unit C.....	44
3.13	N1-114 Density-Neutron cross plot of Unit C.....	45
3.14	X1-114 petrophysical results of Unit A.....	47
3.15	X1-114 Density-Neutron cross plot of Unit A.....	48
3.16	X1-114 petrophysical results of Unit B.....	49
3.17	X1-114 Density-Neutron cross plot of Unit B.....	50
3.18	X1-114 petrophysical results of Unit C.....	51
3.19	X1-114 Density-Neutron cross plot of Unit C.....	52
3.20	Y1-114 petrophysical results of Unit A.....	55
3.21	Y1-114 Density-Neutron cross plot of Unit A.....	56
3.22	Y1-114 petrophysical results of Unit B.....	57
3.23	Y1-114 Density-Neutron cross plot of Unit B.....	58
3.24	Y1-114 petrophysical results of Unit C.....	59
3.25	Y1-114 Density-Neutron cross plot of Unit C.....	60
3.26	Z1-114 petrophysical results of Unit A.....	62
3.27	Z1-114 Density-Neutron cross plot of Unit A.....	63
3.28	Z1-114 petrophysical results of Unit B.....	64
3.29	Z1-114 Density-Neutron cross plot of Unit B.....	65
3.30	Z1-114 petrophysical results of Unit C.....	66
3.31	Z1-114 Density-Neutron cross plot of Unit C.....	67
4.1	Depth structure map of Lower Acacus reservoir.....	70
4.2	Isopach map of Lower Acacus reservoir.....	71
4.3a	Time Slice of Lower Acacus reservoir @1548 ms.....	72

4.3b	The proposed delta geometry at this level.....	72
4.4	Sand/Shale Ratio map of Lower Acacus reservoir.....	74
4.5a	Net sandstone Reservoir map of Unit A.....	76
4.5b	Net pay map of Unit A.....	76
4.6a	Net sandstone Reservoir map of Unit B.....	77
4.6b	Net pay map of Unit B.....	77
4.7a	Net sandstone Reservoir map of Unit C.....	78
4.7b	Net pay map of Unit C.....	78
4.8	Seismic Sections among two different direction in the study area.....	81
4.9	Stratigraphic cross section in SE-NW direction.....	82
4.10	Stratigraphic cross section in SSW-N direction.....	83
4.11	Structural cross section in SE-NW direction.....	84
4.12	Structural cross section in SSW-N direction.....	85
5.1	FMI tool shape and design.....	88
5.2	FMI Standard processing parameters.....	88
5.3	Shale Facies compared to core image.....	92
5.4	Shaly-Sand Facies bounded by two cross bedding units.....	92
5.5	Cross-bedding Facies compared to core image, Core#3.....	93
5.6	Heterolithic Bedding Facies compared to core image, Core#4.....	93
5.7	Facies distribution, major trend of the structural bedding, and major trend of the Paleocurrent of Cross-bedding, all for Unit A of Well N1-114. ....	95
5.8	The facies distribution within Unit A1, Well N1-114.....	96
5.9	The facies distribution within Unit A2, Well N1-114.....	97
5.10	The facies distribution within Unit A3, Well N1-114.....	98
5.11	The facies distribution within Unit A4, Well N1-114.....	99
5.12	Facies distribution, major trend of the structural bedding, and major trend of the Paleocurrent of Cross-bedding, all for Unit B of Well N1-114. ....	100
5.13	The facies distribution within Unit B1, Well N1-114.....	101
5.14	The facies distribution within Unit B2, Well N1-114.....	102
5.15	The facies distribution within Unit B3, Well N1-114.....	103
5.16	The facies distribution within Unit B4, Well N1-114.....	104
5.17	Facies distribution, major trend of the structural bedding, and major trend of the Paleocurrent of Cross-bedding, all for Unit C of Well N1-114. ....	105
5.18	The facies distribution within Unit C, Well N1-114.....	106
5.19	Facies distribution, major trend of the structural bedding, and major trend of the Paleocurrent of Cross-bedding, all for Unit A of Well X1-114. ....	108
5.20	The facies distribution within Unit A1, Well X1-114.....	109
5.21	Zoom-in to the reservoir showing an indicator of vertical burrow.....	110
5.22	The facies distribution within Unit A2, Well X1-114.....	111
5.23	The facies distribution within Unit A3, Well X1-114.....	112
5.24	The facies distribution within Unit A4, Well X1-114.....	113
5.25	Facies distribution, major trend of the structural bedding, and major trend of the Paleocurrent of Cross-bedding, all for Unit B of Well X1-114. ....	114
5.26	The facies distribution within Unit B1, Well X1-114.....	115

5.27	The facies distribution within Unit B2, Well X1-114.....	116
5.28	The facies distribution within Unit B3, Well X1-114.....	117
5.29	The facies distribution within Unit B4, Well X1-114.....	118
5.30	Facies distribution, major trend of the structural bedding, and major trend of the Paleocurrent of Cross-bedding, all for Unit C of Well X1-114.....	119
5.31	The facies distribution within Unit C, Well X1-114.....	120
5.32	Facies distribution, major trend of the structural bedding, and major trend of the Paleocurrent of Cross-bedding, all for Unit A of Well Y1-114. ....	121
5.33	The facies distribution within Unit A1, Well Y1-114.....	122
5.34	The facies distribution within Unit A2, Well Y1-114.....	123
5.35	The facies distribution within Unit A3, Well Y1-114.....	124
5.36	The facies distribution within Unit A4, Well Y1-114.....	125
5.37	Facies distribution, major trend of the structural bedding, and major trend of the Paleocurrent of Cross-bedding, all for Unit B of Well Y1-114.....	126
5.38	The facies distribution within Unit B1, Well Y1-114.....	127
5.39	The facies distribution within Unit B2, Well Y1-114.....	128
5.40	The facies distribution within Unit B3, Well Y1-114.....	129
5.41	The facies distribution within Unit B4, Well Y1-114.....	130
5.42	Facies distribution, major trend of the structural bedding, and major trend of the Paleocurrent of Cross-bedding, all for Unit C of Well Y1-114.....	131
5.43	The facies distribution within Unit C, Well Y1-114.....	132
5.44	Detailed stratigraphic correlation of Unit A1 & Unit A2 among the studied wells.....	135
5.45	Detailed stratigraphic correlation of Unit A3 & Unit A4 among the studied wells.....	136
5.46	Detailed stratigraphic correlation of Unit B1 & Unit B2 among the studied wells.....	137
5.47	Detailed stratigraphic correlation of Unit B3 & Unit B4 among the studied wells.....	138
5.48	Detailed stratigraphic correlation of Unit C among the studied wells....	139

## List of Abbreviation

Abbreviation	Meaning
AGOCO	Arabian Gulf Oil Company
APLC	APS Near/Array Limestone Porosity Corrected
APS	Accelerator Porosity Sonde ‘Neutron log’
CGR	Corrected Gamma Ray
DT	Sonic log
DST	Drill Stem Test
IP	Interactive Petrophysics
FMI	Fullbore Formation MicroImager
GR	Gamma Ray
HCAL	Six-arm Caliper Logging Tool
HRLA	High Resolution Laterolog Array tool
LRP	Low Resistivity Pay
NMR	Nuclear Magnetic Resonance
NPHI	Neutron Porosity Log
PEFZ	Photo-Electric Factor Log
PT	Production Test
RHOZ	Density log
RW	Water Resistivity
SW	Water Saturation
Vcl	Volume of Clay

**Subsurface Reservoir Evaluation and Image Log Analysis of the Shaly-Sand Lower Acacus Reservoir, Block-114,  
Northern Ghadames Basin**

**By  
Abraheem Elmasli**

**Supervisor  
Mohamed Abdelmalik**

**Abstract**

The Lower Acacus reservoir in the northeastern part of Ghadames Basin (Block-114) forms a tidally influenced deltaic system. Structural and stratigraphic cross-sections that were constructed using Petrel (Schlumberger Trademark) have shown a general thickening of the reservoir formation towards the north-northeast. Petrophysically, this reservoir is divided into three main units based on log characters; these are (Unit A, B, and C) with Unit A being at the bottom followed by B & C. The petrophysical analysis using IP (Lloyd's Register Trademark) indicates that Lower Acacus reservoir is hydrocarbon bearing in the study area with very good reservoir parameters. Average volume of shale is around 25 percent, porosity ranges from 15 to 20 percent, and water saturation is around 35 percent in the oil wells. Hydrocarbon distribution and reservoir intervals are both mainly controlled by depositional facies and to a lesser extent by structural influence. Consequently, FMI and core images were analyzed using Techlog (Schlumberger Trademark) to define the main sedimentary structures in the available wells. These sedimentary structures were grouped into four main facies in order to delineate the vertical and lateral variation among the wells in the study area. The identified facies are heterolithic bedding, crossbedding sandstone, shaly-sand bedding, and laminated shale facies. The bioturbation activity on these facies might have a direct influence on the reservoir performance by destroying the rock primary fabric. However, the association of these facies reflect the tidal effect on the delta as supported by paleocurrent direction analysis. Additionally, the paleocurrent measurements from the cross-bedded facies show a dominant bimodal trend towards NW-SE, with modest polymodal and unimodal models.

# Chapter One

## Introduction

### 1.1 Introduction

This study was embedded in a detailed aspect by integrating core images, image logs, well logs and production data to define the characterization of the U. Silurian sequence (Lower Acacus shaly sandstone reservoir) in northern Ghadames Basin, NW Libya. Due to the confidential nature of the information used in this thesis, the study area was renamed to Block-114 and the names of the studied wells were omitted. Block-114 is one of the most profitable field in Ghadames Basin that has been operated by the Arabian Gulf Oil Company (AGOCO) since 2002.

Thus, data integration from FMI images and core images with other open hole logs is the key element for detecting and interpreting the subsurface geological sequences in the study area. From the subsurface dataset, a detailed investigation of Lower Acacus reservoir in term of petrophysical evaluation, facies analysis, and their stratigraphic contribution to oil play in the Block-114 is going to be accomplished in this study. Five wells have been used in this case study to define the Lower Acacus depositional setting of the Silurian succession in the Block-114. Three out of the five exploration wells, have image logs along with some core image control as well, to better define the main facies packages of Lower Acacus reservoir.

### 1.2 Location of the study area

Block-114 is located in the northeastern part of Ghadames Basin, South of Tripoli and it covers an area about 1,444 km<sup>2</sup>. The study area is represented by five wells (Fig. 1.1).

### 1.3 Previous work

The geology of western Libya was first studied by Italian geologists from 1930 to 1940, and then by French geologists between 1944 and 1950. In the late 1950's and early 1960's petroleum exploration programs in the sedimentary basins of western Libya, were undertaken by a number of companies after the discovery of oil. From that time, research on the Paleozoic

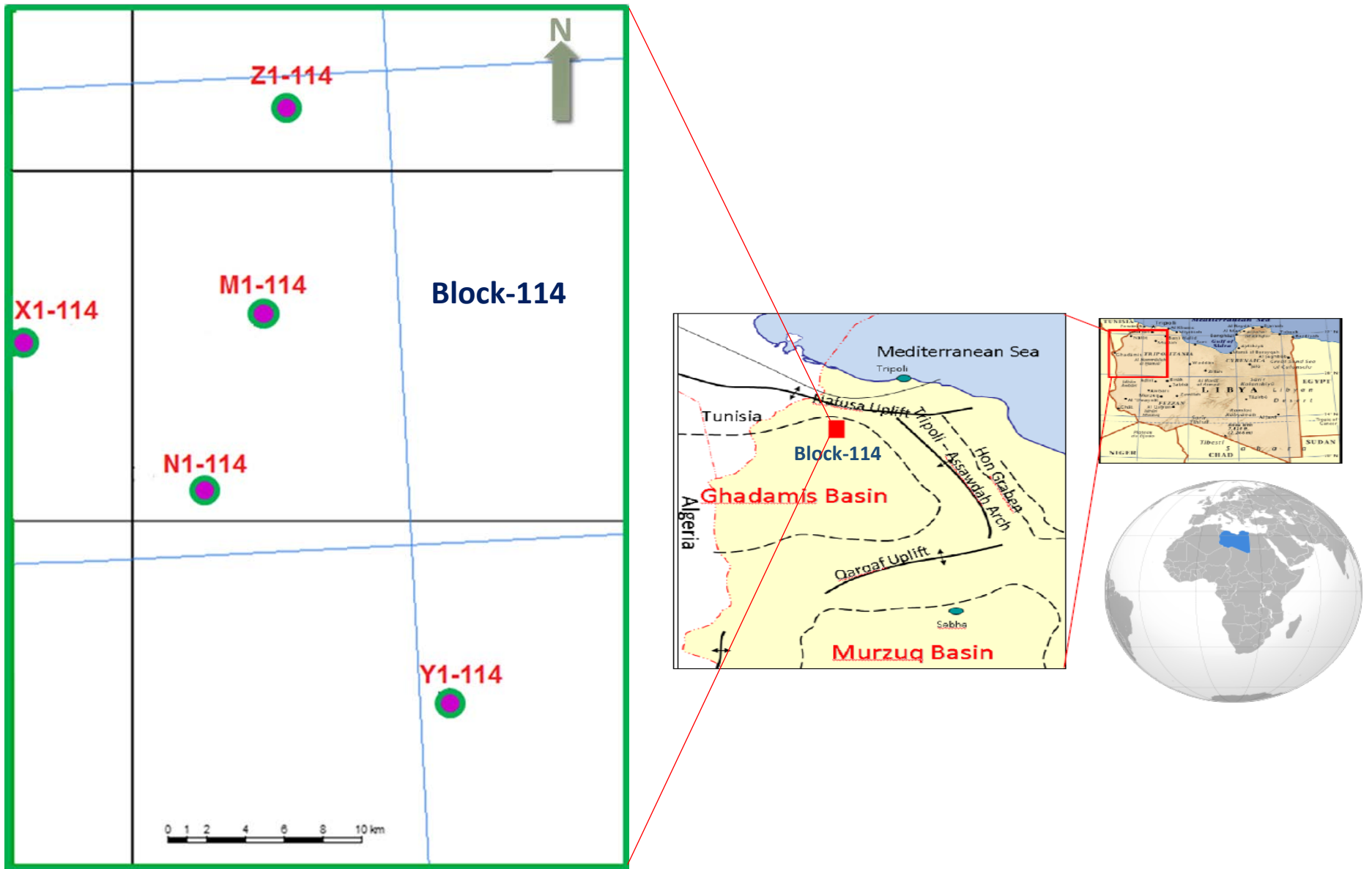


(Fig. 1.1): The location of Ghadames Basin and the location of Block-114, in Libya (AGOCO, 2009).

outcrops of the area continued and a great number of boreholes, mostly in Ghadames basin, were drilled, Boote et al., (1998). Bellini and Massa (1980) reviewed the previous publications on the Palaeozoic of the western sedimentary basins of Libya. Other work that has been done on Ghadames basin include Hammuda (1980), Clark-Lowes (1985), Bracaccia et al., (1991), Sinha and Ben Rahuma (2000), Howlett (2000), Rusk, (2001), Underdown and Redfern (2008), among others.

The Palaeozoic strata in western Libya have been a subject of intensive sedimentological and stratigraphical investigation as it involved the main source and reservoir rocks in the area. Harouda et al (2002) made a detailed investigation for the hydrocarbon potential of Silurian Tanezzuft shale as it is represent the main source rock in Ghadames Basin. Lower Acacus sandstone on the other hand represent the main target reservoir for hydrocarbon exploration in the basin. On the basis of a best-facies-fit-correlation approach, Elfigih (1991) demonstrated that the Lower Acacus Formation consists regionally of at least 14 progradational units which change laterally in a progradational fashion from south to north in the Basin. Consequently Elfigih (2000), made a detailed analysis on the sedimentology and regional diagenesis of Lower Acacus sandstone and identified three diagenetic facies; quartz, carbonate and clay-cemented facies; from the southern basin flanks to the northern basin center respectively.

In addition, the usage of FMI log have been used for structural and sedimentological analysis with emphasis on the identification of the major sequence boundaries. In Murzuq Basin, Ramadan (2008) Utilized FMI Images and open hole logs to define the structural and sedimentological features in the Middle Ordovician Successions, and Najem (2011) integrated subsurface seismic data to FMI images to construct a structural modeling of the Ordovician succession in the South-Central part of Concession NC186. Similarly in Sirt Basin, Bosnina (2010) made an analysis of microfaults and fractures in Southern NC193 concession using FMI Log.

## **1.4 Methodology**

Framework will start with a phase of collection, investigation and preparation of all the available data in the study area; subsequently state of the art software will be used to undertake analysis providing a firm foundation to the overall geological interpretations.



Construction of subsurface maps and subsurface correlations will be methods embraced to achieve this geological study. Below are the main methods, software and products, which will later be integrated to achieve the objectives of the study. AGOCO Company provides the following geological software:

- i. **TechLog Software Version 3.0-2016:** this software used for displaying and interpreting the image log (FMI).
- ii. **Interactive Petrophysics (IP) Version 4.0.:** this software used for displaying and interpreting the conventional well logs.
- iii. **Petrel Software-2016:** this software will be used for visualization and extraction subsurface maps; as well as constructing stratigraphic and structural cross-sections.

Software will help construct geological maps and assist in the following analyses:

1. **Petrophysical Evaluation of Lower Acacus Formation:** the reservoir parameters will be assessed; Volume of Shale, Effective Porosity, and Water Saturation; which will be used as cut-offs to determine the Net Pay intervals.
2. **Petrophysical Maps (sand/shale, and Net-pay):** These maps will be integrated with other facies maps to predict the trend of the reservoir geometry.
3. **Detailed geological facies analysis of Lower Acacus Formation using FMI and core images:** Identifying sedimentary structures along with sand body geometries through integration of logs and core images for the reservoir intervals would delineate the different lithofacies within Lower Acacus Formation.
4. **Stratigraphic and Structural cross sections:** These cross sections will show lateral and vertical relationships as well as the facies identified and their influence on hydrocarbon entrapment.

## 1.5 Data Base

The main dataset were used in this study are summarized in (Table, 1.1). Lower Acacus reservoir in three wells are totally covered by FMI log and they will represent the control points to determine the possible depositional setting.

Table-1.1: Data list of the wells in Block-114, which used in this study.

Well Name	Year	Well Logs	FMI Logs	Core Image	Production Test	Status
M1-114	2005	Yes	-	-	Yes	HC
N1-114	2008	Yes	Yes	Core#4	Yes	HC
X1-114	2009	Yes	Yes	Core#2	Yes	Dry
Y1-114	2009	Yes	Yes	Core#3	Yes	HC
Z1-114	2010	Yes	-	-	-	Dry

## 1.6 Objective of the Study

- i. Integration of all available datasets to provide realistic spatial variations of facies and reservoir intervals throughout the area of interest.
- ii. Lithofacies and rock properties prediction. Infer reservoir qualities of Lower Acacus Shaly-Sandstone in wells with High-resolution Micro-resistivity Image logs.
- iii. Compare and contrast the characteristics of Lower Acacus Sandstone facies within each reservoir.

## 1.7 Observations and Scientific Problem

The hydrocarbon exploration of Lower Acacus Member has always being targeted in Ghadames Basin. Many difficulties are encountered during the evaluation of this reservoir, most important of which is the lateral facies change and reservoir heterogeneity.

The most important observation is, well Y1-114 in southeastern part of the study area, which is an oil producing well fuelled by multi-play horizons in the Lower Acacus, where in well X1-114 in the northwest is a water wet (Table-1.2). Meaning that there are more than structural constrains contributing to the entrapment styles in the area of interest. This observation is supported by the updated structure depth maps for both wells, which both exhibit four-way closers (Fig. 1.2). Correlations and facies analysis might help to understand and resolve this issue.

Table-1.2: production test of well X1-114 and Y1-114 in the study area (AGOCO, 2009).

<b>(Production Test of X1-114)</b>		<b>(Production Test of Y1-114)</b>		<b>Formation</b>
<b>(L. Acacus@8009 ft)</b>		<b>(L. Acacus@8020 ft)</b>		
PT4 (9072-9082)	Water Wet	PT3 (8874–8879) (8885–8892)	HC Bearing	<b>Lower Acacus</b>
PT5 (9022-9037)	Water Wet			
PT6 (8746-8760)	Water Wet	PT4 (8601-8608) (8584-8596)	HC Bearing	
PT7 (8564-8575)	Water Wet			
PT8 (8501-8515)	Water Wet			
PT9 (8078-8088)	Water Wet	PT5 (8022-8036) PT6 (7997-8002) (7943-7950)	HC Bearing	
PT10 (8011-8028)	Water Wet			

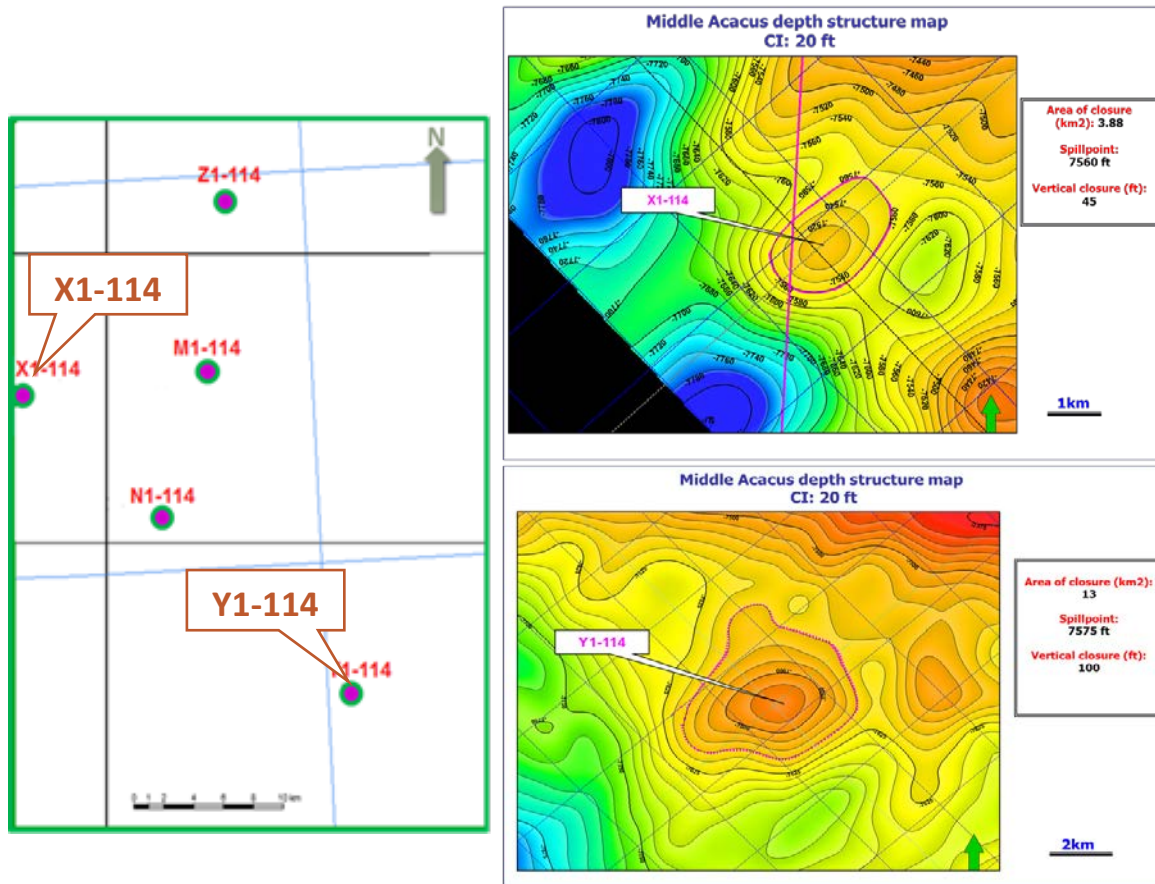


(Fig. 1.2): Depth structure maps of wells Y1-114 and X1-114 in the study area (AGOCO, 2009).

## **Chapter Two**

### **Regional Geological Setting**

#### **2.1 Introduction**

Ghadames Basin is a large intracratonic basin on the North African platform. Formed during the early Paleozoic era, it covers an area of 350,000 km<sup>2</sup> and straddles the borders of Libya, Tunisia, and Algeria. The Libyan portion represents the eastern flank of the basin and covers an area of about 183,000 km<sup>2</sup>. It has been an important hydrocarbon province since the 1950s (Echikh, 1998). Block-114 is located in the northern part of Ghadames Basin close to Jabal Nafusah Uplift and to the South-West of Tripoli City (Fig. 2.1).

The main tectonic elements bounding the Ghadames Basin are the Dahar–Nafusah high to the north, the Qarqaf uplift to the south, and the western flank of the younger Sirt Basin to the east. Many of these structural features were initiated in the late Precambrian Pan-African orogeny, with repeated reactivation of older structures occurring throughout the Phanerozoic. The basin contains up to 5,200 m [~17,000 ft] of Paleozoic and Mesozoic sediments, the Paleozoic section being separated from the Mesozoic deposits by a major regional unconformity of the Hercynian (Devonian-Carboniferous) age (Fig. 2.2). This Hercynian unconformity is represented as the most conspicuous feature of the basin as Palaeozoic succession is overlain by Mesozoic Basin (Hamadah Basin) with a markedly different basin configuration. Erosion patterns and the topography that developed on the surface of this regional unconformity have had a direct influence on the petroleum systems within the basin. The tectonic history of the basin has similarities with Murzug Basin, but with some differences, due to its location closer to the continental margin and to the Tethys Ocean (Hallet, 2002).

#### **2.2 Geological Setting**

In the Ghadames Basin the Paleozoic subsidence created most of its basin fill. Deposition started with the Cambrian to Lower Ordovician succession, a sequence of continental to shallow marine sands (Hassauna and Haouaz Formations), which was followed by the deposition of a package of transgressive marine shales (Melez Chograne Fm) (Fig. 2.3).

During the Late Ordovician the area was covered by a thick ice sheet: this event was a consequence of the southern–near the South Pole–geographic position of the North African Platform during that time. At the beginning of the

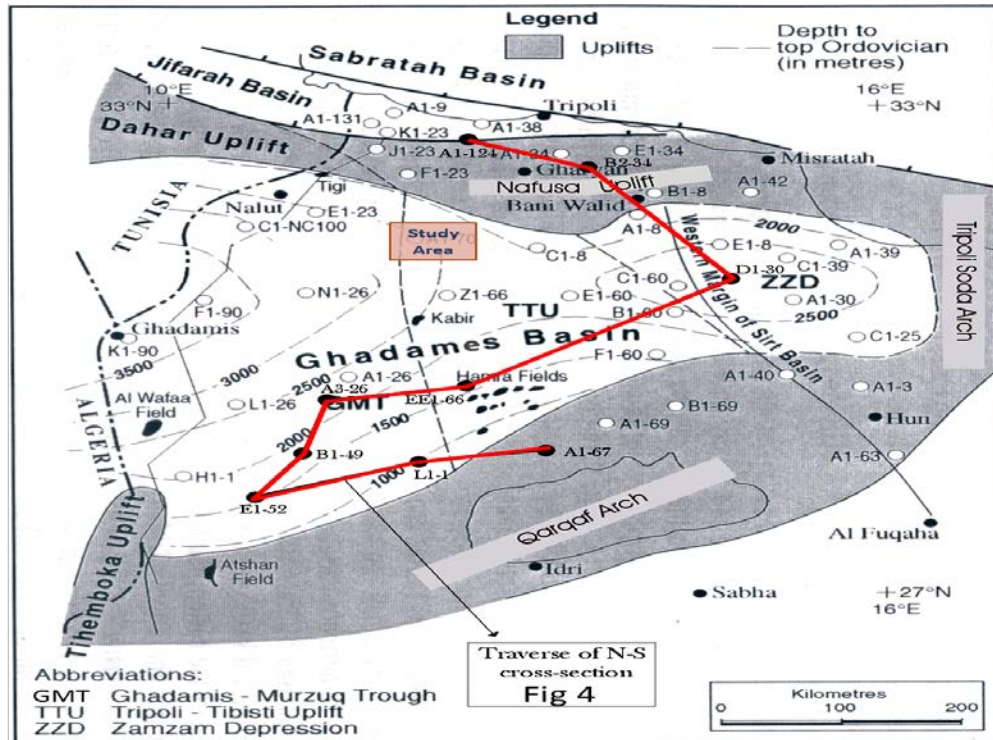


(Fig. 2.1): Tectonic Elements of Ghadames Basin (Hallet, 2002).

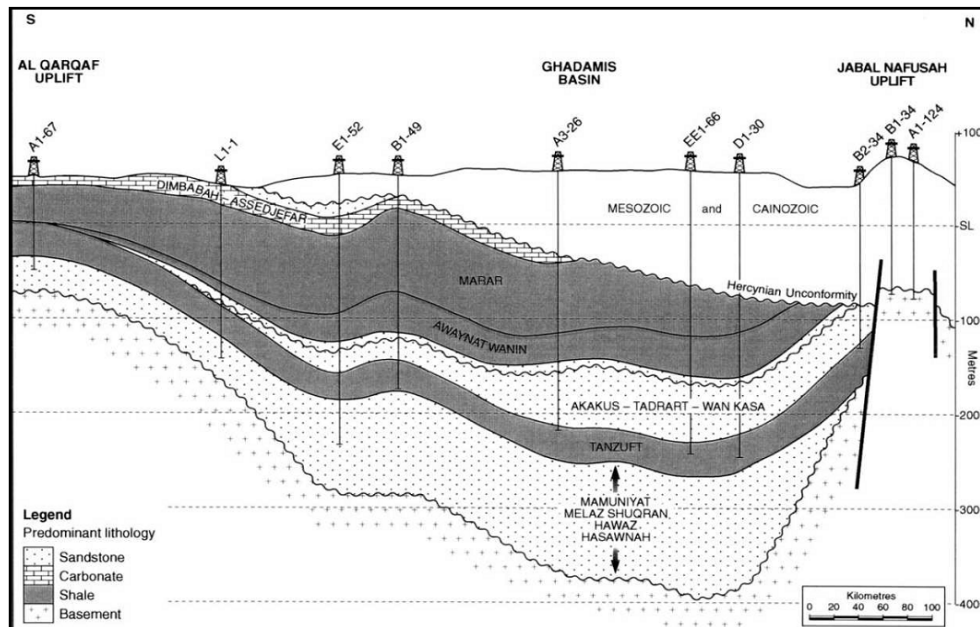


(Fig. 2.2): The section shows the progressive truncation of the Palaeozoic strata by the Hercynian unconformity from south to north, and the abrupt northern termination of the Ghadames Basin against the Jabal Nafusah Uplift (Hallet, 2002).

Late Ordovician (Ashgillina stage), an uplift of the area occurred and the subsequent erosional activity by ice cover determined the creation of a series of large and long troughs, which were filled by fluvio-glacial and glacio-marine deposits of the Memouniat Formation. Memouniat Formation consists of sandy periglacial deposits in the southern part near the Garghaf Uplift and of shaly glacio-marine deposits in the north. Because of the glacial origin, rapid vertical and lateral facies variations are quite common in Memouniat Formation. The distribution of sand bodies is irregular and directly related to the paleo-topography generated by erosive actions of the ice sheet (Letouzy et al., 2005).

The Taconian unconformity marks the transition to the Early Silurian sequences. An extensive marine transgression (Liandoverain stage) occurred leading to the deposition of the Tanezzuft Formation. Tanezzuft Formation is a shaly interval which at the base is highly radioactive and has high organic content (Hot Shales).

The Acacus Formation is one of the most important reservoirs of the Ghadames Basin. The Acacus Formation is identified by varying amounts of sandstones alternating with shaly layers. It represents deltaic depositional system with the progradational trend directed both from SSE to NNW and from East to West (Arduini et al., 2003). Another important tectonic event occurred at the base of the Devonian time. This event is referred to the Caledonian orogeny and determined the uplift of the southeastern area of Ghadames Basin and the erosion of part of the Acacus Formation. Above this unconformity, the fluvio-deltaic and shallow marine sands of the Tadrart Formation were deposited. The subsequent Devonian succession includes the transgressive shallow marine sands of the Ouan Kasa Formation, the Emgyat Shale (maximum flooding event), the Aouinet-Ouenine Formation (shelf sands overlain by shallow marine shales, the latter including some organic rich shale layers in the upper section) and the sandy Tahara Formation in the shelf environment (Hallet, 2002).

During the Carboniferous several mostly shaly units of offshore shelf and shallow marine environment deposited in the basin (e.g. Marar, Assedjefar, tiguentourine Formations). This sedimentation was then abruptly interrupted Hercynian orogeny. This major event affected the entire structural setting of the Ghadames Basin. This phase caused the uplift of the Dahar-Nefusa Arch, as well as a strong but uneven erosion of the area. A regional tilting caused the basin depocenter to shift towards the north.

The Mesozoic sedimentation is characterized by clastic, carbonates and evaporates sequences with an overall wedging towards the north. The fluvio-deltaic sandstones of the Lower Triassic (Ouled Cheb and Ras Hamia Formations) are reservoirs of minor importance. During Tertiary the tectonism of the North Africa Platform was related to the Alpine orogeny. It caused the re-activation and inversion of the Hercynian faults and was rather weak. However, no significant sedimentation occurred in the basin during this era (Letouzy et al., 2005).

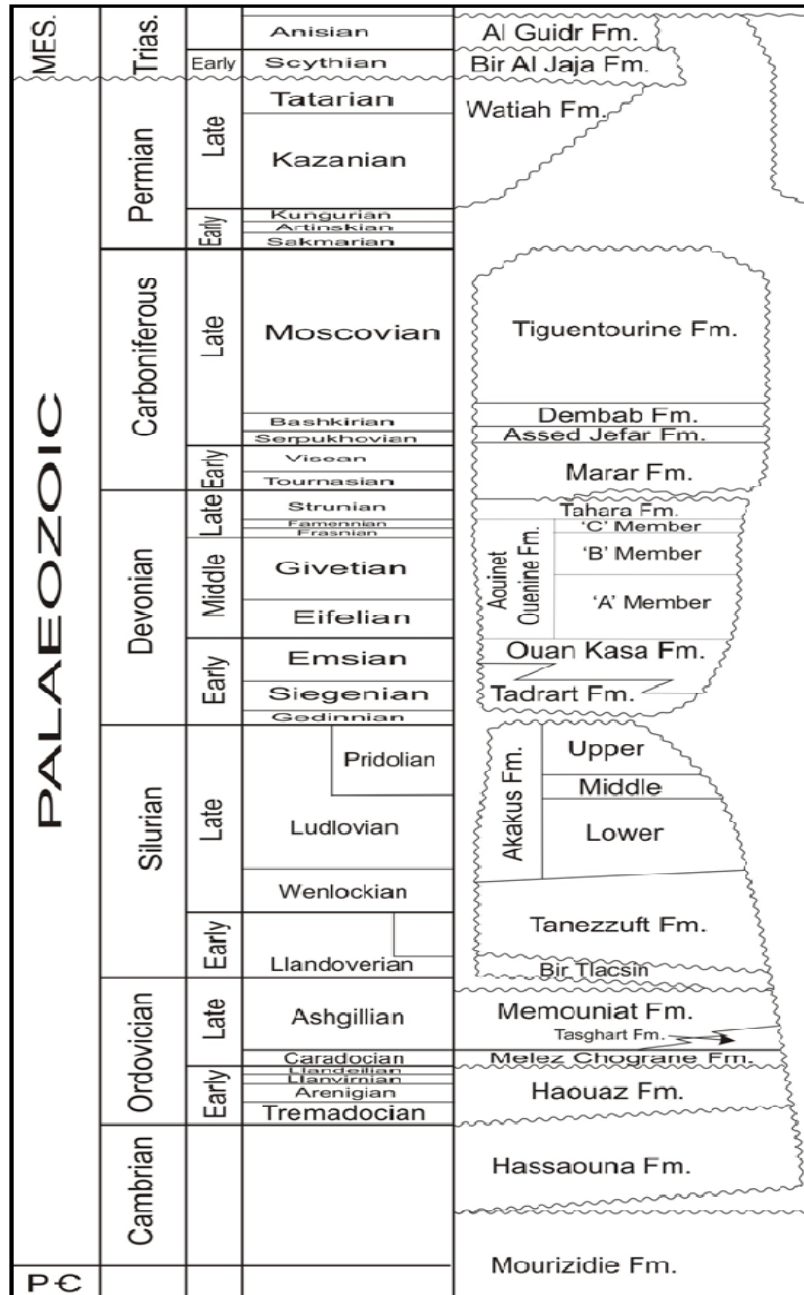


(Fig. 2.3): Paleozoic stratigraphy of Ghadames Basin (Letouzy et al., 2005).

## **2.3 Petroleum System of Ghadames Basin**

The comparison of many prolific source rocks with the different sedimentary cycles confirms that they were mainly deposited during periods of global marine transgressions. In these cases the primary productivity of phytoplankton is high. The algal blooms and anoxic conditions together with the sedimentation provide organic rich source rocks containing the oil-prone type II kerogen. This type of kerogen is typical for Paleozoic North African oils (Lu'ning et al., 2000).

### **2.3.1 Source Rock**

The Lower Silurian (Tanezzuft) and the Middle–Upper Devonian (Frasnian) bituminous mudstones form the main source facies within the Ghadames Basin and are the most important Paleozoic source rocks on the North African platform (Boote et al., 1998). The highest total organic carbon (TOC) content in these Lower Silurian and Middle–Upper Devonian shales occurs in two discrete intervals: the Llandoveryian basal radioactive (hot) shale interval and the Frasnian radioactive shales (Lu'ning et al., 2000; Cochran and Petersen, 2001).

The Lower Silurian (Llandoveryian) radioactive shales range in thickness from 0 to 50 m (0 to 164 ft), averaging about 20–30m (66–98 ft) over the central area (Underdown, 2006). The thickness is strongly controlled by Hercynian erosion over the northern, western, and southeastern flanks. Over the central part of the basin, thickness is only poorly constrained because of limited well penetrations. However, extrapolation of information from the east, confined by available data from the literature (Lu'ning et al., 2000), suggests that the hot shale thickness in this area averages about 20–25m (66–82 ft). This agrees with estimates from literature (e.g., Boote et al., 1998; Cochran and Petersen, 2001).

### **2.3.2 Reservoir Rocks**

Nearly all of the oil-and gas accumulations so far discovered in the Libyan Ghadames Basin occur within Devonian and Silurian sandstones, with only a few small accumulations in the Ordovician, Carboniferous and Triassic (Hammuda, 1980; Echikh, 1998).



The main reservoirs are the Upper Silurian Acacus and the Lower Devonian Tadrart and Ouan Kasa and Memouniat formations. Three other objectives are the Middle Devonian Aouinate Ounian Sandstone, Upper Devonian Tahara Formation, and the Triassic Ras Hamia Formation.

Silurian, Lower Acacus sands represent the most important reservoir of the area with porosities ranging 10-30 % and permeabilities often higher than 100 mD in the productive layers. The Lower Acacus Member has been divided into two parts: a lower package and an upper package. The lower package is sandier than the upper one. From the depocenter into the basin edges the lower package is equivalent and correlates with the Lower Member of the Undifferentiated Acacus formation and the upper package with the lower part of the Upper Member of the Undifferentiated Acacus formation. Deposition of the Lower Acacus Member was a result of eustatic level fall during Upper Silurian times which developed a sedimentary delta complex. The inter-fingering of the delta front sandstones with adjacent prodelta mudstone provides the multipay reservoirs. Along the bottom part of the Lower Acacus Member overlapping basal regressive sandstones are present. The individual sandstone units are typically 10-40 feet thick and represent the main reservoirs and targets for oil production (AGOCO, 2009).

### **2.3.3 Seal Rocks**

As much as 2,000 m of Triassic to Jurassic evaporites, mudstone, and carbonate rocks (Saliferous Units) provides a regional top seal for reservoirs in most of the Tanezzuft Oued Mya Total Petroleum System. The Triassic to Jurassic seal extends from the Saharan Flexure in the north where the thickest section is present to approximately the southern boundary of the Trias/Ghadames Province. Triassic volcanic rocks provide the primary seal for some reservoirs, and intraformational Paleozoic marine mudstone provides secondary, lateral seals when in conjunction with the regional top seal (Boote et al., 1998).

Generally, there is an effective Acacus shale seal above the sandstone. Where it may be absent, however, the overlying Tadrart will form a combined objective with the Acacus sandstone. Shale horizons consistently provide adequate seals for Tadrart, Ouan Kasa, and Tahara sandstones. Throughout most of the area, there are effective shale, carbonate, or

evaporite seals for the Ras Hamia sandstone. Because of a dominant continental siliciclastic facies above the Ras Hamia in the southern part of the area, however, a seal may be lacking. (Rusk, 2001).

In Block-114 area, the sandstones reservoirs of the Lower Acacus Member are top and laterally sealed by the intra-informational shales, some of which may be partially sealing in some zones due to discontinuity. The Middle Acacus Member is transgressive marine shale with a few silty sandstones beds in the middle. It represents an active top sealed of the main sandstone reservoir of Lower Acacus Member (Hallet, 2002).

### **2.3.4 Trap Style**

Most of the fields in the Ghadames Basin have multiple ages of structuring. The younger stages of deformation either enhanced or degraded the traps. In some cases other elements, such as stratigraphic pinchout, are more important than structure in trap formation. Howllett (2000) recognized seven different trapping styles in Ghadames Basin which are: broad regional uplifts, high-amplitude folding associated with reverse faulting, low-amplitude folding associated with reverse or normal faulting, normal fault and dip-closed structures, stratigraphic pinchouts, sub-crop to an unconformity and laccolith-induced structures.

In the study area, the principle traps are structural and consist of small-size anticlines, Hercynic in age. These structures are rather limited in vertical closure, which implies that a relatively small amount of hydrocarbon reserves are usually found. In the northwestern part of the Ghadames Basin, several discoveries of this type have been made at the Lower Acacus reservoirs (Block-114).

Howllett (2000) categorized Al Hamada al Hamra area as normal fault and dip-closed traps while new 3D seismic data reveals these structures are better to be classified in low-amplitude folding associated with reverse or normal faulting trapping styles.

Stratigraphic traps may be found as pinch-outs (e.g. in El Wafa Field, where hydrocarbons are trapped in a large termination of the Aouinet Ouenine sands against Temboka High) or as toplaps against unconformity (e.g. Acacus sands against the Hercynian unconformity in the Tigi Field) (Hallet, 2002).

## 2.4 Oil and Gas Generation and Migration

According to regional evaluation, the geothermal gradient 1.7 °F /100 feet (31 °C /Km) has been accepted for the Ghadames Basin. The top of oil generative window is 5000-6000 ft and the top of gas condensate zone is 9000-10000 ft (Hallet, 2002).

Tanezzuft source rocks of the central part of Ghadames Basin have reached the top of oil window, first, during Permo-Carboniferous subsidence and second during Upper Cretaceous–Lower Jurassic subsidence. Along the basin periphery where the deposits were thinner and shallower Tanezzuft source rocks did not reach the top of oil window during Permo-Carboniferous. The Upper Cretaceous – Lower Jurassic times represent the main hydrocarbon mobilization stage of Tanezzuft source rocks. The Upper Member shales of Ouenine formation source rocks have reached the top of oil window during Cretaceous subsidence in the deepest parts of the basin.

Primary migration during the main phase of hydrocarbon generation generally occurs at depths between 1500-3500 m; proved as a fact in current oil fields. Almost all the sedimentary section in the Ghadames Basin is an intercalation of source rocks, reservoir rocks and seal rocks creating ideal conditions for primary migration from source rocks to reservoir rocks.

In the Ghadames Basin the lateral regional migration from the center of the basin to the edges of the basin is supposed to be common. The basal sandstones of Lower Acacus Member that are the closest reservoir rocks to the Tanezzuft source rocks represent the first environment for both primary and extensive lateral migration (Fig. 2.4). The tectonic faults, fractures and unconformities presence together with the channel development in the sand dominated sequences represent the ways for a vertical migration from source rocks to the shallower reservoirs. The shallower reservoirs help the lateral extensive migration in the other parts of the basin creating so a complex system for the secondary migration and the distribution of oil from the source rocks to the reservoirs rocks of the basin (Underdown and Redfern, 2008).

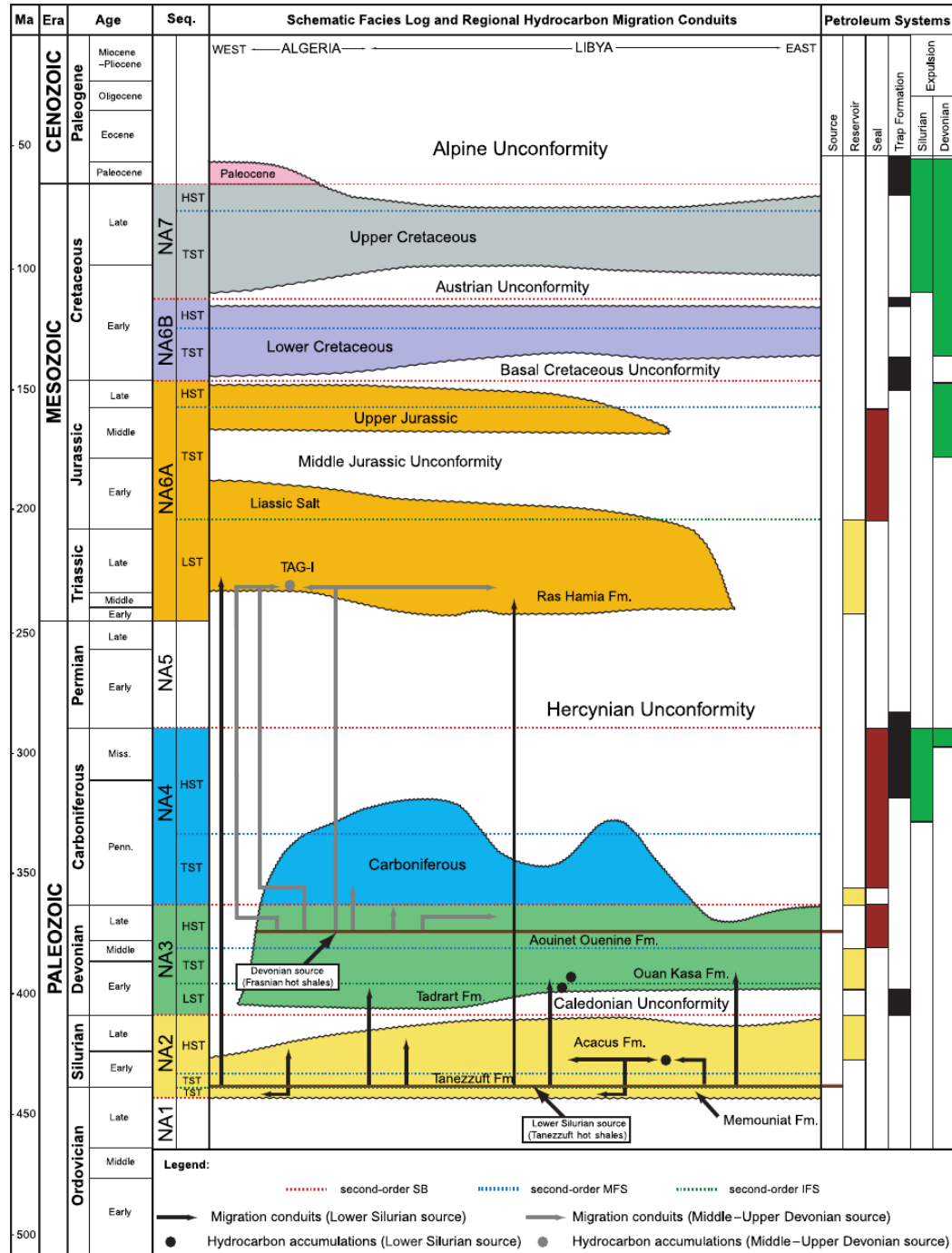


(Fig. 2.4): Petroleum systems event chart for the Ghadames Basin, showing regional chronostratigraphy and migration conduits from the Lower Silurian (Tanezzuft) and Middle Upper Devonian (Frasnian) source rock intervals. LST, TST, and HST = lowstand, transgressive, and highstand systems tracts, respectively. SB = sequence boundary, MF = maximum flooding surface, IFS = initial flooding surface, TAG-I = Triassic (Underdown and Redfern, 2008).

## Chapter Three

### Petrophysical Interpretation

#### 3.1 Introduction

The principal objective of the petrophysical study is to provide a reliable evaluation of Lower Acacus reservoir, capable of predicting the formation properties from the well logs. All the wells were drilled with KCL mud and were surveyed with a full complete logging program. The recent logs include a High Resolution Laterolog Array tool (HRLA), Six-arm caliper logging tool (HCAL), Sonic log (DT), Gamma Ray log (GR), Corrected Gamma Ray (CGR) only in M1-114, Density log (RHOZ), and Neutron log ‘Accelerator Porosity Sonde’ (APS) (Table, 3). Five wells were fully interpreted and the petrophysical data were interpreted using the Interactive Petrophysics (IP) Version 4.0. The following is a summary regarding the wireline logging types in the studied wells:

(Table, 3.1): Log types in the studied wells.

Well Name	Conventional Well Logs
M1-114	GR, CGR, APS, RHOZ, DT, HRLA, HCAL, PEFZ
N1-114	GR, APS, RHOZ, DT, HRLA, HCAL, PEFZ
X1-114	GR, APS, RHOZ, DT, HRLA, HCAL, PEFZ
Y1-114	GR, APS, RHOZ, DT, HRLA, HCAL, PEFZ
Z1-114	GR, APS, RHOZ, DT, HRLA, HCAL, PEFZ

##### 3.1.1 An overview of Wireline Logging

Wire line logging is a conventional form of logging that employs a measurement tool suspended on a cable or wire that suspends the tool and carries the data back to the surface and Wire line logs are created when the drill-bit is removed from the borehole (Glover, 2012).

Many information regarding porosity, permeability, formation thickness, depths, lithology, water saturation, wettability, capillary pressure and grain and pore size distributions can be obtained from the core analysis. This information from core analysis carries very detailed description from the subsurface. Visual examinations of cores are an important method to study formation features but this method has some limitations due to imprecise depth for each sample and high cost for coring process.

One of the earliest goals of wire line logging was to provide a description as detailed as those obtained by coring, but more time-efficient and cheaper (Ekstrom et al., 1987). The wire line logs are providing continuous measurement of data as a function of depth, but they are used as a supplementary method to cores. A brief review of the logs were used in this study is discussed below:

## **3.2 Well Logs used in this study**

### **3.2.1 Mechanical Log (Caliper log)**

The caliper log is a tool for measuring the diameter and shape of a borehole. It uses a tool that has 2, 4, or more extendable arms. The arms can move in and out, as the tool is withdrawn from the borehole, and the movement is converted into an electrical signal by a potentiometer (Glover, 2012). The caliper logs are plotted along with the drilling bit size, for comparison for instance, when a hole has same size as the bit-size, it is called on gauge. This means that the formation is consolidated and non-permeable. When the borehole diameter is larger than the bit-size, the formation consists of a soluble lithology such as a salt formation or brittle shale, but when the diameter is smaller than the bit-size, it is time for the development of mudcake for porous and permeable formations, which indicate the permeable sandstones (Glover, 2012).

The Six-arm Caliper Logging Tool (HCAL) accurately measures the borehole's radius in six 60° angles, and the tool's axis is the center of the radius. Three diameter curves or six radius curves will be obtained in logging process. During open hole logging, the degree of irregularity of the hole will be obtained. During cased hole logging, the position of the casing damage and deformation condition will be obtained (Schlumberger, 2015).

### **3.2.2 Natural Radiation Log (Gamma ray log)**

A Gamma-ray log is a record of a natural formation's radioactivity. It measures the radiation of the combined elements of parent and daughter product, of the three main radioactive families: Uranium, Thorium and Potassium. It is used to identify lithology (shaliness) and to derive the shale volume of a formation.

In sediments, radioactive elements are borne by numerous minerals. Among other, Potassium is found in clay minerals, evaporates, carbonates and in low concentrations within the feldspars contained in sandstones. Thorium is a common constituent of the

detrital fraction of minerals such as continental shale, certain beach-sands and placers. Uranium can be found in clay mineral containing organic matter of vegetable origin, clay particles, and adsorptive material such as amorphous silica, alumina, and coals. Therefore, shale have by far the strongest radiation; then sandstones, dolomite and finally limestone with weak radiation (Rider, 1996).

High gamma ray may not imply shaliness, but a reflection of radioactive sands such as potassium rich feldspathic, glauconitic or micaceous sandstones. Gamma-ray log is usually preferred to spontaneous potential logs for correlation purposes in open holes nonconductive borehole fluids, for thick carbonates intervals, and to correlate cased-hole logs with open-hole logs. The standard unit of measurement of gamma-ray is API (American Petroleum Institute).

### **3.2.3 Electrical Log (Resistivity Logs)**

Electrical logs are perhaps the most important tools available to a petrophysicist. This is because they provide a method for calculating the water saturation, upon which calculations of hydrocarbon reserved are based (Glover, 2012). Electrical logs are divided in to three subcategories: laterolog, induction log and micro resistivity log. The induction log measures conductivity of the formation and can cope with highly resistive muds (oil-base mud). The modern tool for measuring the resistivity in low resistivity mud with high salinity is called laterolog. Micro resistivity is another resistivity tool, which is designed to measure the resistivity of mudcake.

Since the solid components have higher resistivity than pore fluids in most rocks, resistivity is controlled by the conductivity of the pore fluids. Hydrocarbons have higher resistivity than the fresh water and fresh water has higher resistivity than the salt water. The correlation between deep and shallow resistivity and the amount of separation between deep and shallow resistivity is dependent on the depth of invasion and drilling fluid (Glover, 2012). Shale formations should be indicated by a lower resistivity than the sandstone formations due to the presence of bound water in clays. This is not the case in the studied reservoir as the shale layers have a higher resistivity than the reservoir sandstone (law resistivity pay zones).

The high-resolution laterolog Array tool (HRLA) helps resolve the problem of determining true formation resistivity ( $R_t$ ) in thinly bedded and deeply invaded formations to identify and estimate reserves. Because the multiple-frequency HRLA

array measurements are simultaneously made from a common central electrode, they are naturally resolution-matched and depth-aligned for greater intra-data accuracy (Schlumberger, 2015).

### **3.2.4 Acoustic log (Sonic Log)**

The sonic or acoustic log measures the travel time of an elastic wave through the formation. This type of log is designed to indicate porosity, lithologies, facies and stratigraphic correlation. In addition, the identification of fractures, compaction, over pressures and source rocks can be achieved. The sonic log is sensitive only to the primary intergranular porosity. The difference between intergranular porosity measured by sonic tool and total porosity measured by density and neutron tools will give the secondary porosity. The sonic log can identify the lithology; high velocities usually indicate carbonates; middle velocities indicate sands and low velocities, shales (Glover, 2012).

The compacted formations have high velocity of an elastic wave inside themselves. The over pressured zones that have higher pore pressure show an increase in sonic travel time. A relative decrease in sonic transit time and an increase in resistivity indicate an organic-rich layer in impermeable sediments. Where density logs are affected by rugosity of the borehole wall or by the presence of pyrite, sonic logs may prove more reliable reading than density logs (Meyer and Nederlof, 1984).

### **3.2.5 Neutron Log**

The neutron source emits neutrons to the formation and maximum energy is lost when the neutron collides in-line with the nucleus of the same mass like hydrogen. The slowing down of the fast neutrons by hydrogen nuclei is the predominant phenomenon used, and the reading, for given hole conditions, depends mostly on the hydrogen index of the formation (Gaymard and Poupon, 1968).

Shale formations contain clays that have high amount of bound water. Hence, shales can contain a significant proportion of hydrogen despite being of low porosity. The porosity reading from the neutron tool in shale formations is therefore always significantly higher than the real porosity, this phenomena is called shale effect (Glover, 2012).



The (Accelerator Porosity Sonde) APS uses an electronic pulsed neutron generator (PNG) to deliver both epithermal and thermal neutron measurements. The relative insensitivity of the measurements to the borehole environment and formation characteristics, such as lithology and fluid salinity, provides accurate data for evaluating porosity. Because clays and mixed carbonate lithologies have little effect on the hydrogen index measurement made by the APS sonde, true formation porosity is obtained and gas effects are more visible (Schlumberger, 2015).

### **3.2.6 Density Log**

The density tool sends out gamma rays to the formation and the gamma rays will be scattered by an orbital electron. As a result of this interaction the gamma ray lose energy, and the electron is ejected from the orbit. This process with a medium energy is called Compton scattering and is used for density logging. (Glover, 2012). The density log measures the bulk density of the formation that consists of the combined matrix density and the fluid density. The more fluid a formation contains; the more porous it is (Meyer and Nederlof, 1984). The density log is a good porosity indicator and it has the best vertical resolution among other porosity tools.

The neutron log and density log are sketched together in the same track for doing some comparison and the correlation between these two curves leads to better lithology identification. When both the density log, and neutron log show lower value it indicates the sandstone formation, and when the two types of logs overlay the lithology is limestone, and when the neutron and density value increases, it indicates shale. For fluid types identification a comparison of resistivity with other logs is necessary especially for identifying gas zones (Glover, 2012).

### **3.3 Logs Interpretation and Work Flow**

Identifying the lithology types, fluid types and porosity are one of the main goal of this study. For the logs interpretation the data need to be in good conditions. The hole conditions and mud types can effect on the quality of the logs and make some trouble in log reading or cause stationary reading of logs, which is not correct and lead to misinterpretation of logs. Recently, an automatic correction is applied to the logs in the field and it is double-checked by software ‘‘ Interactive Petrophysics’’ (IP).

Gamma ray, which distinguishing between the clean sandstone and clay, in combination with neutron porosity and density logs can be used for interpretation of lithology.

### 3.3.1 Shale Volume Calculation

Because shale is usually more radioactive than sand or carbonate, gamma ray log can be used to calculate volume of shale in porous reservoir. The volume of shale expressed as a decimal fraction or percentage is called *Vsh* shale gamma ray reading log (Schlumberger, 1974):

$$V_{sh} = \frac{GR_{log} - GR_{min}}{GR_{max} - GR_{min}} \quad \text{Equa. (3.1)}$$

$V_{sh}$ : Volume of Shale

$GR_{log}$ : gamma ray reading from log, API (at any depth)

$GR_{min}$ : minimum gamma ray reading API (clean sand or carbonate),

$GR_{max}$ : maximum gamma ray reading, API (Shale)

In some reservoir layers when we can see the effect of the radioactive sandstone, we switch to calculate the volume of shale from density-neutron combination (Worthington, 1985):

$$V_{sh}(nd) = \frac{\emptyset_{neutron} - \emptyset_{density}}{\emptyset_{neutron_{shale}} - \emptyset_{density_{shale}}} \quad \text{Equa. (3.2)}$$

$\emptyset_{neutron}$  = neutron porosity in the sand

$\emptyset_{neutron_{shale}}$  = neutron porosity in the adjacent shale

$\emptyset_{density}$  = density porosity in the sand

$\emptyset_{density_{shale}}$  = density porosity in the adjacent shale

### 3.3.2 Formation Water Resistivity ( $R_w$ )

The total contained water in an otherwise hydrocarbon bearing reservoir rock is best called "formation water". The measurement of resistivity of formation water is essential for accurate assessment of water saturation. Formation water resistivity ( $R_w$ ) is closely related to salinity, salinity varies both vertically and laterally across basin (North, 1985).

Formation water resistivity ( $R_w$ ) can be developed during geologic time, and its value can change in wide spread from well to another in same reservoir because the influence of salinity, temperature and contamination with fresh water and change in depositional environment (Tiab and Donaldson, 1996).

There are some methods to estimate the formation water resistivity from spontaneous potential log, or from formation water analysis in laboratory by known salinity of formation water (selected method), NaCl concentration in formation water at specific interval and temperature and using chart Gen-9 to change salinity to resistivity (Schlumberger, 1997). According to AGOCO Evaluation, the Geothermal Gradient  $1.7^\circ\text{F}/100\text{ft}$  has been accepted for the Ghadames Basin, and in the study area is about  $1.5^\circ\text{F}/100\text{ft}$  (AGOCO, 2009). The Table below (Table, 3.2) represent the depth intervals and their proposed water resistivity according to production tests in the study area.

(Table, 3.2): Average Formation Water Resistivity ( $R_w$ ) through depth intervals in the study area.

Depth (ft)	Salinity (ppm)	Temperature (F)	$R_w$ (ohm-m)
7800-8000	132,000 - 172,000	150-153	0.024 - 0.023
8000-8200	172,000 - 200,000	153-156	0.022 - 0.021
8200-8400	200,000 - 237,000	156-159	0.021 - 0.02
8400-8600	237,000 - 250,000	159-162	0.02 - 0.019
8600-8800	250,000 - 260,000	162-165	0.019 - 0.018
8800-9000	260,000 - 270,000	165-168	0.018 - 0.017
9000-9200	270,000 - 280,000	168-171	0.017 - 0.016

### 3.3.3 Neutron-Density Combination

Both the neutron and the density logs should be show the same formation parameters- porosity. Plotted on compatible porosity scales, they should give identical values and it should be possible to superimpose the two logs. The explanations can be taken in two stages. Firstly, the scales of the two logs are made compatible (normally) on clean limestone scale. A neutron log value of zero (no porosity, 100% matrix) corresponds to a bulk density of  $2.71 \text{ gm}/\text{cm}^3$ , and so on to neutron value of 100% fluid and a density of  $1.0 \text{ gm}/\text{cm}^3$ . A cross plot of density log values against neutron log values will show a straight-line relationship, a point on the line corresponding to a particular porosity. (Rider, 1996).

### 3.3.4 Neutron-Density Cross Plot

There are three lithology lines displayed on the cross plot, sandstone (silica), limestone (calcite) and dolostone (dolomite), the lithology lines are marked with porosity values usually in percent.

The log values for a particular interval or depth are plotted on the cross plot to create a point and the location of the point with respect to the lithology lines is an indication of the lithology and porosity of the points.

If the point fall directly on the lithology line, the lithology of the point corresponds to the lithology of the line and the porosity of the point corresponds to the porosity of the line at that location, when the point falls between two lines it assumed to be a lithological mixture of these two lines that contain a greater percentage of the mineral of the line to which it is closer (Krygowski, 2003).

### 3.3.5 Total Porosity ( $\emptyset$ ) and effective porosity ( $\emptyset_e$ )

Porosities in the reservoir rocks usually range from 8 % to 28 % depending of the arrangement (cubic or rhombohedral), size and sorting of the rock. In general, porosities tend to be lower in deeper and older (consolidated) formations, due to cementation and overburden pressure stress on the rock. Likewise, the porosity of shale decreases rapidly with depth than sand (Rider, 1996). There are many descriptions of porosity, but the two common are the total and the effective porosity.

Total porosity can be estimated from a single log (sonic, density and neutron) or the combination of two logs (neutron – density), while effective porosity involves subtraction between total porosity and volume of shale, and it can be simplified by the equation below:

$$\emptyset_e = \emptyset_t * (1 - V_{sh}) * 100 \quad \text{Equa. (3.3)}$$

$\emptyset_e$  = Effective Porosity

$\emptyset_t$  = Total Porosity

$V_{sh}$  = Volume of Shale

### 3.3.6 Water saturation (Sw)

Shales have moderately low resistivities, as can be seen on any resistivity log and their presence as a component of shaly sandstones introduces a conductivity contribution that should be included together with the conductivity of the pore formation water in detailed reservoir analysis. As a general statement, if uncorrected resistivities are used in a conventional clean reservoir calculation of a shaly sand zone, the result will be an overestimation of water saturation, since the resistivities have been reduced below their true values by the conductivity of the shale component. Different methods can be used to evaluate the water saturation of a reservoir formation:

- I. The Archie method that involves clean sandstone formations.
- II. The shaly sand method comprising the resistivity approach (Simandoux model, Poupon and Leveaux model, Schlumberger model, Indonesian model) and the conductivity approach (Waxman-smith model, Dual-water model, Juhasz model).

Archie (1942) developed an equation resulting from his experiment on voids saturation. He found that water saturation of the rocks could be related to their resistivity. The formula showed that increasing porosity will reduce the water saturation for the same resistivity in a clean (homogenous) formation.

Simandoux (1963) developed adequate equations for shaly (heterogeneous) formations with relative simplicity and limited demand comparing to other methods, as well as it was generally found to give reasonable estimates of water saturation in reservoir with higher salinity formation water (Doveton, 2014), as in Lower Acacus reservoir. This gives the privilege of using Simandoux equation in this study:

$$\frac{1}{R_t} = \frac{\Phi^m S_w^n}{a R_w} + \frac{V_{sh} S_w}{R_{sh}} \quad \text{Equa. (3.4)}$$

Where:

SW = Water Saturation

a = Tortuosity factor

m = Cementation factor

n = Saturation exponent

$\Phi$  = Porosity of the formation

Rt = Deep resistivity of the formation

Rsh = Resistivity of a shale unit

### 3.4 Petrophysical Interpretation

Petrophysical interpretation was performed for 5 wells drilled in Block-114 using Interactive Petrophysics. Environmental corrections were applied on all logs, to compensate for the effect of mud and borehole size. Production Tests (PT) results were integrated in the final petrophysical interpretation.

The following are the main outcomes and recommendations from petrophysical analysis:

- All available data were integrated to evaluate the lithology, saturation, and porosity profiles of the Lower Acacus reservoir.
- Potential oil intervals were detected as per resistivity and porosity profiles and were confirmed with test results.
- For each well, the average net reservoir and net pay petrophysical properties of the zones were generated.
- Due to no special core analysis, the default saturation equation parameters for tortuosity, cementation factor was taken as 2. This assumption implies some uncertainty regarding the saturation results. To reduce this uncertainty, special core analysis of “ $m$   $n$  &  $a$ ” would be needed.
- Pay zones that produce low resistivity or low contrast log responses are influenced by a variety of factors associated with mineralogy (Iron rich minerals), water salinity, and microporosity, clay distribution as well as bed thickness (Darling and Sneider, 1992). Probably the most common cause of low resistivity pay is the simple combination of thin beds containing highly conductive clay (and their associated bound water), along with thin pay sands which are below the vertical resolution of the logging tool. It is recommended to acquire Nuclear Magnetic Resonance log (NMR) on core sample in these kinds of sand.

Lower Acacus Member is a low resistivity reservoir, in which it is very difficult to obtain reliable saturations measurement during petrophysical interpretation. After detailed integration of petrophysical interpretation and test results it was decided that the saturation estimation from petrophysical interpretation have to be modified using

the PT results; (ex. if petrophysical interpretations show high water saturation and PT produced oil, then this zone was considered to be oil bearing and vice versa).

### 3.4.1 Net reservoir and Netpay Cutoffs

Since the production tests are available, some approximations were made to establish the final cutoffs and the resulted net reservoir and pays were compared with the test results (Table, 3.3).

Net reservoir was established to determine the best clean and porous interval, while net pay is for determining the hydrocarbon zones.

(Table, 3.3): The selected net reservoir and net pay cut-offs

<b>Net Reservoir</b>	<b>Porosity</b>	<b>Volume of clay</b>	<b>Water Saturation</b>
L. Acacus	>10%	<35%	-

<b>Net Pay</b>	<b>Porosity</b>	<b>Volume of clay</b>	<b>Water Saturation</b>
L. Acacus	>10%	<35%	<50%

The Gross, net-to-gross, average net reservoir and net pay, porosity, volume of clay and Water Saturations, are all summarized for every well in the study area.

### 3.5 Petrophysical Evaluation of M1-114

An Interactive Petrophysical evaluation was performed to evaluate the formations and rock properties in terms of accurate lithology, water saturation and effective porosity for well M1-114, which is located in center of the study area. Open hole log data of the interval from 7745 to 8776 ft MD that comprises of intercalation of sand and shale sequence of Silurian Lower Acacus reservoir are used for this purpose. The lithology of this formation is dominated by a clean to shaly sandstone interbedded with shale and siltstone beds. The presences of clays and conductive minerals in the sand units, along with the high value of the irreducible water saturation, make confusing in the hydrocarbon evaluation due to the effect of those materials on the resistivity measurements. Low Resistivity Pay (LRP) is very remarkable of Lower Acacus reservoir in Ghadames Basin and it is a tremendous challenge to be discussed and worked out. However, this issue is not going to be a part of this study, and any resistivity derived RW value would be unreliable for petrophysical evaluation. Furthermore, by considering the field knowledge and production tests, RW is best estimated from formation water as in (Table, 3.4) and all computation will be calibrated to fit the test result.

(Table, 3.4): Production test summary of M1-114 well.

Depth (ft)	M1-114
7780-7800	Oil & Gas (PT#4)
7920-7930 7954-7964	Oil & Gas (PT#5)
8172-8180 8152-8158 8134-8140	water (CH DST#13) 160,000 ppm (RW=0.025 ohm-m)
8286-8294 8272-8278 8252-8258	water (CH DST#12) 252,000 ppm (RW=0.019 ohm-m)
8480-8494	water (CH DST#11) 270,000 ppm (RW=0.017 ohm-m)
8710-8724	Oil & Gas (PT#3)
8542-8556	Oil & Gas (PT#2)



The petrophysical interpretations (effective porosity “Phie”, volume of shale “Vcl” and water saturation “Sw”) of Lower Acacus reservoir show several units could be considered as interesting reservoirs, three main units (A, B, & C) with various thicknesses and different reservoir characteristic were observed (Fig. 3.1).

### **3.5.1 Unit A**

This unit occupies the bottom section of the studied reservoir, which is characterized by a sandstone-dominated succession overlaying the deep marine Tanezzuft shale. The gross thickness of this unit ranges from 309 ft in the southeast (Y1-114) to 485 ft toward the north (Z1-114) among the study area. The unit has the cleanest, thickest and the most porous sandstone interval thorough the reservoir as it is shown in the log and cross plot of M1-114 well (Fig. 3.2 &3.3).

### **3.5.2 Unit B**

This unit placed in the middle part of the reservoir and it indicates a deeper sediment succession in which the sand-shale interbedded is very pronounced. In similar pattern, the thickness increase toward the north-northwest from 642 ft in X1-114 to 599 ft in Z1-114 and 562 ft in M1-114. The gross thickness of Unit B represents the thickest sequences among the study area, and the log and cross plot of in this unit in M1-114 well are showing that (Fig. 3.4 &3.5).

### **3.5.3 Unit C**

This is the thinnest unit among the studied wells that is ranging in thickness from 70 to 100 increasingly toward the north. It marks the top of the studied reservoir, which is actually distinctive by sandstone layers usually saturated with hydrocarbon and superimposed by Middle Acacus marine shale that represents a good cap of this unit.

In M1-114 Unit C has good porosity value and it is composed of shale and sandstone interbedding (Fig. 3.6 &3.7). The density-neutron cross plots display the main lithology and average porosity of every unit along with mineral identification cross plots between thorium-potassium. These plots show that the dominant clay type is mixed clay layers with two or more components probably due to chemical alteration via weathering reaction or diagenesis. As it is shown in the cross plot show there could be some contributions of chlorite and montmorillonite in the reservoir intervals. The chlorite-

bearing reservoir sandstones are deposited in specific settings, namely in the transitional environments, where mixing between Fe-rich fresh waters and marine waters occurs (Arduini et al., 2003). The mentioned author referred to Fe-chlorite coating as the most affected diagenetic feature in Lower Acacus reservoir as it has preserved the primary porosity by preventing the precipitation of occlusive cements, and it could be one of the reasons behind the low resistivity pay in the reservoir. Montmorillonite on the other hand is a well-known member of the Smectite family of swelling clay minerals, and it probably represents the shale intervals. When this clay imbibes fresh water, it swells to several times its original (dry) volume and retains a good deal of water between layers in its mineral structure. This change in volume can cause montmorillonite clays to dislodge and migrate within the pore system, thus resulting in plugged pore throats (McHardy et al., 1982). This simply reveal the complexity of the Lower Acacus reservoir.

The results of the petrophysical parameters of these sand units are summarized in the table below (Table, 3.5). In this well all the unit have hydrocarbon accumulations with total net pay 115 ft, from which Unit C only has 22 ft, with average porosity 14% and SW 24.7%. Unit B in the middle has the best porosity value 18%, SW 29%, and net pay 48 ft. Unit A has the thickest sandstone reservoir intervals with average porosity (17%), water saturation 32% and net pay 45 ft.

(Table, 3.5): Reservoir and Pay summary of well M1-114.

#### Reservoir Summary

Unit Name	Top	Bottom	Gross	Net	N/G	Av Phi	Av Sw	Av Vcl
Unit C	7745	7840	95	22	0.232	0.14	0.25	0.175
Unit B	7840	8402	562	124	0.221	0.19	0.51	0.22
Unit A	8402	8776	374	208	0.556	0.19	0.63	0.21
All Units	7745	8776	1036	378	0.343	0.188	0.57	0.21

#### Pay Summary

Unit Name	Top	Bottom	Gross	Net	N/G	Av Phi	Av Sw	Av Vcl
Unit C	7745	7840	95	22	0.232	0.14	0.247	0.174
Unit B	7840	8402	562	48	0.085	0.183	0.287	0.206
Unit A	8402	8776	374	45	0.12	0.173	0.317	0.262
All Units	7745	8776	1036	115	0.112	0.171	0.293	0.222

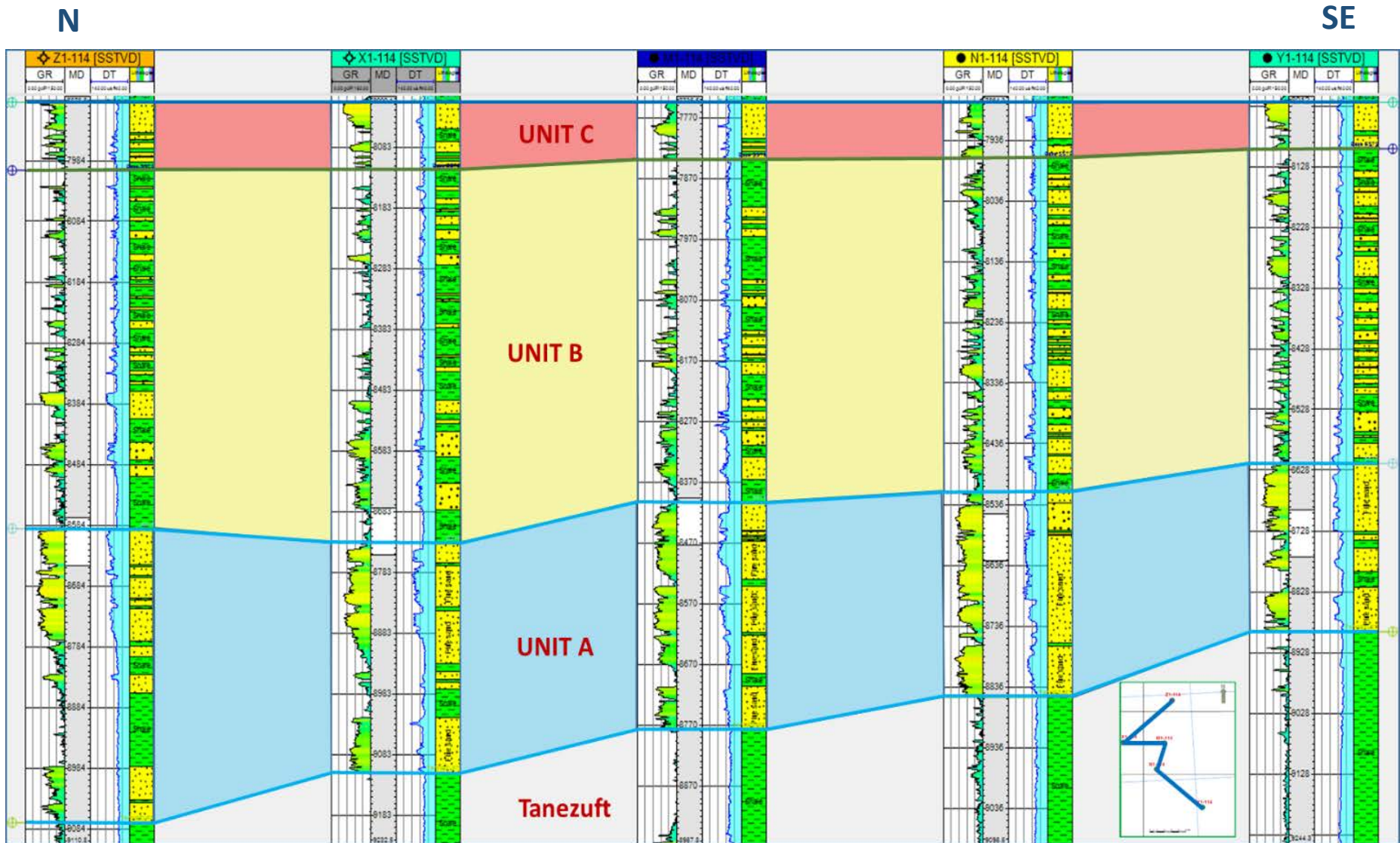


(Fig. 3.1): Stratigraphic cross section among the studied wells showing the three units (A, B, & C). Top of L. Acacus is used as a datum.

### 3.5.4 Presentation of Plot Results

The final deliveries include the plot integrating the open hole logs with the computed saturations and minerals volumes. Below is the IP\* (Interactive Petrophysics) plot presentation summary track.

order from left to right:

Track # 01: Measured Depth and vertical scale in feet.

Track # 02: Caliper, and GR.

Track # 03: DT, RHOZ and NPHI.

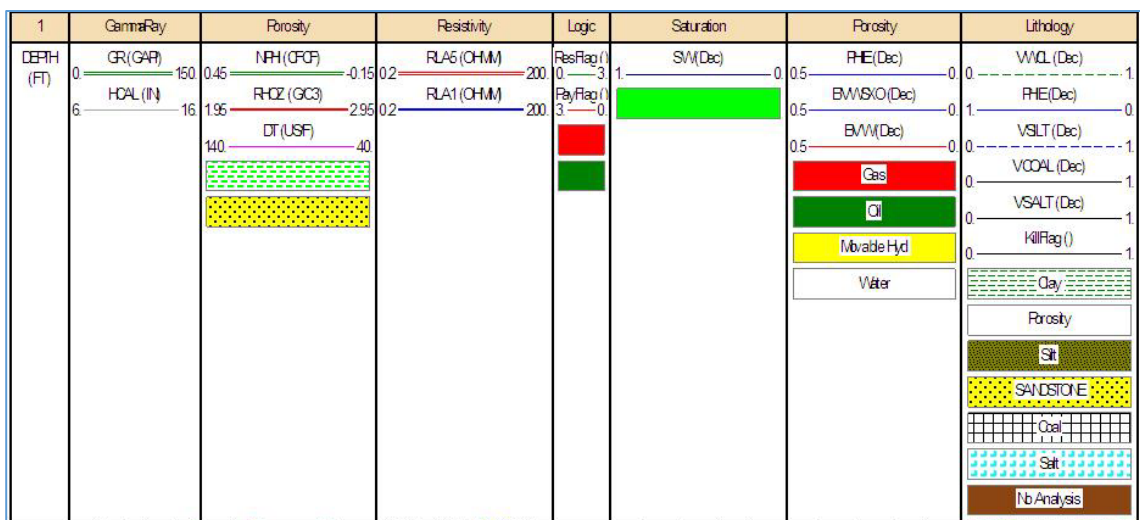
Track # 04: Deep and shallow resistivity logs.

Track # 05: Net reservoir Area in green and net Pay in red.

Track # 06: Water Saturation (SW).

Track # 07: IP\* fluids volume of Oil, Gas, water, and Effective Porosity.

Track # 08: IP\* mineralogy Quartz in yellow, Silt in dark green and Shale in Green.



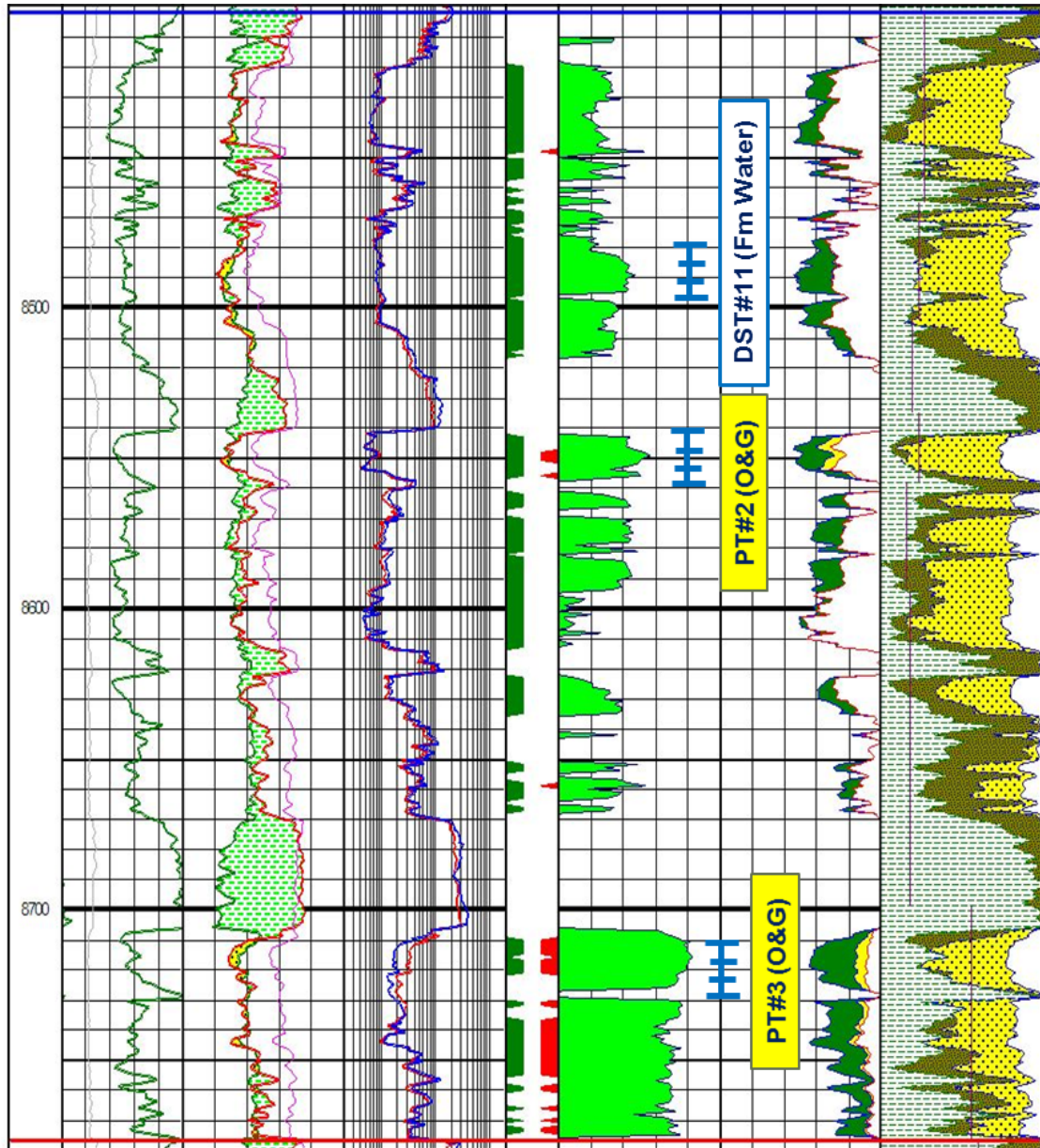


(Fig. 3.2): Lithologic/Petrophysical panel of hydrocarbon bearing sandstone reservoir of unit A in Well M1-114.

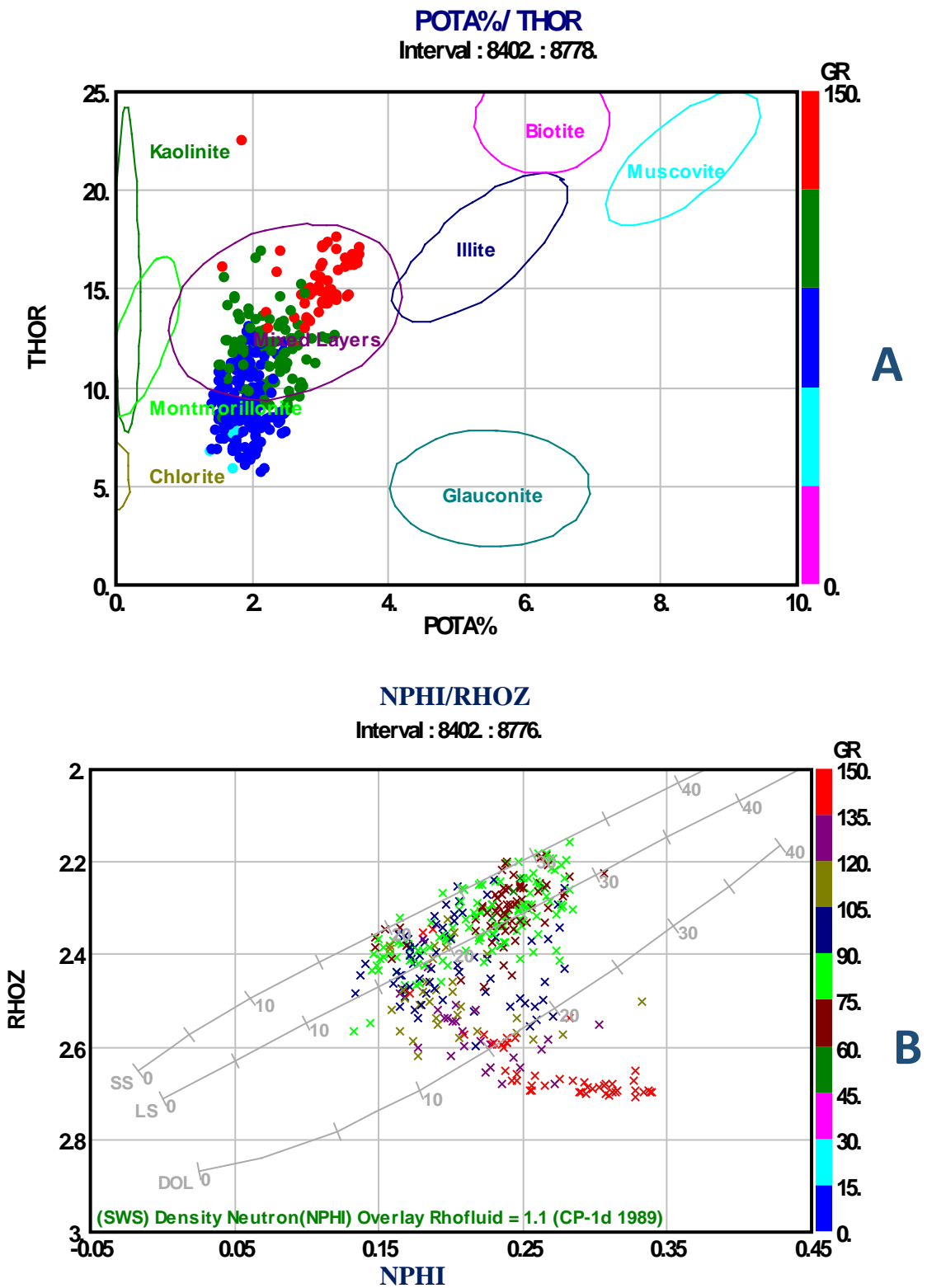


(Fig. 3.3): Unit A in M1-114 (A) POTA-THOR cross plot showing that mixed layers clays are the dominant type in the reservoir with some kind of trend from the chlorite. (B) Density-Neutron cross plot showing that this unit is mainly composed of clean sand stone unit with a very good porosity.

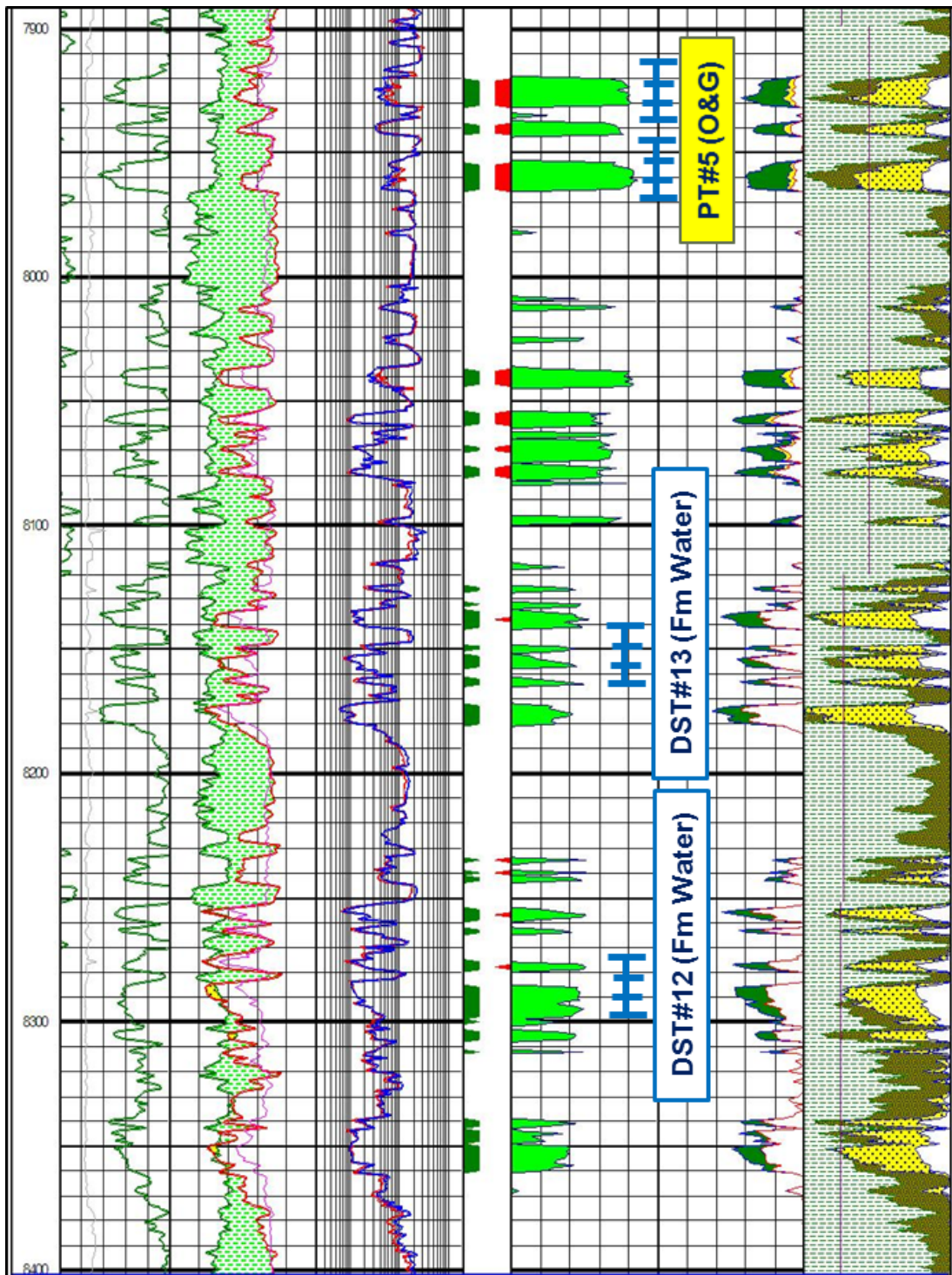


(Fig. 3.4): Lithologic/Petrophysical panel of hydrocarbon bearing sandstone reservoir of unit B in Well M1-114.

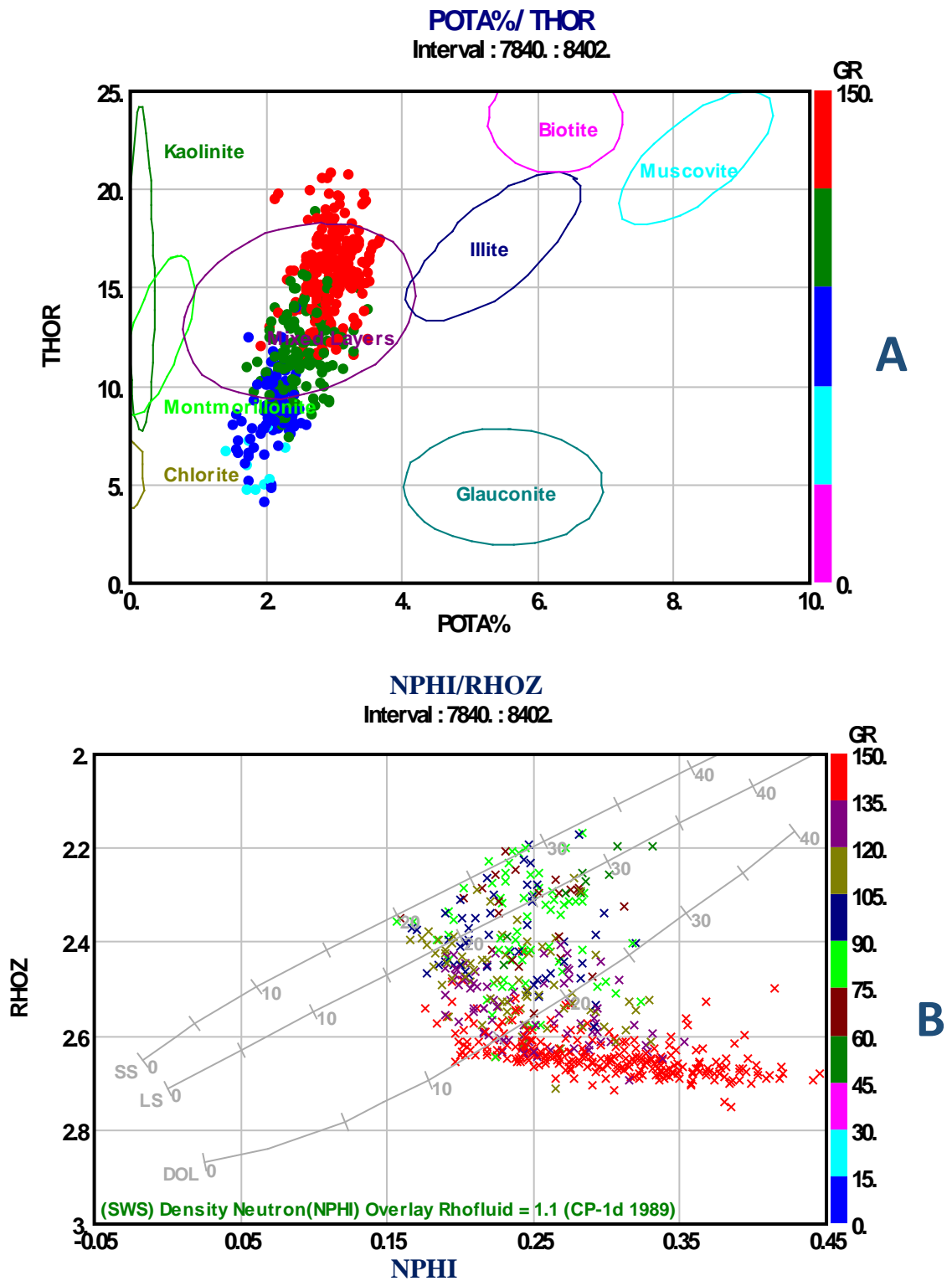


(Fig. 3.5): Unit B in M1-114 (A) POTA-THOR cross plot showing that mixed layers clays are the dominant type in the reservoir with some kind of trend from the chlorite. (B) Density-Neutron cross plot showing that this unit is mainly composed of interbedded of sand and shale with good porosity of the sand reservoir.



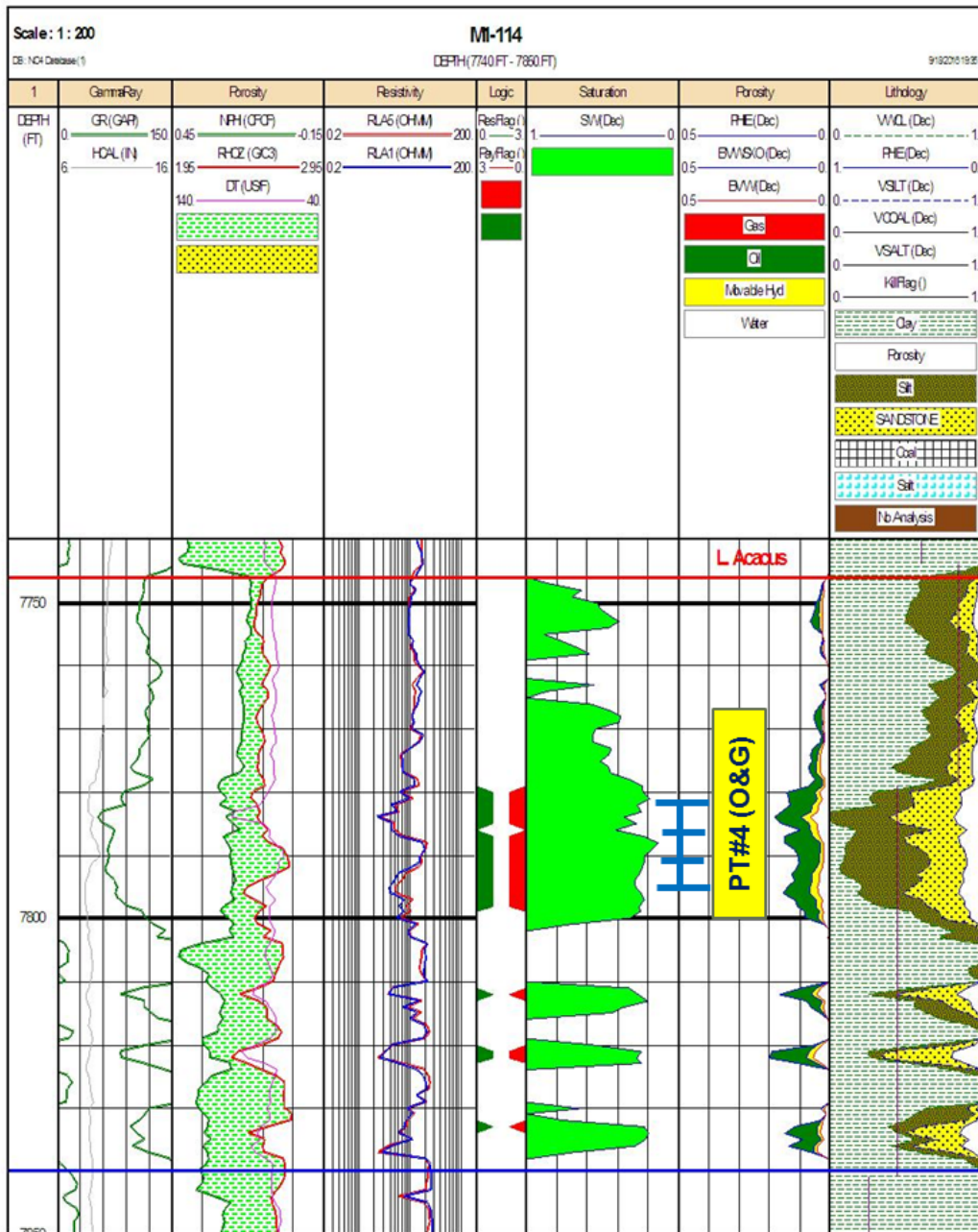


(Fig. 3.6): Lithologic/Petrophysical panel of hydrocarbon bearing sandstone reservoir of unit C in Well M1-114.

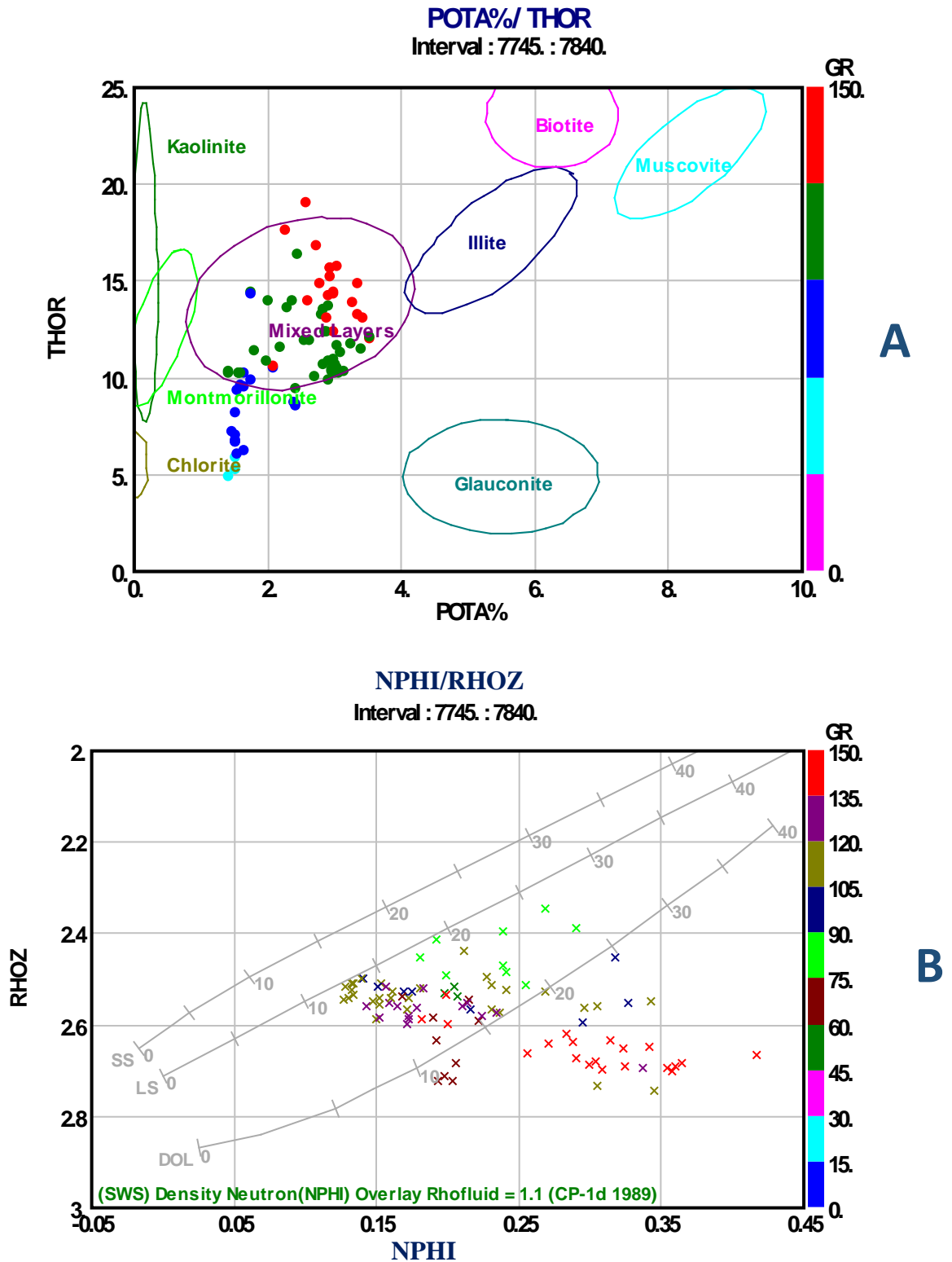


(Fig. 3.7): Unit C in M1-114 (A) POTA-THOR cross plot showing that mixed layers clays are the dominant type in the reservoir with some kind of trend from the chlorite. (B) Density-Neutron cross plot showing that this unit is mainly composed of interbedded of sand and shale with good porosity of the sand reservoir.

### 3.6 Petrophysical Evaluation of N1-114

N1-114 is located to south of M1-114, in which Lower Acacus reservoir covers an interval of around 1000 ft (7873-8852) and the analysis will be based on the result of production test as summarized in (Table, 3.6). All production tests produced oil and gas in this well indicating a very good hydrocarbon accumulation. The petrophysical results shows that this well has the best hydrocarbon accumulation through all zones with total net pay 160 ft, and total net reservoir 417 ft. This well represent one of the most successful wells in the Ghadames Basin with total oil production more than 10,000 BBL/D and around 8.5 MMSCF/D of gas at ½ inch choke size.

(Table, 3.6): Production Test summary of N1-114 well.

<b>Depth (ft)</b>	<b>N1-114</b>
7900-7908 7919-7924	Oil & Gas (PT# 8)
7949-7960	Oil & Gas (PT# 7)
8048-8056 8006-8012 8018-8026	Oil & Gas (PT# 6)
8158-8165 8246-8252	Oil & Gas (PT# 5)
8348-8356 8388-8394	Oil & Gas (PT#4)
8515-8519 8531-8542	Oil & Gas (PT#3)
8748-8754 8768-8775	Oil & Gas (PT#2)

Unit C at the very top has a good reservoir characterization, which mainly composed of sandstone with total net reservoir 27.5 ft (Fig. 3.8 &3.9). This unit has a good average porosity 16.5%, water saturation 33%, and net pay 24 ft. In this well Unit B is has a thick reservoir interval around 140 ft which is clean (Vsh 23%), porous 17%, and very productive with accumulative net pay around 100 ft (Fig. 3.10 &3.11). Unit A has the thickest reservoir sand unit with around 250 ft net reservoir, but only 35 ft net pay at the top of this unit is hydrocarbon saturated intervals (SW 40%) with very good porosity 18% and Vsh 22% (Fig. 3.12 &3.13). A noticeable radioactive sandstone interval at the top of Unit A (8530-8540) has been recognized in this well, the volume of shale in this

unit has been calculated from Density-Neutron method to better evaluate this interval especially it is a hydrocarbon bearing interval (PT#3).

The results of the petrophysical parameters of these sand units are summarized in the table below (Table, 3.7).

(Table, 3.7): Reservoir and Pay summary of well N1-114.

#### Reservoir Summary

Unit Name	Top	Bottom	Gross	Net	N/G	Av Phi	Av Sw	Av Vcl
Unit C	7873	7965	92	27.5	0.299	0.163	0.35	0.199
Unit B	7965	8514	549	140	0.255	0.169	0.437	0.224
Unit A	8514	8852	338	250	0.74	0.202	0.717	0.169
All Units	7873	8852	979	417.5	0.426	0.189	0.612	0.19

#### Pay Summary

Unit Name	Top	Bottom	Gross	Net	N/G	Av Phi	Av Sw	Av Vcl
Unit C	7873	7965	92	24	0.261	0.166	0.328	0.207
Unit B	7965	8514	549	101	0.184	0.168	0.376	0.228
Unit A	8514	8852	338	35	0.104	0.181	0.396	0.221
All Units	7873	8852	979	160	0.163	0.17	0.374	0.223

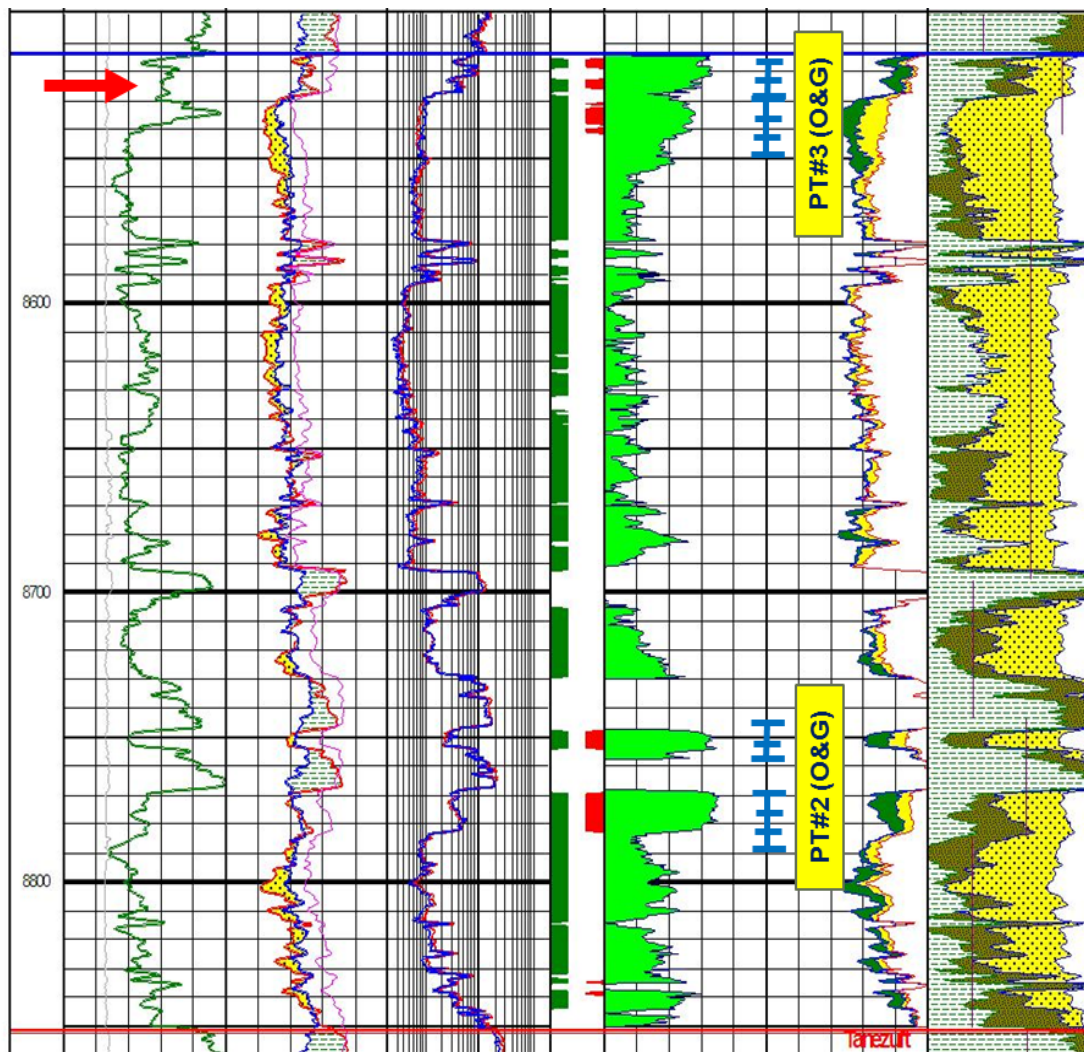


(Fig. 3.8): Lithologic/Petrophysical panel of hydrocarbon bearing sandstone reservoir of unit A in Well N1-114.

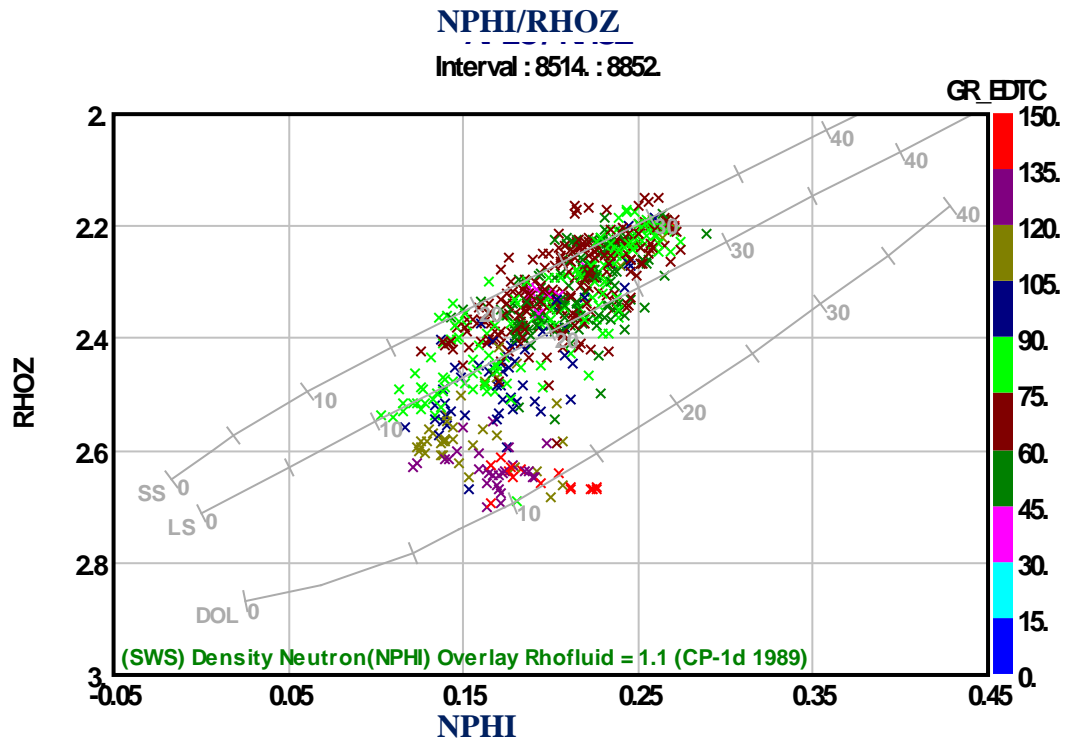


(Fig. 3.9): N1-114 Density-Neutron cross plot of Unit A showing that this unit is mainly composed of clean sand stone unit with a very good porosity.

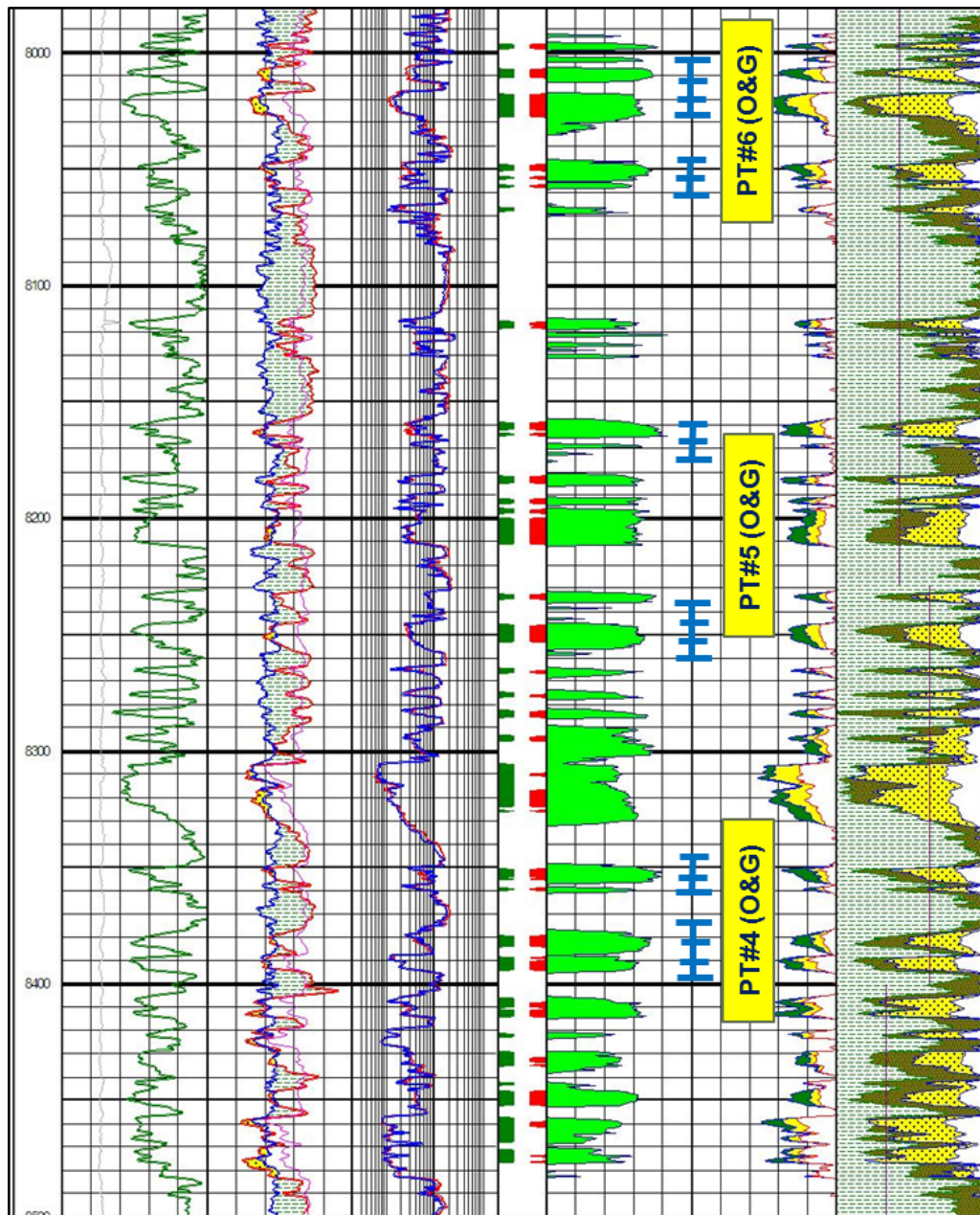


(Fig. 3.10): Lithologic/Petrophysical panel of hydrocarbon bearing sandstone reservoir of unit B in Well N1-114.

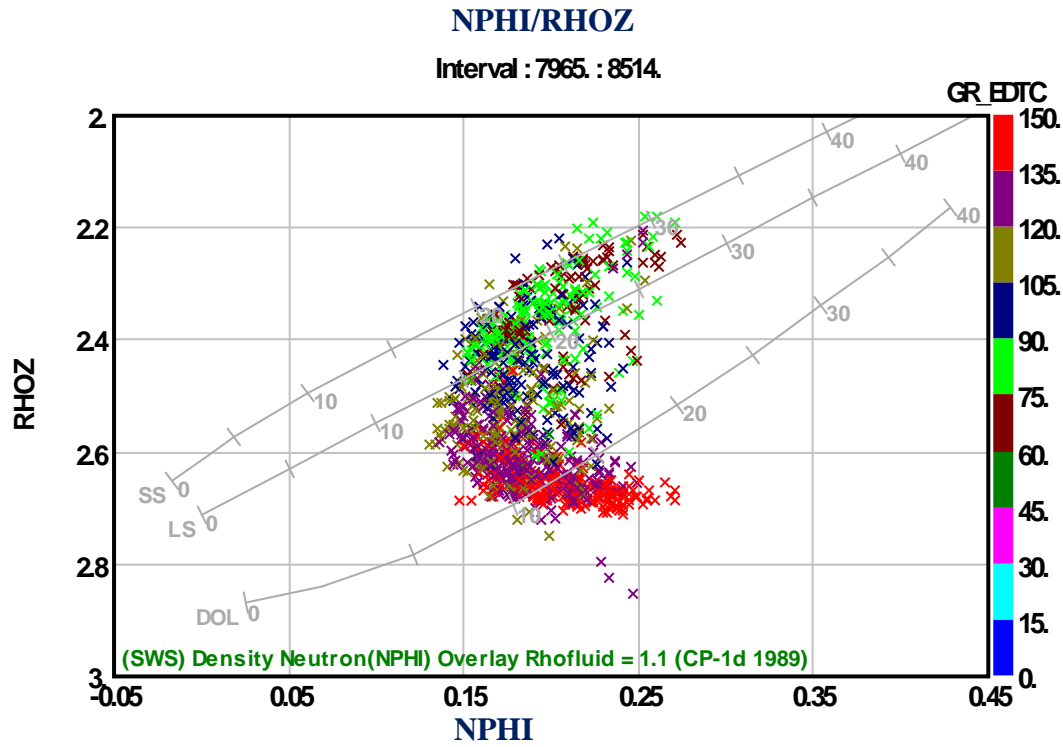


(Fig. 3.11): N1-114 Density-Neutron cross plot of Unit B showing that this unit composed of interbedded of sand and shale with good porosity of the sand reservoir.



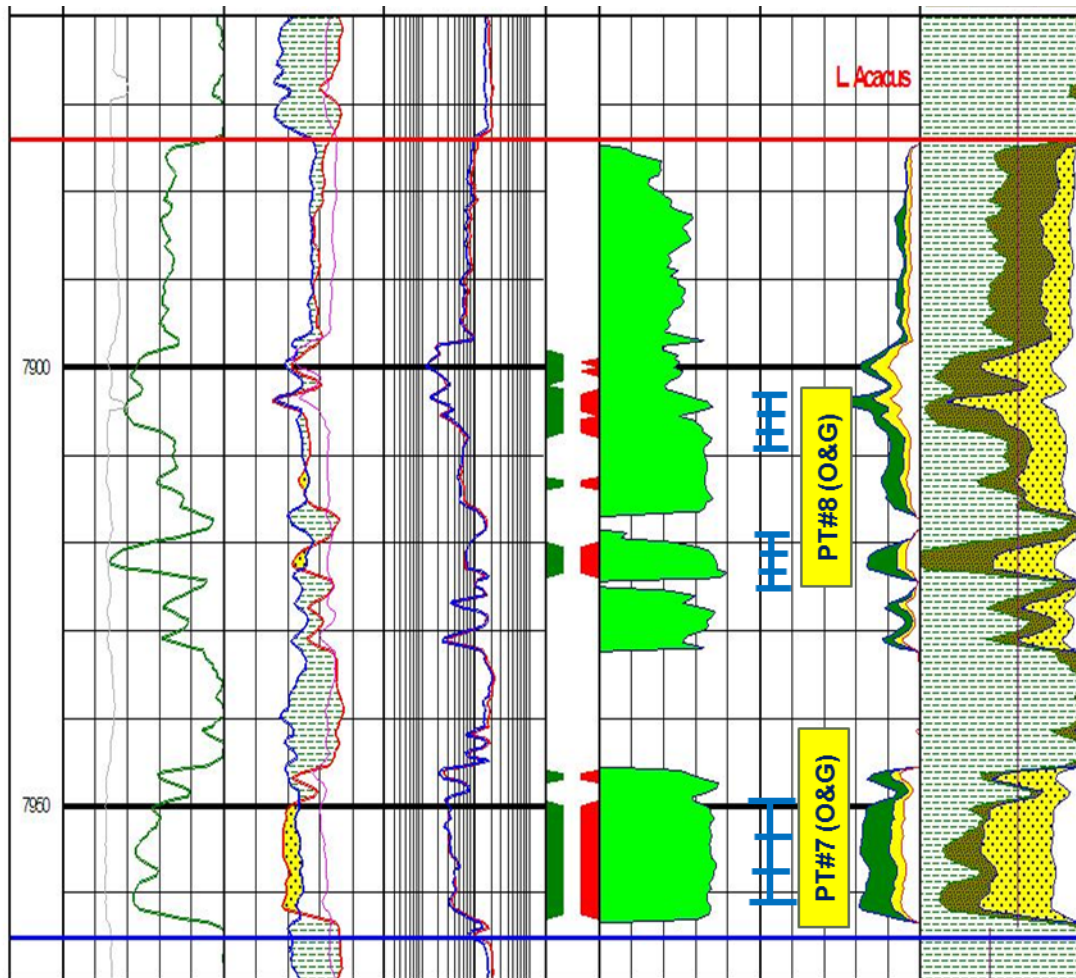


(Fig. 3.12): Lithologic/Petrophysical panel of hydrocarbon bearing sandstone reservoir of unit C in Well N1-114.

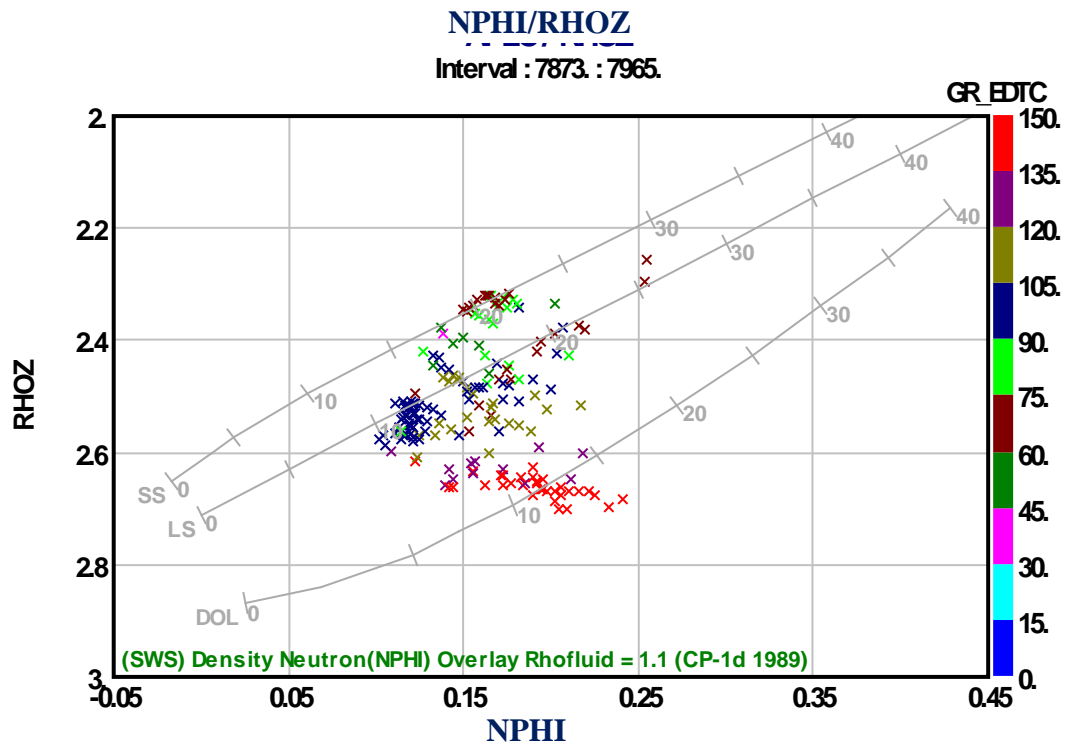


(Fig. 3.13): N1-114 Density-Neutron cross plot of Unit C showing that this unit composed of sandstone

### 3.7 Petrophysical Evaluation of X1-114

X1-114 is located to west of M1-114, in which Lower Acacus reservoir covers an interval of around 1100 ft (8009-9113) and the analysis will be based on the result of production test as summarized in (Table, 3.8). All the test results show that the formation water salinity is high indicating RW ranging from (0.02-0.016 ohm-m). The petrophysical results shows that this well has no hydrocarbon accumulation and it is classified as a dry well. The increase in shale layers is very remarkable with total net reservoir about 281 ft, which is less than other wells in the area. This suggest that Lower Acacus in this well could be deposited in deeper settings.

(Table, 3.8): Production Test summary of X1-114 well.

<b>Depth (ft)</b>	<b>X1-114</b>
8011-8028	water (PT#10) 237,000 (RW=0.02 ohm-m)
8078-8089	water (PT#9) 237,000 (RW=0.019 ohm-m)
8501-8515	water (PT#8) 270,000 (RW=0.018 ohm-m)
8564-8575	water (PT#7) 270,000 (RW=0.018 ohm-m)
8746-8760	water (PT#6) 270,000 (RW=0.017 ohm-m)
9022-9037	water (PT#5) no measurement
9072-9082	water (PT#4) 280,000 (RW=0.016 ohm-m)

Unit C at the very top is tested water, although it has a good reservoir characterization (Fig. 3.14 &3.15) with average porosity 15.5%, Vsh 20%, and 48 net reservoir. Unit B has Volume of shale 26% which is relatively high comparing to the offset wells, porosity 16%, and net reservoir 80 ft (Fig. 3.16 &3.17). Unit A has the thickest reservoir sand unit which is around 153ft net reservoir, water saturation is very high (SW 85%) with very good porosity 18% and Vsh 20% (Fig. 3.18 &3.19). The results of the petrophysical parameters of these sand units are summarized in the table below (Table, 3.9).

(Table, 3.9): Reservoir and Pay summary of well X1-114.

Reservoir Summary

Unit Name	Top	Bottom	Gross	Net	N/G	Av Phi	Av Sw	Av Vcl
Unit C	8009	8092	83	48	0.578	0.156	0.786	0.203
Unit B	8092	8734	642	80	0.125	0.161	0.773	0.263
Unit A	8734	9113	379	153	0.404	0.2	0.854	0.205
All Units	8009	9113	1104	281	0.255	0.181	0.823	0.221

Pay Summary

Unit Name	Top	Bottom	Gross	Net	N/G	Av Phi	Av Sw	Av Vcl
Unit C	8009	8092	83	0	0	---	---	---
Unit B	8092	8734	642	0	0	---	---	---
Unit A	8734	9113	379	0	0	---	---	---
All Units	8009	9113	1104	0	0	---	---	---

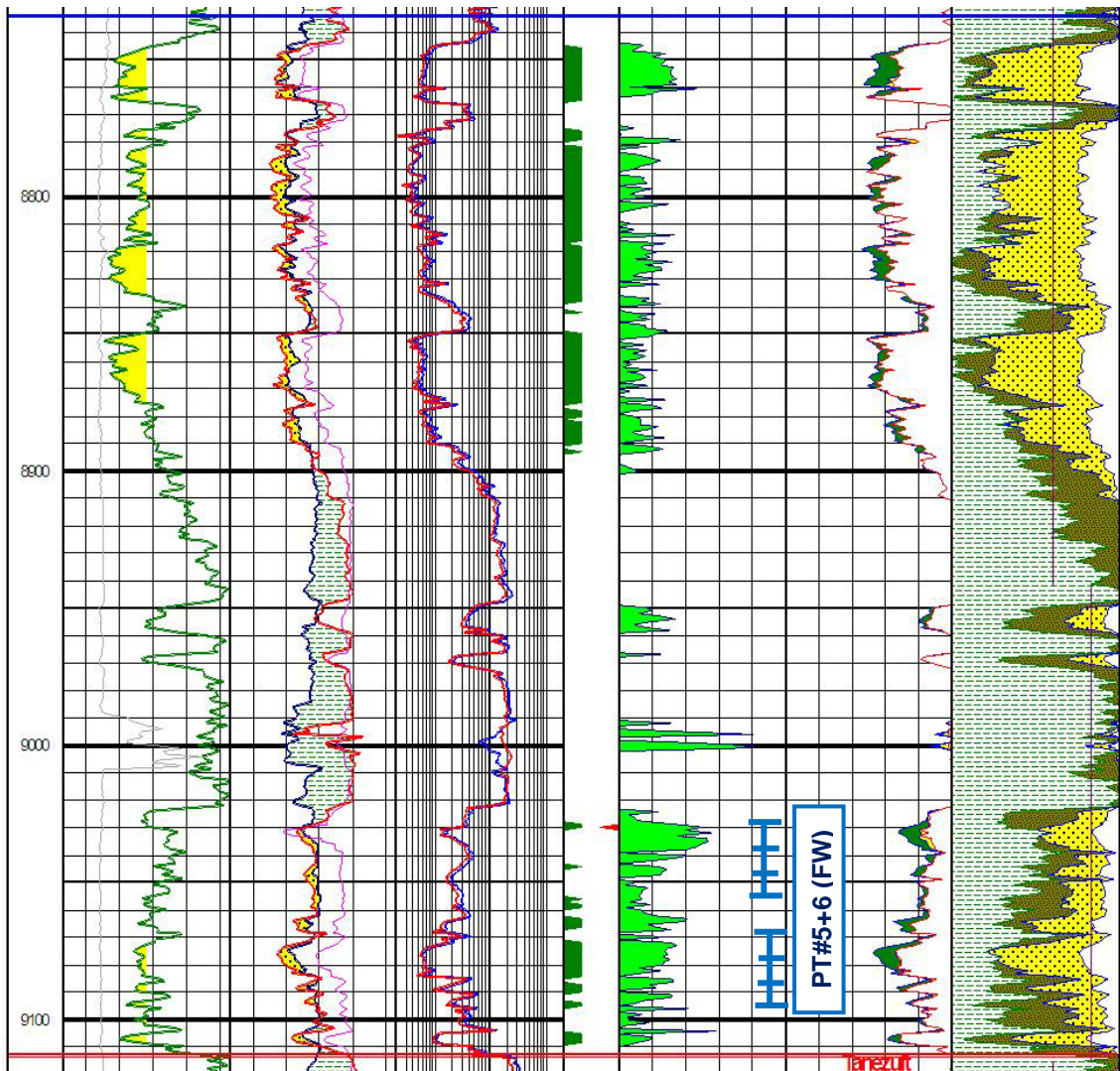


(Fig. 3.14): Lithologic/Petrophysical panel of hydrocarbon bearing sandstone reservoir of unit A in Well X1-114.

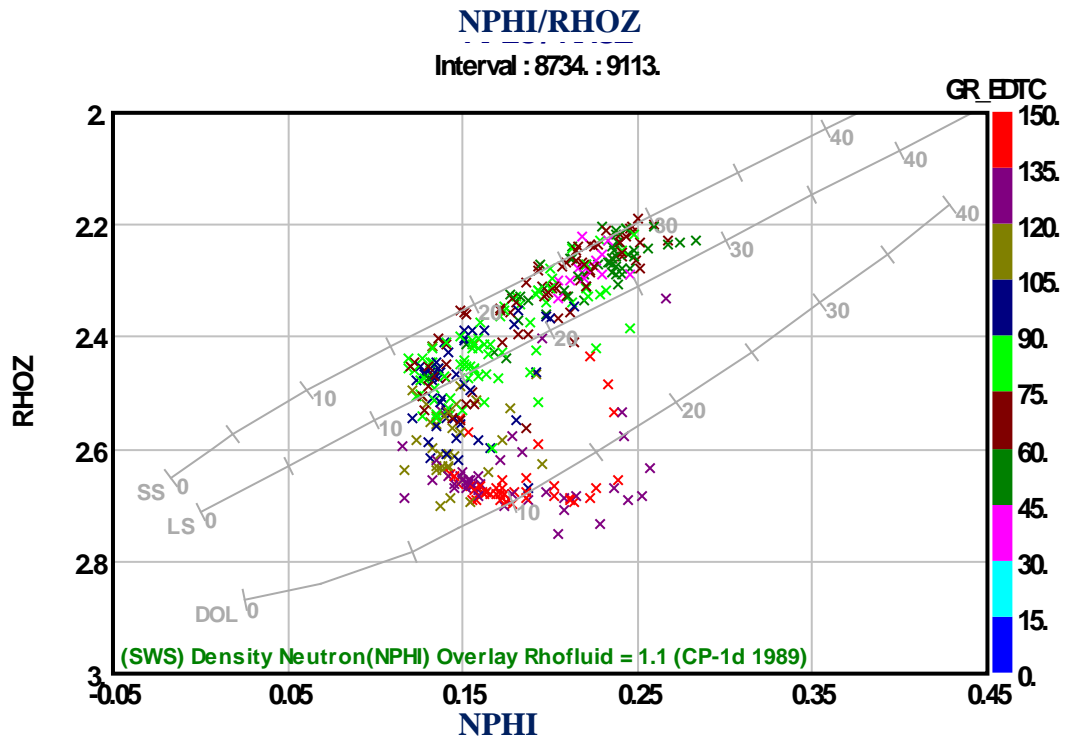


(Fig. 3.15): X1-114 Density-Neutron cross plot of Unit A showing that this unit is mainly composed of clean sand stone unit with a very good porosity.

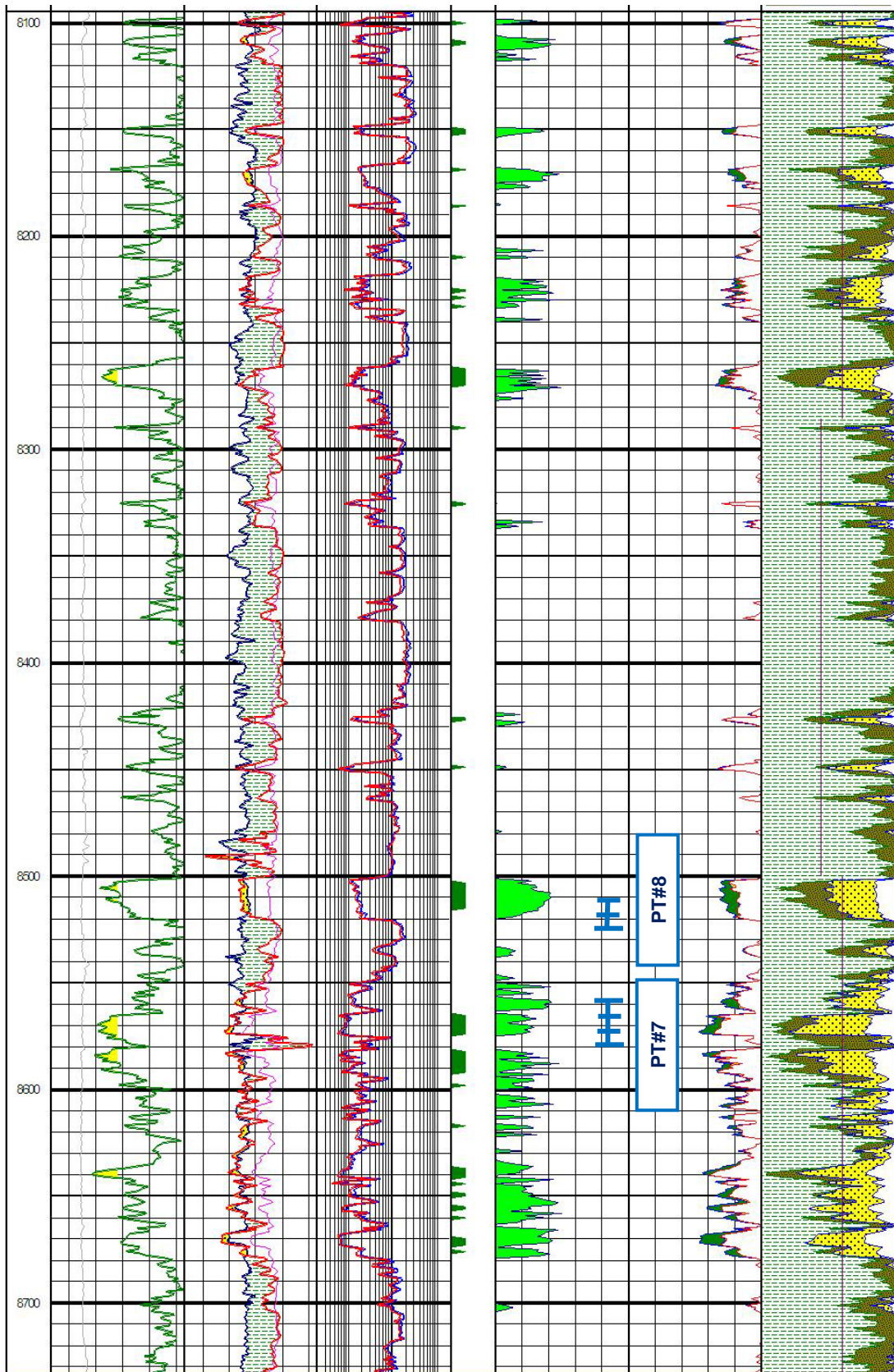


(Fig. 3.16): Lithologic/Petrophysical panel of hydrocarbon bearing sandstone reservoir of unit B in Well X1-114.

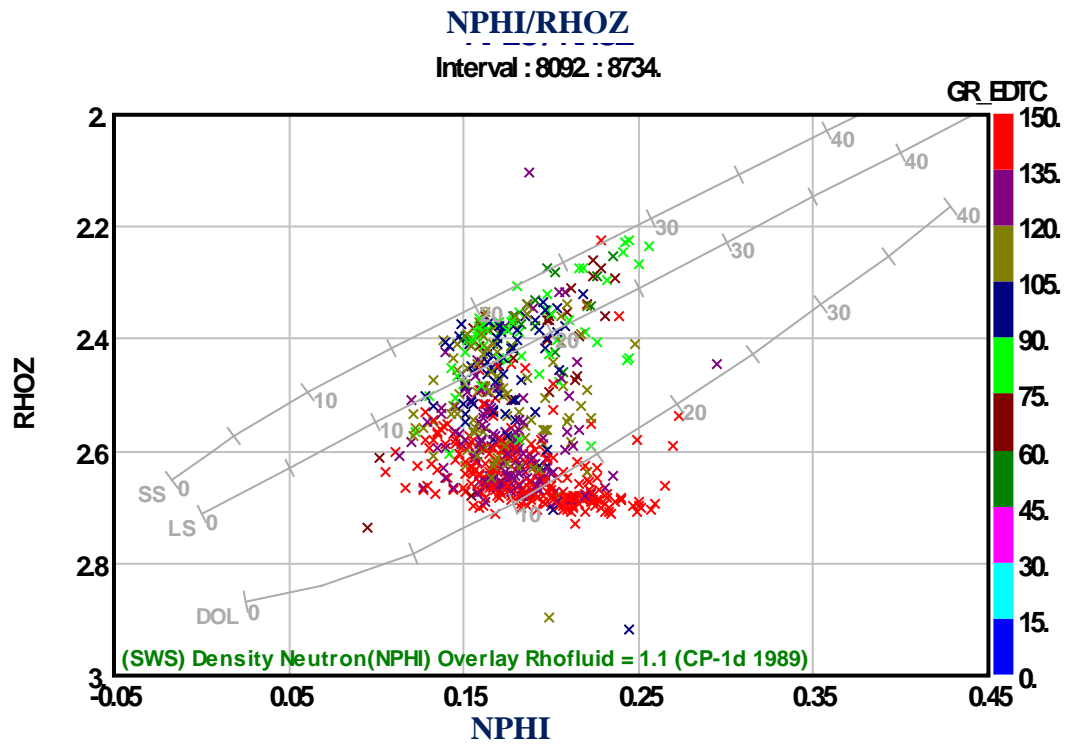


(Fig. 3.17): X1-114 Density-Neutron cross plot of Unit B showing that this unit composed of interbedded of sand and shale with good porosity of the sand reservoir.

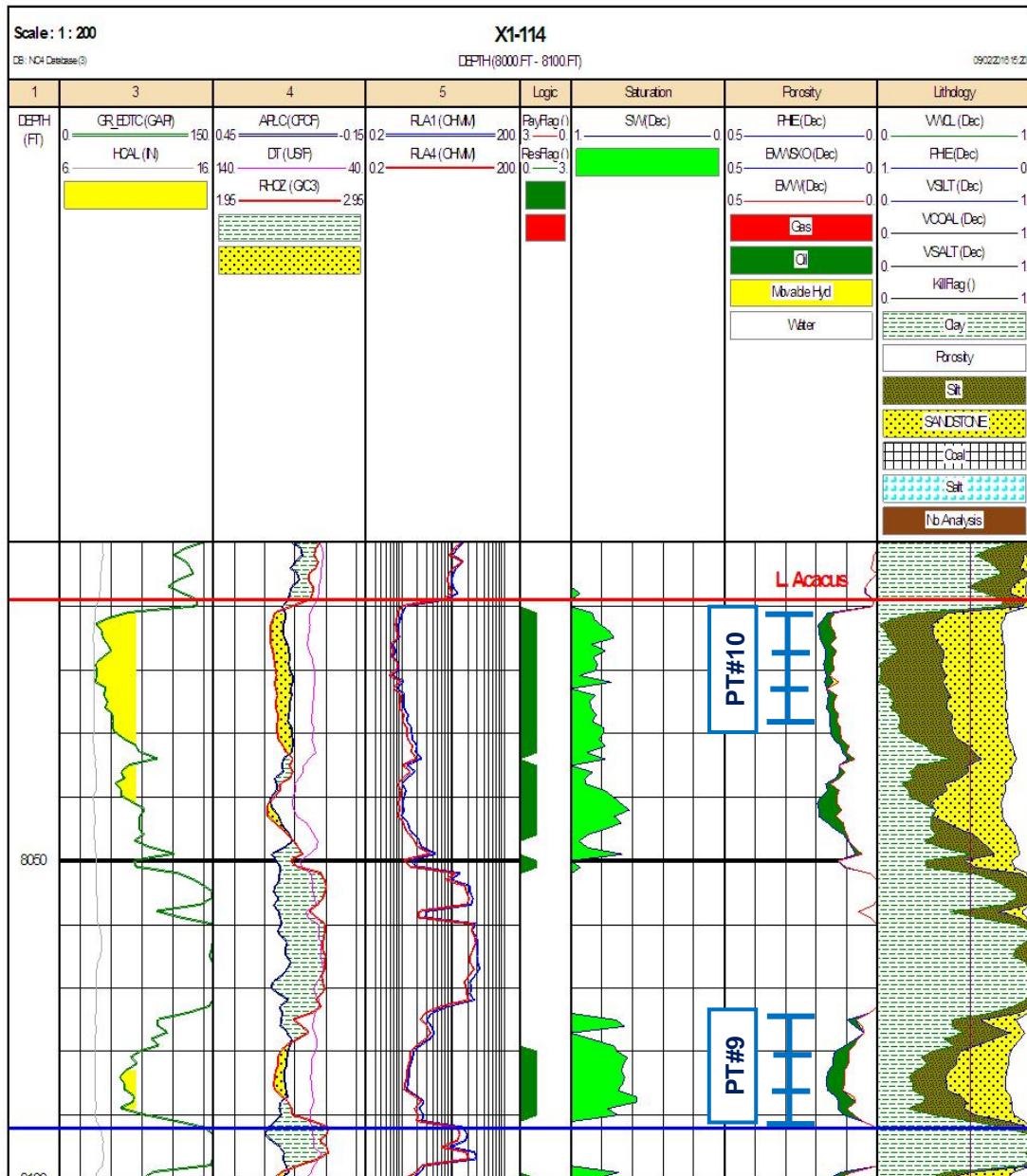


(Fig. 3.18): Lithologic/Petrophysical panel of hydrocarbon bearing sandstone reservoir of unit C in Well X1-114.



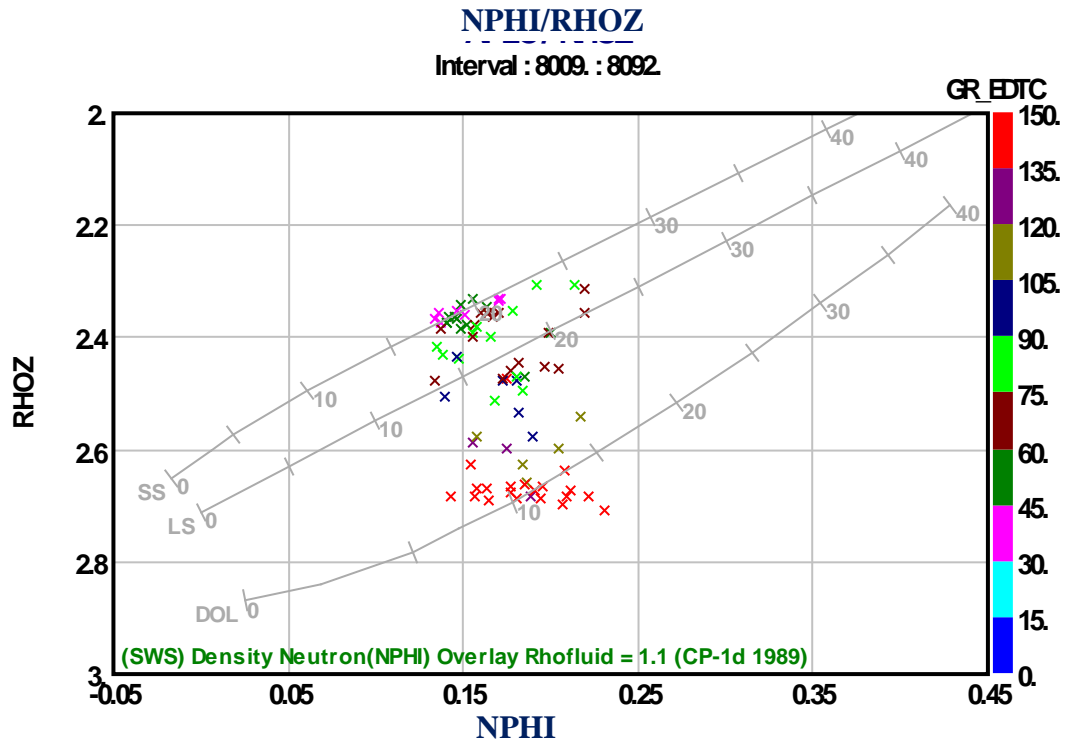


(Fig. 3.19): X1-114 Density-Neutron cross plot of Unit C showing that this unit composed of sandstone with some shale beds.

### 3.8 Petrophysical Evaluation of Y1-114

Y1-114 is located in the southeast of the study area, in which Lower Acacus reservoir has the thinnest gross thickness that covers an interval of around 873ft (8020-8893) and the analysis is calibrated to fit the result of production test as summarized in (Table, 3.10) with adjustment of RW value to the other horizons from the offset wells. The petrophysical results shows that this well has very good hydrocarbon accumulation through all zones with total net pay 50ft, and total net reservoir 276 ft.

(Table, 3.10): Production Test summary of Y1-114 well.

Depth (ft)	Y1-114
8022-8036	Oil & Gas (PT#5)
8601-8608 8584-8596	Oil & Gas (PT#4)
8874-8879 8885-8892	Oil & Gas (PT#3)

Unit C at the very top is mainly composed of thick sandstone intervals that have good reservoir characterizations (Fig. 3.20 &3.21) with average porosity 16%, water saturation 41%, and net pay 23 ft. In this well Unit B is clean (Vsh 21%), porous 13%, but water wet with accumulative net reservoir 78 (Fig. 3.22 &3.23). Unit A has a thick reservoir sand unit with around 171ft net reservoir, but only 27ft net pay at the top of this unit is hydrocarbon saturated intervals (SW 42%) with very good porosity 18% and Vsh 20% (Fig. 3.24 &3.25). A noticeable radioactive sandstone interval at the top of Unit A (8603-8616) has been recognized in this, and as a result, the volume of shale in this unit has been calculated from Density-Neutron method to better evaluate this interval especially since it is a hydrocarbon-bearing reservoir. The results of the petrophysical parameters of these sand units are summarized in (Table, 3.11).

(Table, 3.11): Reservoir and Pay summary of well Y1-114.

## Reservoir Summary

Unit Name	Top	Bottom	Gross	Net	N/G	Av Phi	Av Sw	Av Vcl
Unit C	8020	8098	78	27	0.346	0.152	0.427	0.11
Unit B	8098	8584	486	78	0.16	0.145	0.803	0.227
Unit A	8584	8893	309	171	0.553	0.182	0.642	0.185
All Units	8020	8893	873	276	0.316	0.169	0.662	0.189

## Pay Summary

Unit Name	Top	Bottom	Gross	Net	N/G	Av Phi	Av Sw	Av Vcl
Unit C	8020	8098	78	23	0.295	0.159	0.41	0.089
Unit B	8098	8584	486	0	-	-	-	-
Unit A	8584	8893	309	27	0.087	0.182	0.422	0.201
All Units	8020	8893	873	50	0.191	0.171	0.416	0.145

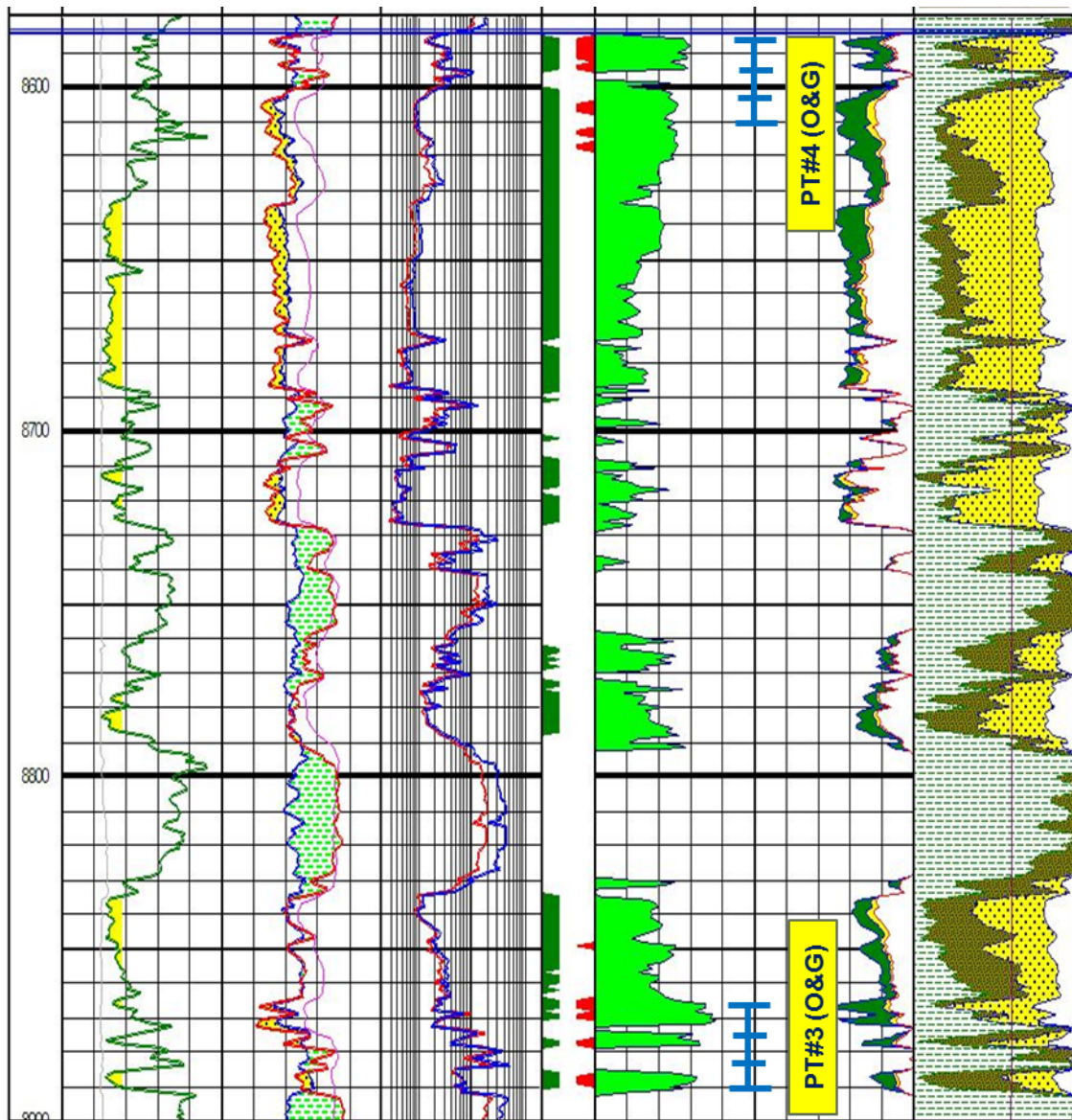


(Fig. 3.20): Lithologic/Petrophysical panel of hydrocarbon bearing sandstone reservoir of unit A in Well Y1-114.

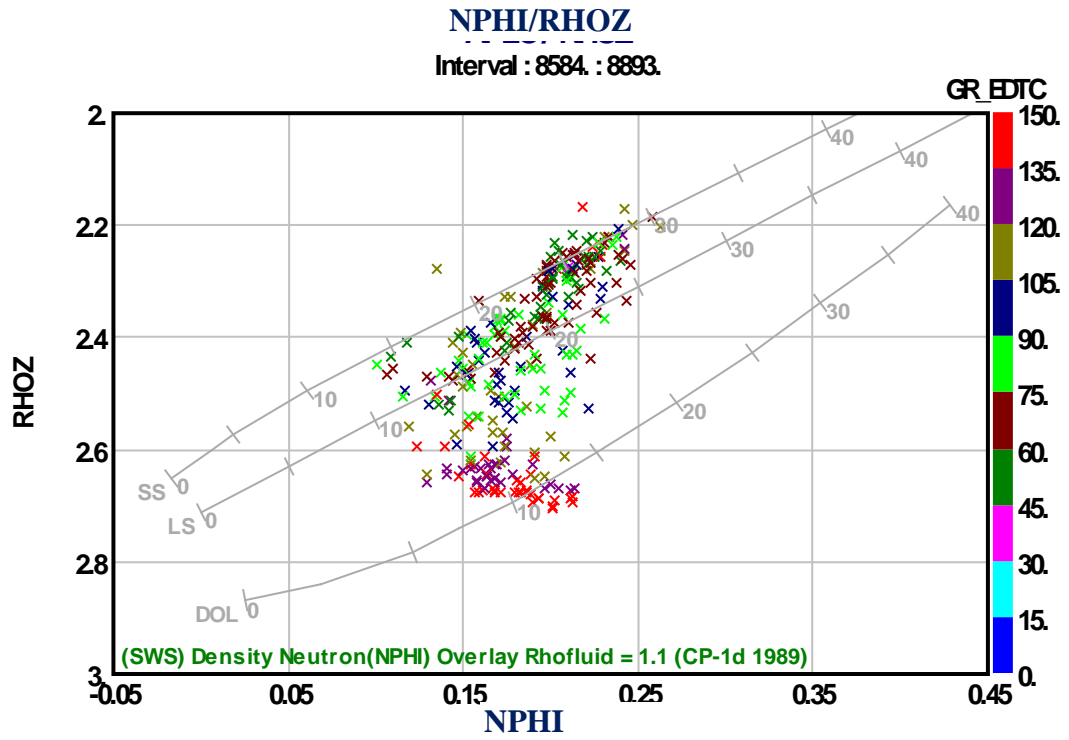


(Fig. 3.21): Y1-114 Density-Neutron cross plot of Unit A showing that this unit is mainly composed of sand stone unit with a very good porosity, interbedded with less shale layers.

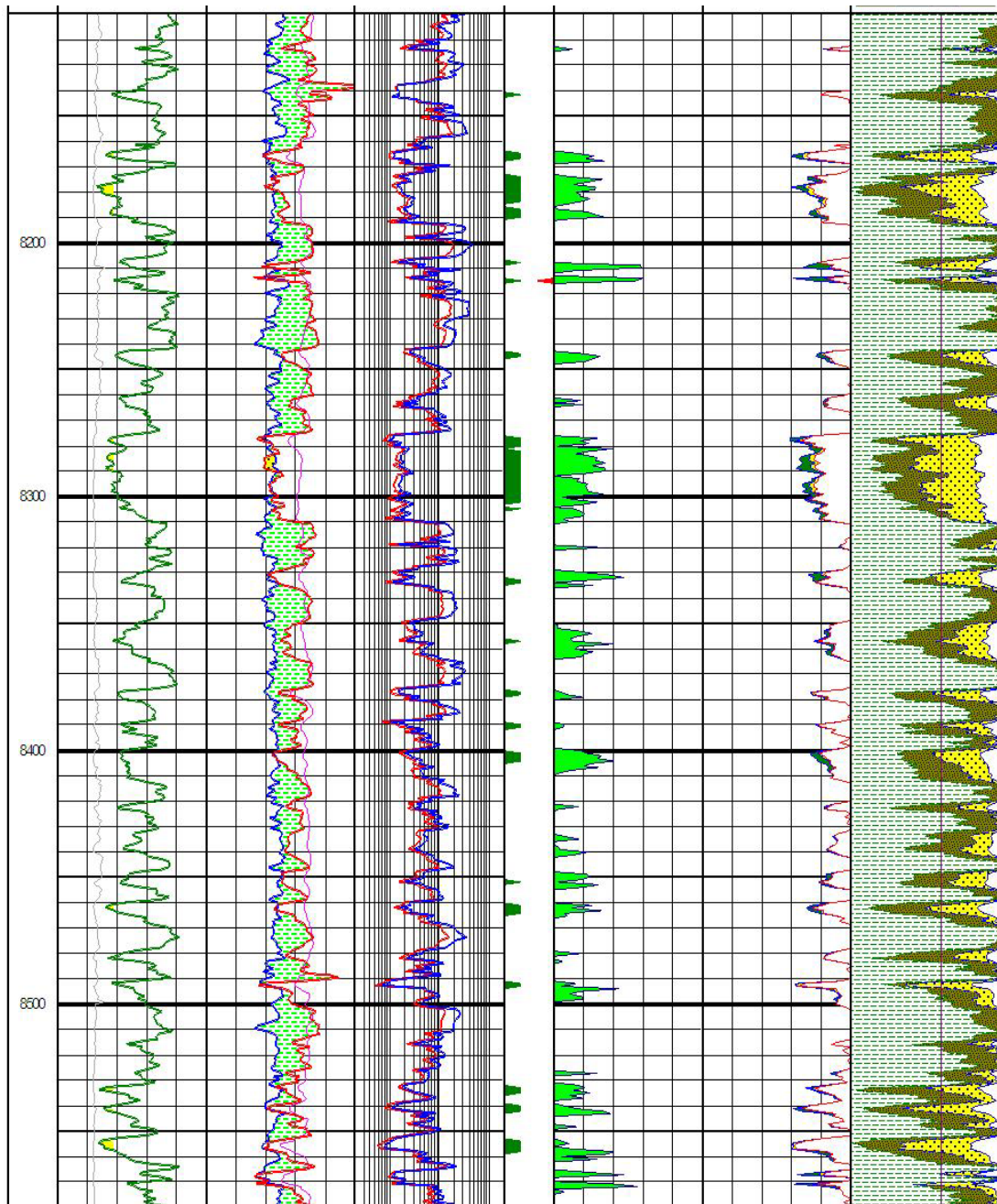


(Fig. 3.22): Lithologic/Petrophysical panel of hydrocarbon bearing sandstone reservoir of unit B in Well Y1-114.

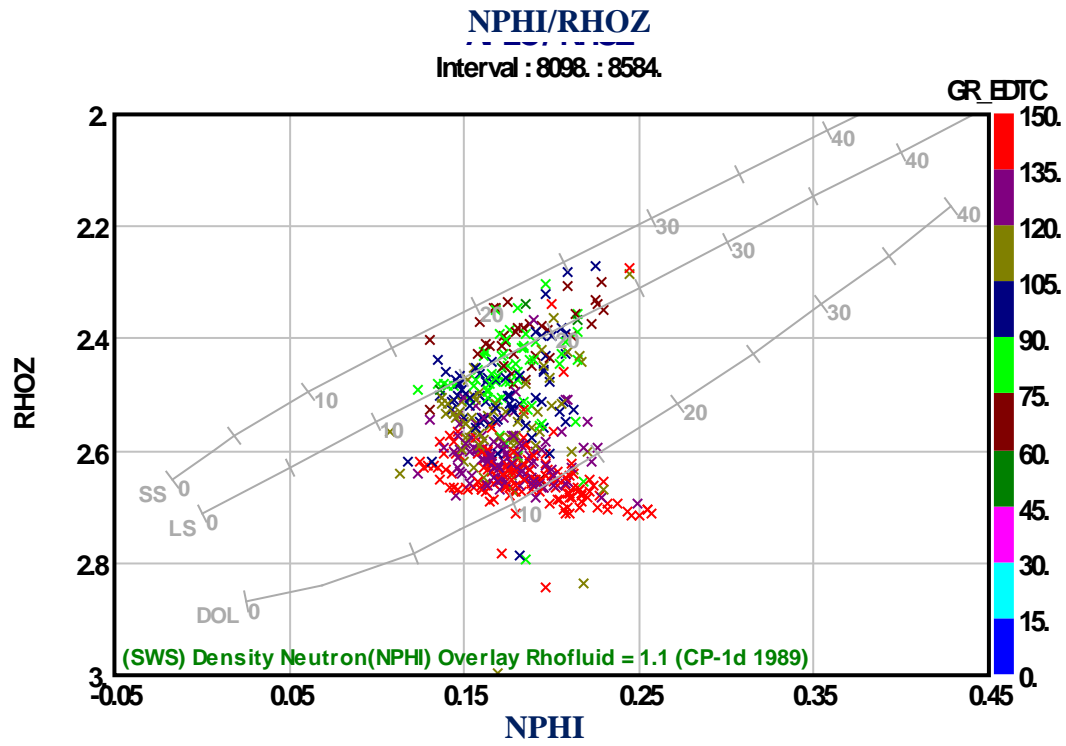


(Fig. 3.23): Y1-114 Density-Neutron cross plot of Unit B showing that this unit composed of interbedded of sand and shale with good porosity of the sand reservoir.

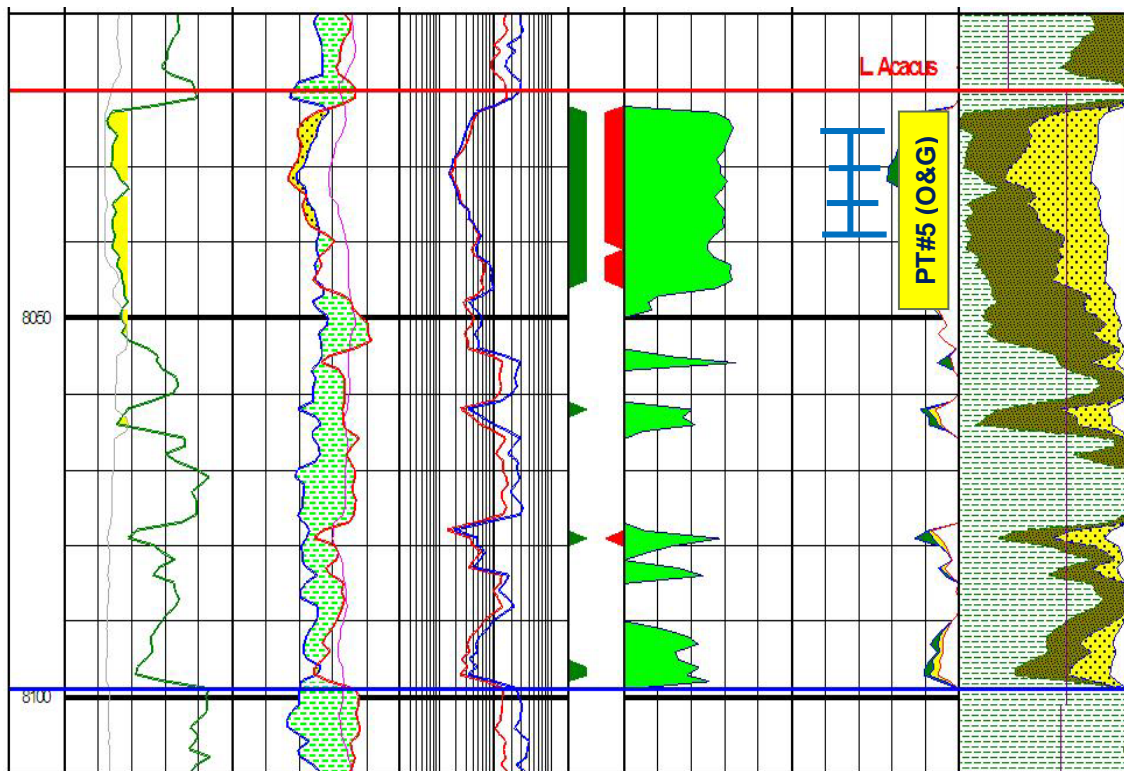


(Fig. 3.24): Lithologic/Petrophysical panel of hydrocarbon bearing sandstone reservoir of unit C in Well Y1-114.



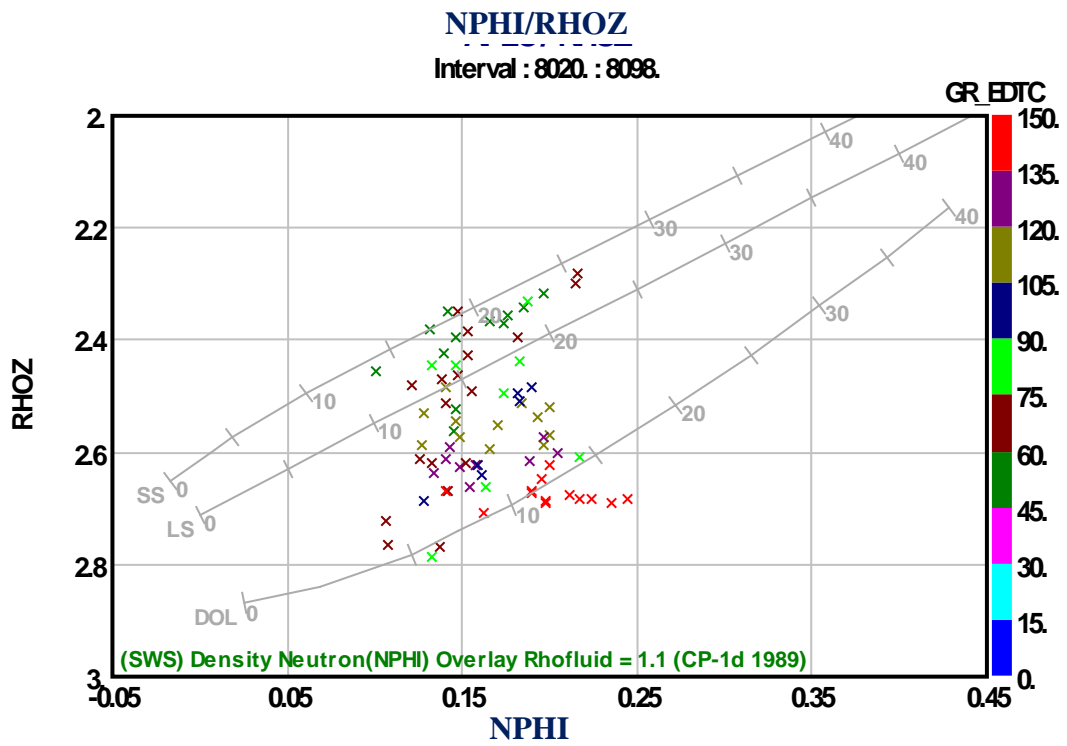


(Fig. 3.25): Y1-114 Density-Neutron cross plot of Unit C showing that this unit composed mainly of sandstone.

### 3.9 Petrophysical Evaluation of Z1-114

Z1-114 is located in the northern part of the study area and to the north of M1-114, in which Lower Acacus reservoir has the maximum thickness and covers an interval of around 1186ft (7888-9074) and the analysis will be based on the result of the offset wells as no test were performed in this well. No oil shows nor significant gas measurement were detected while drilling the well. The petrophysical results support the field observations and shows that this well has no hydrocarbon accumulation and it is classified as a dry well. The total net reservoir is about 263 ft, which is the least in the study area. Similarly to X1-114 the increase in the shale bedding suggest that this well is deposited in deeper settings.

All the units in this well are considered water well although they show good petrophysical parameters. Unit C at the very top is has good reservoir characterization (Fig. 3.26 &3.27) with average porosity 15%, and Vsh 28% and 12 net reservoir. In this well Unit B has Vsh 25%, porosity 13%, and net reservoir 92 ft (Fig. 3.28 &3.29). Unit A has a thick reservoir sand unit with around 159ft net reservoir, (SW 73%) with very good porosity 21% and Vsh17% (Fig. 3.30 &3.31). The results of the petrophysical parameters of these sand units are summarized in the table below (Table, 3.12).

(Table, 3.12): Reservoir and Pay summary of well Z1-114.

#### Reservoir Summary

Unit Name	Top	Bottom	Gross	Net	N/G	Av Phi	Av Sw	Av Vcl
Unit C	7886	7988	102	11.5	0.113	0.154	0.616	0.281
Unit B	7988	8589	599	92	0.154	0.191	0.655	0.246
Unit A	8589	9074	485	159.5	0.329	0.213	0.731	0.17
All Units	7888	9074	1186	263	0.222	0.202	0.702	0.198

#### Pay Summary

Unit Name	Top	Bottom	Gross	Net	N/G	Av Phi	Av Sw	Av Vcl
Unit C	7886	7988	102	0	-	-	-	-
Unit B	7988	8589	599	0	-	-	-	-
Unit A	8589	9074	485	0	-	-	-	-
All Units	7888	9074	1186	0	-	-	-	-



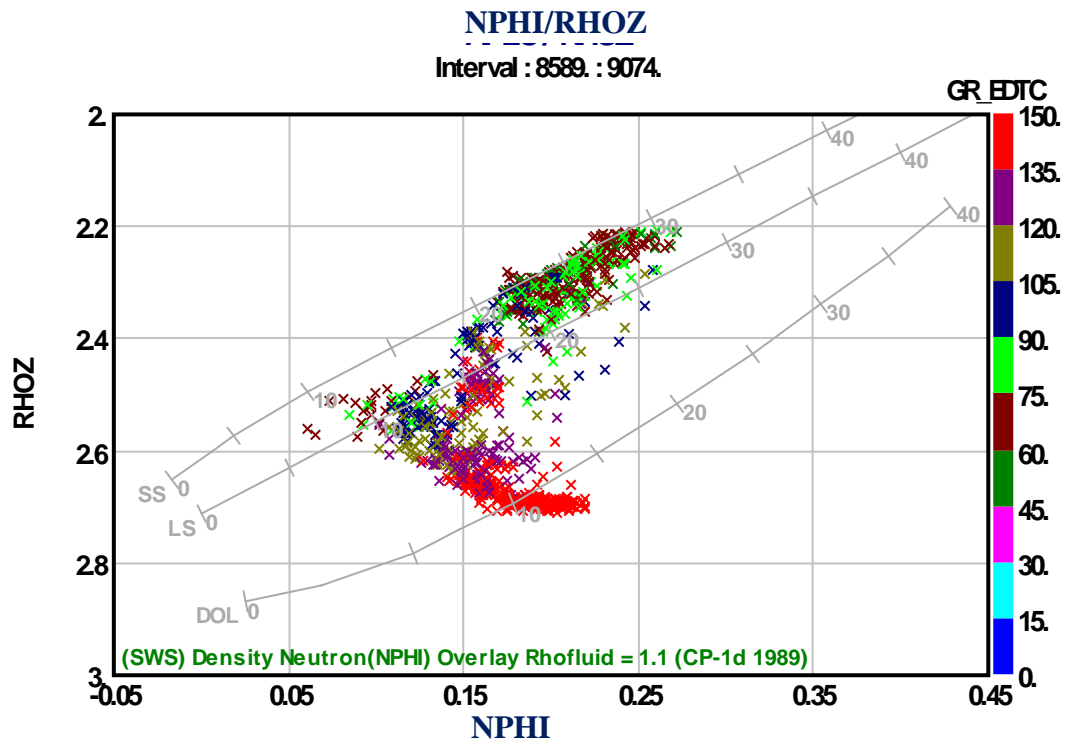


(Fig. 3.27): Z1-114 Density-Neutron cross plot of Unit A showing that this unit is mainly composed of clean sand stone unit with a very good porosity, along with some shale layers.

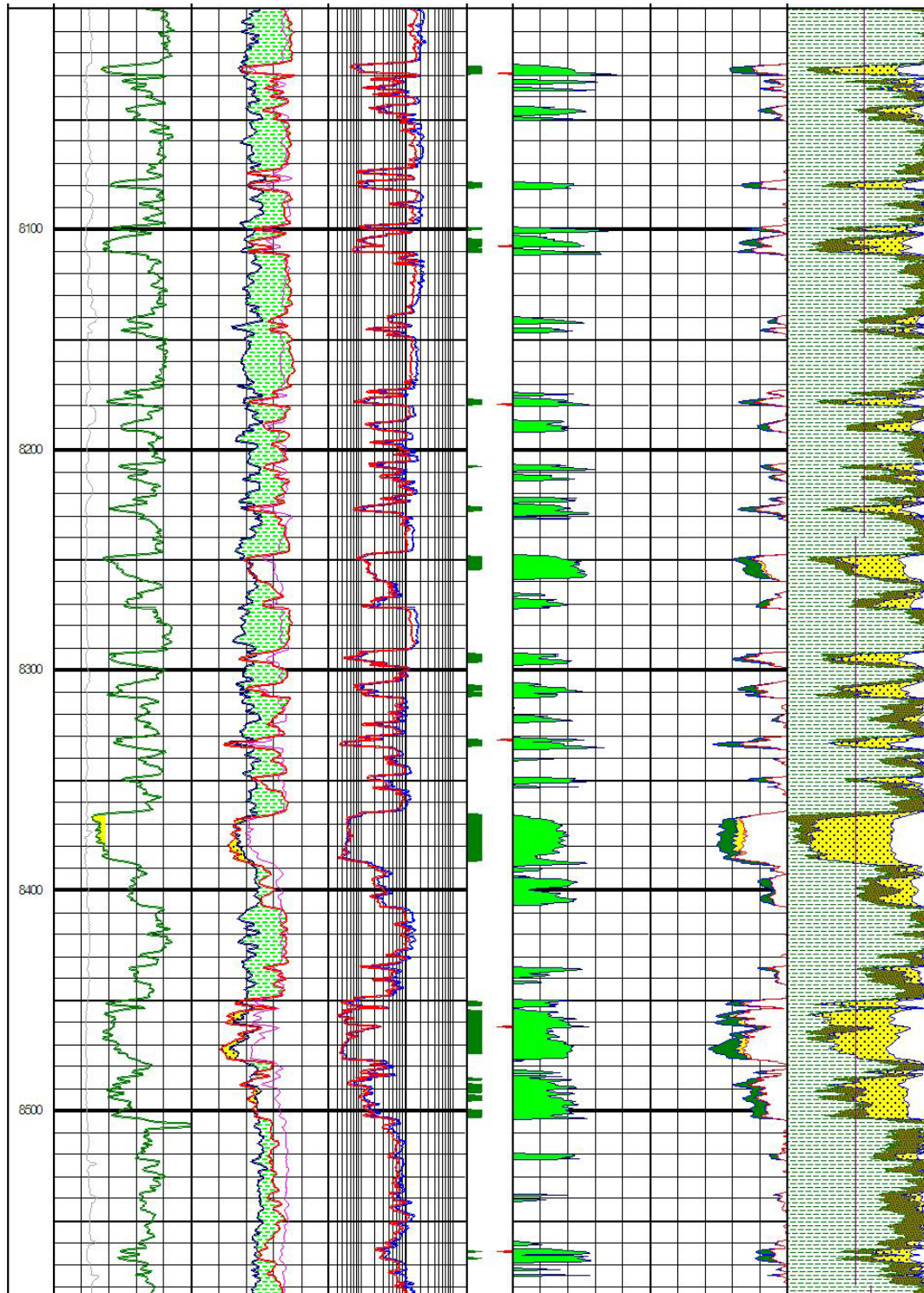


(Fig. 3.28): Lithologic/Petrophysical panel of hydrocarbon bearing sandstone reservoir of unit B in Well Z1-114.

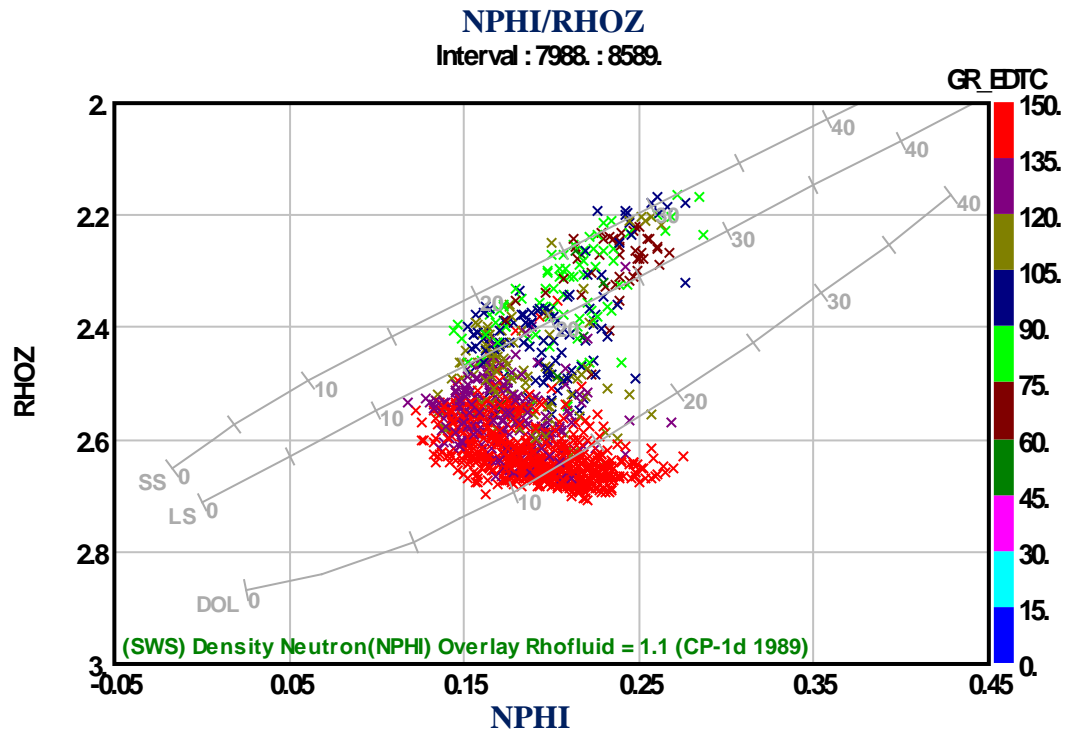


(Fig. 3.29): Z1-114 Density-Neutron cross plot of Unit B showing that this unit composed of interbedded of sand and shale with good porosity of the sand reservoir.

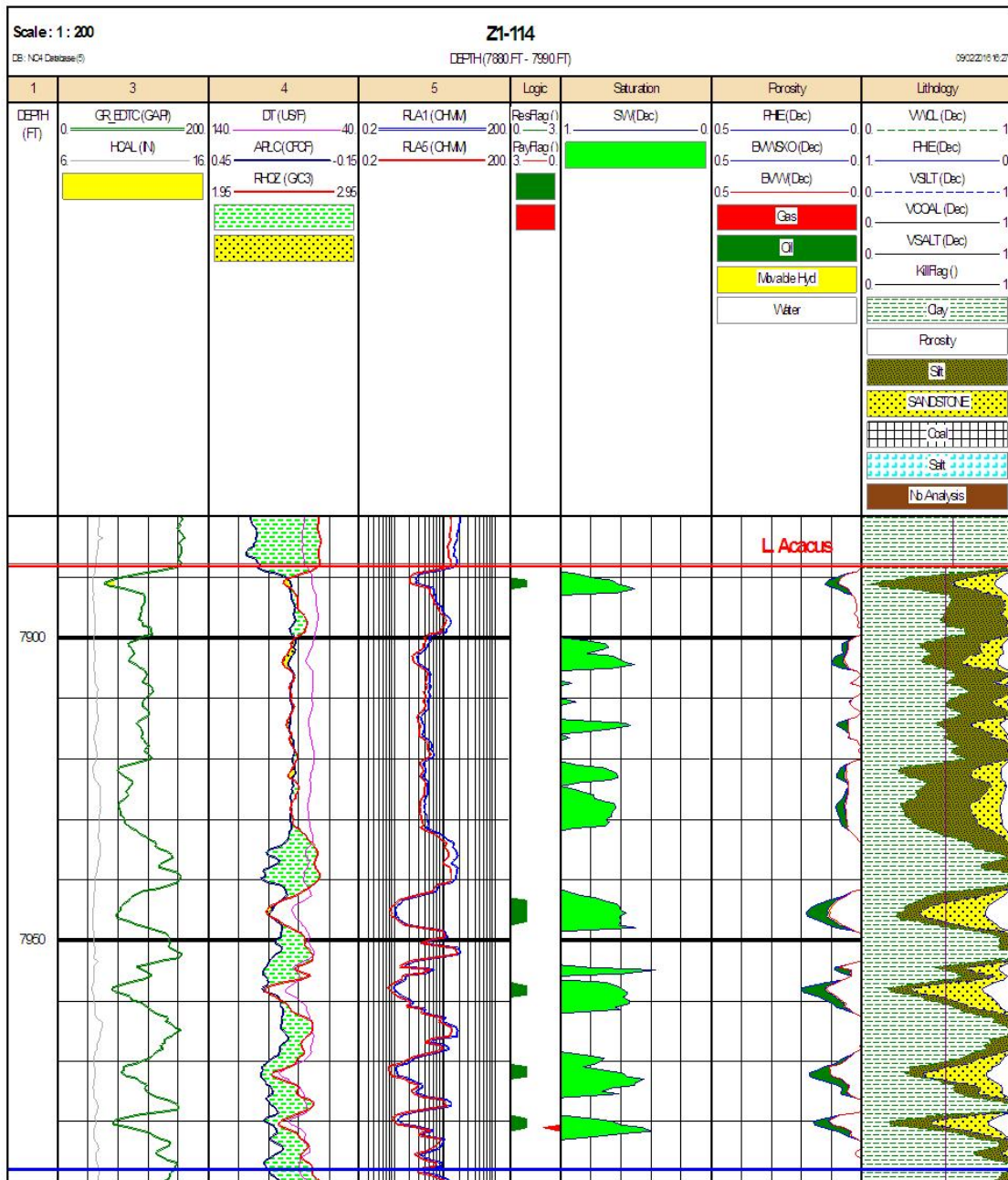


(Fig. 3.30): Lithologic/Petrophysical panel of hydrocarbon bearing sandstone reservoir of unit C in Well Z1-114.

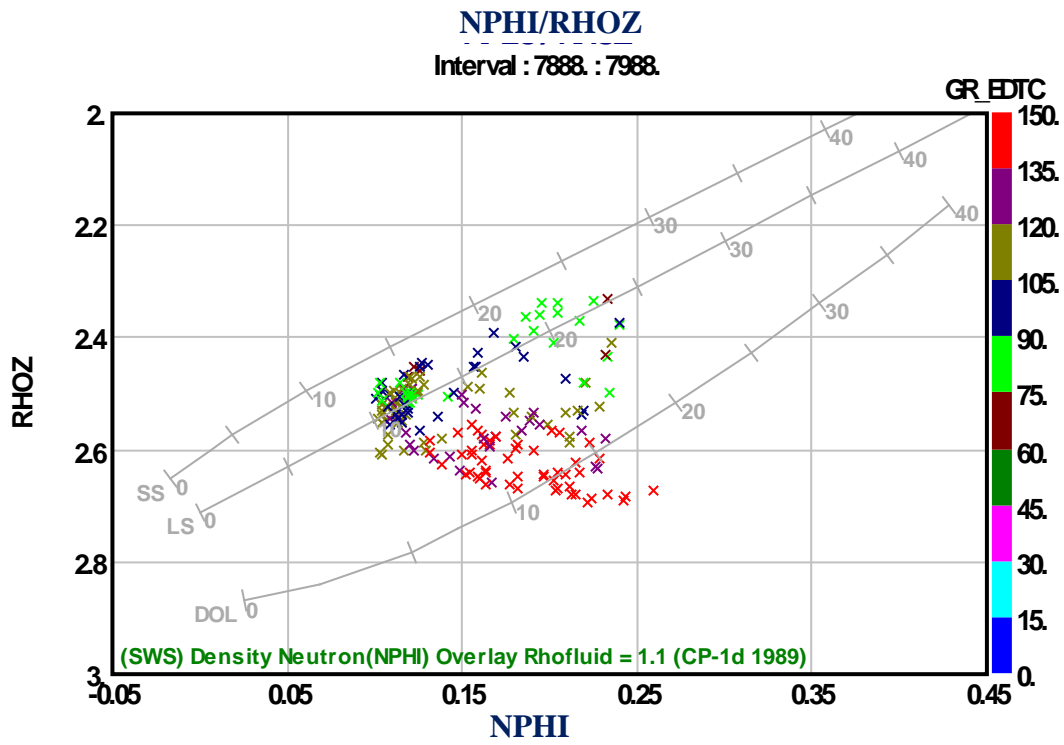


(Fig. 3.31): Z1-114 Density-Neutron cross plot of Unit C showing that this unit composed of sandstone



## **Chapter Four**

### **Subsurface Mapping and Cross Section**

#### **4.1 Introduction**

In the broadest scientific sense, mapping is the transferring of information from one coordinate system to another. The original information is subject to a consistent mathematical transformation so that it appears in a new format. Usually, the purpose is to show some aspects of the data more clearly since many data sets, especially in the natural sciences, have variables that require many dimensions for their precise description. For the geologist, “mapping” is used in a simplified sense, which is merely reduced in size and ideally cleared of any spurious information not pertinent to the needs of geology (Lisle et al., 2011). Cross-sections similarly can show changes vertically and laterally in stratigraphy and structure from place to place.

The integration of the various datasets is required to conclude, recommend and finalize all of these analyses and suggest future work and research. As far as seismic data is concerned, there will be seismic maps used for this study to better understand the reservoir geometry and aerial distribution. Available wells for the study are distantly located from each other, where the shortest distance is about 10 km between Well M1-114 and N-114, while the longest distance is about 17 km between Y1-114 and N1-114. A seismic structural depth map illustrates that structural elevations are the highest in the northern part of the area of interest where Well Z1-114 is located, following that in the middle part of the area is well M1-114 which is close to Z1-114 in elevation. Y1-114 is the well located in the southern part of the area of interest with lowest structural elevation (Fig. 4.1). The isopach map of Lower Acacus gross reservoir display an obvious increase in thickness towards the north (Fig. 4.2). Although the northern part of the study area is structurally higher and stratigraphically thicker, it accommodates no hydrocarbon accumulations, this perhaps gives more room for other driving mechanisms of hydrocarbons accumulation and entrapment, which is thought to be governed by stratigraphic control rather than only structural control.

The isopach map could also assist in the establishment of the general reservoir geometry reflecting the environment of deposition as well as the source of sedimentation in the area of interest. As discussed in chapter three, wells Z1-114 and X1-114 have a higher

shale content. This could indicate that the sediment influx direction is towards the north-northwest. The increase in thickness towards the north does not necessarily reflect the increase in sandstone content as it is controlled by the source sediment area location. Another important contribution comes from the time slice of seismic data at the horizontal display to see the lateral change in the formation (Fig. 4.3). This will help to outline the stratigraphic variation and spatial architecture of the specific interval and could provide insights onto creation of a depositional model in the future. This time slice at 1548 ms equivalent to specific depth of almost 8620 ft within a sandy dominated unit (Unit A), reveal recognizable feature very similar to a deltaic lobe that is trending NW-SE advancing towards the sea direction.

It was decided that work on the maps was to be made by hand, due to the fact that Software could not handle the number of wells relevant for the study. It was seen convenient to take snapshots of Petrel generated structure and isopach maps. Reservoir body geometry was transferred from software-generated maps and fitted on the hand drawn contours for better illustration of the peripheries extent of the reservoir.

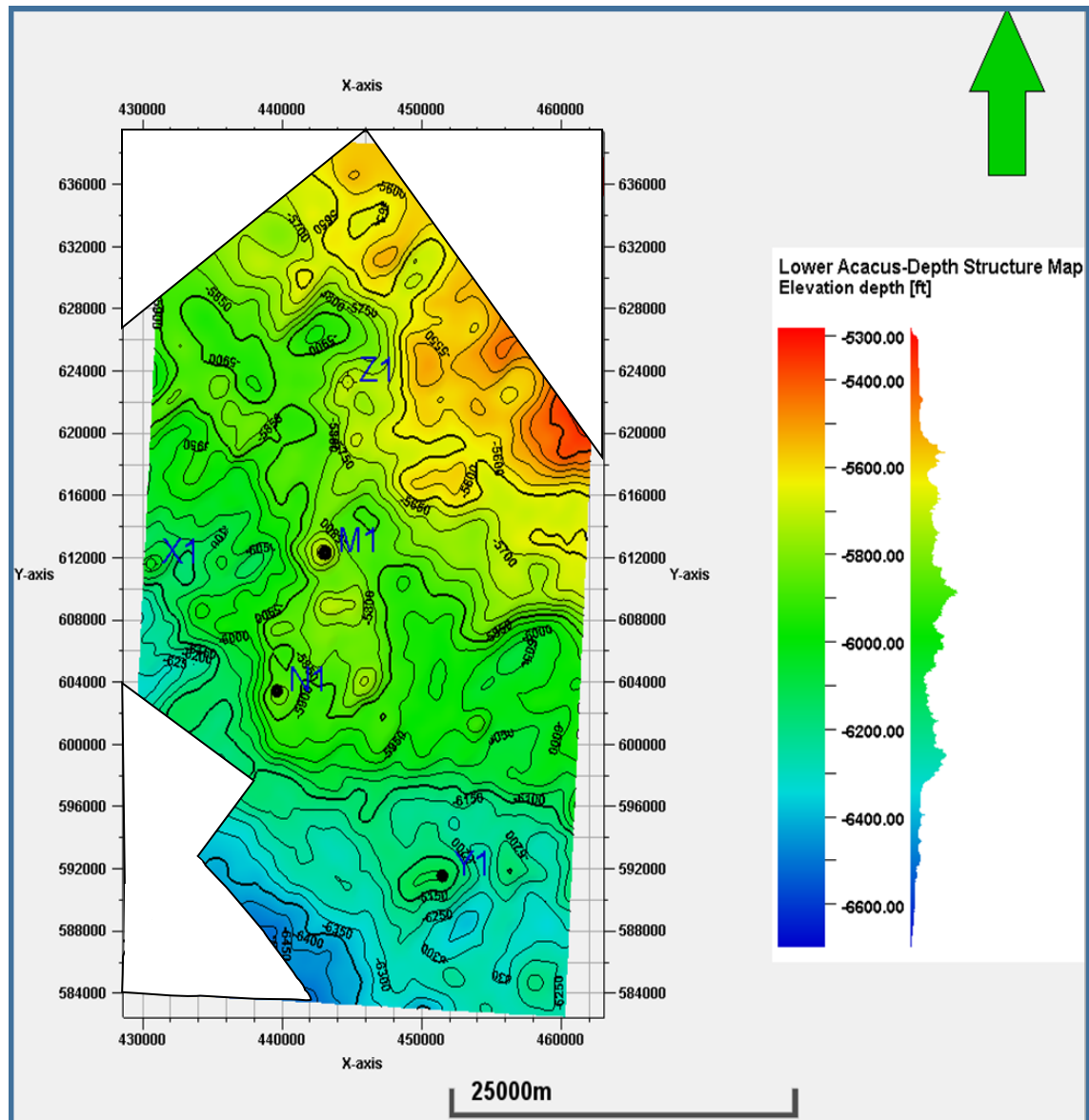


(Fig. 4.1): Depth structure map of Lower Acacus reservoir (AGOCO, 2009).

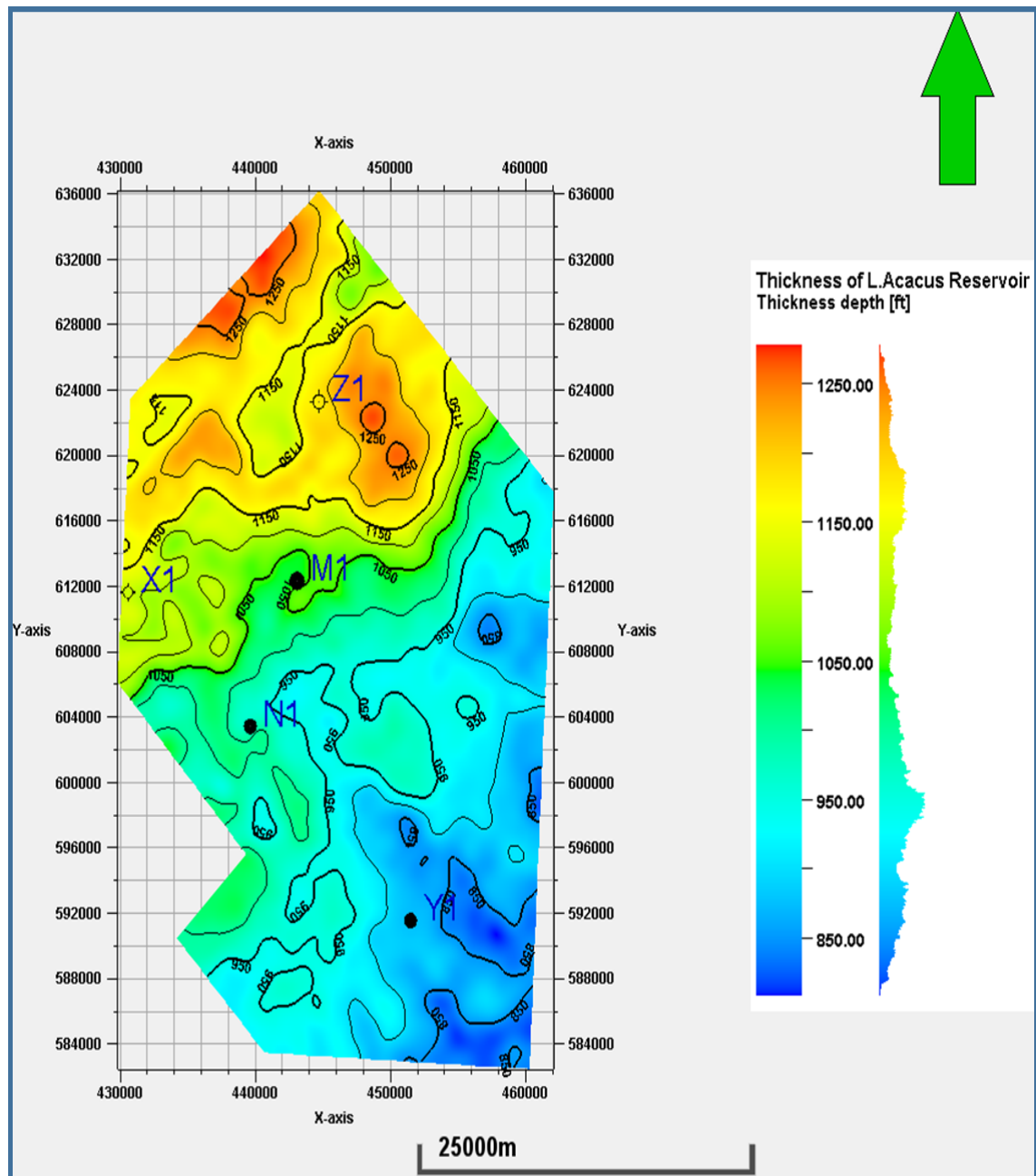


(Fig. 4.2): Isopach map of Lower Acacus reservoir (AGOCO, 2009).

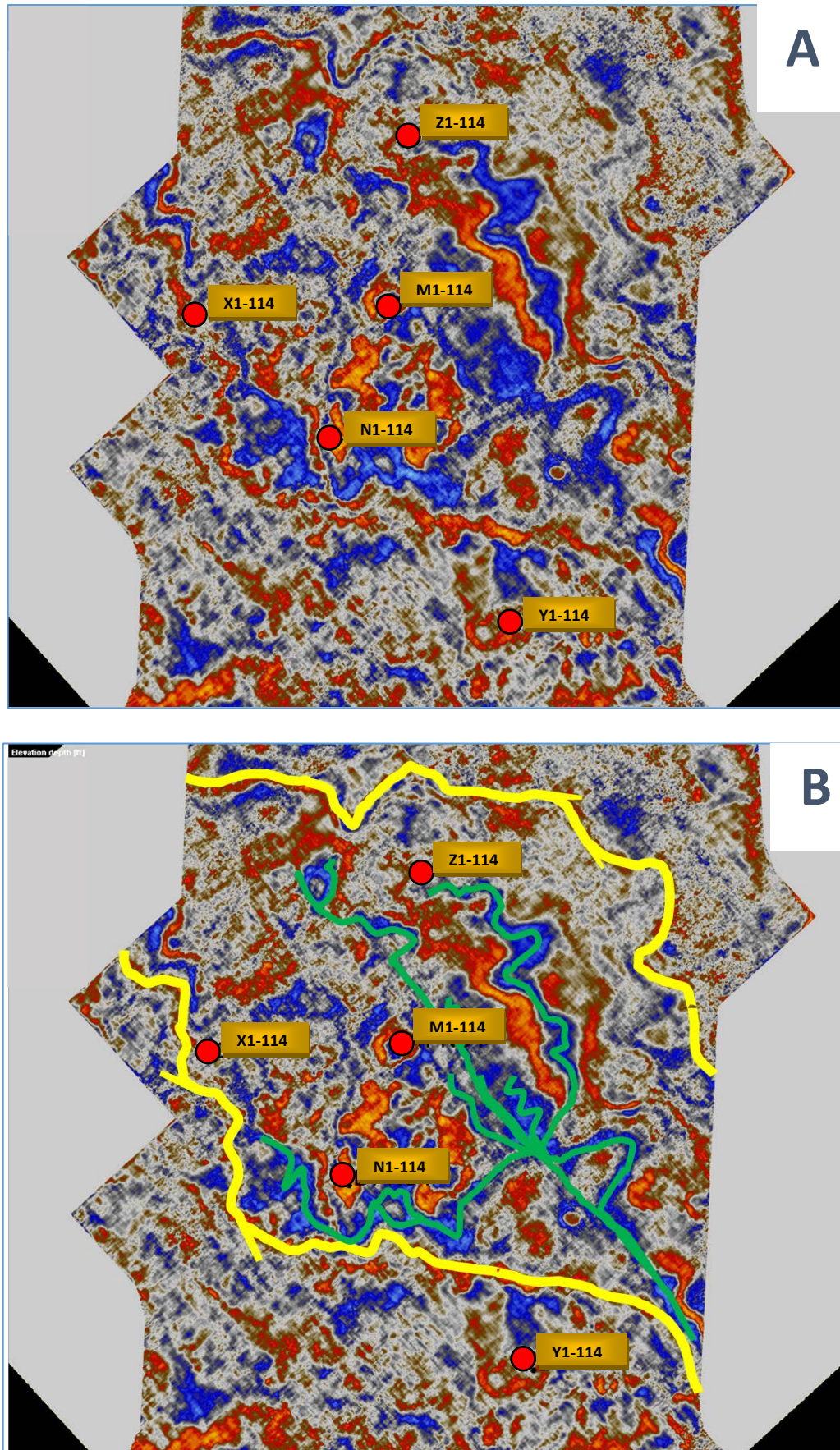


(Fig. 4.3): Time Slice of Lower Acacus reservoir @1548 ms (A), the proposed delta geometry at this level (B), (Red Color indicates High Amplitude, while Blue indicates Low Amplitude) (AGOCO, 2009).

## 4.2 Maps

### 4.2.1 Sand/shale ratio Map

The Sand/shale ratio map is probably one of the easiest methods to relate to current system (Potter and Pettijohn, 1977). It is represented by thickness ratio of sand relative to shale reveals the interrelation between these two lithologic components (Krumbein and Sloss, 1963). The net sandstone layers were identified by applying a cut-off of the shale volume ( $V_{sh} \leq 0.4\%$ ) which is better than using a direct cut-off on GR log (ex.  $GR \leq 75$  API) as we had encountered some radioactive sandstone in which volume of shale were calculated from Density-Neutron log. Table (4.1) represent the sand/shale ratio of Lower Acacus reservoir for all the wells in the study area.

(Table, 4.1): Sand-Shale ratio of the wells in the study area.

Well Name	Total thickness (ft)	Sand layers (ft)	Shale layers (ft)	Sand/shale (%)
M1-114	1031	378	653	0.58
N1-114	979	456	523	0.87
X1-114	1104	327	777	0.42
Y1-114	873	291	582	0.5
Z1-114	1186	302	884	0.34

According to the used cutoffs, we managed to distinguish between sand and shale intervals. Consequently, subdivided the total thickness of sand layers to the total thickness of shale in order to compute the sand/shale ratio. The resulted values range from (0.87%), which indicates sandy-dominated sequences, to (0.34%) representing shaly-dominated sequences. Thus, the sand/shale ratio map of Lower Acacus reservoir was adjusted to fit the geometry presented in the time slice.

The generated map (Fig. 4.4) shows that the highest sand percentage was accumulated nearly in the center of the study area at well N1-114 and gradually decreases toward M1-114 and Y1-114. This may indicate an area of delta front setting. FMI analysis will confirm the existence of this kind of deposition. The sand percentage continues to decrease towards the east (X1-114) and north (Z1-114) of the study area, which suggests more distal deposits or marginal setting.

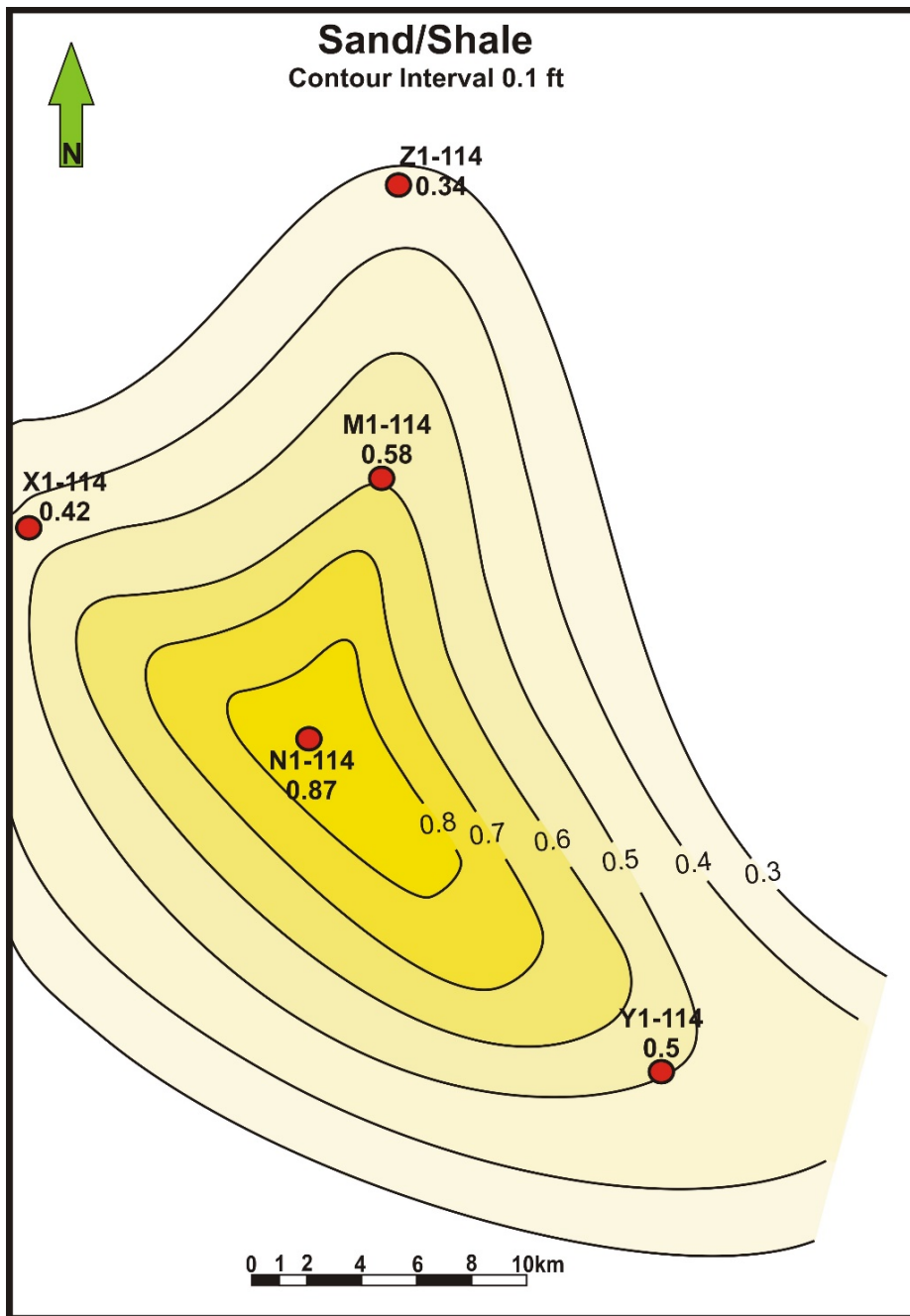


(Fig. 4.4): Sand/Shale ratio map of Lower Acacus reservoir in Block-114.

### 4.2.2 Net pay and net reservoir Maps

The contour map of equal value of true stratigraphic thickness is an isopach map (Maltman, 1990). Considering that, the net sandstone reservoir and net pay maps were generated for every unit in the study area after applying specific cut-offs on the total thickness. The net sandstone reservoir maps indicate area with clean and porous sandstone layers (cutoffs include;  $V_{sh} \leq 0.4\%$  &  $\phi \geq 10\%$ ), while net pay maps indicate area of hydrocarbon accumulations ( $V_{sh} \leq 0.4\%$ ,  $\phi \geq 10\%$ , &  $SW \leq 50\%$ ). The table below (Table, 4.2) represent the net reservoir and net pay values of every unit in the study area:

(Table, 4.2): Net reservoir and net pay of the wells in the study area.

Unit C	Well Name	Total Thickness (ft)	Net Reservoir (ft)	Net Pay (ft)
	M1-114	95	22	22
	N1-114	92	28	24
	X1-114	83	48	0
	Y1-114	78	27	23
	Z1-114	102	12	0

Unit B	Well Name	Total Thickness (ft)	Net Reservoir (ft)	Net Pay (ft)
	M1-114	562	124	48
	N1-114	549	140	101
	X1-114	642	80	0
	Z1-114	599	92	0

Unit A	Well Name	Total Thickness (ft)	Net Reservoir (ft)	Net Pay (ft)
	M1-114	374	208	45
	N1-114	338	250	35
	X1-114	379	153	0
	Z1-114	485	160	0



### 4.2.2.1 Unit A

The generated net sand map of this unit shows relatively high accumulation of a good sandstone reservoir in the center of the area with around 208 ft in M1-114 and 250 ft in N1-114 of clean porous sandstone. Although the highest concentration of sand is present at well N1-114, the highest hydrocarbon content is seen to be at the M1-114 with 45 ft filled of hydrocarbon and 35 ft in N1-114 (Fig. 4.5). This brings about a suggestion of M1-114 is located at higher structural elevation than well N1-114. In X1-114 and Z1-114 wells net pay is almost zero because they are located in the distal part of the delta setting with less likelihood of containing promising sand intervals.

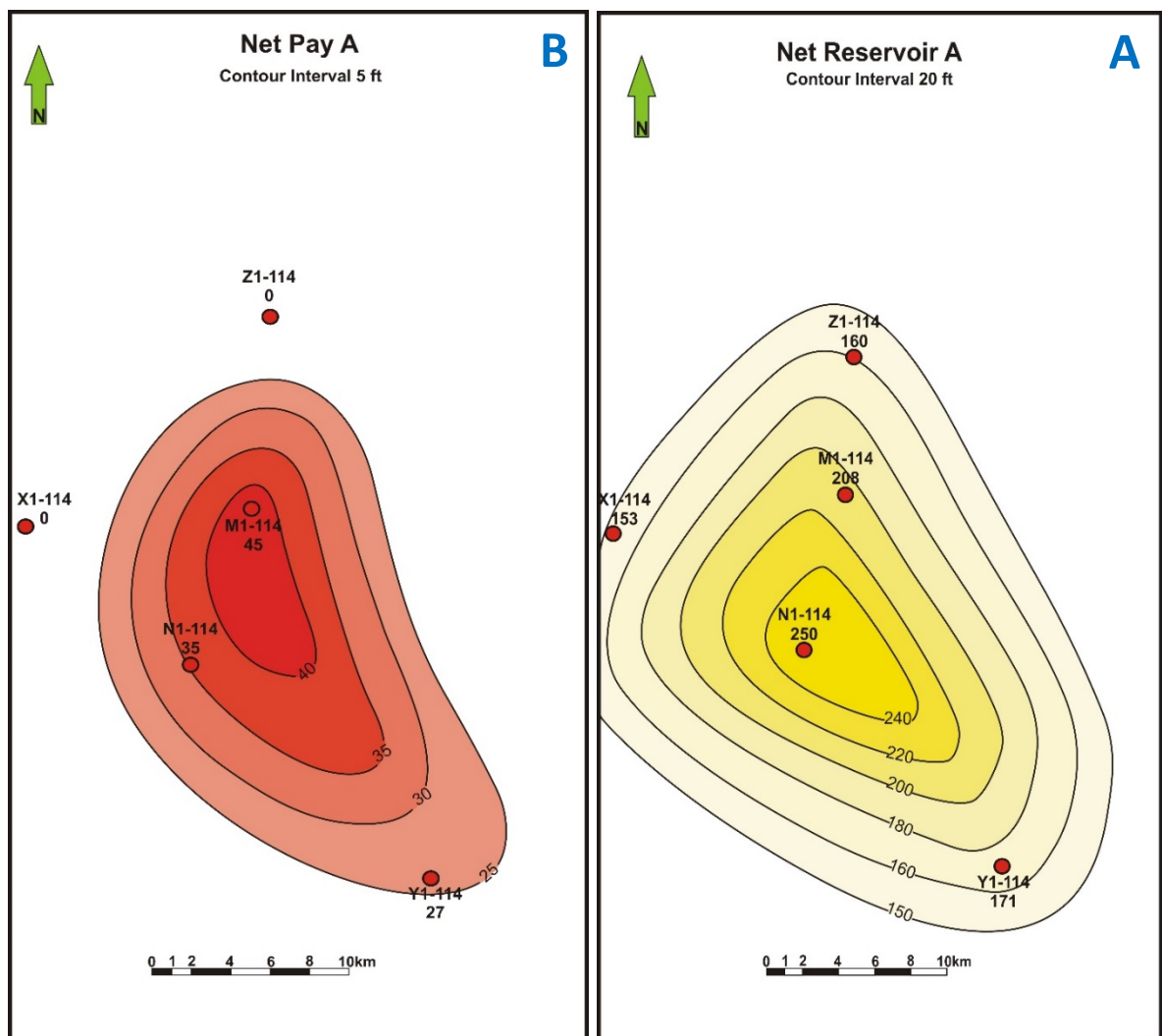


(Fig. 4.5): Net sandstone reservoir map (A), and net pay map (B) of Unit A of Lower Acacus reservoir.

### 4.2.2.2 Unit B

The generated net sand map of this unit shows another pattern of sandstone accumulation somehow similar to the previous unit with an ideal scenario of net pay map fitting with the net reservoir map (Fig. 4.6), illustrating that well N1-114 represents the best hydrocarbon accumulation with more than 100 ft of net pay thickness. M1-114 has half of the accumulation in N1-114 leaving all other wells with no hydrocarbon.

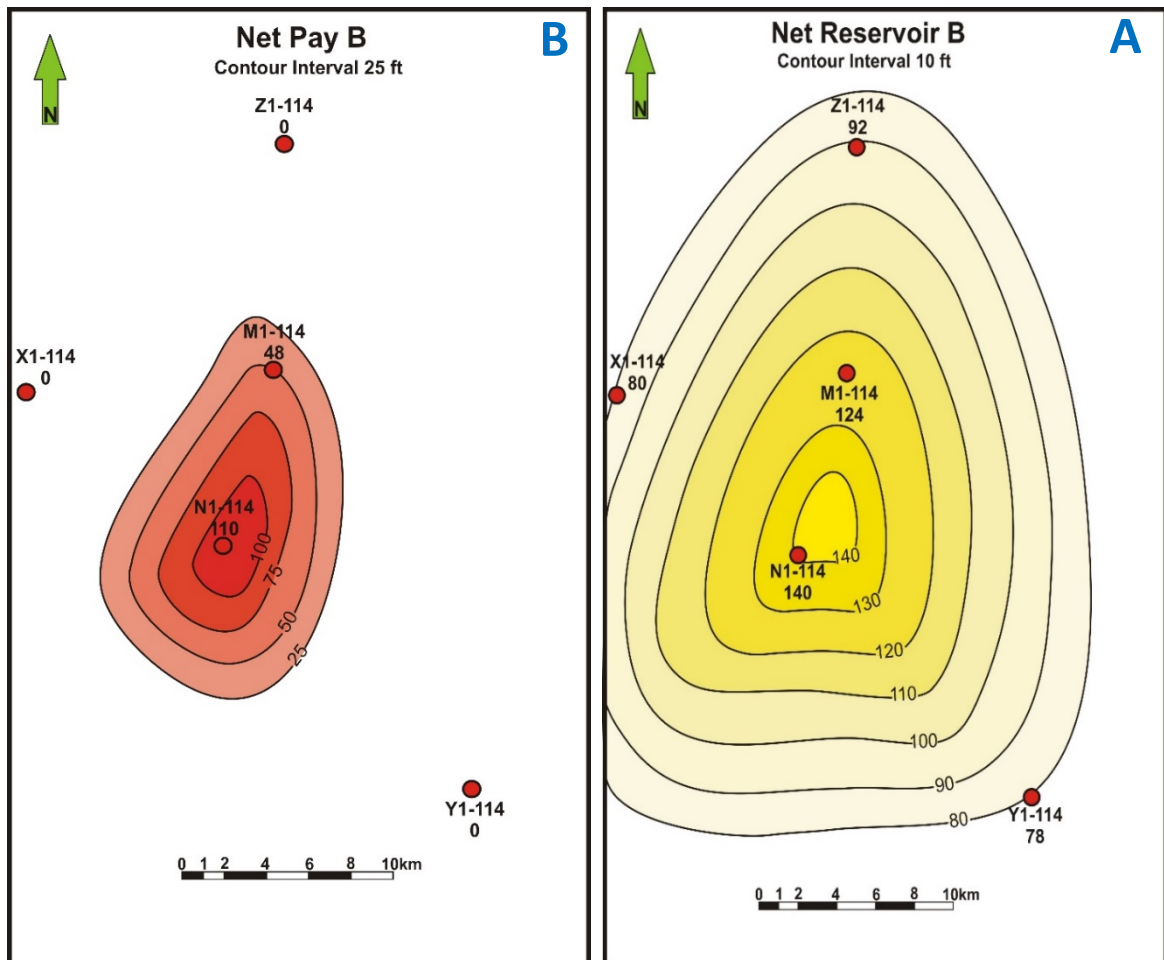


(Fig. 4.6): Net sandstone reservoir map (A), and net pay map (B) of Unit B of Lower Acacus reservoir.

### 4.2.2.3 Unit C

The generated net sand map of this unit shows a completely different pattern of sand accumulation in which the delta pattern seems progressed a little towards the west and the sandstone accumulation concentrated further towards the west (Fig. 4.7). Contradictorily the net pay map shows a fair accumulation in the center area towards S-SW but no accumulating hydrocarbons towards the north Z1-114 nor toward the west X1-114.

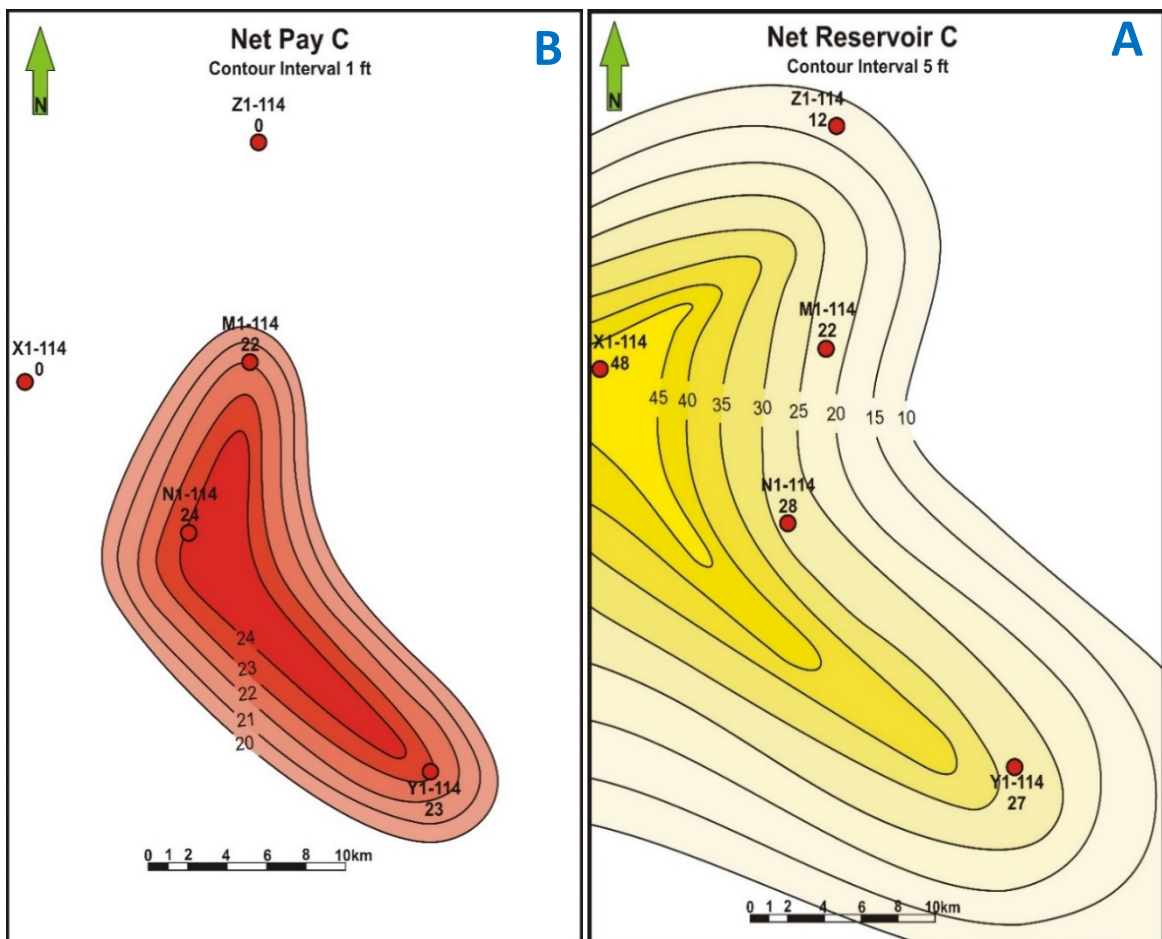


(Fig. 4.7): Net sandstone reservoir map (A), and net pay map (B) of Unit C of Lower Acacus reservoir.

Based on all the previous maps, well N-114 and M1-114 represent the most prospective hydrocarbon wells with the highest accumulation net pay of 160 ft and 115 respectively. Both wells lie at the center of the area of interest making it the best region for further hydrocarbon exploration.

### 4.3 Cross sections

Cross-sections portray the arrangement of the rocks as seen in a vertical plane (Maltman, 1990). In order to see vertical and lateral variation in shaly-sand reservoir, structural and stratigraphic cross sections are generated to trace the continuity of the individual sand layers. Seismic sections (Fig. 4.8) in two directions were generated to observe the general effect of any large-scale structural or stratigraphic features.

After examination of the seismic sections, it is noticed that the structural configuration of the traps is represented by subtle anticlines with small magnitudes, though with good extent. Moreover, no indication of major faults or pinch-out is recognized. Looking at the well logs, coastal log signatures are clear (shallowing upwards) with good sand quality and thickness, the best at N1-114 then sand quality decreases towards the north at Z1-114 confirming rather Stratigraphic control on presence of hydrocarbons.

#### 4.3.1 Stratigraphic cross section

Two stratigraphic cross sections were constructed with the top of Lower Acacus as a datum in order to see the stratigraphic effect on the studied wells. This correlation is based on best match of lithology and log response, while facies lateral change is applied in the next chapter. Fundamentally, Unit A, as well as Unit B, are subdivided into four subunits, showing a lateral continuity with minor thickness changes, while Unit C is left undivided due to small thickness and homogenous sand unit. (Table, 4.3), shows the gross thickness of these horizon in the wells of the study area. The first cross section (Fig. 4.9) is among (Y1-114, N1-114, and X1-114) on the SE-NW direction showing a noticeable general thickening towards X1-114 with increasing in shale percentage.

(Table, 4.3): Determined subunits in the studied wells, (colored cells indicate HC accumulation)

Unit Division		Layer Thickness				
		M1-114	N1-114	X1-114	Y1-114	Z1-114
Unit C	C1	95	91	80	77	102
	B4	77	51	58	72	87
Unit B	B3	255	214	352	206	288
	B2	81	166	63	155	84
	B1	150	119	171	85	142
Unit A	A4	138	130	115	73	130
	A3	81	56	98	67	110
	A2	85	68	75	78	151
	A1	70	85	92	59	93

In Y1-114, the subunits (A1, B1 and C1) are the most prospective among the subdivided units, whereas in well N1-114 all existing subunits are prospective with the exception of subunit A3 & B1. On the other hand, X1-114 well displays a different scenario where all subunits are water wet. This probably indicates that the eastern part of the area of interest would not be prospective for hydrocarbon accumulation, where lateral change in depositional setting may have taken a place. Furthermore, FMI analysis could be a good tool to verify the source and type of sediments. Another cross section (N1-114, M1-114, and Z1-114) on the N-SSW direction (Fig. 4.10) displays more shale increasing towards Z1-114. The subunits in this cross section illustrate a lateral decrease in prospectivity from N1-114 well, which has seven prospective subunits decreasing to four towards well M1-114. This decrease continues until no hydrocarbons detected further north in well Z1-114. As a result, having two dry wells (X1-114 and Z1-114) in the north-northeast portions of the study area reduce the chances of prospectivity in these parts of the area of interest.

### **4.3.2 Structural cross section**

Similarly, two structural cross sections were generated in order to see the structural effect on the study wells. The first cross section (Fig. 4.11) was run among (Y1-114, N1-114, and X1-114) on the SE-NW direction. This cross section shows that the area near the central part at well N1-114 exhibits the highest structural position with relative decrease in elevation towards the oil well Y1-114 in SE, and the dry well X1-114 in NW direction. Although X1-114 and Y1-114 wells lie almost at the same structural elevation, Y1-114 in SE-direction is an oil well while X1-114 in NW-direction is a water wet. The second cross section (Fig. 4.12) is among (N1-114, M1-114, and Z1-114) and it clearly shows that the dry well Z1-114 is located on a high structural position while N1-114 is structurally lower but with high hydrocarbon productivity. Thus, as they are no obvious sealed faults present in the seismic sections preventing the oil to migrate toward X1-114 in the east or Z1-114 in the north, this could indicate that the structural influences on the hydrocarbon entrapment are not highly effective while the stratigraphic play has the strongest contribution on the hydrocarbon trapping mechanism.

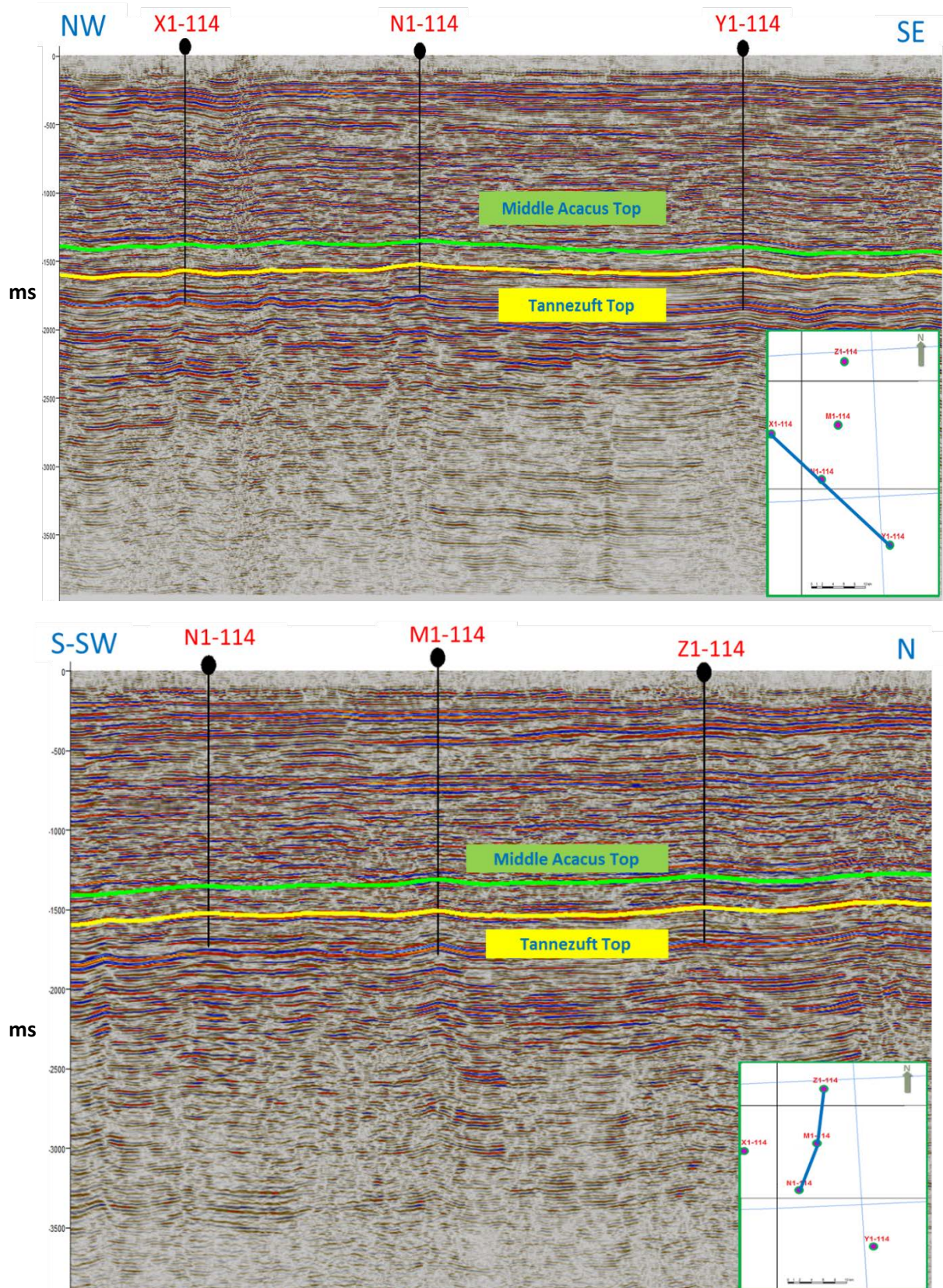


(Fig. 4.8): Composite seismic sections through wells in the study area (AGOCO, 2009).

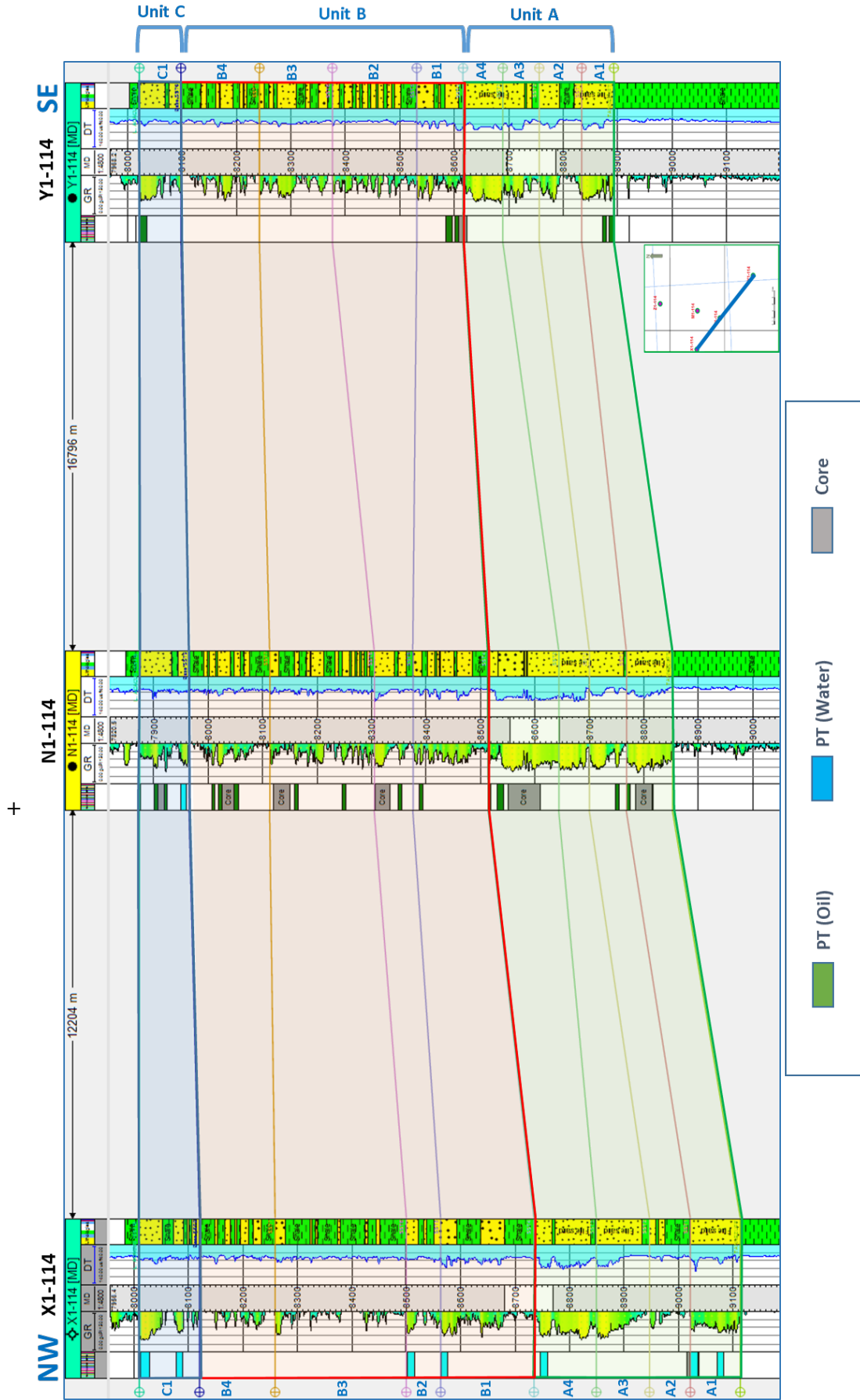


(Fig. 4.9): Stratigraphic cross section in SE-NW direction among wells (Y1-114, N1-114, and X1-114).



(Fig. 4.10): Stratigraphic cross section in SSW-N direction among wells (N1-114, M1-114, and Z1-114).



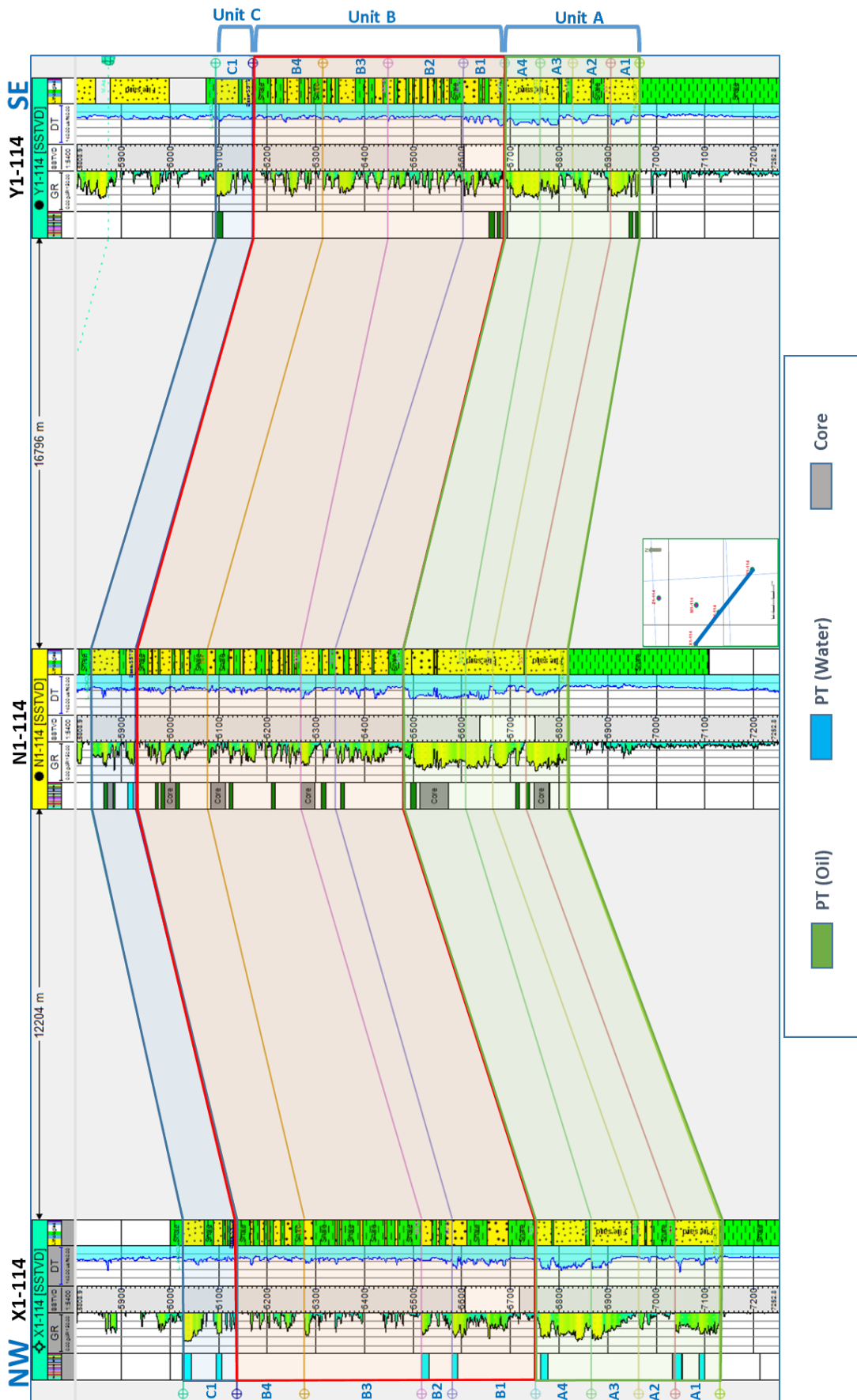


(Fig. 4.1): Structural cross section in SE-NW direction among wells (Y1-114, N1-114, and X1-114).

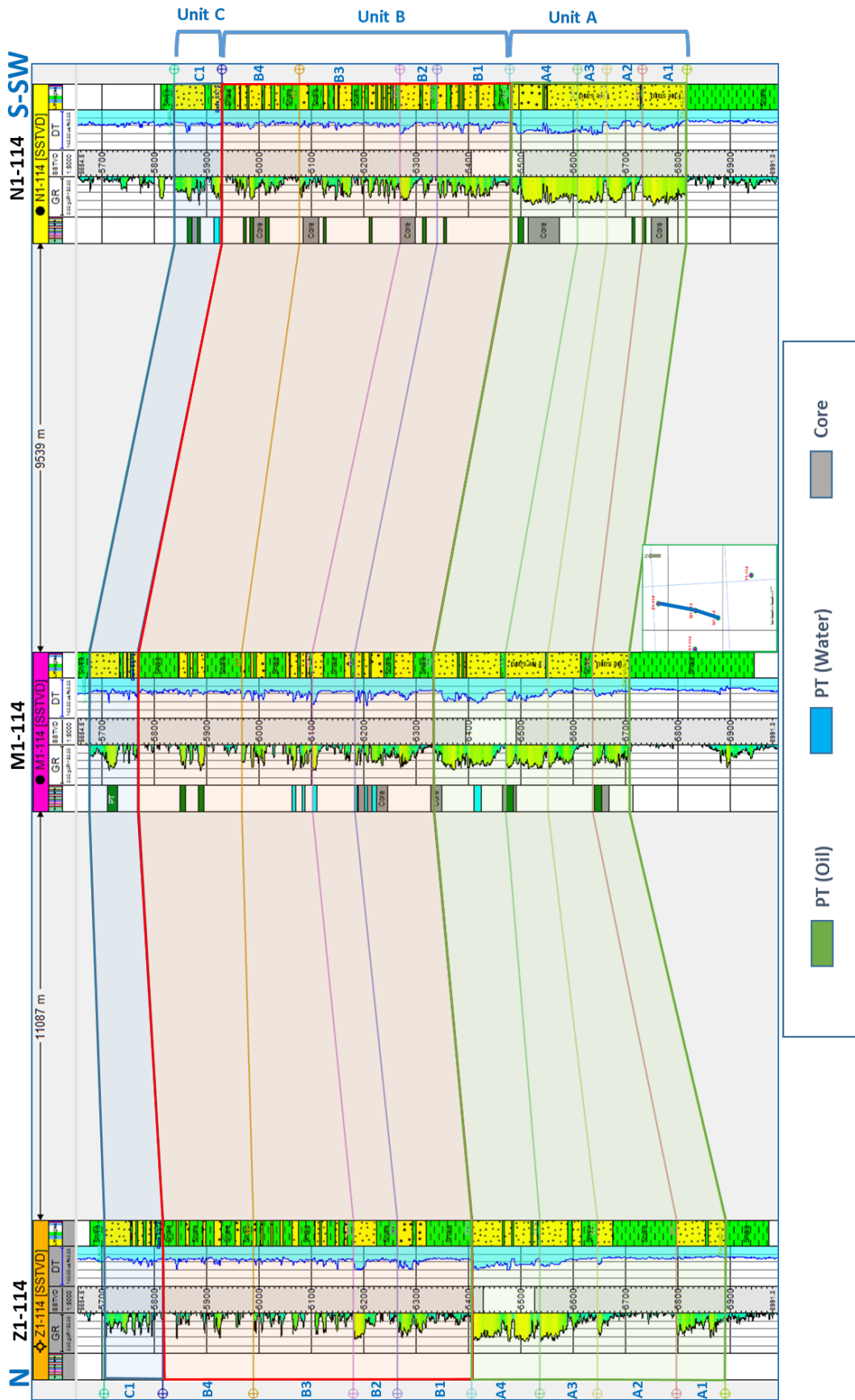


(Fig. 4.12): Structural cross section in SSW-N direction among wells (N1-114, M1-114, and Z1-114).

## **Chapter Five**

### **Subsurface Facies Analysis**

#### **5.1 Introduction**

Facies is a body of rock with specified characteristics which can be any observable attribute of rocks such as their overall appearance, composition, or condition of formation, and the changes that may occur in those attributes over a geographic area (Reading, 1996). Yet, sedimentary facies are bodies of sediment that are recognizably distinct from adjacent sediments that resulted from different depositional environments (Reading, 1996). Sedimentary structures are important attributes of sedimentary rocks and they indicate original position of strata in geologically complex terrains as well as reveal the depositional environment of the sediment. They occur on the upper and lower surfaces of beds as well as within beds. They can be used to deduce the processes and conditions of deposition, the directions of the currents that deposited the sediments, and in areas of folded rocks, the way-up of the strata (Tucker 2003). The sedimentary structures that are observed in borehole images are diverse. Some of the easiest to discern occur at bed boundaries, typically between sand and mud, as these lithofacies usually have very different electrical conductivity. Similarly, internal fabric is most readily observed when clasts and matrix have contrasting conductivities. Many structures internal to a bed such as fining-up grading or cross-bedding are more difficult to resolve because there is a smaller conductivity contrast between the bed constituents in these deposits.

As Lower Acacus sandstones were deposited on a low gradient ramp platform with occurrence of a large number of coalescing sandstone bars forming sedimentary bodies, which could be arranged in tabular sheets for tens of kilometers. These bodies may be separated laterally by fine-grained facies better developed in the offshore domain. This implies that the individual sandy bodies are not correlatable over large distances (Arduini et al., 2003). Geological descriptions of the imaged cores are not available and the images covered a limited number of wells with irregularly distribution across the Lower Acacus sub-layers. Therefore, the core data was insufficient for generating facies classification in all the wells. Nevertheless, they will be used to support and improve the FMI analysis, as it is easier to recognize sedimentary structures on cores. Consequently, the entire facies breakdown will be based on FMI analysis as it covers the entire section of Lower Acacus reservoir. To interpret these variations in terms of sedimentary structures and lithofacies

types, calibration with real rock is needed. Donselaar and Schmidt (2005) recommended calibration of the image logs with the corresponding outcrop rocks or cores in order to correctly recognize the sedimentary structures that are seen in the imaging tools. This reduces the uncertainty in the interpretation of the sedimentary features.

## **5.2 Imaging Tool**

Borehole imaging has been an integral part of logging programs for exploration well since long due to its application in deciphering the geological complexities. The sedimentological applications of the image logs have been in place since the dipmeter days as well. Borehole image tools such as Schlumberger's Fullbore formation MicroImager (FMI) is micro-electrical imaging tool that is based on dipmeter principle. The logs produce an oriented high-resolution image of the variations in micro-resistivity around borehole wall (Serra, 1989).

## **5.3 Schlumberger Fullbore MicroImager (FMI)**

The FMI tool generates high-resolution electrical images of the borehole using micro-resistivity measurements in water-base drilling mud systems. Two pads from each of the four tool arms are fitted with electrode arrays that measure variations in the formation micro-resistivity, giving eight imaging arrays in total. Each array has two rows of 12 button electrodes that give a vertical and horizontal data sampling of 0.2 inches (Fig. 5.1). A total of 192 electrodes are monitoring and responding to the resistivity variations within a small cylindrical portion of the borehole with high vertical variations. There is also a navigation system with accelerometers and magnetometers, which is also part of the FMI toolstring (Schlumberger, 2002). Therefore, in this research FMI log analysis were matched and correlated with the available core data in the study area.

## **5.4 Signal processing**

The data was processed at the Schlumberger data services center. The main objective has been to provide a continuous log of formation structure in the form of interpreted dip results and near-wellbore images. Microresistivity variations recorded by the tool are converted into color images after speed correction, depth alignment, electrode equalization and 'static' normalization using a histogram equalization technique (Fig 5.2).

Further contrast enhancement was achieved using a sliding 2 ft normalization window to produce the ‘dynamic’ images.

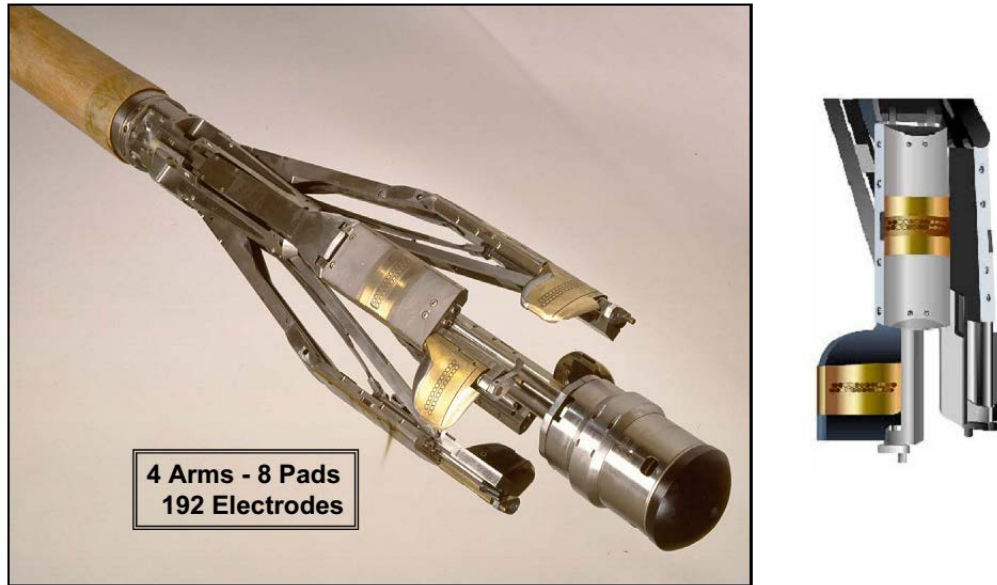


(Fig. 5.1): FMI tool shape and design (Schlumberger, 2002)

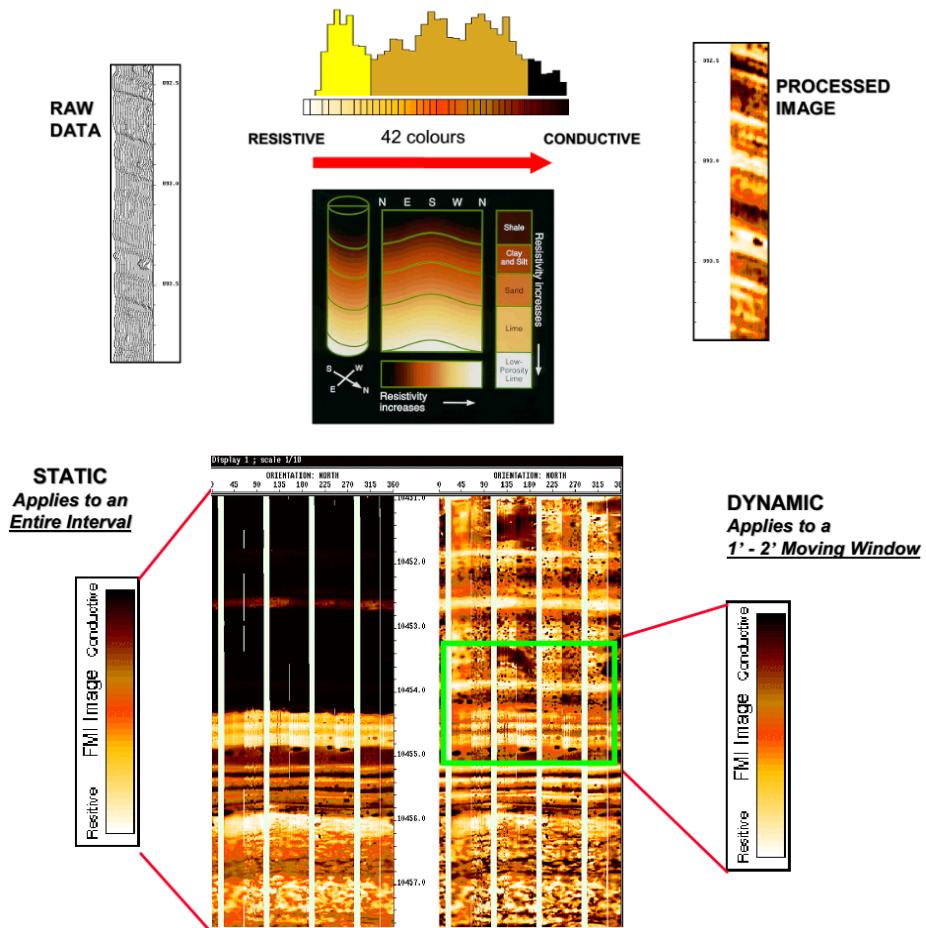






(Fig. 5.2): FMI Standard processing parameters (Schlumberger, 2002)

## 5.5 Geological Classification of Image Features

The dip data extracted from the geological log images was obtained interactively using a workstation Techlog software. Surfaces intersecting the well were manually traced and assigned to one of the following color coded dip categories in the table below:

(Table, 5.1): symbols of geological features on the image log

Dip Type	Symbol	Description	Comments
Bedding		Planar surfaces between lithologies and/or common in argillaceous rocks.	Used for structural determination
Cross Bedding		Coherent sets of sedimentary structure within grain dominated lithologies. Lithology dependent	Indicative of the paleo-transport direction.
Set Boundary		The upper and lower bounding surfaces of cross bedding set except if the surface is erosional	Indicator of sedimentary package architecture.
Erosional Surface		Surfaces in which clear signs of erosion is detected (abrupt change in dip pattern)	They could be interpreted as scour surface or reactivation surface

## 5.6 Image Integration Using Core Data

Because of possible ambiguity such as very short lines or irregular, noisy images, some features are difficult to interpret even with the help of the other open hole logs. Calibration against core observation is needed in this setting (Serra, 1989). The fundamental benefit of core/log image integration is that it builds an understanding of the geology around the well. Once calibration to core indicate an appropriate result, same features outside the core interval could be interpreted with more confidence. According to the observation of the core images, the facies identified in the Lower Acacus reservoir is correlated and calibrated with FMI image log to best determine the main facies within the reservoir interval, which includes (Shale facies, shaly-sand facies, heterolithic bedding facies, and cross bedding sandstone facies). These facies could reflect the depositional setting of the target reservoir in which shale facies represent the lowest energy setting, and it progresses through shaly-sand facies to higher energy with abundance of cross bedding sandstone,

while the heterolithic bedding is a good indicator of tidal activity supported by some bidirectional cross bedding. However, if erosional surfaces were associated with fining upward sequences they shall be considered as scour surface while in the coarsening upward sequences they might be considered as reactivation surfaces especially when associated with the bidirectional cross bedding.

### **5.6.1 Shale facies**

Shale facies is widely distributed in the study area notably from the middle upward and it represents non-reservoir facies. It could be both deep and shallow marine (period of energy loss) settings. In the targeted wells, it is usually laminated and associated with few lenses of sandstone (Fig. 5.3). This shale usually interbedding with the heterolithic facies, which might indicate some periods of marine flooding. In the study area, shale layers on FMI log appears as a bright color (resistive layers contradictory to the common situation). Some dark spots associated with this facies may characterize bioturbation with variable abundance. In the study area Shale facies deposited in flat sheets with low dipping ( $2 - 6^\circ$ ) which is ideal for local structural dip determination. Moreover, in order to see the very thin layer of sand and shale, a new technique in Techlog Software called (Sand Counting) is used to define the sand intervals using the resistivity response of the FMI tool. In the resulted track three lithology are created; shale in green, silt in orange, and sand in yellow.

### **5.6.2 Shaly-Sand (Silty) Bedding Facies**

The shaly-sand bedding facies is quite dominated within the study area, and it represents a transitional period between sand and shale depositional setting. It rarely represents reservoir sections and therefore no cores were cut in these facies. Moreover, GR reads around 100 API, and as a result it is grouped into shale facies when using conventional logging. It is occasionally thinly bedded, in which the image log appears in shade of yellow between black and bright color, and usually bioturbated (Fig. 5.4).

### **5.6.3 Cross Bedding (Lamination) Sandstone Facies**

The red color code was used for sedimentary planar features identified within sandstone (low - medium GR) characterized by higher dip magnitudes than structural beds (generally  $10-25^\circ$ ) and varying or consistent azimuths (Fig. 5.5). Cross bedding were deposited in a high energy environment and are indicators of the direction of sediment

transport “paleocurrent”. The variation of their magnitudes and azimuths provides clues on the energy level of sediment transport and the sinuosity of the currents. Moreover, the increase in dip magnitudes usually reflect the increase of the energy-level, especially if they associated with upward increase in the log motif indicating a probable prograding delta. Additionally, when two population of laminae dip abruptly and practically in opposite direction, they indicate bimodal direction of the current. This kind of feature is typical of sediments deposited under tidal action (Serra, 1989). This facies deposited in high-energy setting and represents the best reservoir quality.

#### **5.6.4 Heterolithic Bedding (include wavy, flaser and lenticular)**

Heterolithics are thin alternations of sand/shale or sand/silt or silt/shale. They are formed mainly in tidal flats and found extensively throughout the wells. Mud content varies, with a combination of muddy Heterolithics (lenticular bedding) with some clay drapes which often reworked into elongate mudclasts. If mud and sand deposits are equal, wavy bedding is produced, while flaser bedding is characterized by dominant of sandstone layers with thin shale or mud drapes. These three types of bedding will be considered as one facies, as it is hard to be distinguished between them in the FMI log (Fig. 5.6). These facies are usually setting where fluctuating currents or sediment supply permit the deposition of both sand and mud, which is a good tidal signature along with the abundant mud drapes and bidirectional cross stratifications (Kreisa and Moiola, 1986). It appears as white and dark zones join on the images as lenses of more conductive (dark) or resistive (white) material.

The vertical association of these facies in conjunction with paleocurrent direction are gathered to delineate the genetically related facies into specific cycles. The vertical stacked of these cycles will be correlated laterally to define the possible depositional settings. However, the deltaic successions will overall shallow upward, but the contribution of the tidal processes could show some fining and blocky sequences especially when tidal channels dominated.



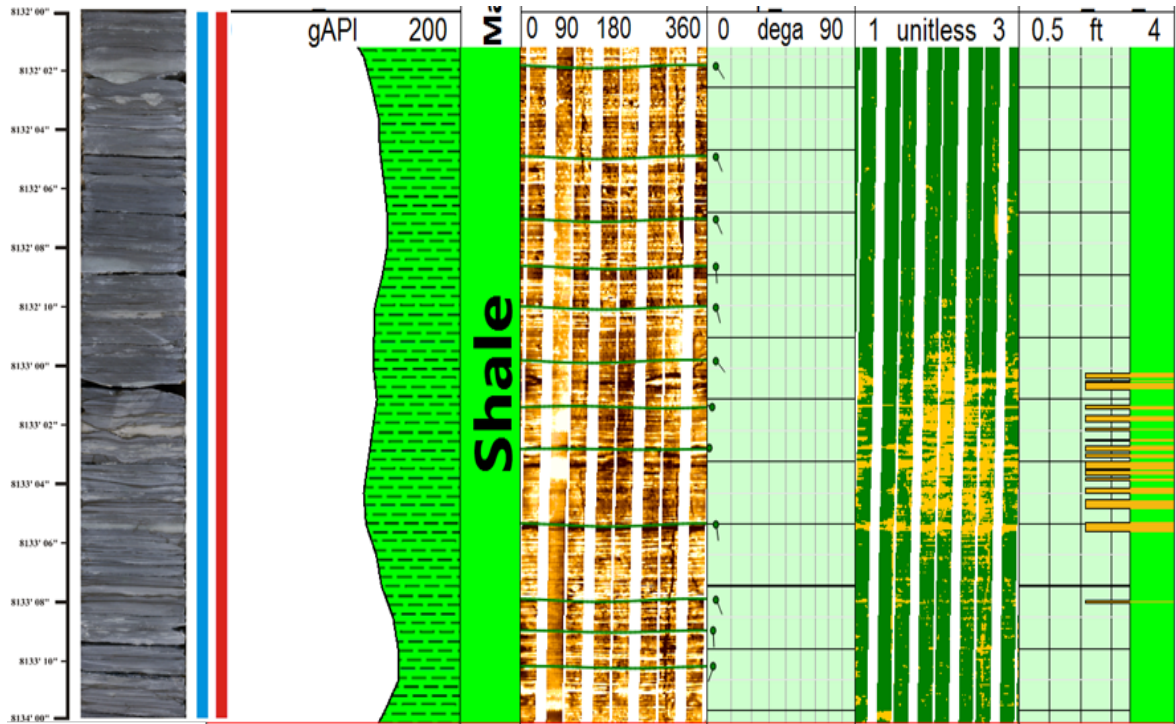


(Fig. 5.3): Shale Facies compared to core image, Core#4 in N1-114.

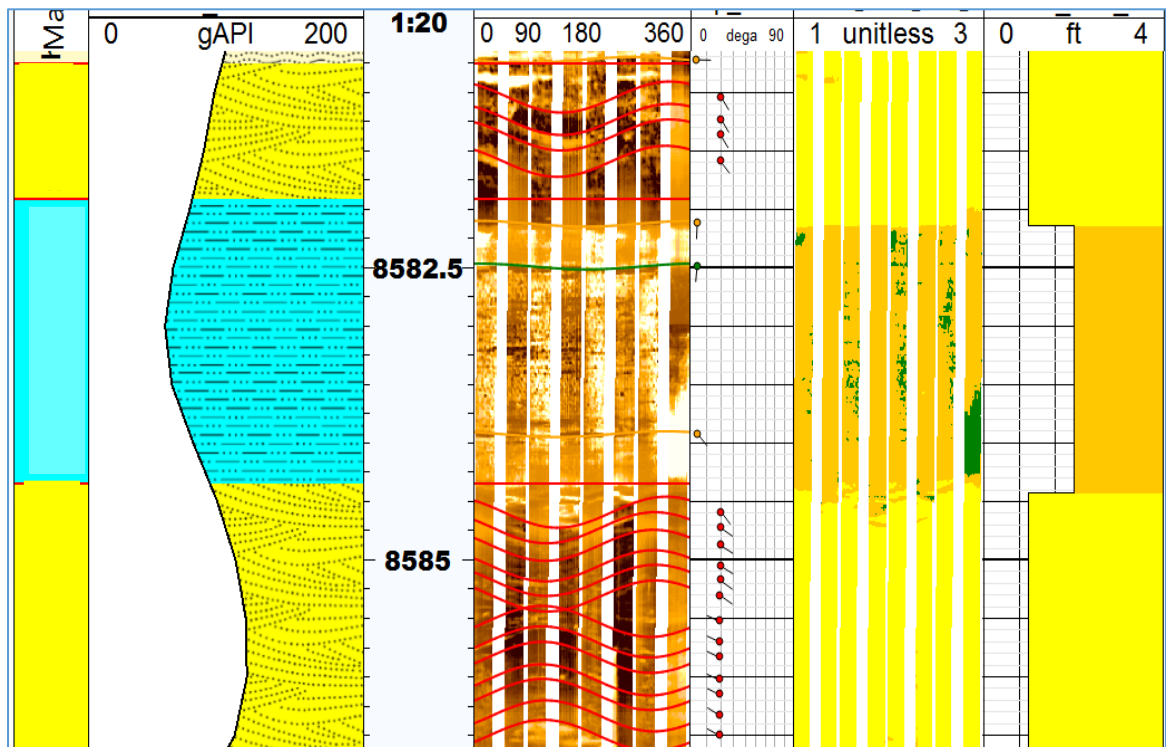


(Fig. 5.4): Shaly-Sand Facies bounded by two cross bedding units.

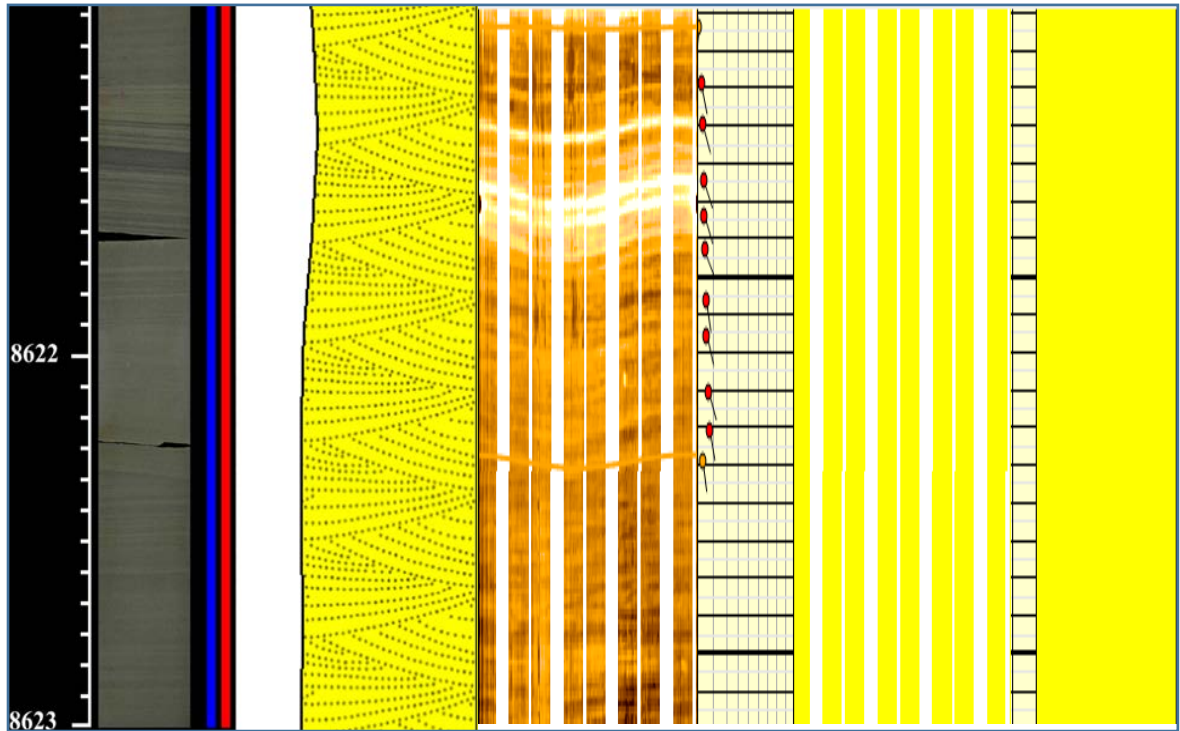


(Fig. 5.5): Cross-bedding Facies compared to core image, Core#3 in Y1-114.

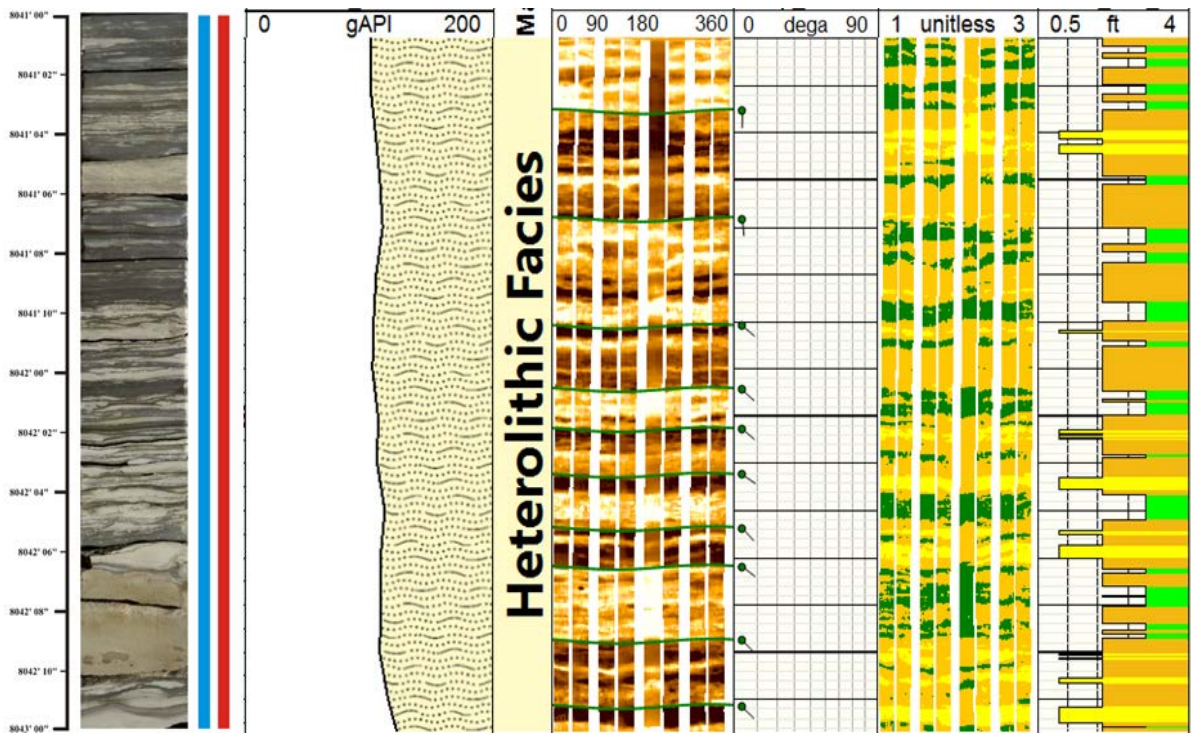


(Fig. 5.6): Heterolithic Bedding Facies compared to core image, Core#4 in N1-114.

## 5.7 FMI Interpretation

The FMI data has been fully interpreted in three wells (N1, X1, and Y1-114) in the study area to determine the main facies within Lower Acacus reservoir. The high resolution of the tool assists in the facies distinctions and added more details to the internal reservoir architecture, allowing detailed description of various units.

### 5.7.1 FMI Analysis of N1-114 well

The reservoir is mainly comprised of clastic sequences (sandstone, siltstone and shale facies). The interpreted FMI interval between (7873 – 8852 ft) revealed different facies within the reservoir, and cores image helps to better define the determined facies. The cross-bedding and heterolithic bedding represent the majority facies, while shale and shale sand facies are less dominate.

The reservoir shows variations in the sequence patterns from coarsening to fining upwards as well as changes in the sedimentary structures and nature of paleoflow. Sedimentary features and paleocurrent type and direction were used to indicate the possible environmental setting within the Lower Acacus reservoir. As an example, blocky to fining upward sequence composed of bidirectional cross-bedding, heterolithic bedding and some erosional surfaces may indicate deposition within a possible subtidal channel. On the other hand, the cross-bedding coarsening upward sequences shall indicate deltaic (coastal) dominating intervals.

Normally, in the study area the Lower Acacus reservoir sectioned into three main units (as shown in chapter three):

- The sandstone dominated unit (Unit A) between 8852 – 8514 ft, mainly characterized by blocky to coarsening upward sequence with highly dominated cross bedding facies around 45% (Fig. 5.7a). The clear blocky trend with a strong unimodal dip azimuth (Fig. 5.7b), shall indicate a distributary mouth bar depositional setting. The analysis of the structural bedding shows that the overall structural dip is around  $4^{\circ}$  which indicate that the bedding was subjected to negligible structural tectonic. On the other hand, the paleocurrent analysis indicates that the cross beddings exhibit low to medium dip angles with a clear uni-modal direction towards SE (Fig. 5.7c), pointing to the paleo flow direction (sediments source). This unit could be subdivided into four subunits as shown in chapter four, (A1, A2, A3, and A4) and each of them possess more than sandstone interval.

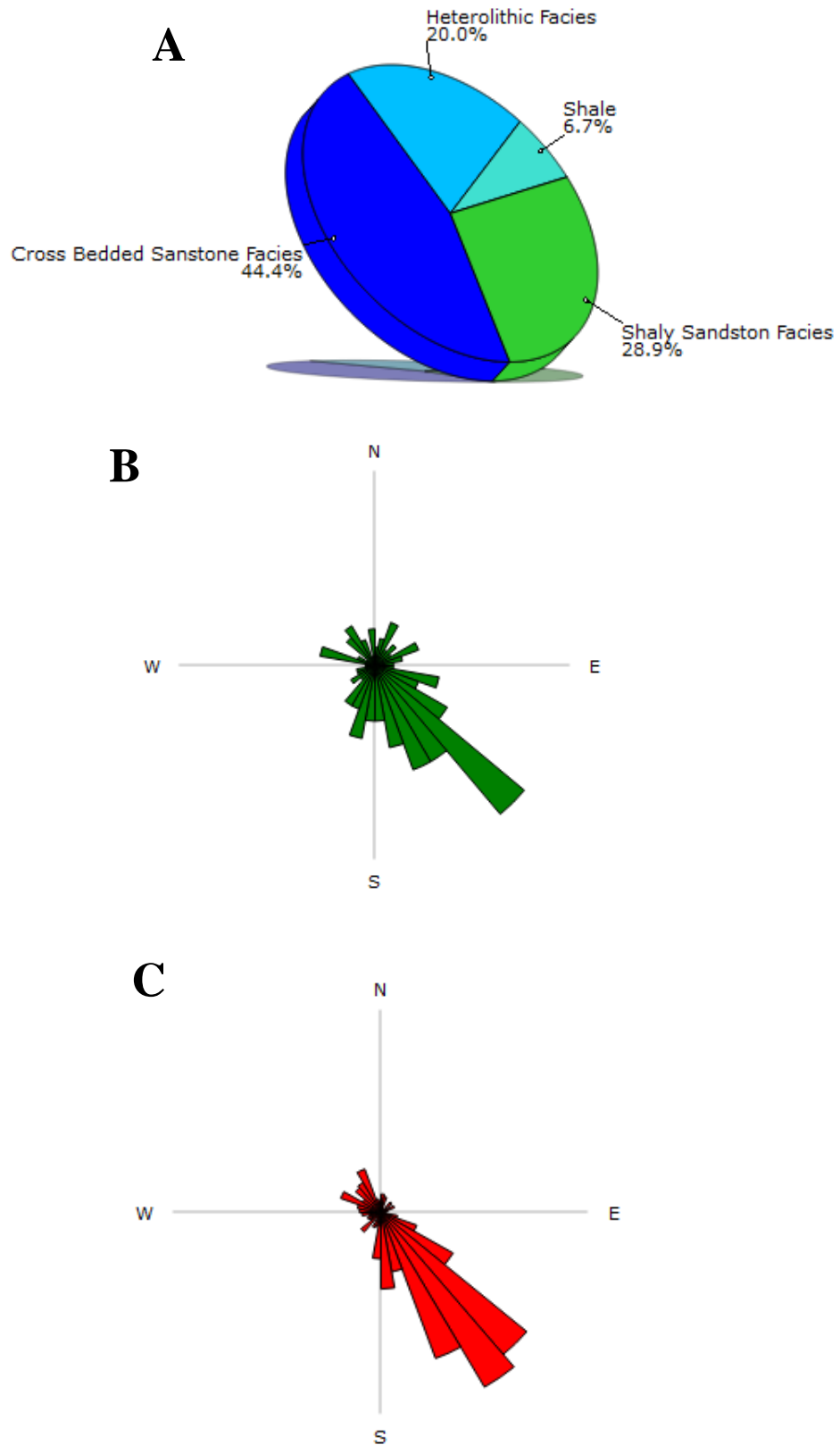


(Fig. 5.7): (A) Facies distribution in, (B) dip azimuth major trend of the structural bedding, (C) major trend of the Paleocurrent of Cross-bedding, all for Unit A of Well N1-114.

- A1 subunit: represent around 75 ft of blocky GR that consist of alteration of cross bedding and heterolithic bedding associated with some erosional surface that could represent the feeder (distributary) channels of the prograding delta. Some oil and gas production come from the heterolithic bedding facies at the top of this unit (Fig. 5.8).

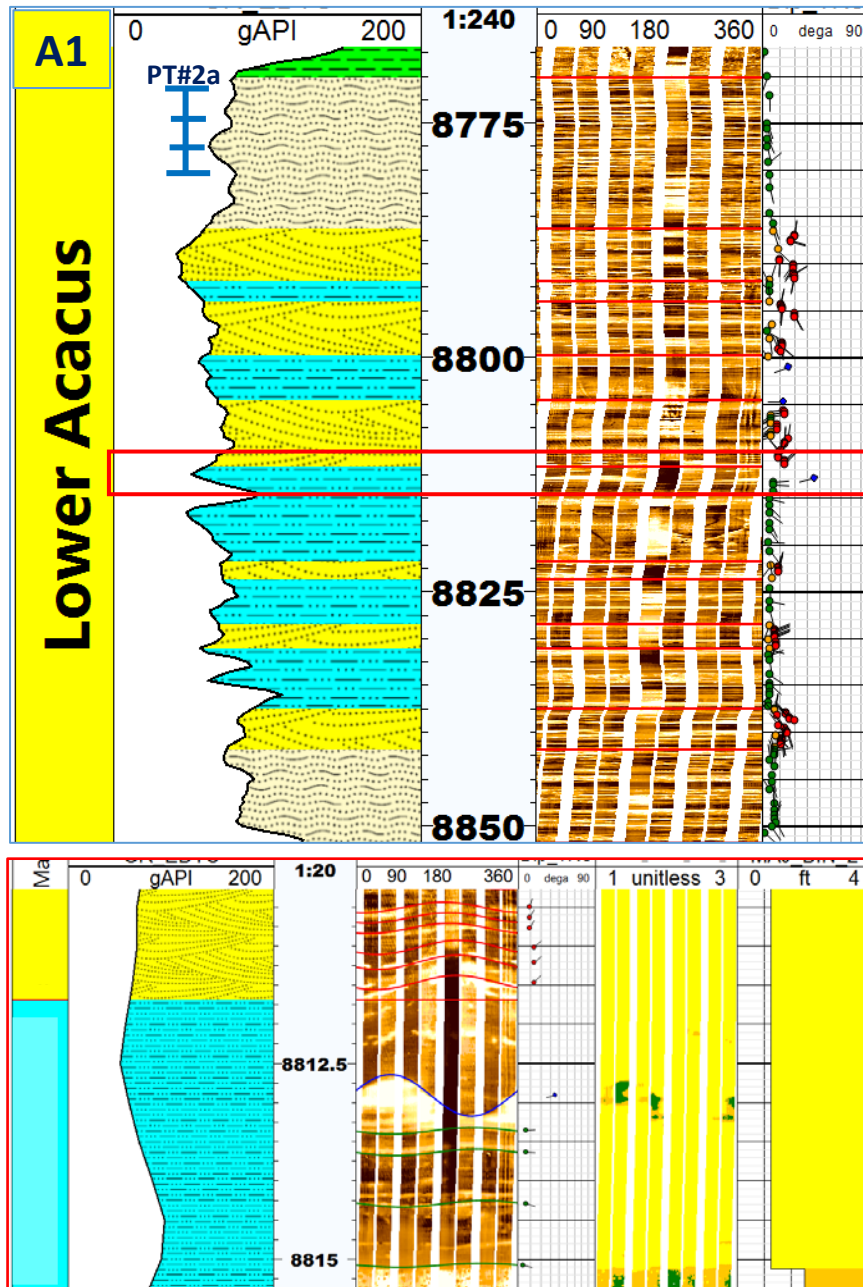


(Fig. 5.8): The facies distribution within Unit A1, Red Box represent a Zoom-in into the blocky GR sand body, in which the erosional surface is clear.

- A2 subunit: composed of two coarsening upward sand interval that is well cross bedded which is typical of prograding deltaic (coastal) deposits, with less effect of tidal processes. The lower delta is highly productive as proven from production test with increase in cross bedding thickness upward, while the upper prograding coarsening was eventually followed by fining upward sequence, which might indicate channel cut especially with evidence of erosional surface (Fig. 5.9).

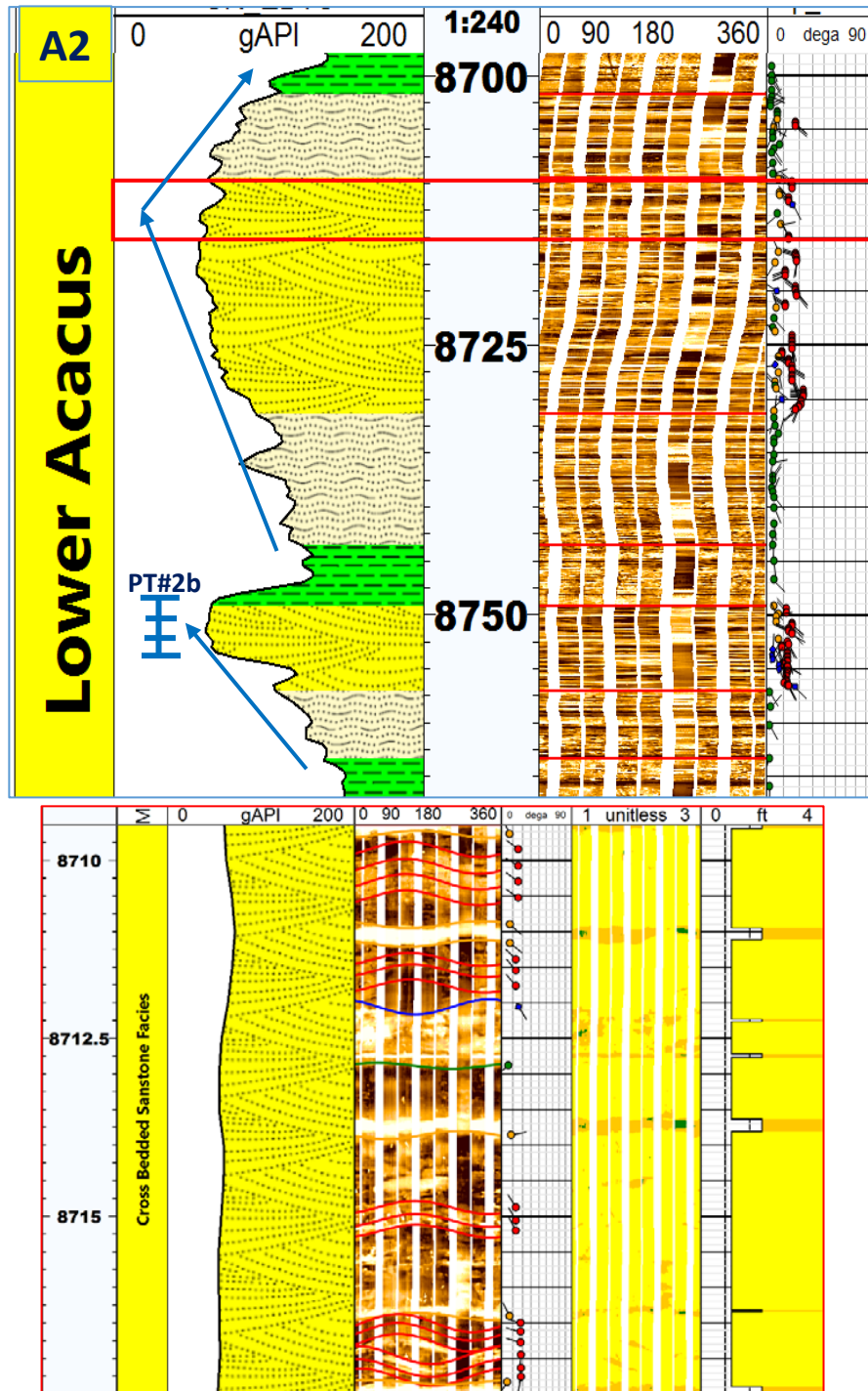


(Fig. 5.9): The facies distribution within Unit A2, Red Box represent a Zoom-in into the cross bedding facies that mainly dips opposite to the major dipping trend.

- A3 subunit: represent around 95 ft of blocky GR that consist mainly of unimodal cross bedding sandstone dipping toward SE. The thick blocky cross bedding could represent sequences of multi distributary mouth bar as uniform reading dips shall indicate an aggradation stage of deposition (Fig. 5.10).

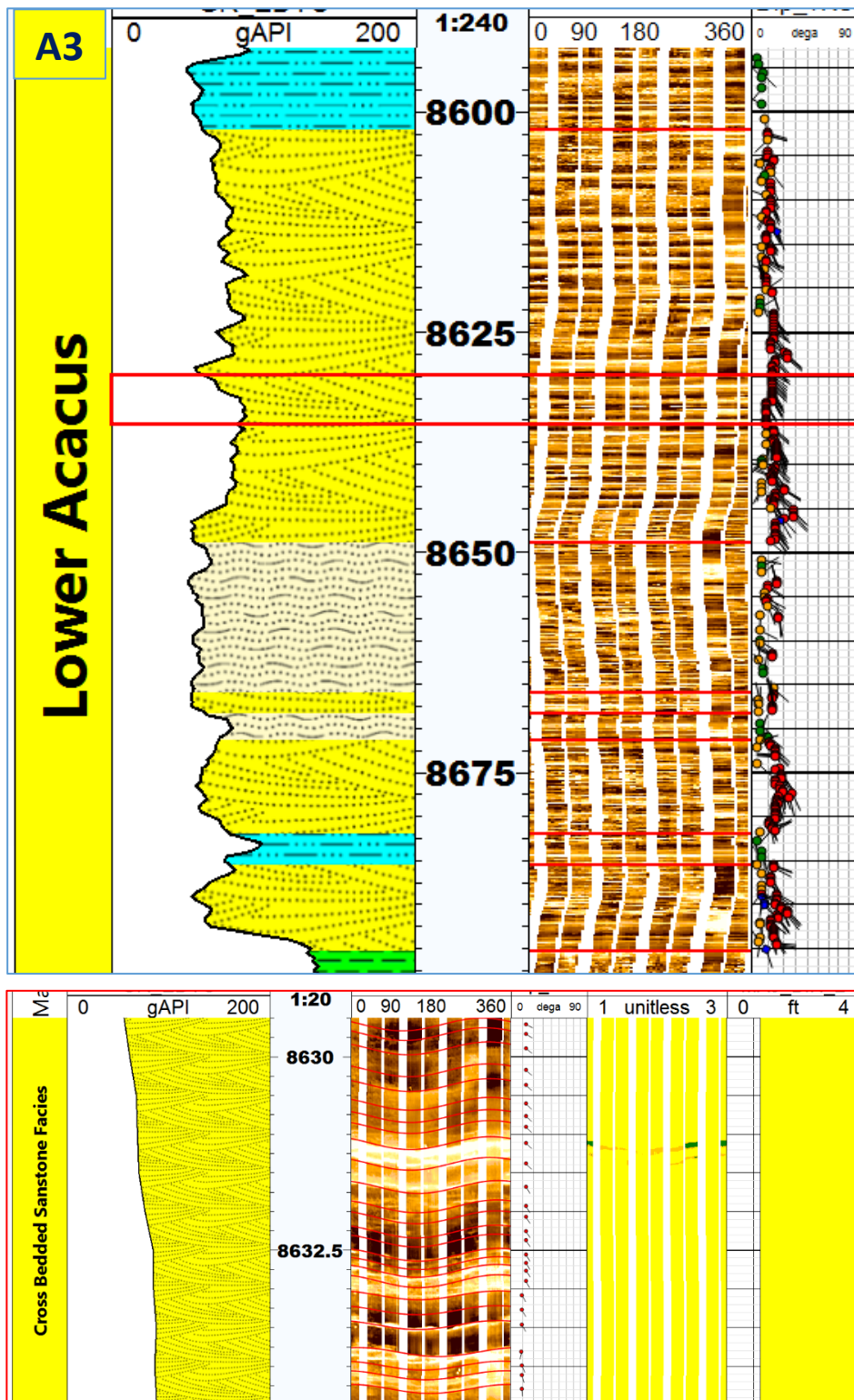


(Fig. 5.10): The facies distribution within Unit A3, Red Box represent a Zoom-in into the cross bedding facies, in which the unimodal trend is clear toward SE.

- A4 subunit: represent around 75 ft of blocky GR with clear indicating of paleo-flow direction towards SE, and fewer towards NW. This subunit consists of alteration of cross bedding and heterolithic bedding associated with some shaly-sand bedding facies especially at the top of this unit that is actually produced some oil and gas (Fig. 5.11).

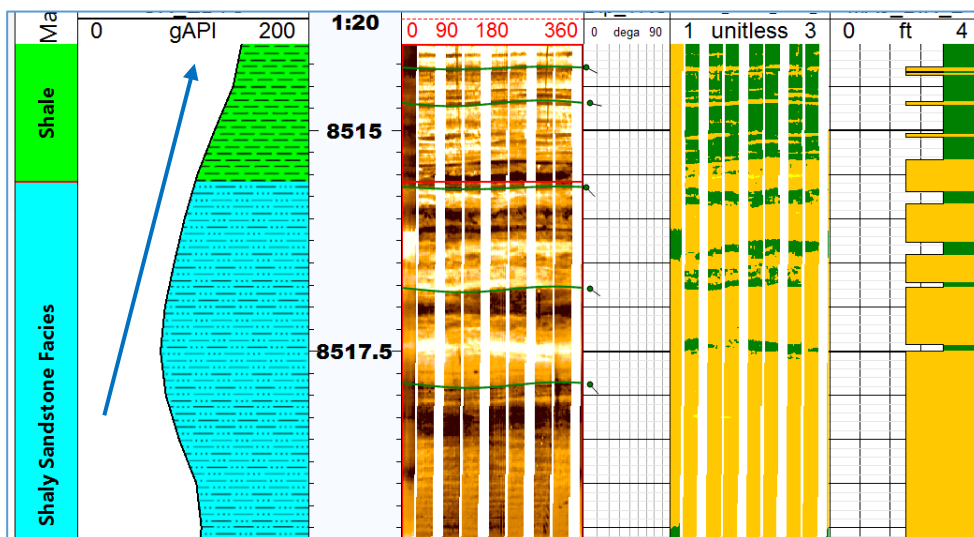
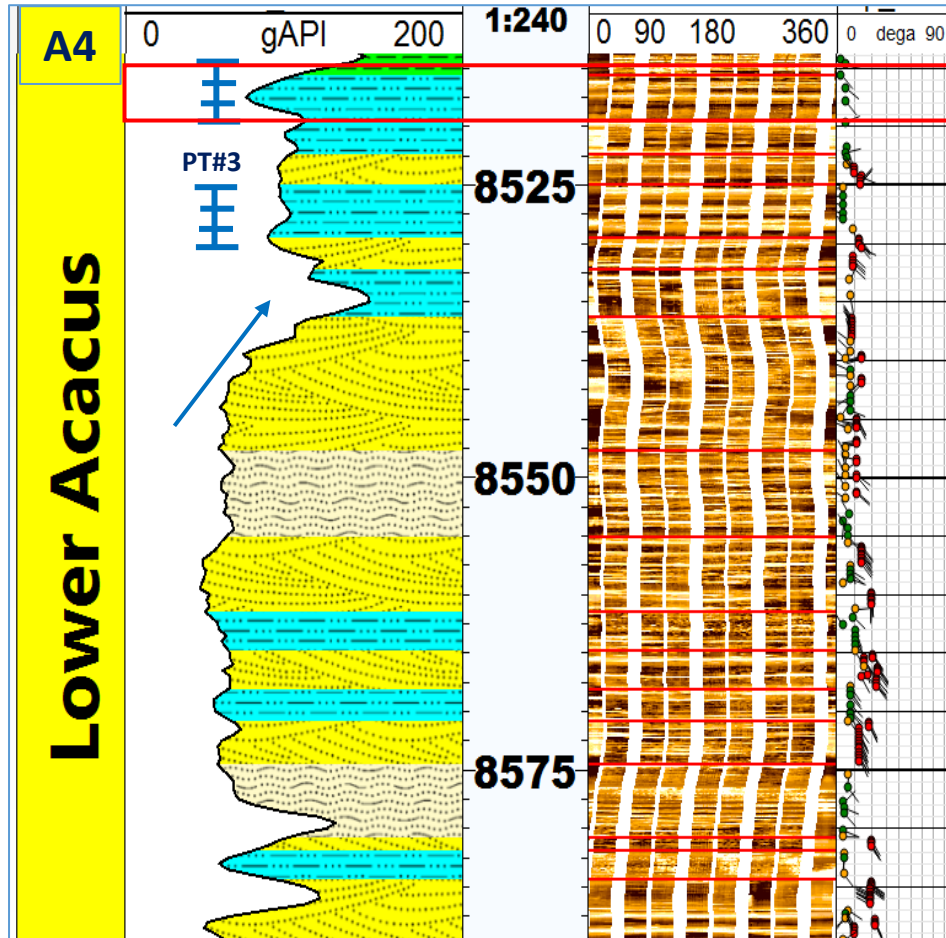


(Fig. 5.11): The facies distribution within Unit A4, Red Box represent a Zoom-in into the reservoir in which silty sand layers is productive.



- Unit B between 8514 – 7965 ft, mainly characterized by shale-sand interbedding with domination of the heterolithic bedding facies (37%) as in (Fig. 5.12a) that is usually associated with fining upward sequence. On the other hand, around thirteen coarsening upward sequences that were highly dominated by cross bedding facies (around 45%) represent the coastal delta depositional setting. The analysis of the structural bedding shows similar result to Unit A, with structural dip magnitude around  $5^{\circ}$  which indicates that the bedding was deposited on relatively flat setting dipping toward SE (Fig. 5.12b). On the other hand, the paleocurrent analysis shows that the cross beddings exhibit low to medium dip angles with a clear Bi-modal direction towards SE-NW, which is typical indicator to the effect of tidal processes (Fig. 5.12c). Equally, this unit could be subdivided into four subunits, (B1, B2, B3, and B4) and each of them possess more than sandstone interval.

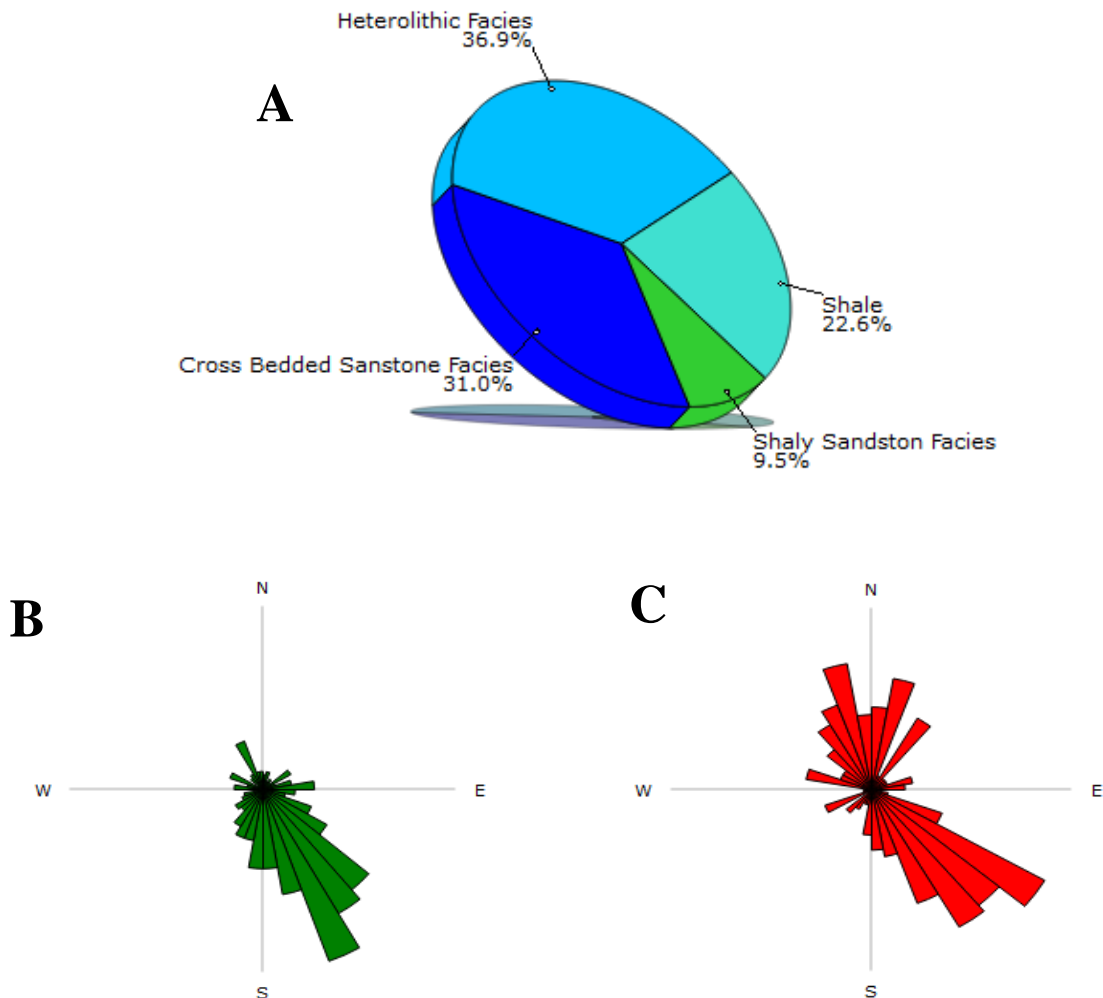


(Fig. 5.12): (A) Facies distribution in, (B) dip azimuth major trend of the structural bedding, (C) major trend of the Paleocurrent of Cross-bedding, all for Unit B of Well N1-114.

- B1 subunit: represent around 75 ft of blocky to kind of serrated GR that mainly consist of heterolithic bedding associated with less percentage of cross bedding and shaly-sand facies. Even though the cross bedding occurs in small sets, it indicates oblique bidirectional paleo-flow which is typical of tidal processes (Fig. 5.13).

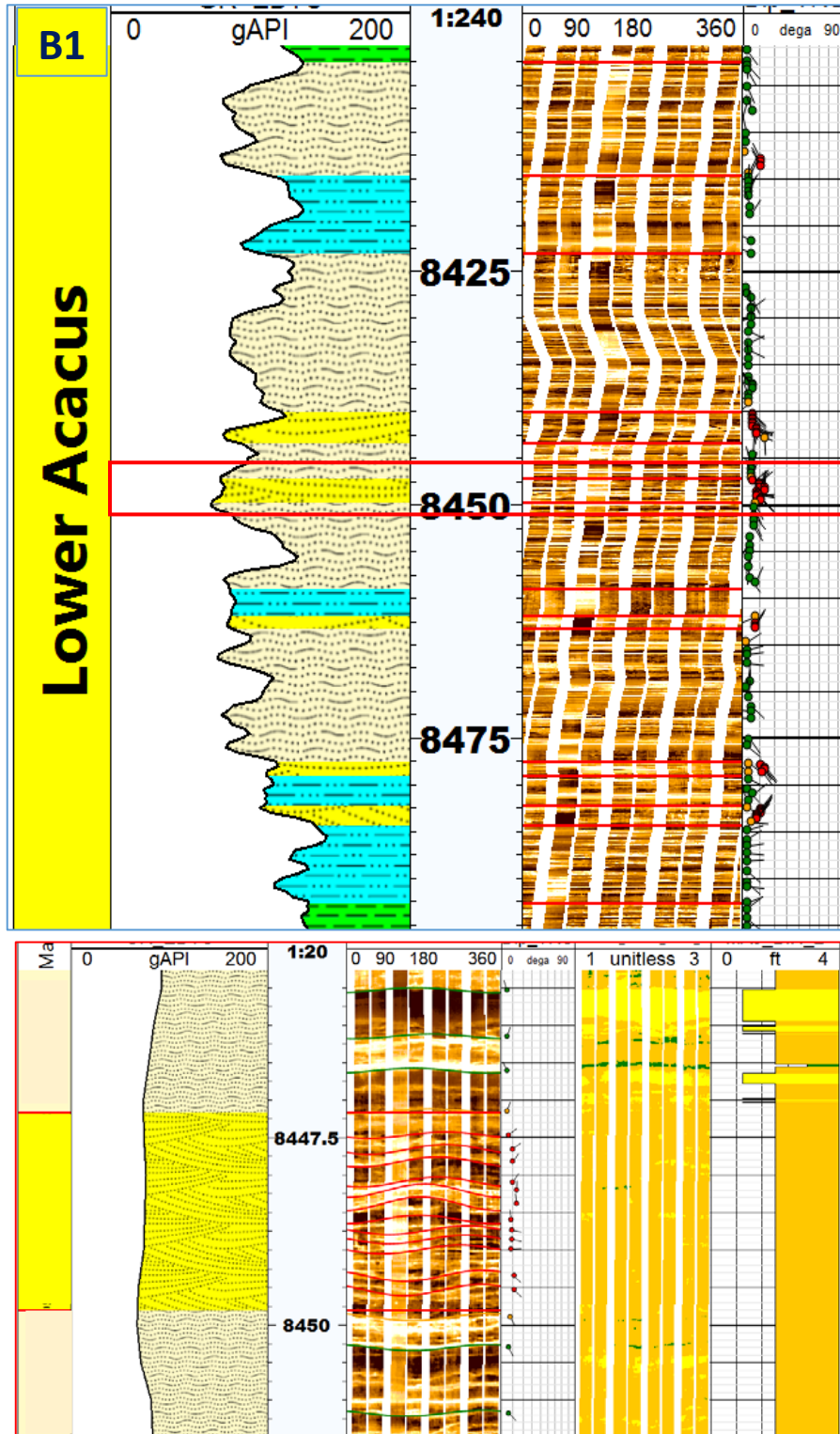


(Fig. 5.13): The facies distribution within Unit B1, Red Box represent a Zoom-in to the bidirectional cross bedding.

- B2 subunit: represent a thick interval around 105 ft that is actually composed of four coarsening upward sand interval that is eventually followed by fining upward sequences and separated by shale facies. This might be a good indicator of cyclicity in deposits with clear effect of tidal processes. It worth to say that the sand unit in the middle of two shale facies is highly saturated with oil as proven from production test (Fig. 5.14), signifying the stratigraphic influence on entrapment mechanism.

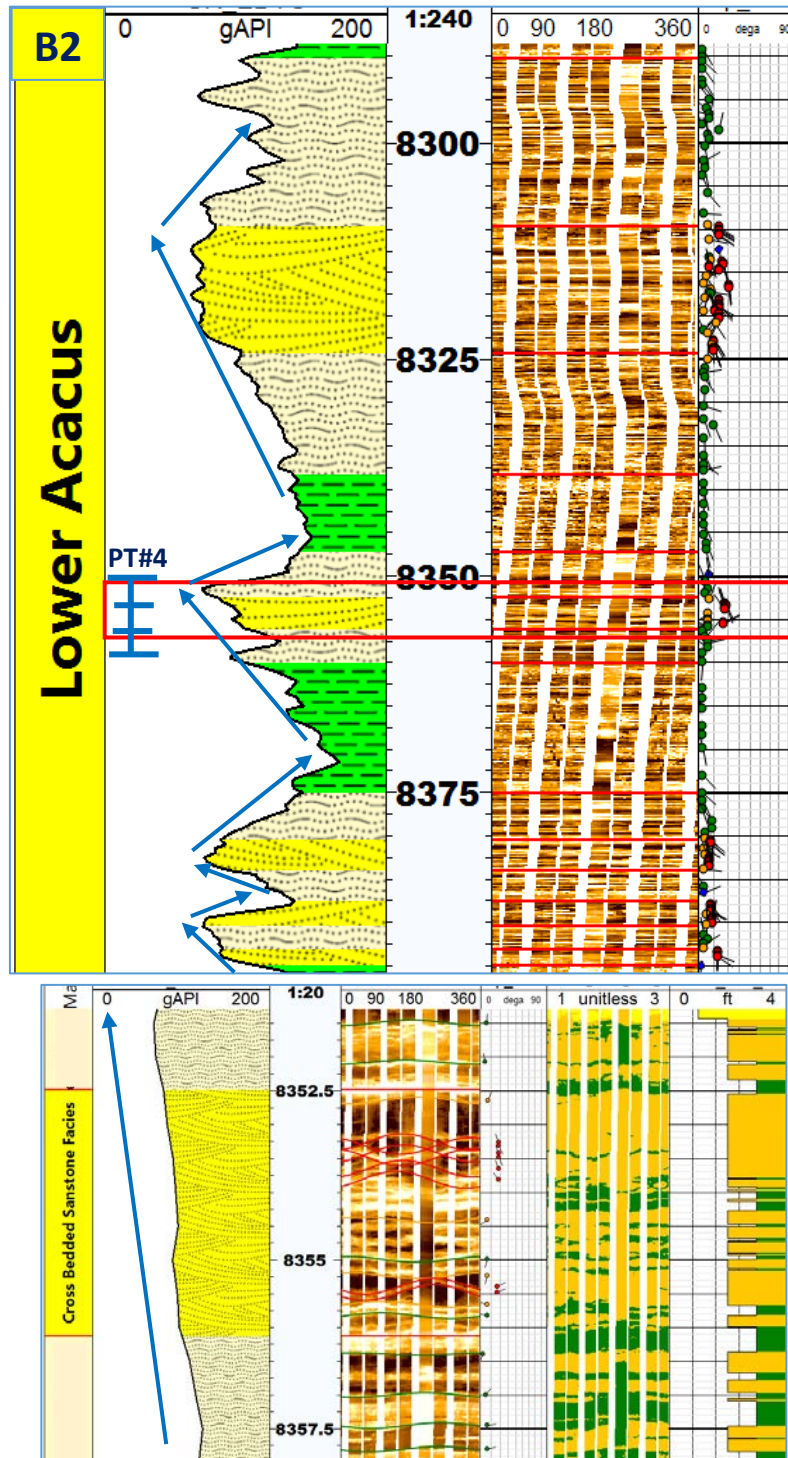


(Fig. 5.14): The facies distribution within Unit B2, Red Box represent a Zoom-in into the reservoir in which the cross bedding is clearly dipping in two directions.

- B3 subunit: represent around 100 ft composed of sand interval that is separated by shale facies with multi fining and coarsening upward sequences that is actually dominated by heterolithic facies with evidence of erosional surface. The top and bottom of this subunit are highly productive zones (Fig. 5.15).

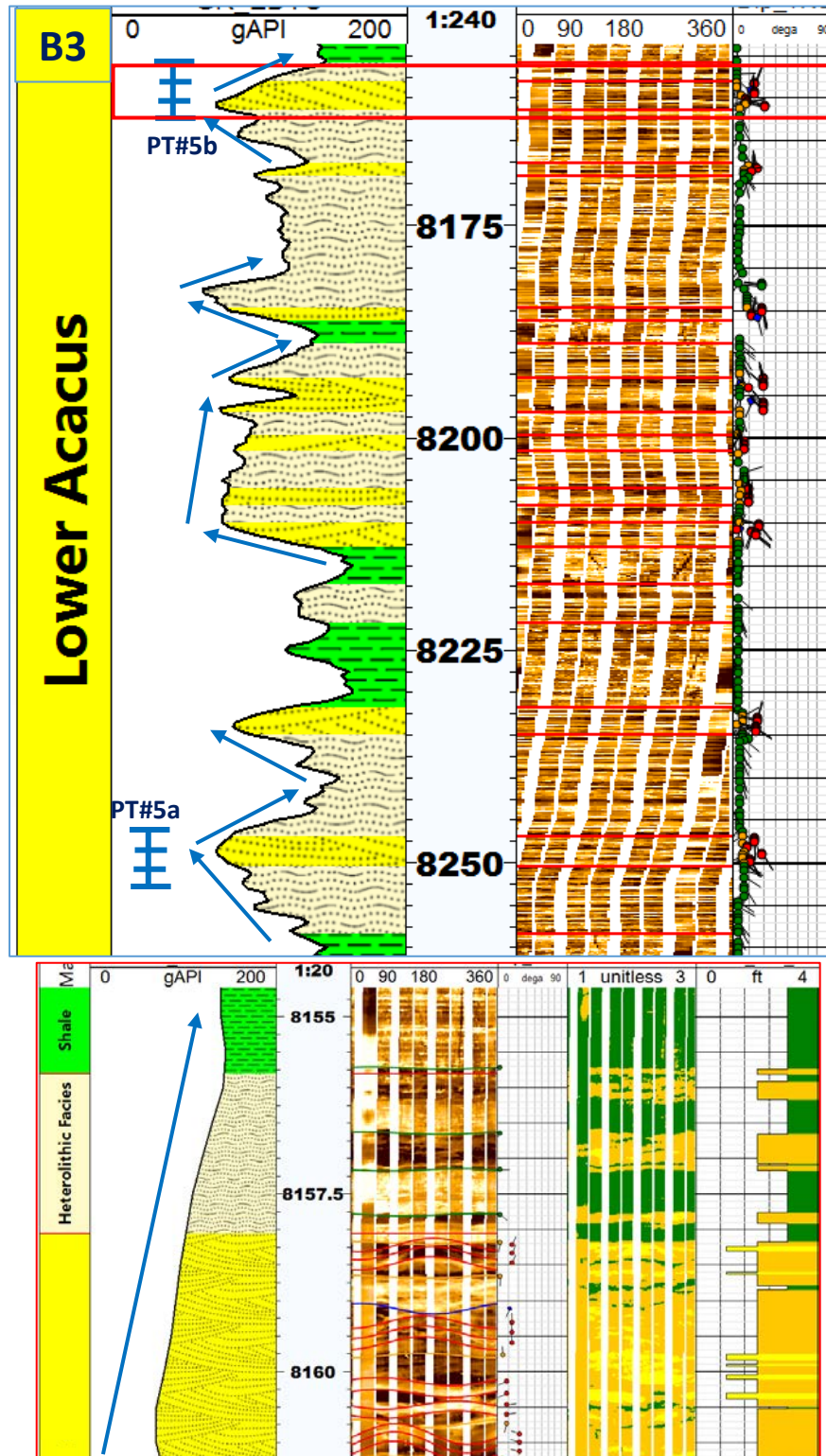


(Fig. 5.15): The facies distribution within Unit B3, Red Box represent a Zoom-in into the reservoir in which the bidirectional cross bedding and erosional surface is clear.

- B4 subunit: represent around 90 ft composed of multi coarsening and fining upward sequences that is separated by shale facies. This subunit is dominated by heterolithic facies and cross bedding, as the core image showed in (Fig. 5.16). However, this subunit is highly productive as it contains hydrocarbon within three different sand bodies.

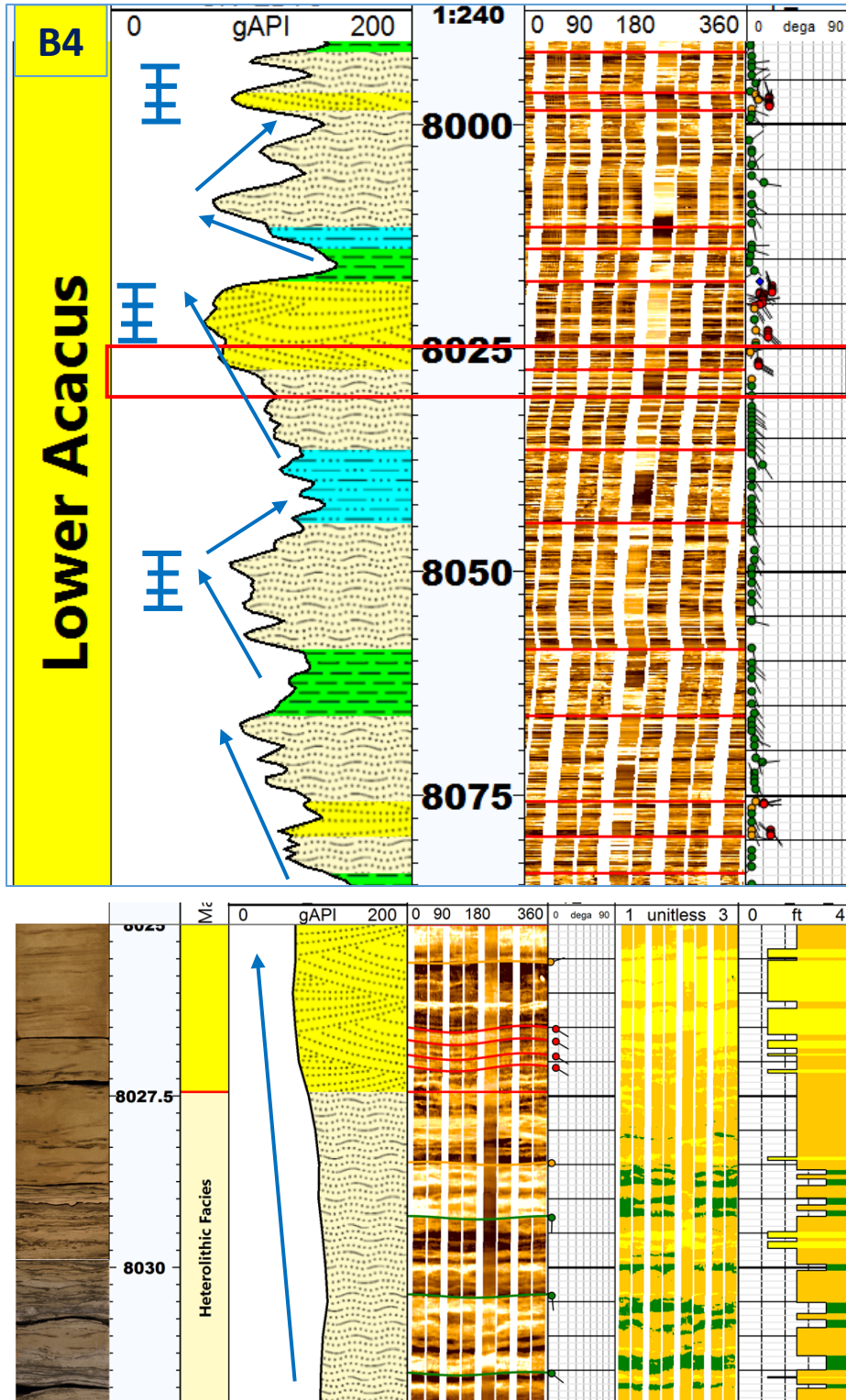


(Fig. 5.16): The facies distribution within Unit B4, Red Box represent a Zoom-in, in which the core image almost fitted with FMI image.

- Unit C between 7965 – 7873 ft, started with fining upward sand body followed by two coarsening upward sequences and capped by blocky heterolithic facies. The heterolithic bedding facies and cross bedding facies are equally ruled the unit with 35% each (Fig. 5.17a). The analysis of the structural bedding indicates low value mainly dipping toward the south (Fig. 5.17b), while the paleocurrent analysis shows dominate Bi-modal to somehow less poly-modal trend (Fig. 5.17c). The tide effect is present on these kind of coastal sandstone intervals, and the fining sand bodies are probably representing tidal channels especially with some indication of erosional surfaces. The unit mainly composed of three sand intervals, started with fining upward sequences followed by two coarsening up sequences and topped with kind of blocky heterolithic interval probably representing a tidal flat setting. Nevertheless, the three sequences produced oil and gas (Fig. 5.18).

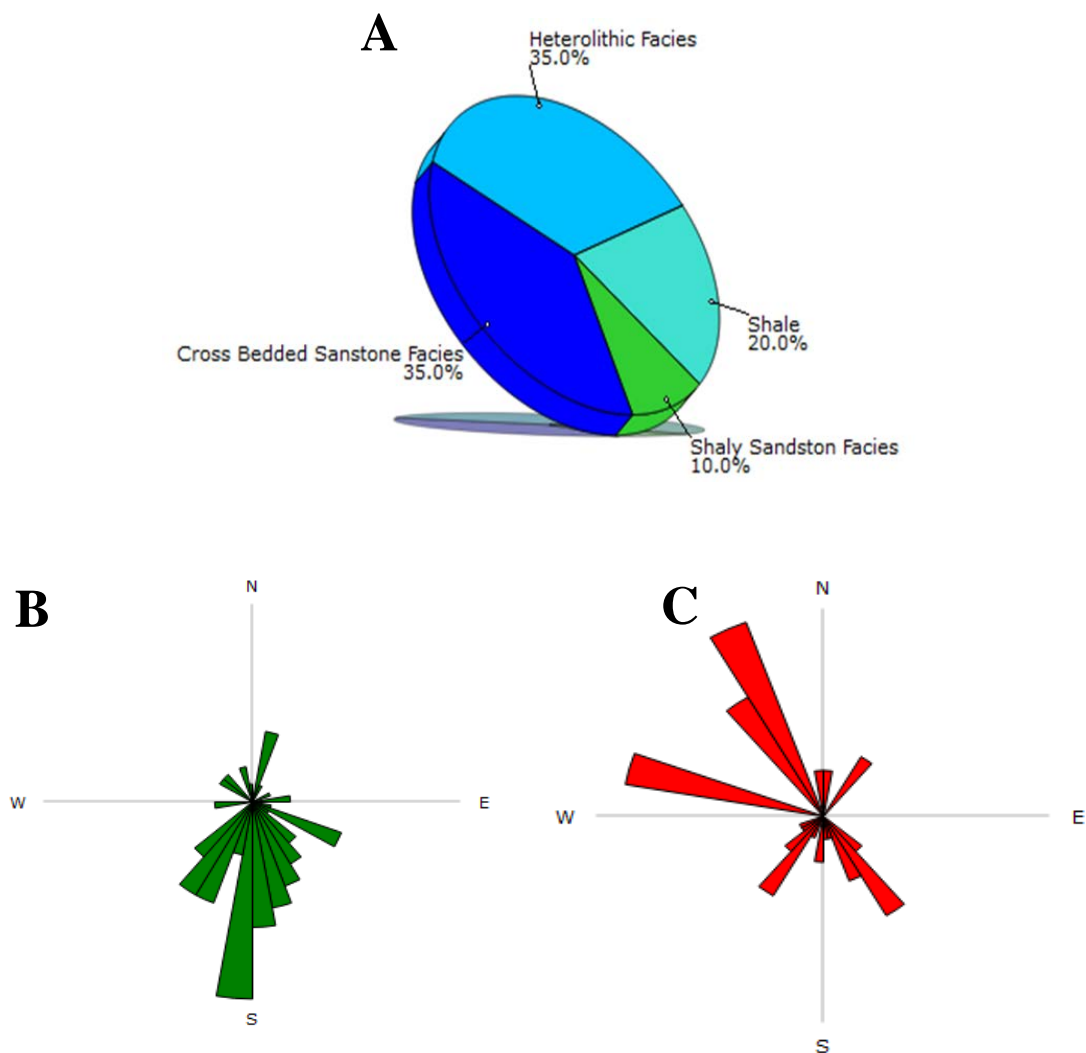


(Fig. 5.17): (A) Facies distribution in, (B) dip azimuth major trend of the structural bedding, (C) major trend of the Paleocurrent of Cross-bedding, all for Unit C of Well N1-114.

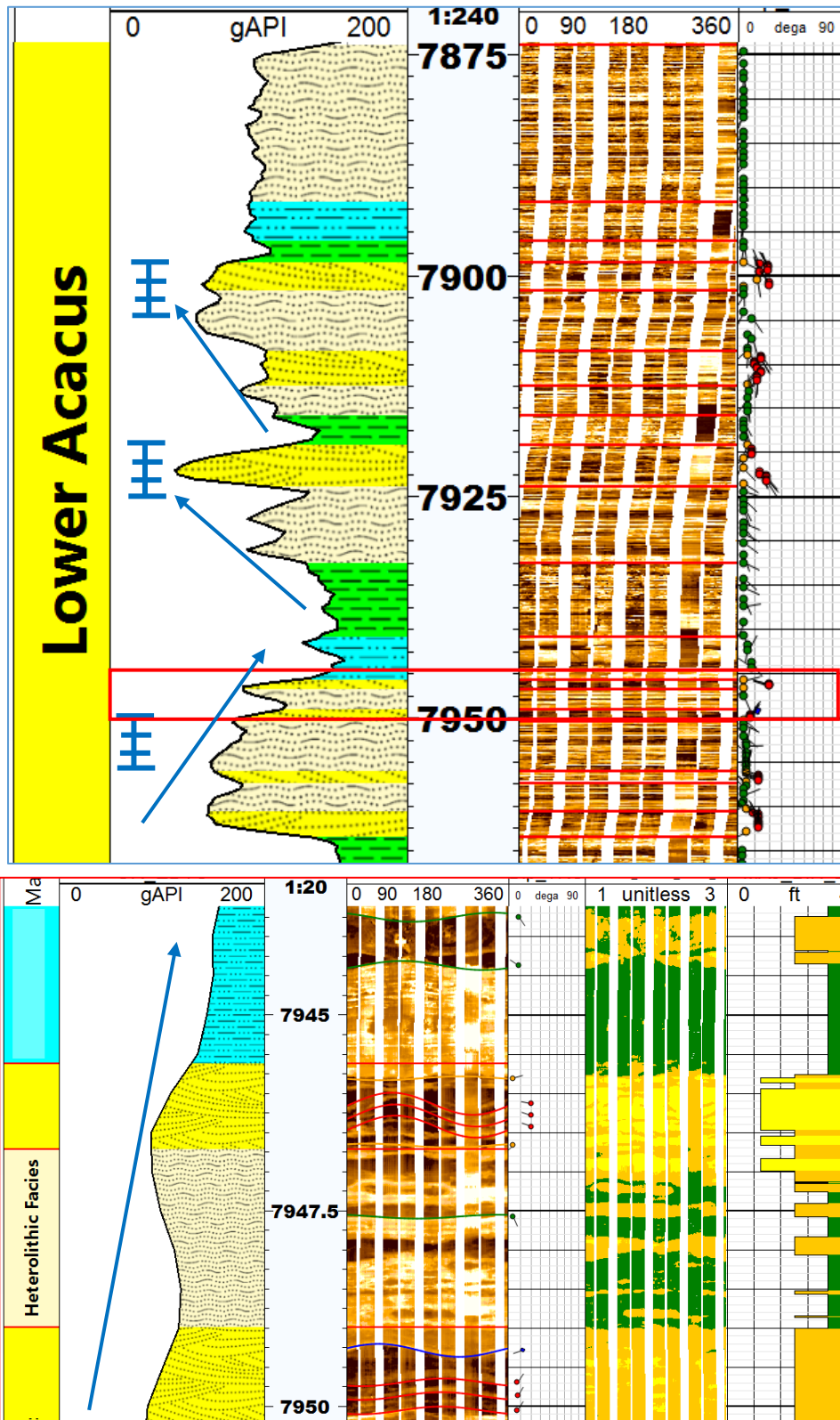


(Fig. 5.18): The facies distribution within Unit C, Red Box represent a Zoom-in into the reservoir in which the erosional surface is clear.

### 5.7.2 FMI Analysis of X1-114 well

The interpreted FMI interval between (8009 - 9131ft) revealed different lithofacies within Lower Acacus reservoir, and the available core image in this well help to better define the determined lithofacies. All the same, the cross-bedding were picked and interpreted over the logged interval to be used for paleocurrent analysis. The Lower Acacus reservoir, shows an overall polymodal to bimodal trend to the NW and SE, which strongly indicate an environmental setting of tide processes to a deltaic setting.

Lower Acacus reservoir is characterized by very frequent alternation of sandstone, siltstone and shale. The reservoir shows variations in the sequence patterns from coarsening to fining upwards as well as changes in the sedimentary structures and nature of paleoflow. Sedimentary features and paleocurrent type and direction were used to indicate the possible environmental setting within the Lower Acacus reservoir. One of the main observation in this well is the increase of bioturbation activity which might destroy the reservoir internal texture and make a kind of diagenetic barrier to the other well especially this well proved to be a water wet. Cyclicity wise, there are very evident coarsening upward cycles on the log response with variable thicknesses ranging from 40 to 100 ft, as thicker cycles are more feasible at the base of the member than the upper part. The coarsening up-ward cycles are mostly comprised of laminated shale at the base changing vertically to heterolithic bedding and are usually overlaid by cross-bedding sandstone indicating increase in energy level. Normally, in the study area the Lower Acacus reservoir sectioned into three main units:

- The sandstone dominated unit (Unit A) between 9113 – 8734 ft, mainly characterized by blocky to coarsening upward sequence with highly dominated cross bedding facies around 44% (Fig. 5.19a). The slight amount of shale facies (9%) indicate the high energy depositional processes were dominated. The analysis of the structural bedding shows that the general trend of dip azimuth is toward north (Fig. 5.19b), with low dip magnitude which indicate the bedding was subjected to insignificant structural tectonic. The paleocurrent trend is mainly polymodal pattern toward north, south and east (Fig. 5.19c) indicating different energy sources within every sand interval of this unit. The cross beddings exhibit medium-high dip magnitude representing the high energy level. Bioturbation activity was noticed especially with the heterolithic bedding which makes the picking of the bedding difficult. This unit could be subdivided into four subunits as shown in chapter four, (A1, A2, A3, and A4) and each of them possess more than sandstone interval.



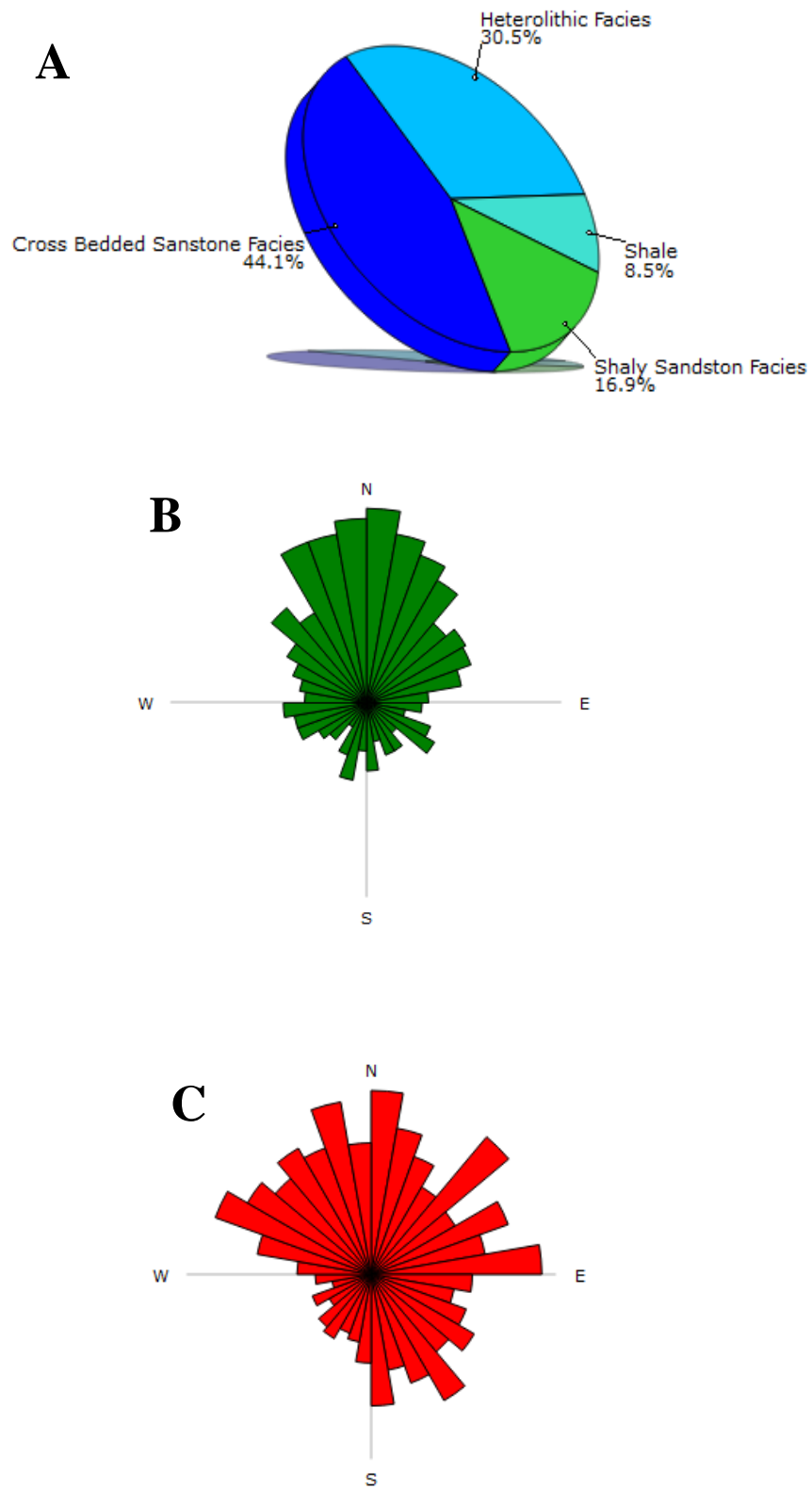


(Fig. 5.19): (A) Facies distribution in, (B) dip azimuth major trend of the structural bedding, (C) major trend of the Paleocurrent of Cross-bedding, all for Unit A of Well X1-114.

- A1 subunit: represent around 90 ft of blocky GR that consist of alteration of cross bedding and heterolithic bedding associated with some erosional surface (Fig. 5.20). The cross bedding shows high random dip patterns which indicate different energy source, and as a result it might represent an area where both deltaic and tidal processes are present. The dip magnitude of the cross bedding is around 30° especially the upper part proving the upward increase in depositional regime. However, production tests flowed formation water with high water salinity.

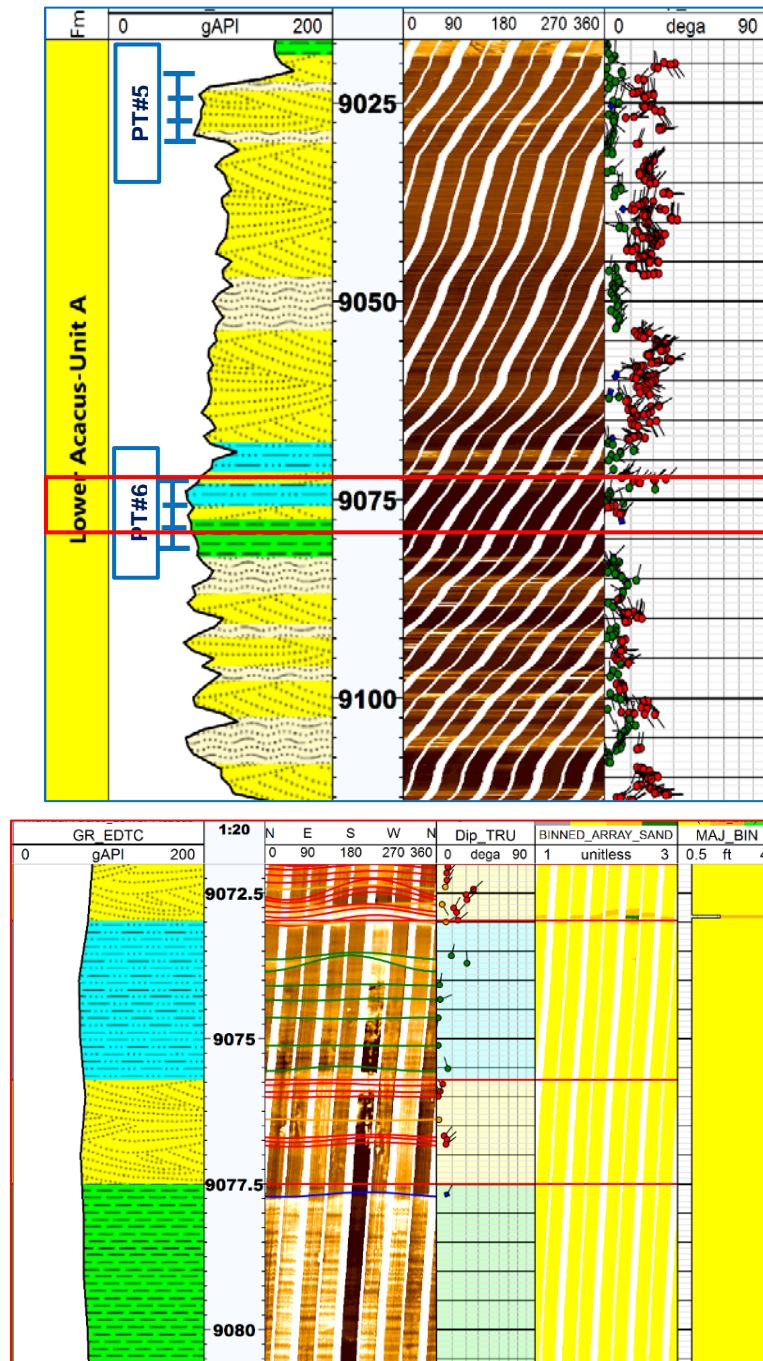


(Fig. 5.20): The facies distribution within Unit A1, Red Box represent a Zoom-in into the reservoir in which erosional surface separate shale facies from cross bedding facies.

Bioturbation has a strong impact on reservoir quality and its flow behavior, and subsequently influence on diagenetic processes (Knaust, 2013). Within this subunit some bioturbations were detected especially vertical burrows, which might create a lateral barrier to the fluid flow or hydrocarbon migration (Fig. 5.21).

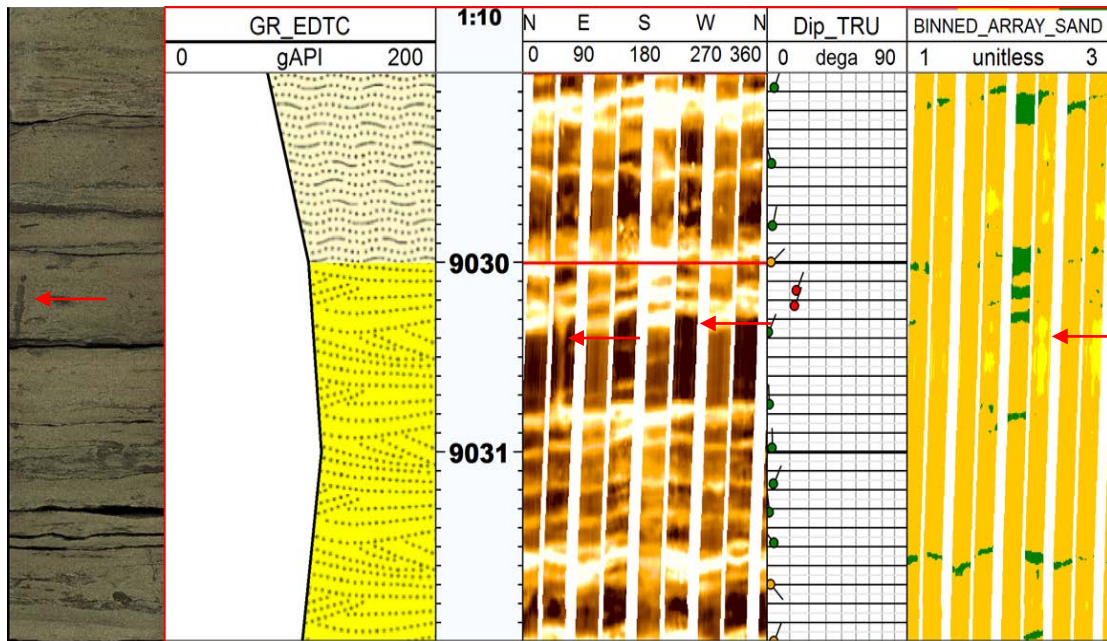


(Fig. 5.21) Zoom-in into the reservoir section showing an indicator of vertical burrow in the FMI and core image as well.

- A2 subunit: composed of one thick coarsening upward sand interval, which compose of sets of cross bedded facies with relative upward increase in dip magnitudes indicating a possible prograding deltaic toward NW (Fig. 5.22).

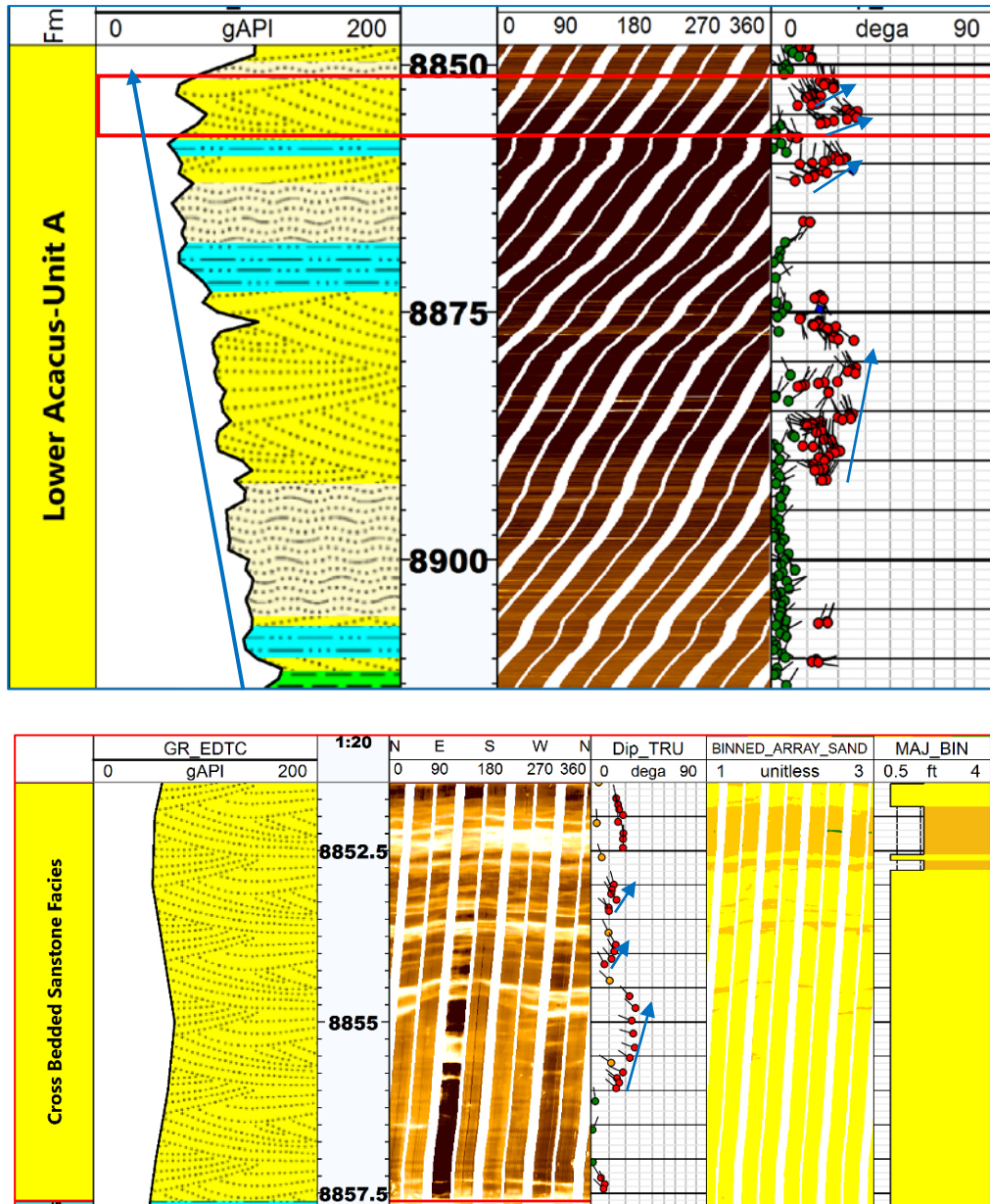


(Fig. 5.22) The facies distribution within Unit A2, Red Box represent a Zoom-in into the coarsening upward sandstone body associated with upward increase in the dipping of cross-bedding.

- A3 subunit: represent around 65 ft of blocky GR that consist mainly of polymodal cross bedding sandstone, with bioturbated heterolithic bedding in some parts (Fig. 5.23). Some light spots or ships were recognized which may indicate rip-up clasts (or mudclasts), which usually represent an erosive current containing suspended sediments that were flowed for some distance. However, small fining upward interval overly the blocky sequence indicating a possible subchannel activity.

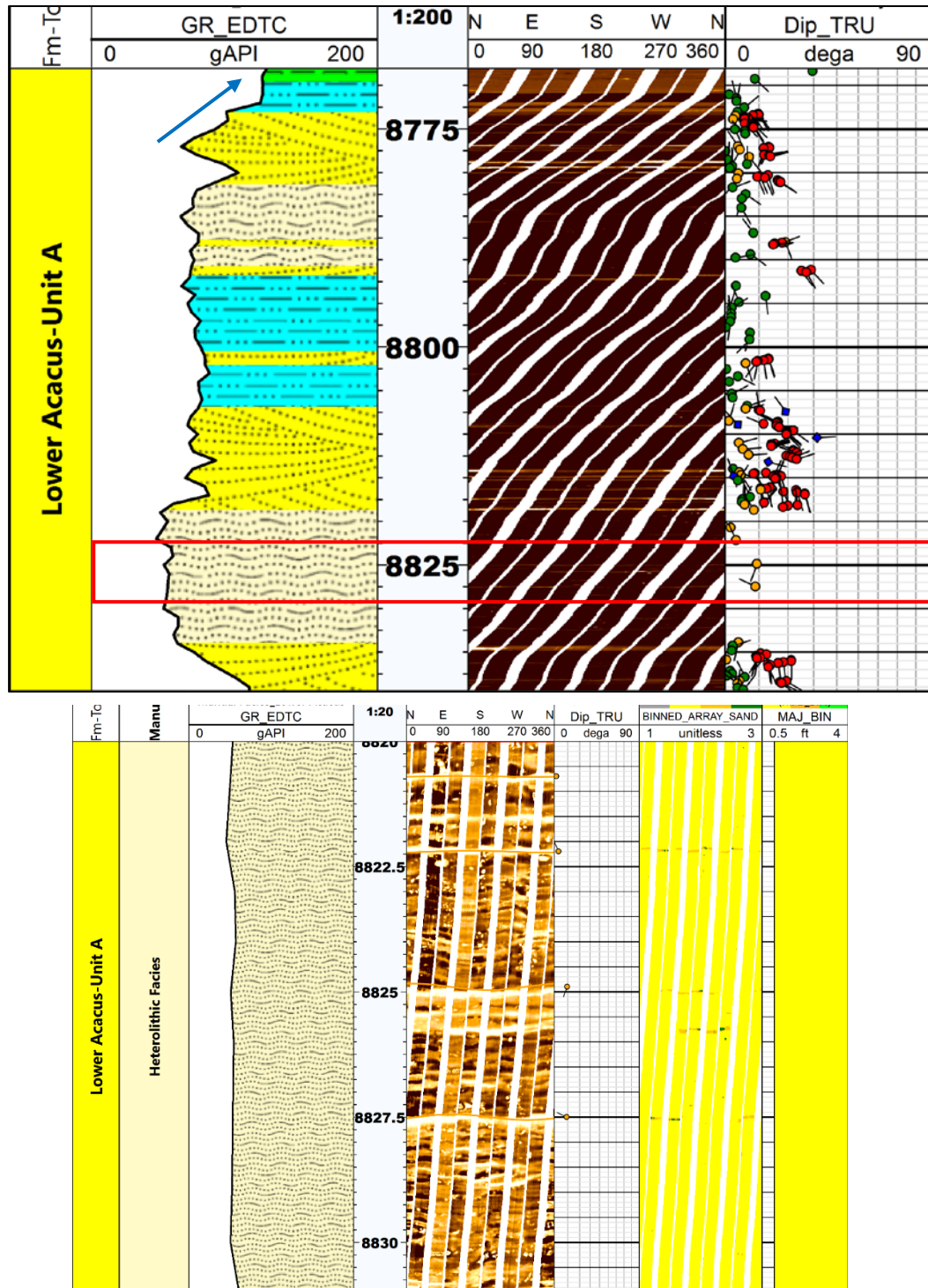


(Fig. 5.23) The facies distribution within Unit A3, Red Box represent a Zoom-in into the heterolithic facies, in which the bioturbation and mudclasts occur.

- A4 subunit: represent around 30 ft of blocky to fining GR of highly bioturbated heterolithic bedding. The sand-counting method shows some spots that could reflect the bioturbated parts (Fig. 5.24).

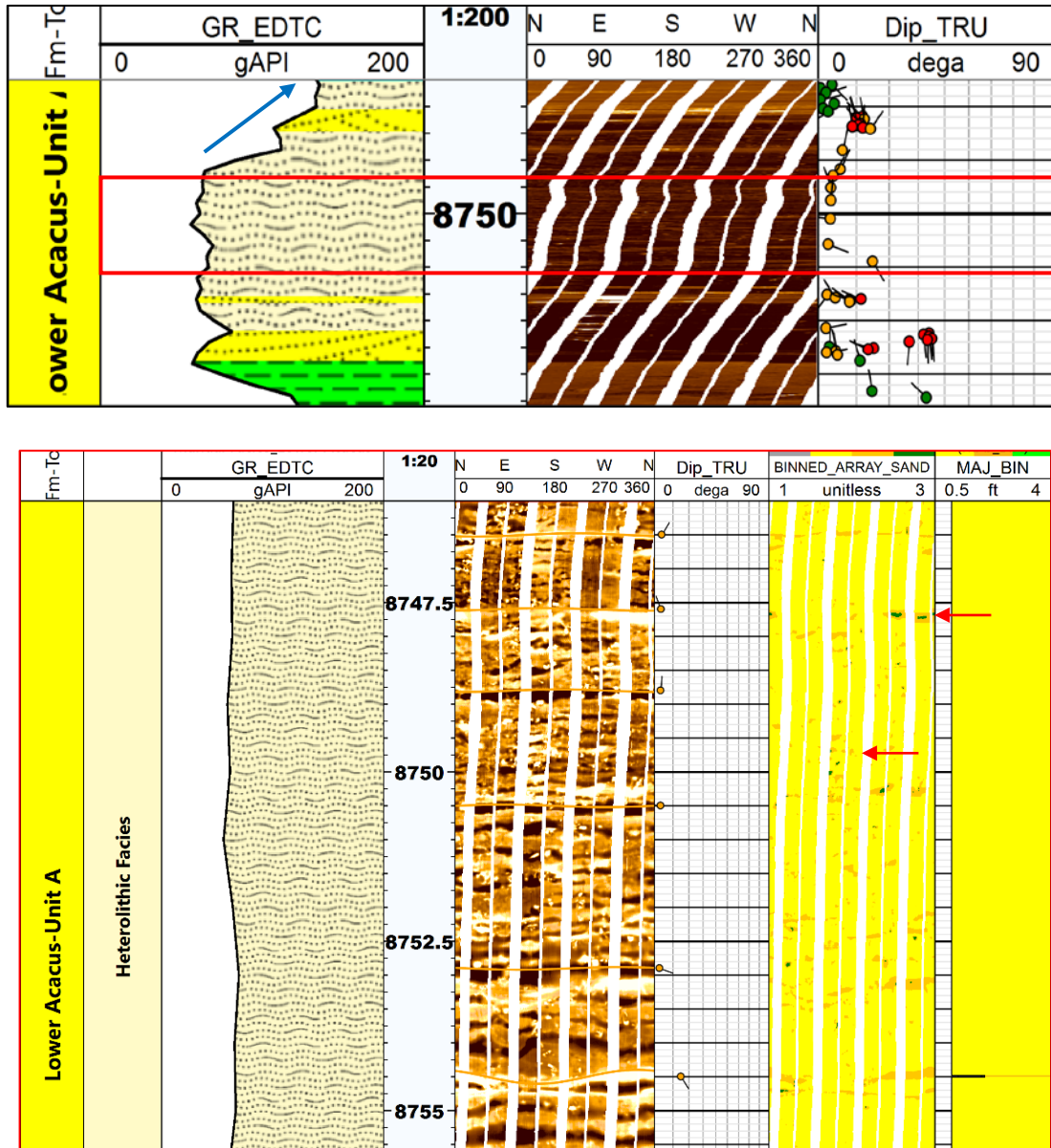


(Fig. 5.24) The facies distribution within Unit A4, Red Box represent a Zoom-in into the heterolithic facies, in which the bioturbation and mudclasts are clear, as red arrow in the sand counting tracks indicate the bioturbated parts.

- Unit B between 8092 – 8734 ft, mainly characterized by shale-sand interbedding with domination of the cross bedding sandstone facies (37%) as in (Fig. 5.25a) while the shale and shaly sand facies dramatically increase in this unit to reach around 43%. On the other hand, some coarsening upward sequences that were noticed mainly dipping toward SE representing the coastal delta depositional setting. The analysis of the structural bedding shows similar result to Unit A, with low structural dip magnitude dipping toward north (Fig. 5.25b). The paleocurrent trend is mainly polymodal which mean no major energy flow were dominated (Fig. 5.25c) and indicating different energy sources for each sand interval. Bioturbation activities were detected in some zones. Equally, this unit could be subdivided into four subunits, (B1, B2, B3, and B4) and each of them possess more than sandstone interval.

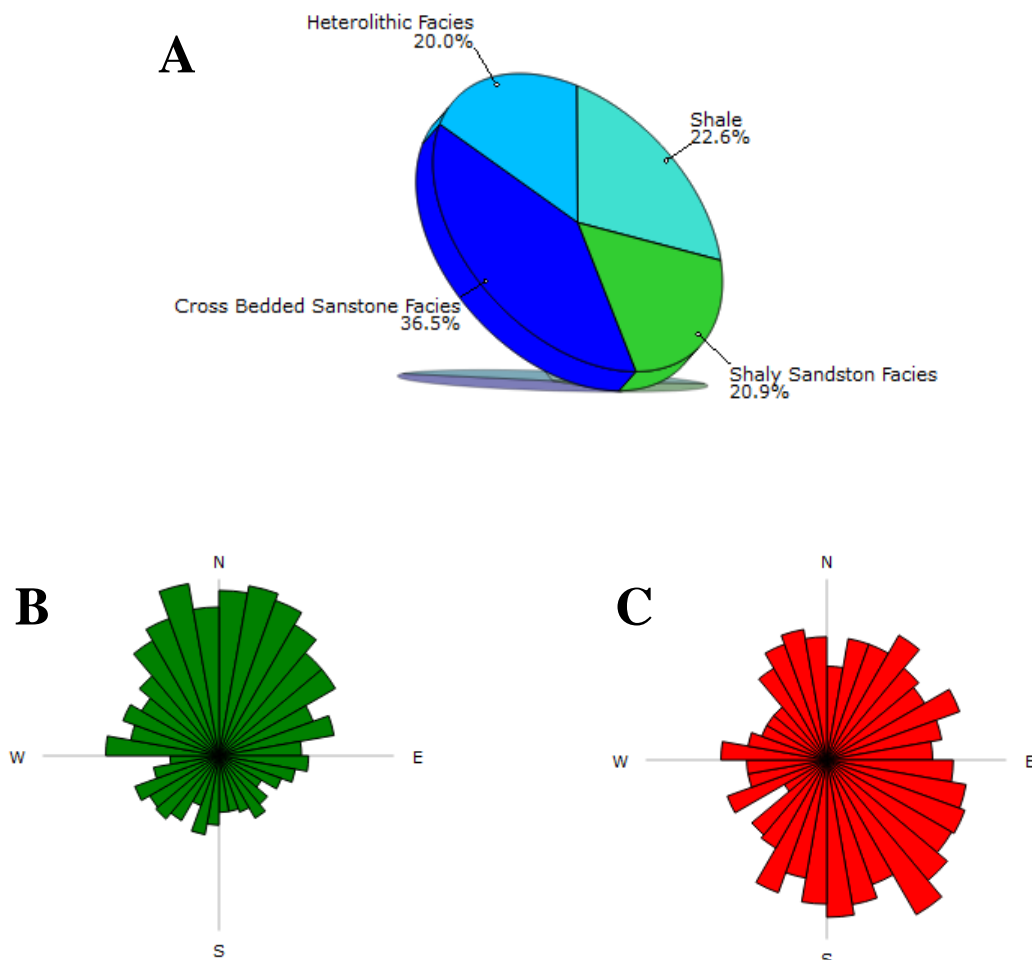


(Fig. 5.25): (A) Facies distribution in, (B) dip azimuth major trend of the structural bedding, (C) major trend of the Paleocurrent of Cross-bedding, all for Unit B of Well X1-114.

- B1 subunit: represent a thick sequence (around 100 ft) of serrated to blocky GR that mainly consist of heterolithic bedding associated with cross bedding and shaly-sand facies. The cross bedding indicates clear bidirectional paleo-flow which is typical of tidal processes (Fig. 5.26). Bioturbation is less abundant and the test in upper part indicate a highly water saturated interval.

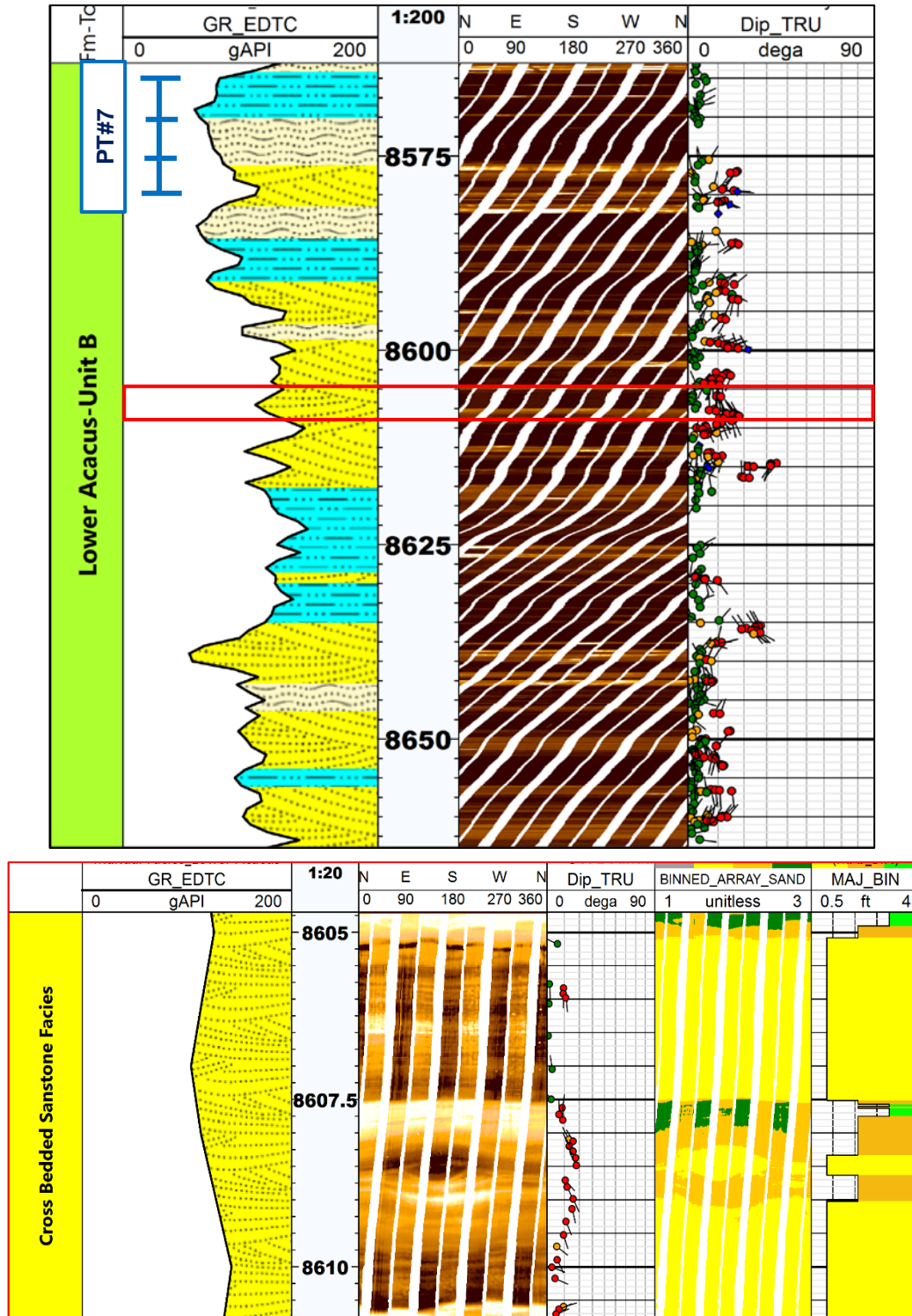


(Fig. 5.26) The facies distribution within Unit B1, Red Box represent a Zoom-in into the cross bedding facies, in which bidirectional current making an eye-like feature.



- B2 subunit: represent a thick interval around 65 ft that is actually composed of one noticeable coarsening upward sand interval that is clearly dipping toward SE (Fig. 5.27). This highly dipping cross bedding sandstone interval was tested and flowed formation water. However, bidirectional cross bedding within fining upward sequences is also observed in the middle and lower parts, which might represent subtidal channels.

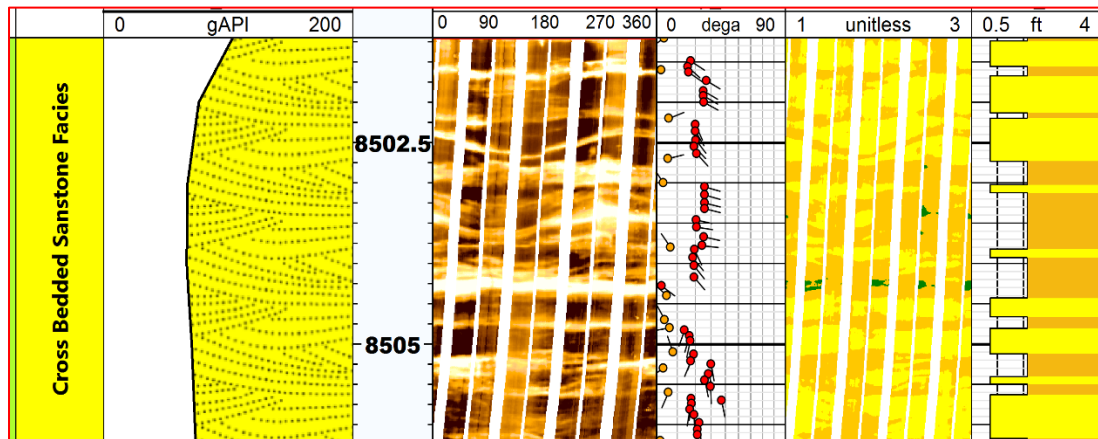
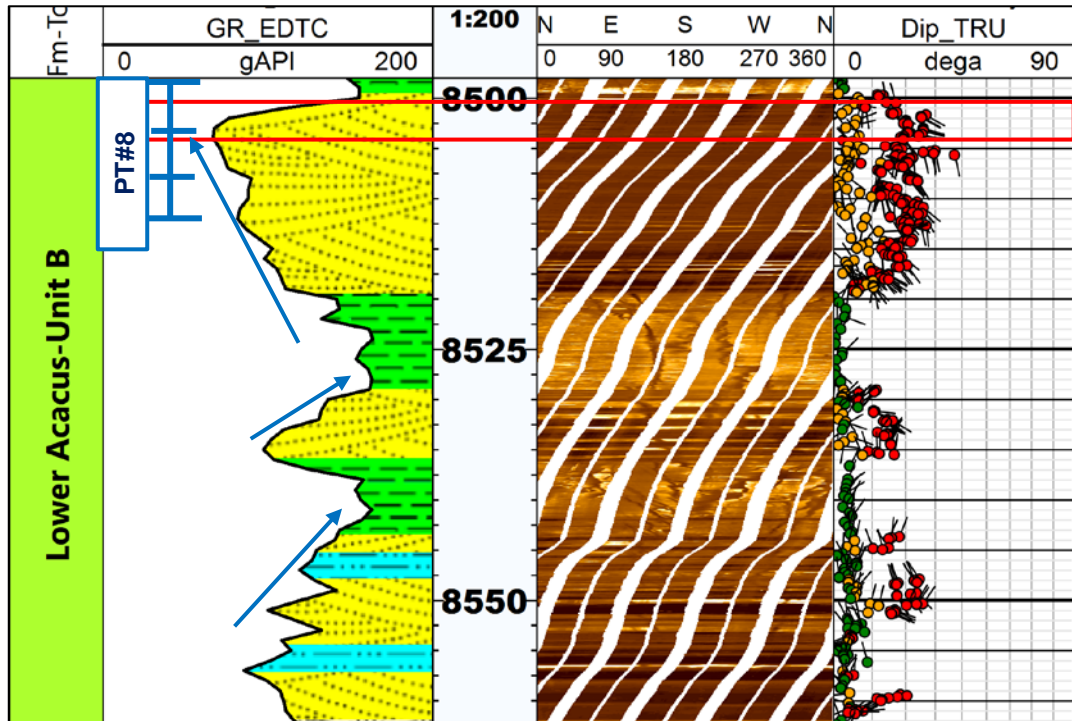


(Fig. 5.27) The facies distribution within Unit B2, Red Box represent a Zoom-in into the reservoir in which the cross bedding shows SE dipping.

- B3 subunit: this unit represent around 70 ft of coarsening upward sequences. The dipping is mainly unimodal toward the south in the lower part while tide effect is more visible at the upper part. The heterolithic facies is highly dominated and their contact with the cross bedding facies is clearly seen (Fig. 5.28).

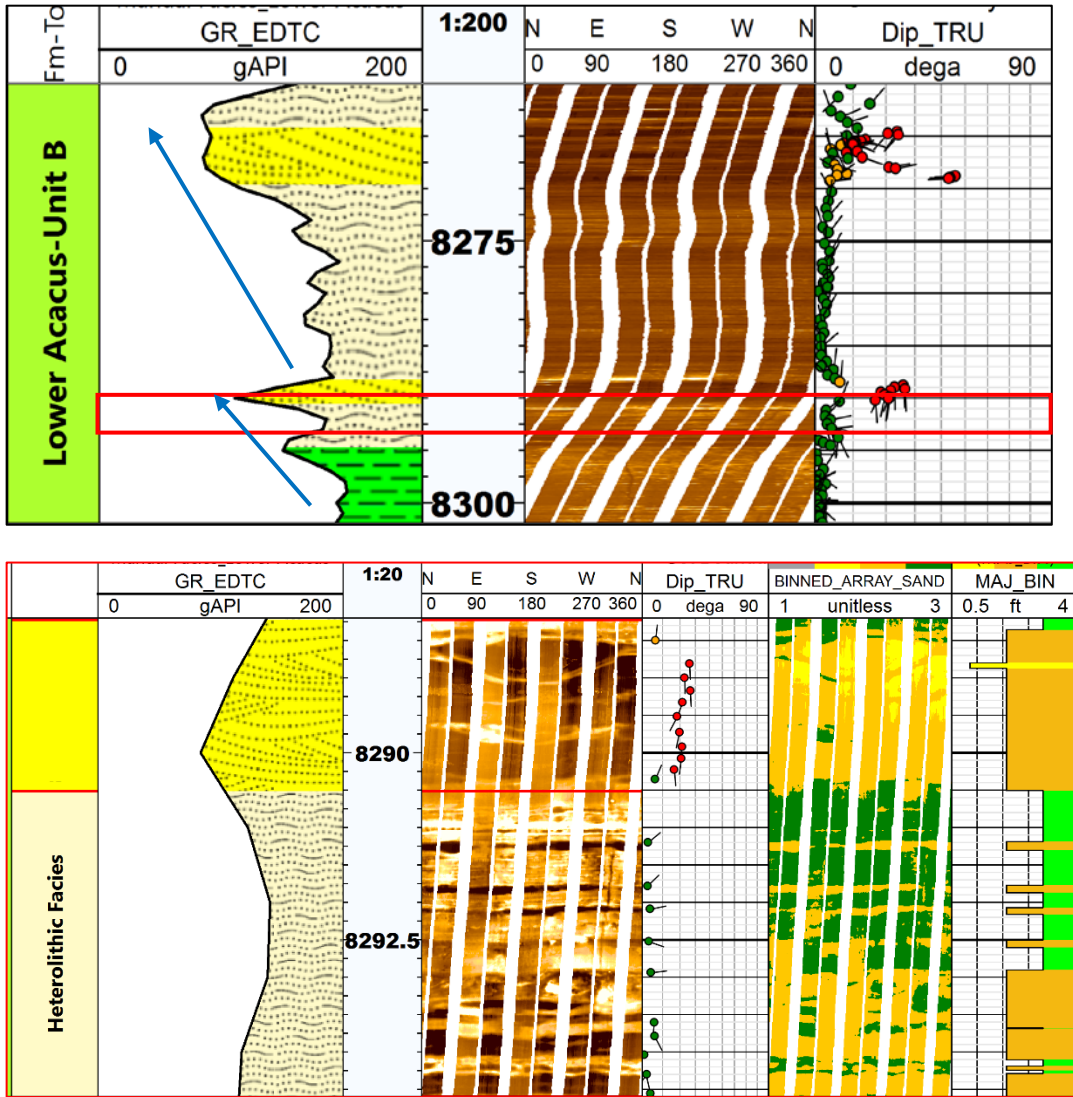


(Fig. 5.28) The facies distribution within Unit B3, Red Box represent a Zoom-in showing the contact between cross bedding and heterolithic bedding facies.

- B4 subunit: represent around 70 ft composed of multi coarsening and fining upward sequences that is separated by shale facies. This subunit is dominated by heterolithic facies while cross bedding has less occurrence. Moreover, the shale facies is laminated and bioturbated in some parts, besides a vertical induce fracture is identified (Fig. 5.29).

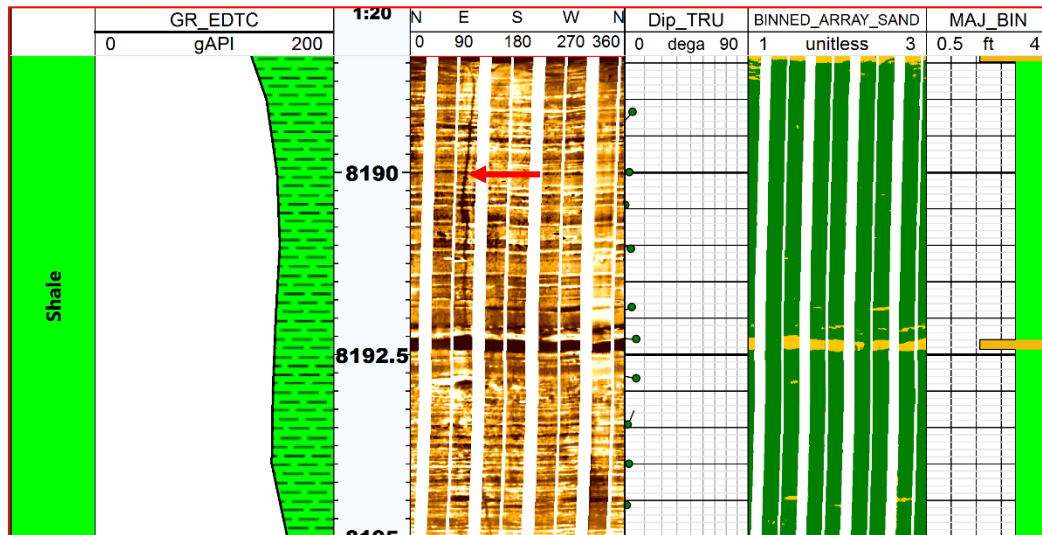
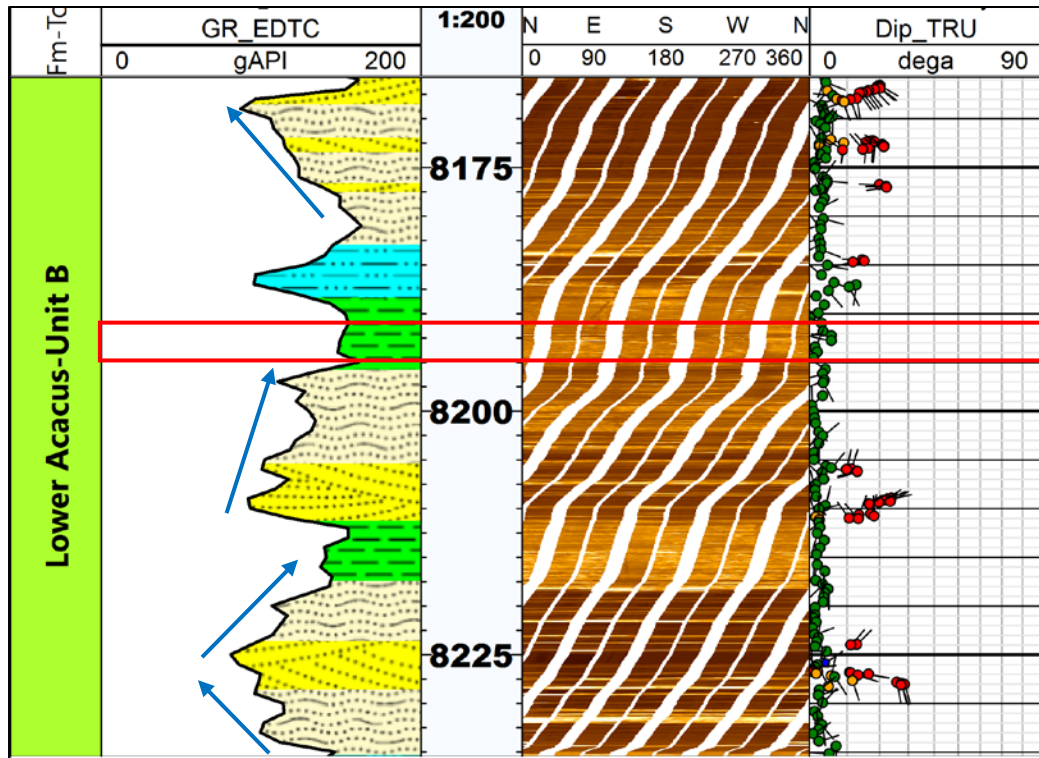


(Fig. 5.29) The facies distribution within Unit B4, Red Box represent a Zoom-in into the shale facies in which a vertical induced fracture is observed.

- Unit C between 8009 – 8092 ft, started with fining upward sand body followed by coarsening upward sequence. The cross bedding facies is almost ruled the unit with 47% (Fig. 5.30a), while shale and heterolithic facies both represent 20% each. The analysis of the structural bedding indicates low value mainly dipping toward the N-NW (Fig. 5.30b), whereas the paleocurrent trend is mainly bimodal pattern toward NW-SE (Fig. 5.30c) indicating the tide processes. Nevertheless, the minor trend (NE-SW) perpendicular to the main trend might indicate a component of longshore current. The tide effect is present on these kind of coastal sandstone intervals, and the fining sand bodies are probably represent tidal channels. The bioturbation activity is very remarkable and could make a kind of diagenetic barrier to the adjacent sandstone units (Fig. 5.31). This unit proved to be water wet reservoirs as indicated in the production tests.

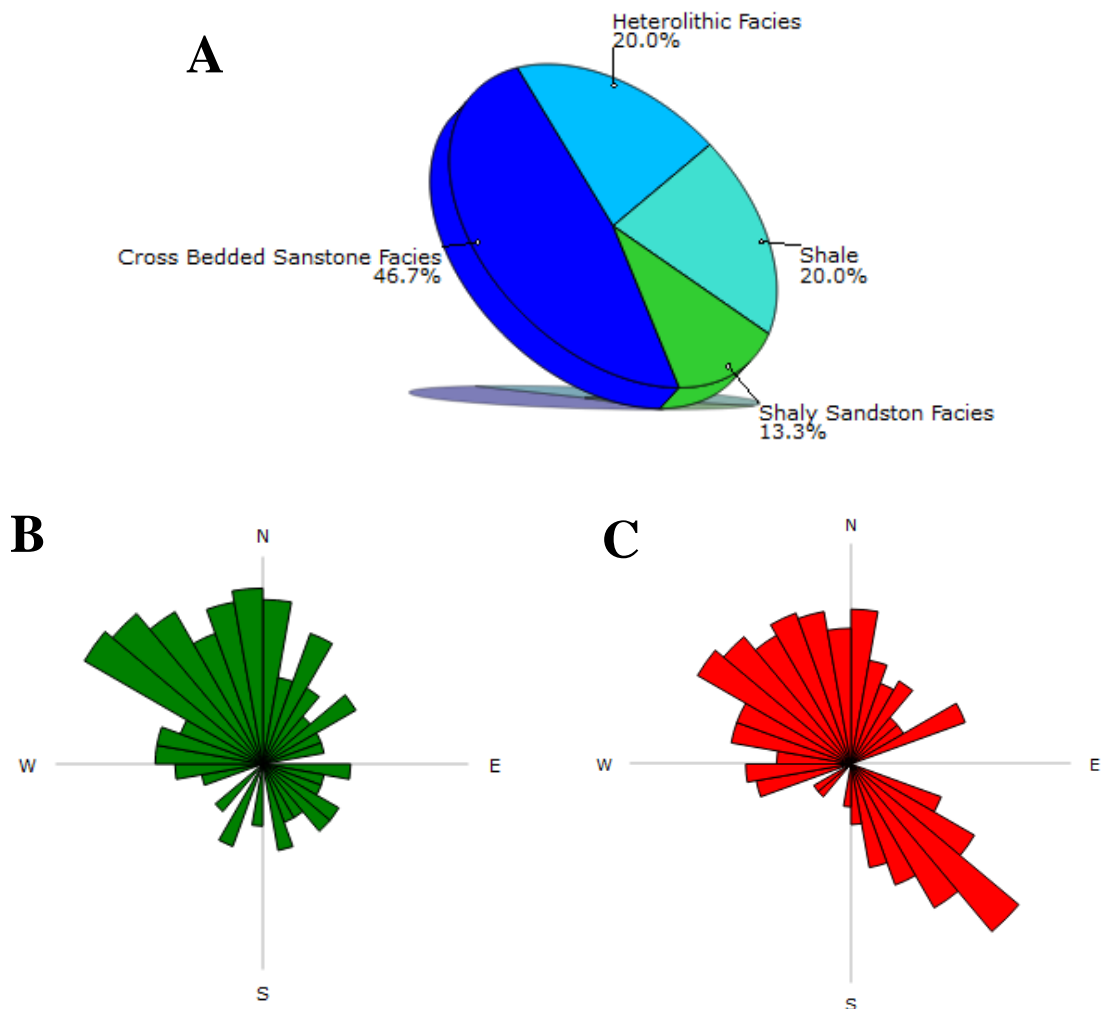


(Fig. 5.30): (A) Facies distribution in, (B) dip azimuth major trend of the structural bedding, (C) major trend of the Paleocurrent of Cross-bedding, all for Unit C of Well X1-114.

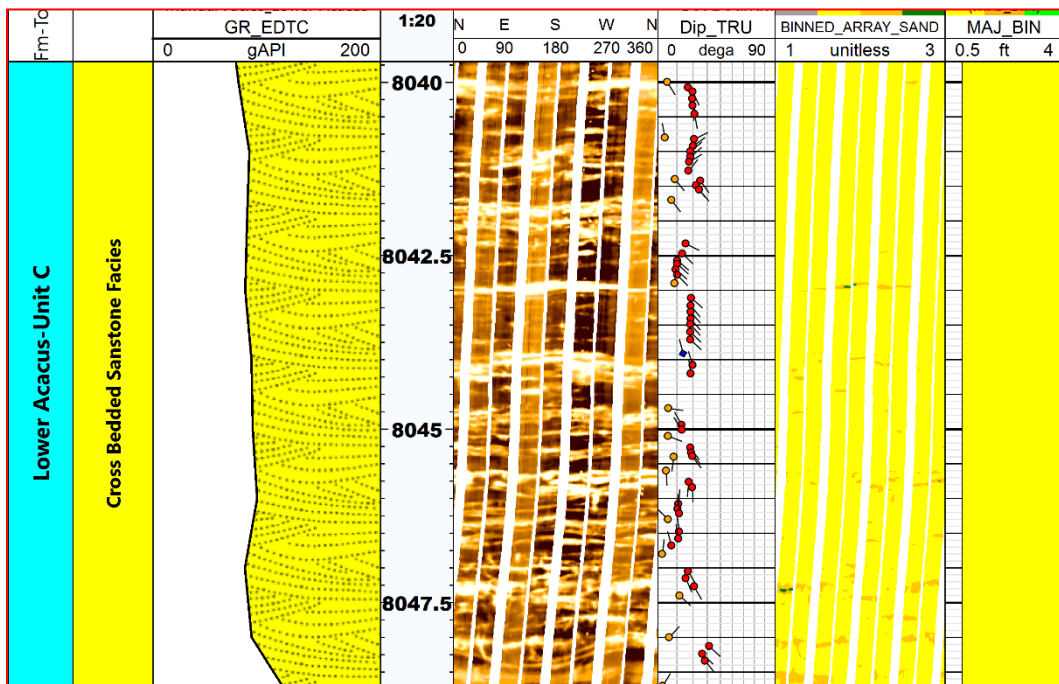
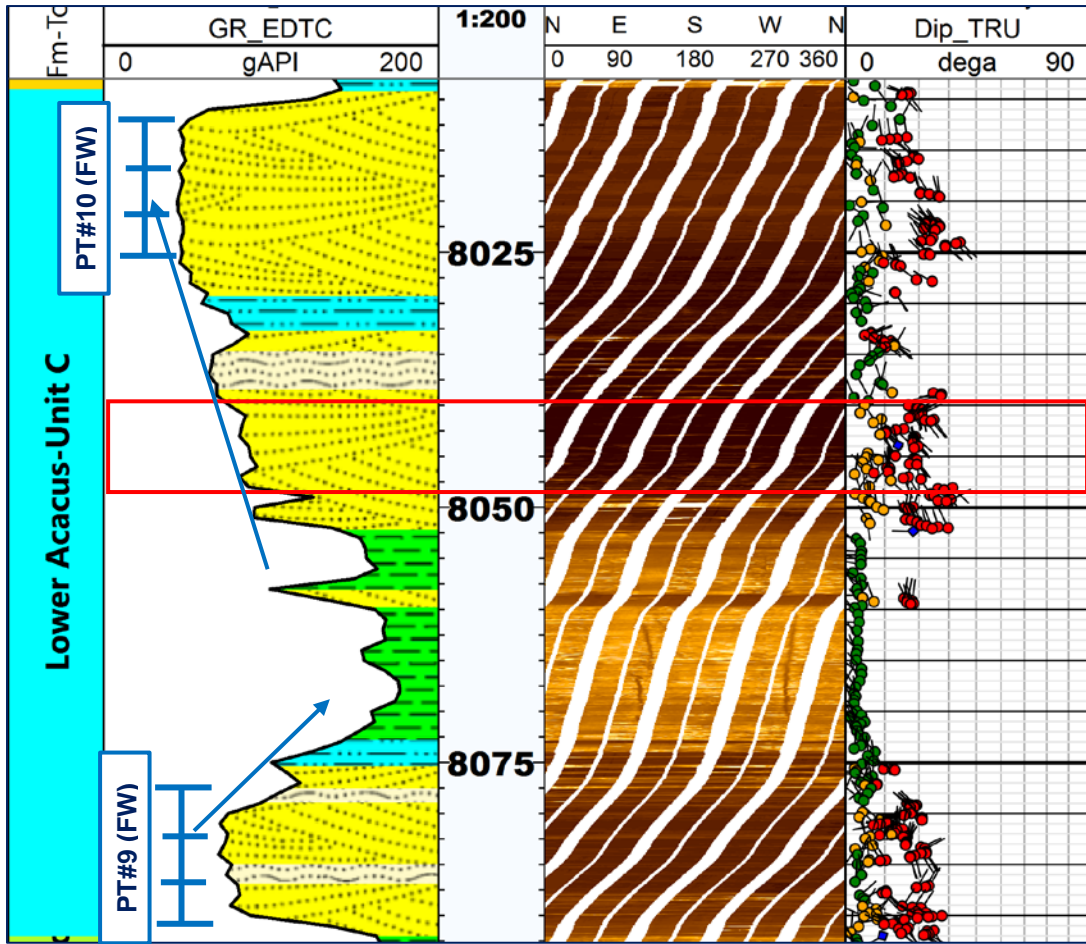


(Fig. 5.31) The facies distribution within Unit C, Red Box represent a Zoom-in into the cross bedding facies, in which a bioturbation is quite common.

### 5.7.3 FMI Analysis of Y1-114 well

The interpreted FMI of Y1-114 has the best quality among the studied wells, and the targeted interval between (8020 - 8893ft) revealed the different lithofacies within Lower Acacus reservoir, in which images for one core is available to better define the determined lithofacies. In this well the cross bedding facies is easily recognized on core image. The major directional trend in most units is towards the SE-NW in bimodal behaviors, which signify the tide effect on the depositional setting. Some trends are directed to the SE in unidirectional model as in subunit A3. The reservoir shows variations in the sequence patterns from coarsening to fining upwards as well as changes in the sedimentary structures. Normally, in the study area the Lower Acacus reservoir sectioned into three main units (as shown in chapter three):

- The sandstone dominated unit (Unit A) between 8584 – 8893 ft, mainly characterized by blocky to coarsening upward sequence as well abundance of fining channelized sand bodies. cross bedding is dominating with around 41% (Fig. 5.32a), with slight amount of shale facies (10%) indicate the high energy depositional processes were dominated. The analysis of the structural bedding shows that the general trend of dip azimuth is typically polymodal (Fig. 5.32b), which might indicate that beddings were subjected to mixed settings (probably subaerial and subaqueous processes). The paleocurrent trend is mainly bimodal toward NW-SE (Fig. 5.32c) signifying the tide effect on the area. This unit could be subdivided into four subunits and each of them possess more than sandstone interval.

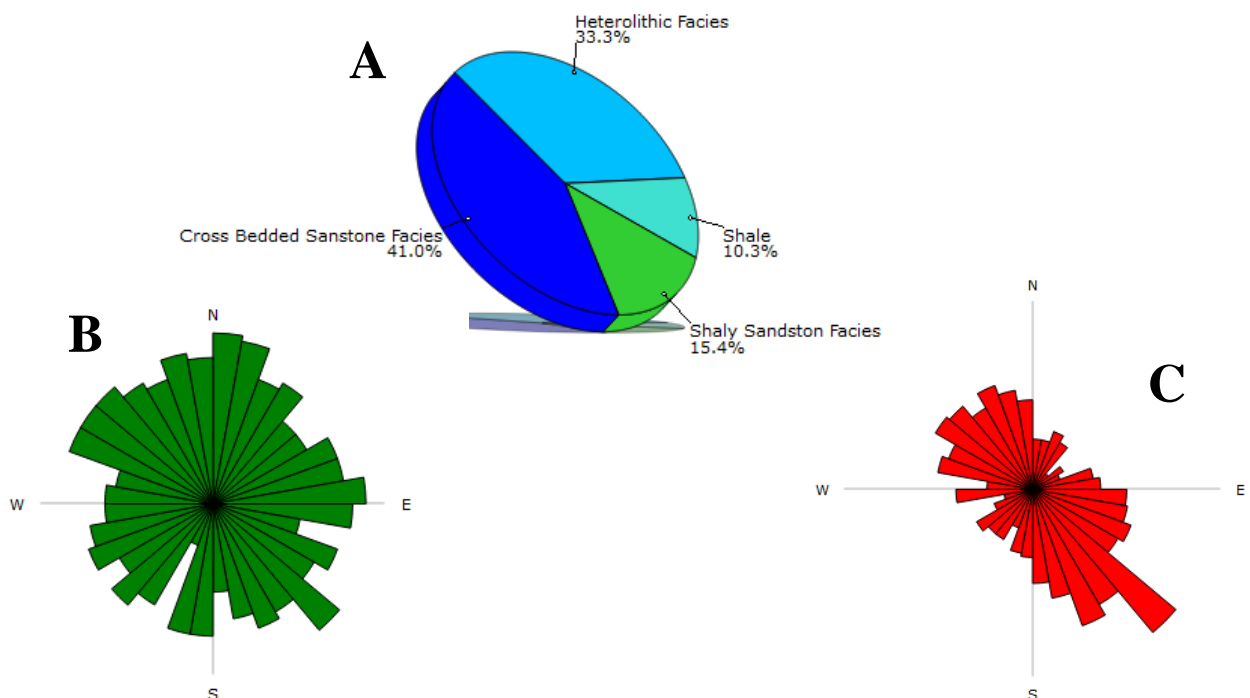


(Fig. 5.32): (A) Facies distribution in, (B) dip azimuth major trend of the structural bedding, (C) major trend of the Paleocurrent of Cross-bedding, all for Unit A of Well Y1-114.

- A1 subunit: represent around 75 ft composed of small coarsening upward sand body that mainly consist of small sets of bidirectional cross bedding (Fig. 5.33). This interval proves to be highly hydrocarbon productive, and eventually overlay by another thick coarsening upward sequence that composes of thicker bidirectional cross bedding. Fining upward interval lay at the top of this unit surface indicating a possible channel that is actually grades to shale facies.

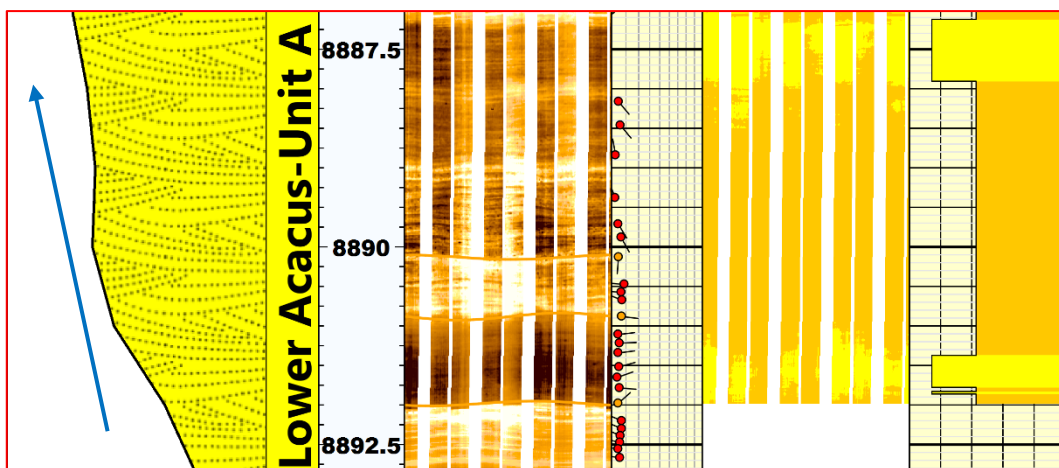
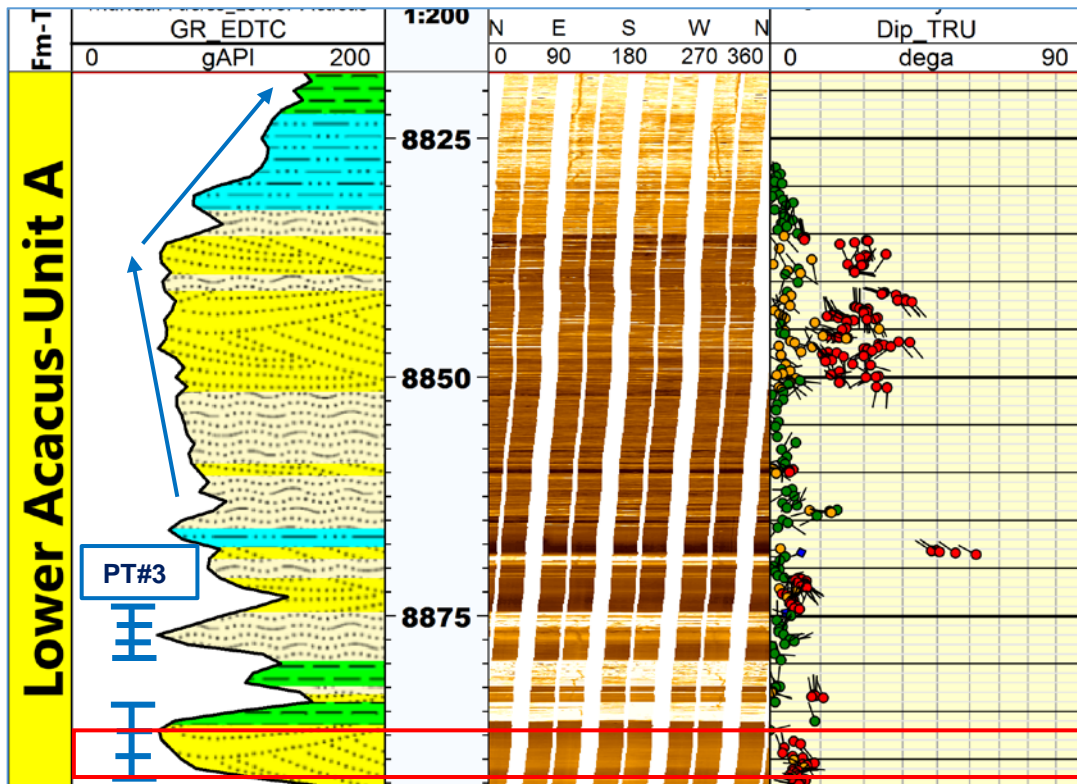


(Fig. 5.33) The facies distribution within Unit A1, Red Box represent a Zoom-in into the reservoir in which low angel bidirectional cross bedding is clear.

- A2 subunit: composed of two coarsening upward sand interval that is eventually followed by fining upward sequences. The cross bedding mainly dips toward the SE with less tide effect. The clear cut between the cross bedding sets might represent erosional surfaces (Fig. 5.34).

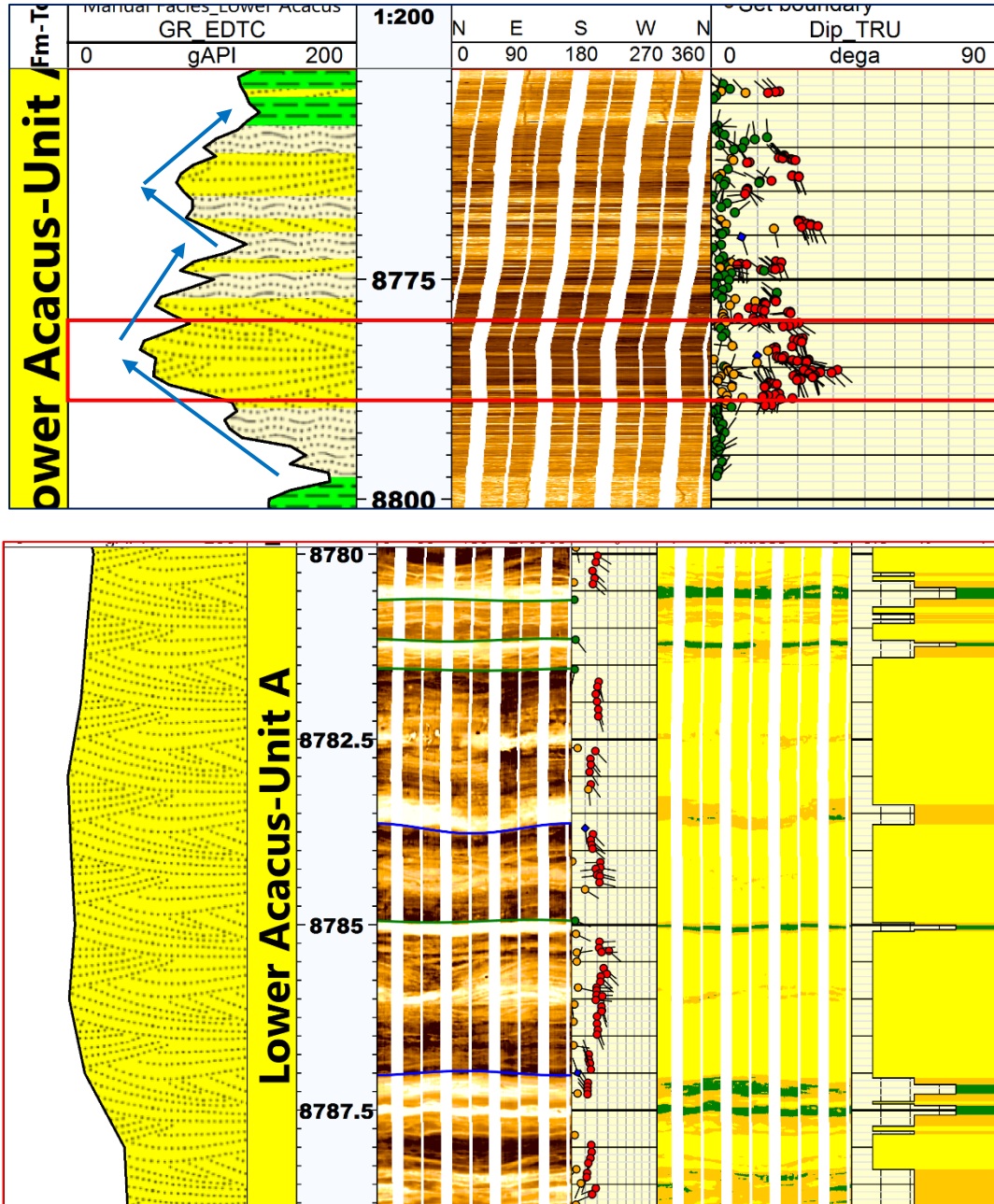


(Fig. 5.34) The facies distribution within Unit A2, Red Box represent a Zoom-in shows the erosional surfaces that separate the cross-bedding sets.



- A3 subunit: represent 50 ft of mainly cross bedded fining upward sequences that dips toward SE in unimodal pattern, which might represent the feeder channels. The tadpole of the cross bedding goes straight in uniform pattern with depth that might signify the steady stage of sediment deposition (Fig. 5.35).

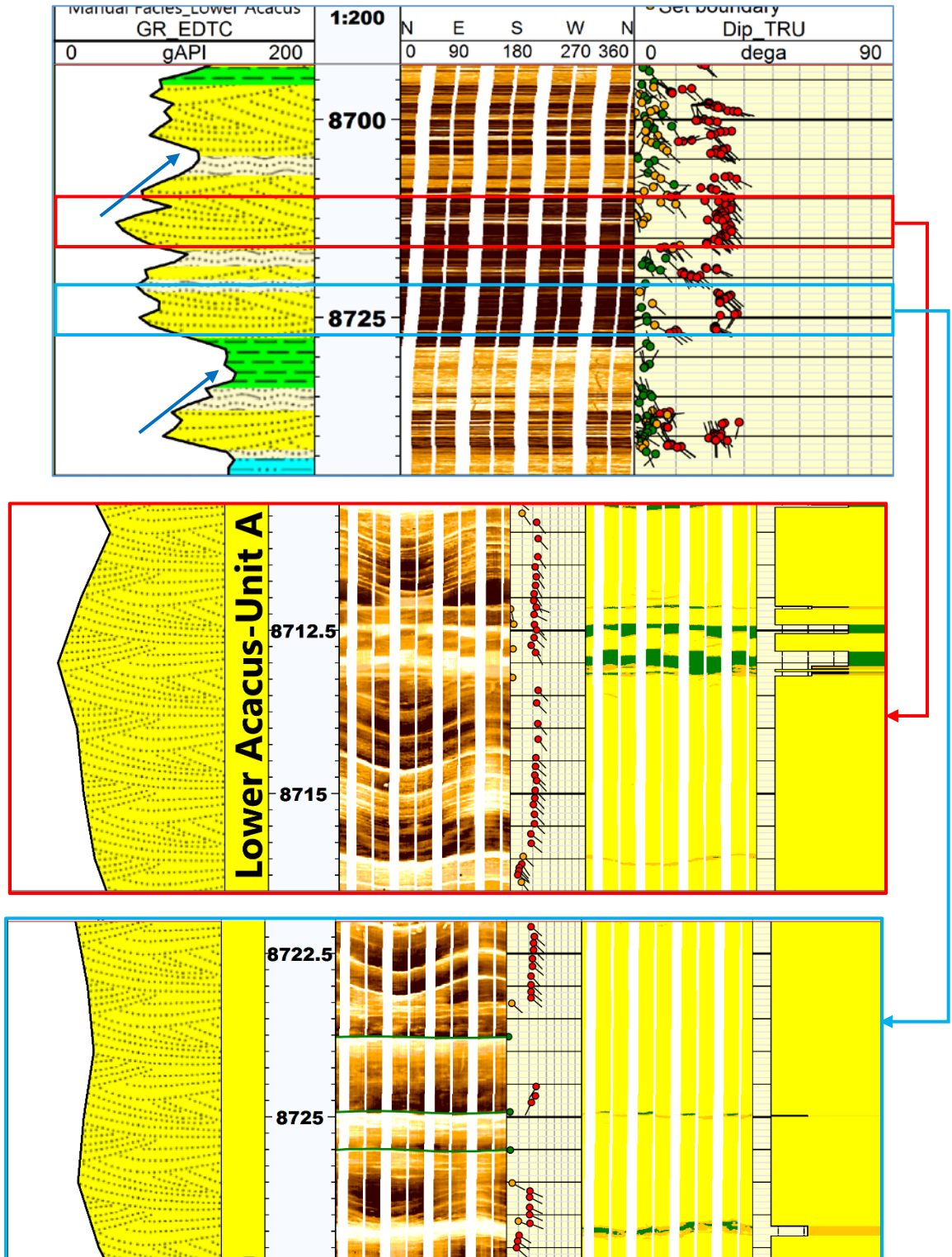


(Fig. 5.35) The facies distribution within Unit A3, the boxes represent a Zoom-in into the cross-bedding facies in which almost straight reading of cross bedding dips.

- A4 subunit: represent around 110 ft of blocky to kind of serrated GR with bidirectional indicator of paleo-flow. Repeated erosional surfaces at the top of this unit indicate the increase in channel activity (Fig. 5.36), especially the upper part that was flowed gas and oil.

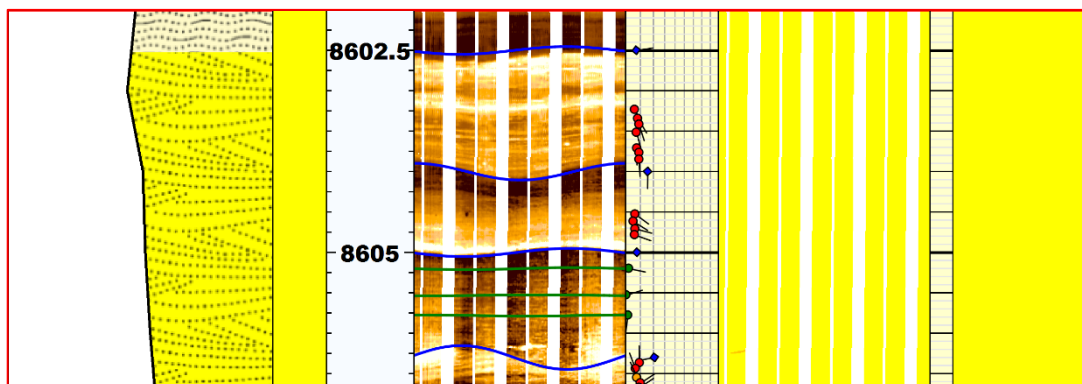
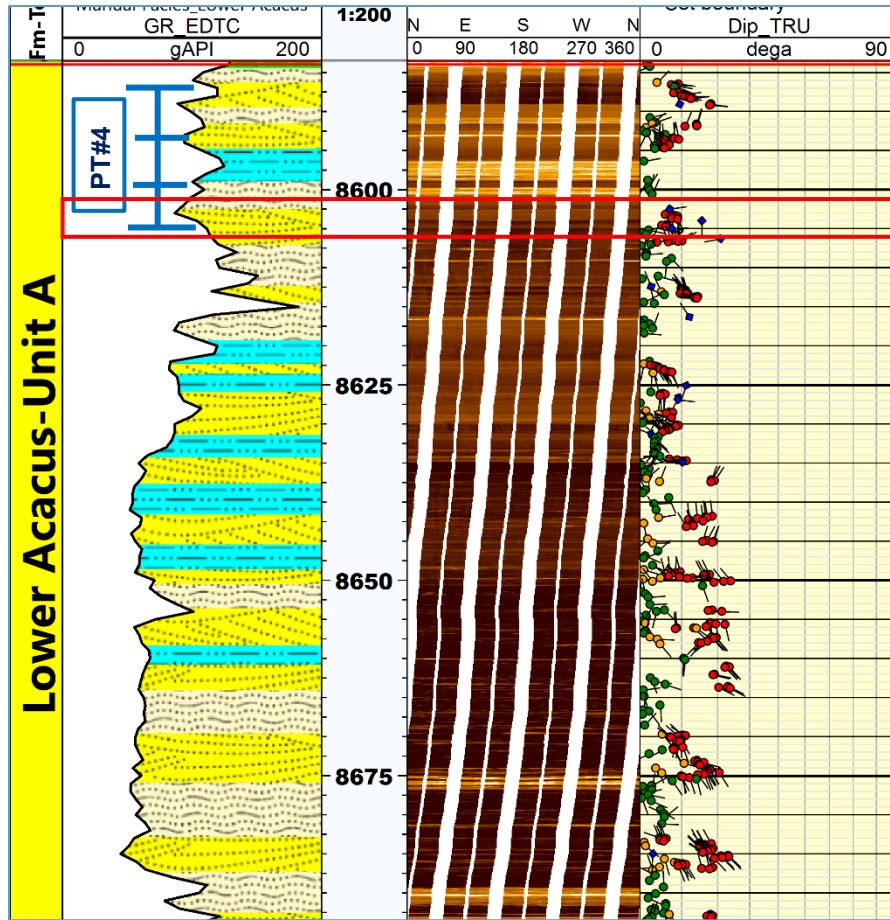


(Fig. 5.36) The facies distribution within Unit A4, Red Box represent a Zoom-in into the reservoir in which the erosional surfaces are quite common.

- Unit B between 8092 – 8734 ft, mainly characterized by shale-sand interbedding with domination of both the cross bedding sandstone facies (30%) and heterolithic bedding (29%) as in (Fig. 5.37a). Furthermore, the repeating pattern of coarsening upward sequences that were mainly dipping toward NW-SE representing the tide dominated-deltaic depositional setting. The upper part of this unit shows a clear change in deposition pattern to dominate the fining upward sequences. The analysis of the structural bedding shows similar result to Unit A dipping in polymodal pattern (Fig. 5.37b). The paleocurrent trend is mainly bimodal toward NW-SE, which indicating the tide processes. Nevertheless, another minor trend (NE-SW) perpendicular to the main trend might indicate a component of longshore current (Fig. 5.37c). Equally, this unit could be subdivided into four subunits, (B1, B2, B3, and B4) and each of them possess more than sandstone interval.

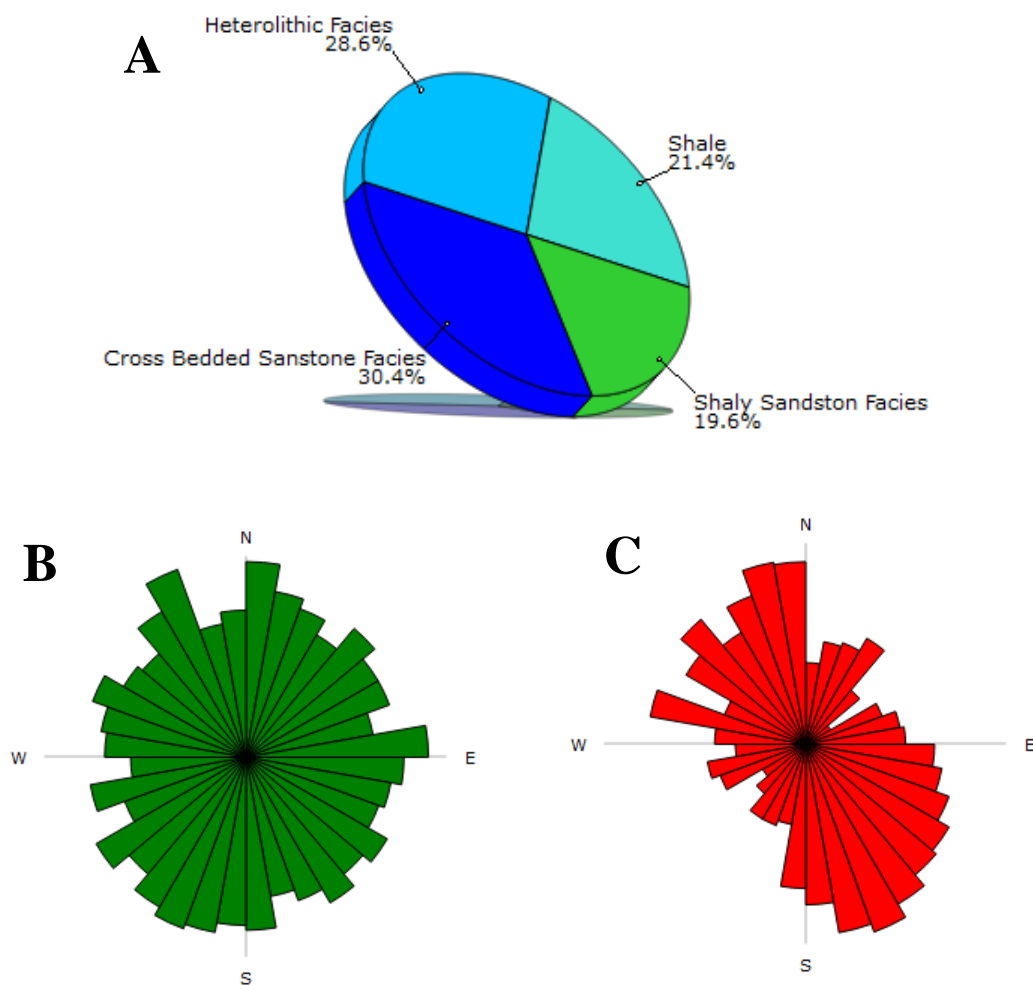


(Fig. 5.37): (A) Facies distribution in, (B) dip azimuth major trend of the structural bedding, (C) major trend of the Paleocurrent of Cross-bedding, all for Unit B of Well Y1-114.

- B1 subunit: represent thick sequences (around 70 ft) of about five coarsening upward intervals that mainly consist of heterolithic bedding associated with cross bedding and shaly-sand facies. The cross bedding indicates clear bidirectional paleo-flow which is typical of tidal processes, while the erosional surfaces could represent reactivation surfaces (Fig. 5.38).

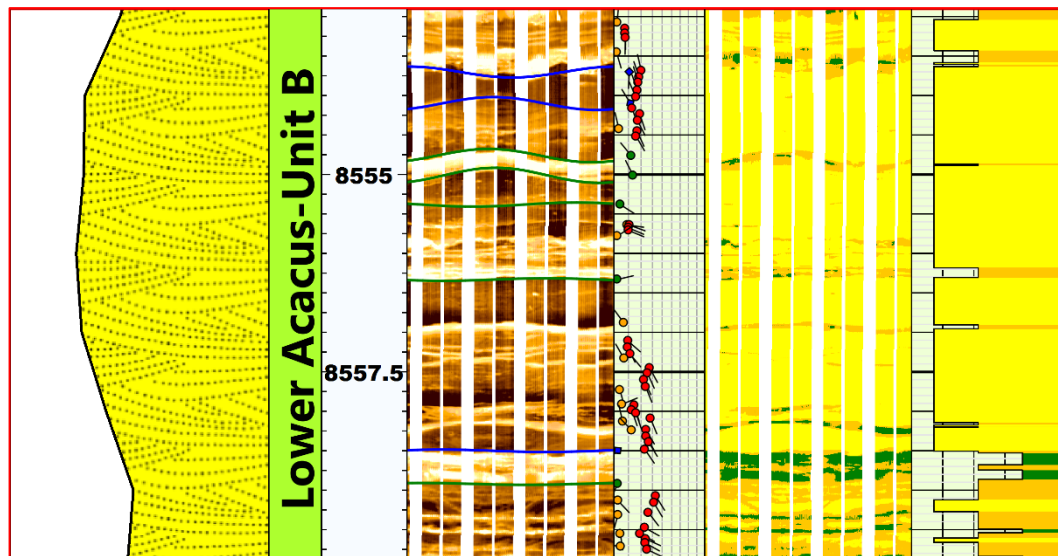
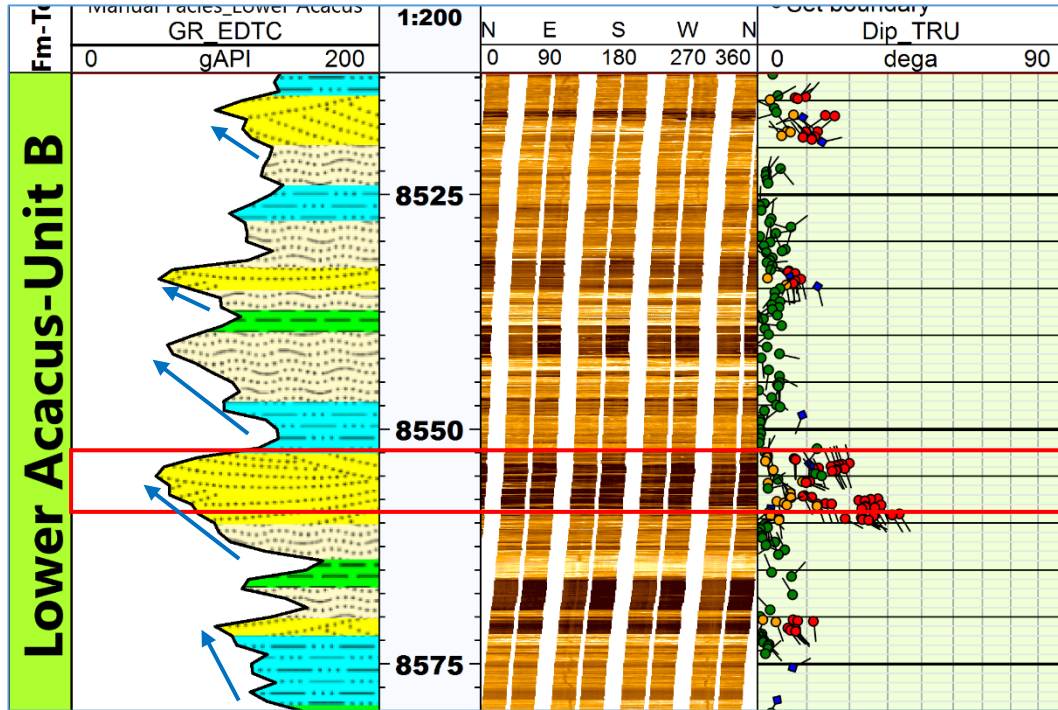


(Fig. 5.38) The facies distribution within Unit B1, Red Box represent a Zoom-in into the cross bedding facies with some indicator of erosional surface.

- B2 subunit: represent a thick interval around 125 ft that is actually composed of multi-coarsening upward sand intervals that is clearly dipping toward NW-SE (Fig. 5.39). However, bidirectional cross bedding within fining upward sequences is also observed, which might represent subtidal channels.

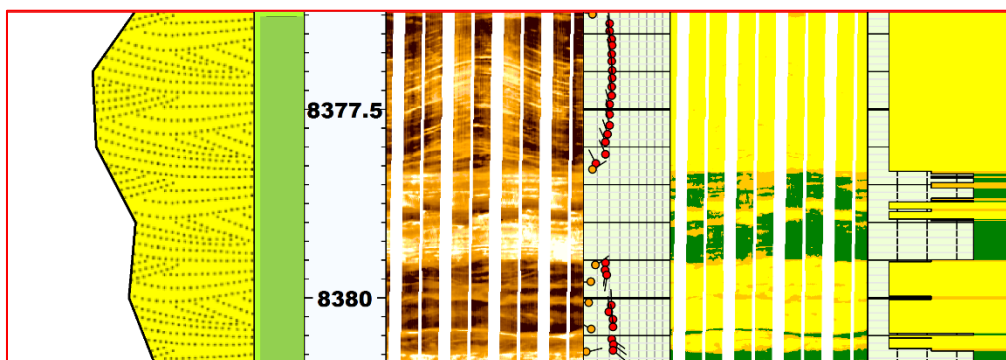
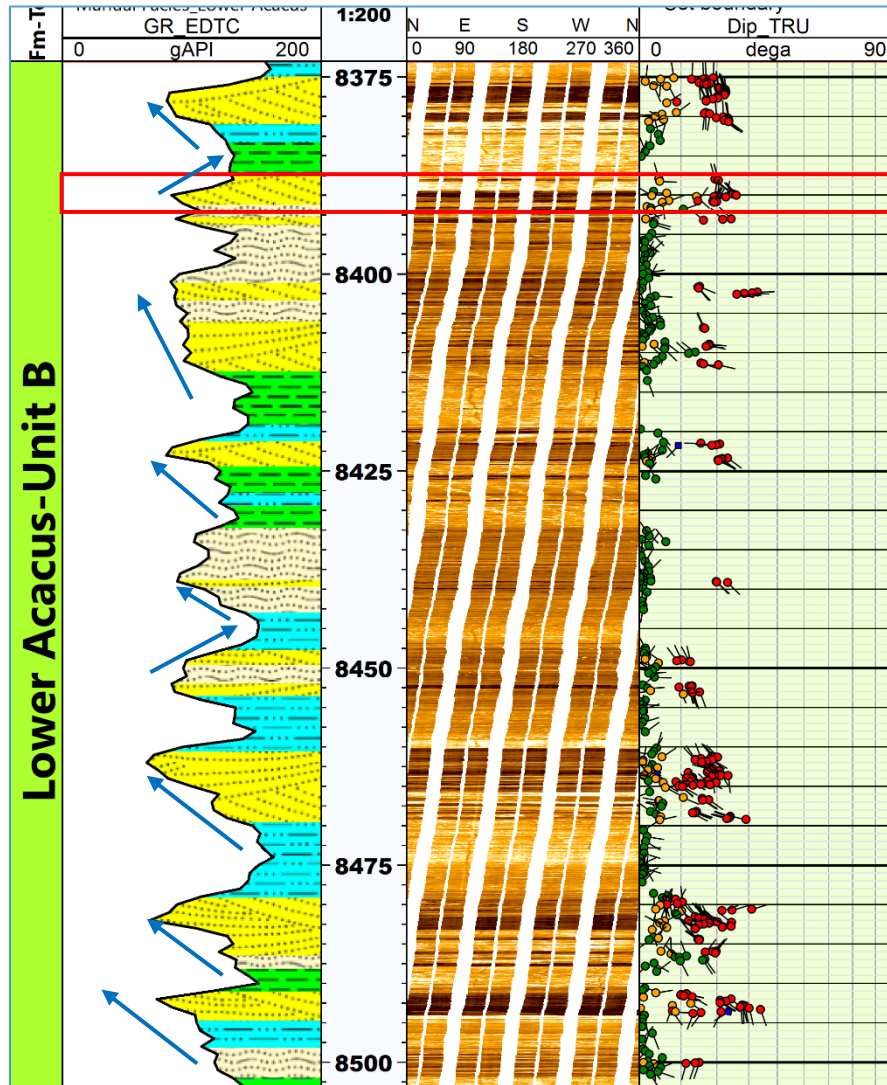


(Fig. 5.39) The facies distribution within Unit B2, Red Box represent a Zoom-in into the cross bedding facies, in which bidirectional trend is observed.

- B3 subunit: this unit represent around 120 ft mainly heterolithic at the base of fining upward channel eventually switch to thick cross bedded coarsening upward sequence and overlie by another smaller one. The cross bedding dips mainly in bimodal pattern similar to the dominate trend (Fig. 5.40).

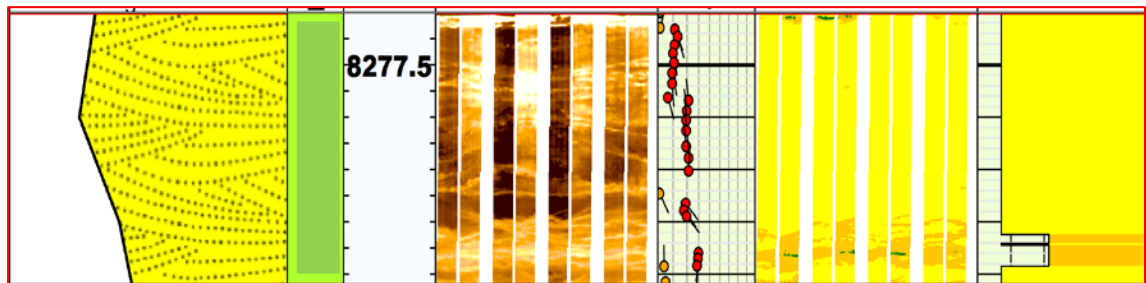
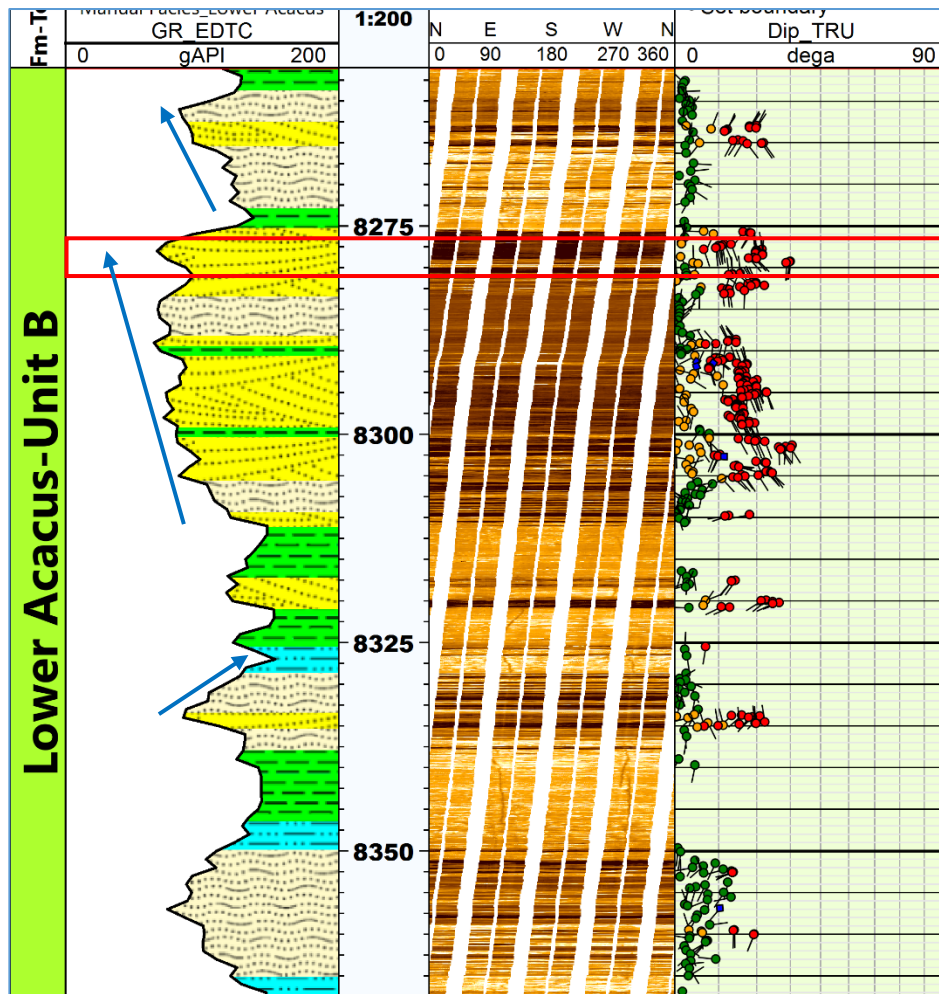


(Fig. 5.40) The facies distribution within Unit B3, Red Box represent a Zoom-in into the cross bedding (or lamination) facies, in which bidirectional trend is observed.

- B4 subunit: represent around 60 ft composed of one coarsening upward sand body followed by multi fining upward sequences. This subunit is dominated by cross bedding facies of bidirectional trend, while the erosional cut within the proposed channel bodies could be signposted by the scour surfaces (Fig. 5.41).

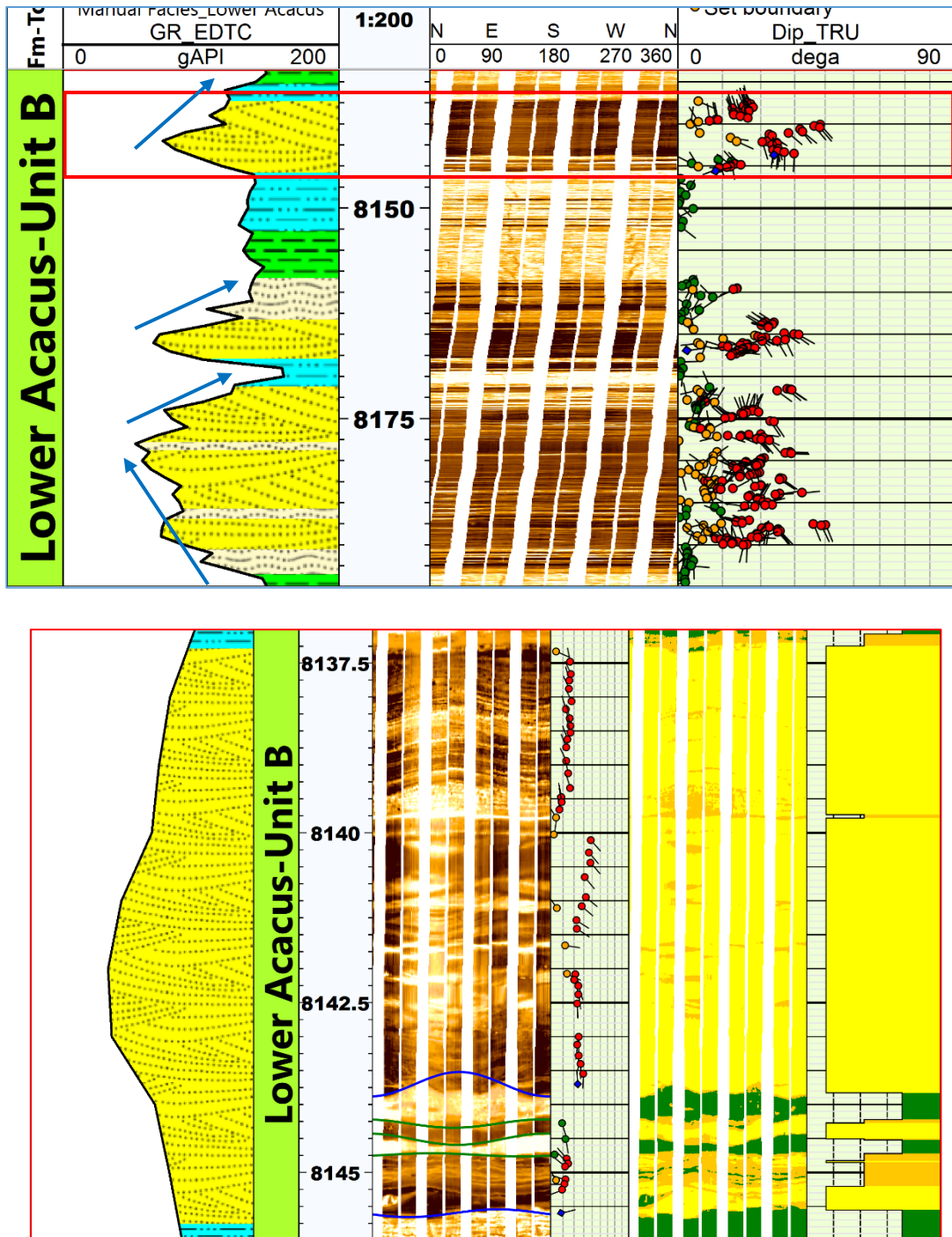


(Fig. 5.41) The facies distribution within Unit B4, Red Box represent a Zoom-in into the cross bedding (or lamination) facies, in which bidirectional trend is observed along with erosional surfaces.

- Unit C between 7965 – 7873 ft, started with fining upward sand body followed by around three coarsening upward sequences mainly composed of cross bedding facies 44% (Fig. 5.42a). The analysis of the structural bedding indicates polymodal dip azimuth (Fig. 5.42b), and the paleocurrent analysis shows almost similar trend (Fig. 5.42c), reflecting the mixed depositional settings. The tide processes are present on these kind of coastal sandstone intervals, and the fining sand bodies are probably representing tidal channels. Nevertheless, the upper coarsening sequence produced oil and gas (Fig. 5.43).

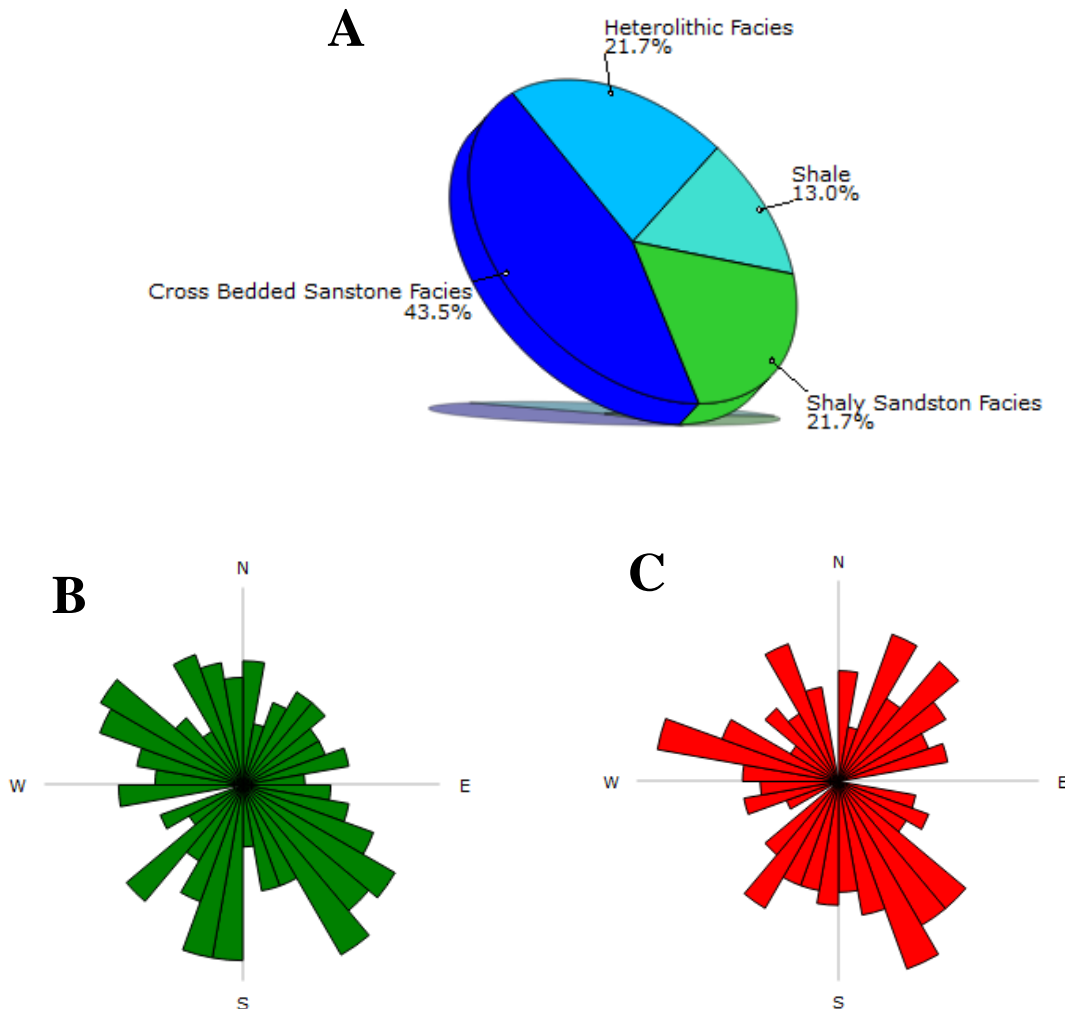


(Fig. 5.42): (A) Facies distribution in, (B) dip azimuth major trend of the structural bedding, (C) major trend of the Paleocurrent of Cross-bedding, all for Unit C of Well Y1-114.



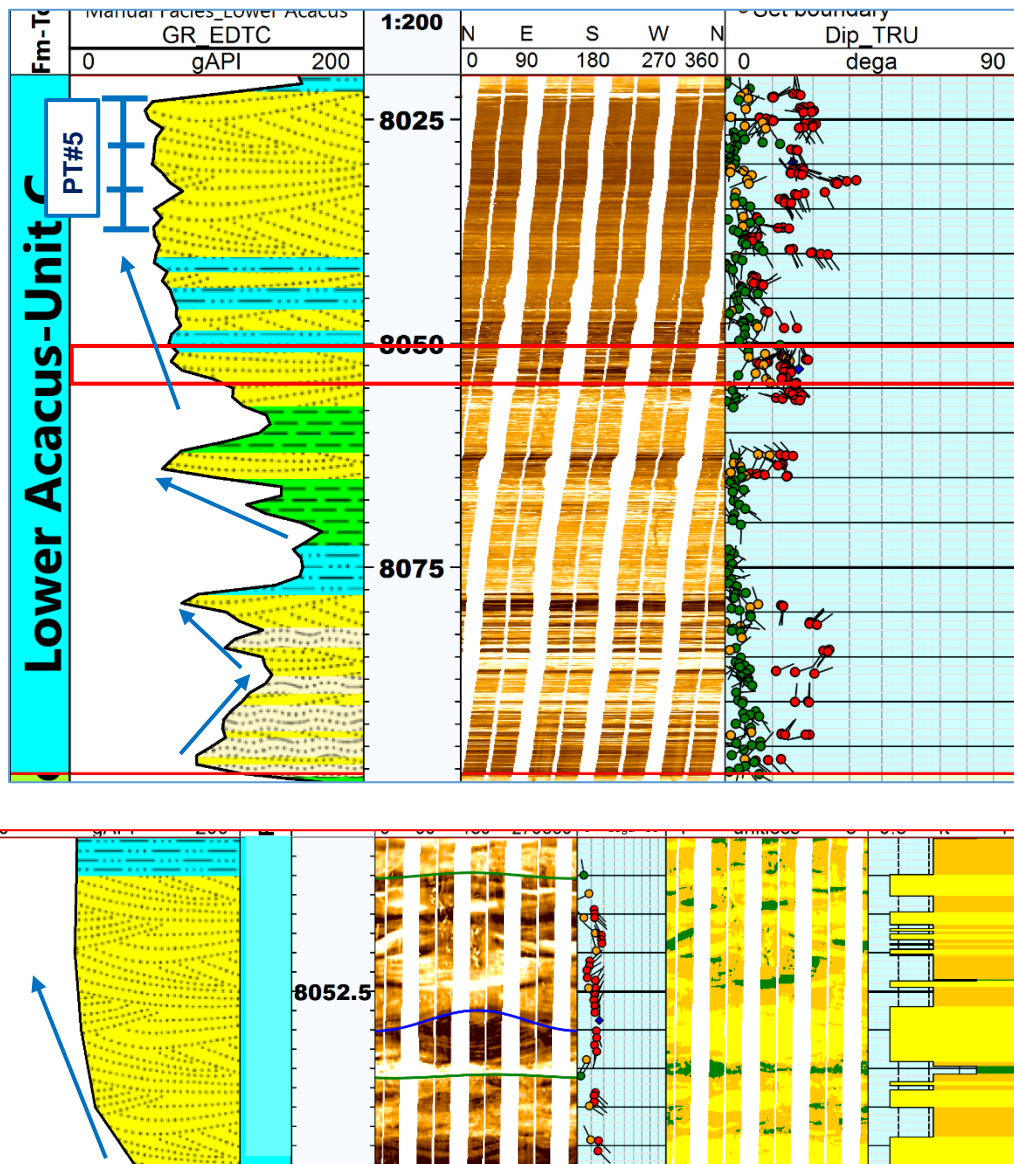


(Fig. 5.43) The facies distribution within Unit C, Red Box represent a Zoom-in into the cross bedding facies, in which bidirectional trend is observed along with erosional surfaces.

## **5.8 Stratigraphic Cross-Section and Lateral Facies Continuity**

The previous discussion represents the vertical association of the determined facies and sand bodies, while the lateral facies change and heterogeneities pose a challenge, particularly for hydrocarbon exploration. Relevant scales were used to better visualize every two units at a time with clarity in terms of dip fans trends, shape of sand bodies, dominant facies, and coarsening and fining upwards cycles.

### **5.8.1 Lateral Facies Change of Unit A1 &A2**

Unit A1 deposited at the very bottom of Lower Acacus reservoir clearly overlies the marine shale of Tanezzuft Formation representing fall of sea level, and beginning of clastic material deposition into the basin from several directions. At Y1-114 in the SE coarsening upward sequences representing the first onset of the prograding delta while the thick blocky sequences shall represent stacked sequences of distributary channel mouth bars.

The coarsening upwards prograding delta is more evident in Unit A2 in which clear bidirectional trend appear on N1-114 and Y1-114 indicating the tidal effect on deltaic sequences, while in X1-114 the thick coarsening upward sequence, which progrades towards the sea with clear unimodal direction towards NW, away from the tide influence. This is also marked by the increase of shale facies thickness towards the NW. On the other hand, the fining upward sequences of channel appear towards the SE, and gradually decrease towards the NW before it disappeared in X1-114, as most of the sequences show lateral discontinuities (Fig. 5.44).

### **5.8.2 Lateral Facies Change of Unit A3 &A4**

Unit A3 presents thick sequences of dominant unimodal trend of paleocurrent towards the SE, which probably indicate the paleo-slope of the delta feeder-channel. The thick cross bedded sandstone shall indicate the channel mouth bars where tide effect is less influential. The tide impact increases toward the SW, associated with increase in bioturbation activity as in well X1-114. The unit does not contain any hydrocarbon accumulation probably due to the lack of lateral and vertical seals (Fig. 5.45).

On the other hand, the tide influence could be more recognized in unit A4 as heterolithic bedding and bidirectional currents are dominant. Fining upward sequences could present tidal channels that were actually overlaid by the shale of Unit B providing a good cap of hydrocarbon accumulations.

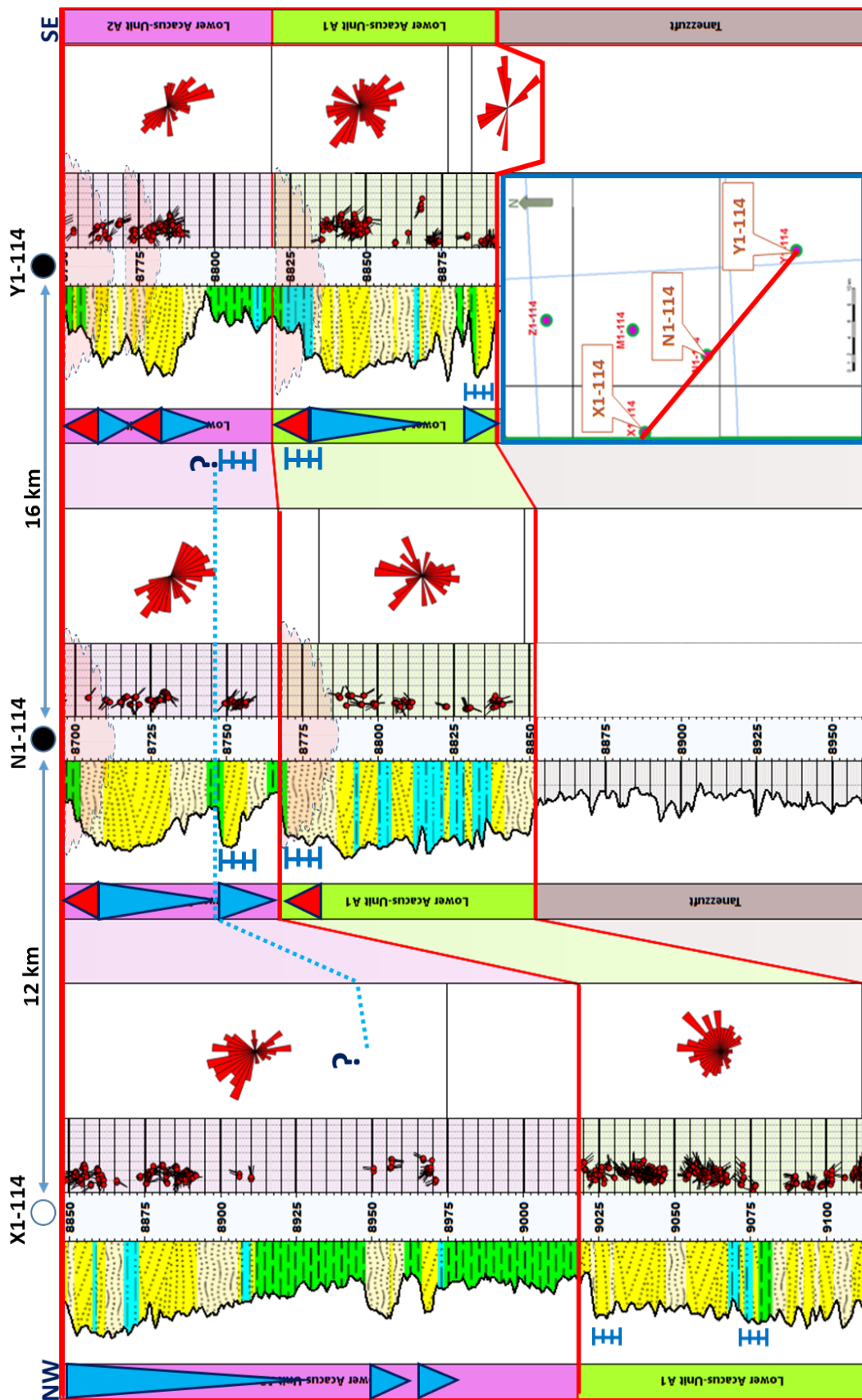


(Fig. 5.44) Detailed stratigraphic correlation of Unit A1 & Unit A2 among the studied wells.

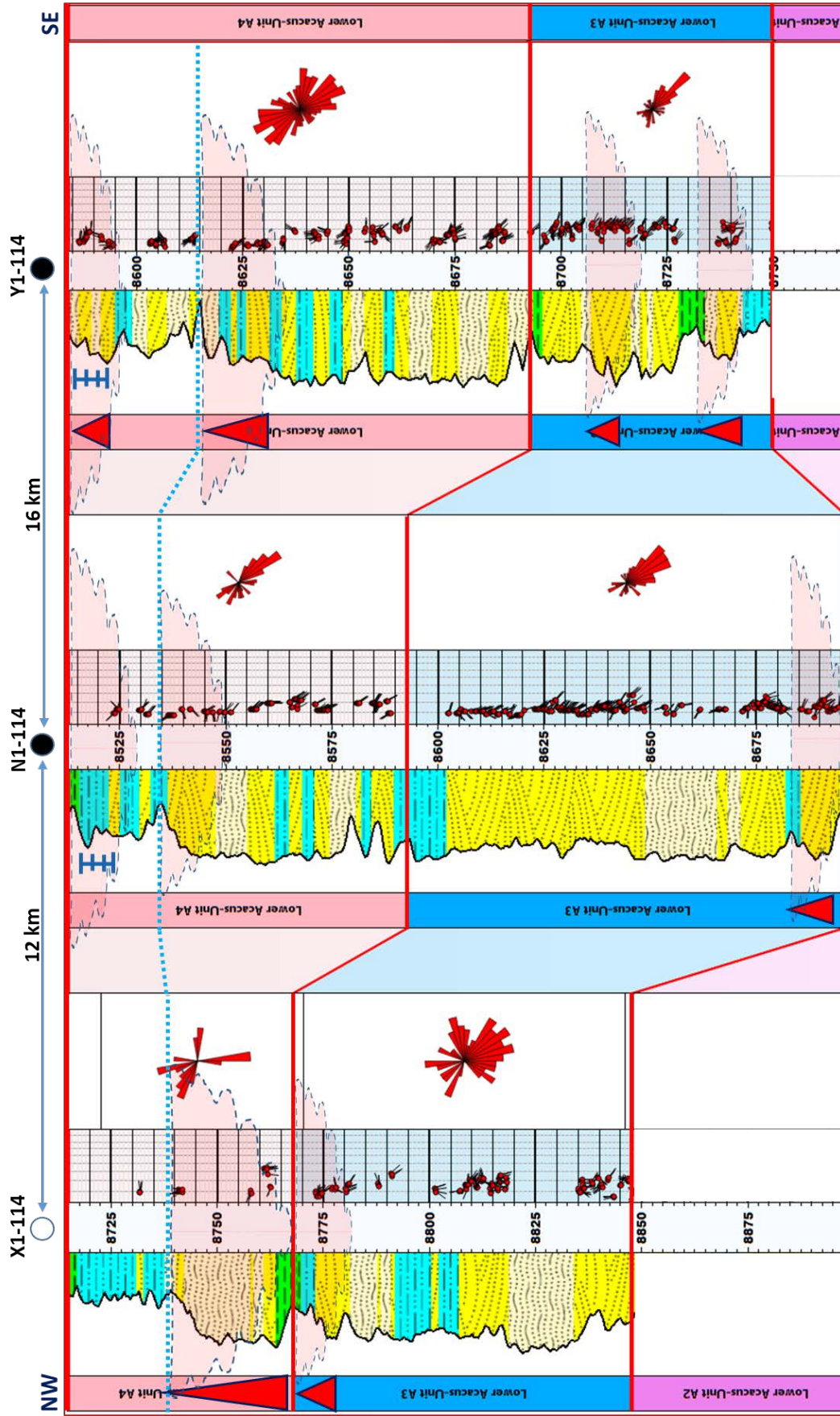


(Fig. 5.45) Detailed stratigraphic correlation of Unit A3 & Unit A4 among the studied wells.

### **5.8.3 Lateral Facies Change of Unit B1 & B2**

Unit B1 and B2 are characterized by interbedded of shale and the small coarsening upward sandstone that is actually reflecting the local change in sea level especially in Y1-114. The coarsening upward sequences increase in thickness towards NW where bimodal to polymodal current are present. These thick coarsening upward intervals were tested water in X1-114, while the tested interval in N1-114 is well-bounded by shale facies that had flowed a good amount of hydrocarbon (Fig. 5.46).

### **5.8.4 Lateral Facies Change of Unit B3 & B4**

Unit B3 shows a clear increase in thickness towards NW with increase in shale facies. The paleocurrent indicate gradual increase from mainly unimodal dominated in Y1-114 to bimodal in N1-114 up to polymodal further towards NW in X1-114. This reflects the lateral change in energy source, although the top part of this unit has good signature of horizontal continuity with oil production in N1-114. The analogue interval in the other wells ought to be tested (Fig. 5.47).

Unit B4 in N1-114 is highly productive and mainly dominated by heterolithic bedding with major bimodal direction that reflect the tide influence. The cross bedding percentage is higher in NE especially associated with the small channels that shows bimodal trend.

### **5.8.5 Lateral Facies Change of Unit C**

This unit is capped by the Middle Acacus Shale, and very characterized by fining upward channels at the base, followed by coarsening upward prograding delta. In Y1-114 the unit shows change in cyclicity at the base altering to coarsening upward bodies with obvious increase in thickness. These coarsening upward sequences laterally decreased into SW until become one thick sequence in X1-114 that was tested water probably due to the high bioturbation activity. However, the top unit was tested and flowed hydrocarbon in the other two wells. The paleocurrent indicate one major trend NE-SW representing the trend of delta with the tide effect, while minor trend perpendicular to the main trend might indicate a component of longshore current. N1-114 is highly dominated by the heterolithic bedding facies that actually reflects the tidal fingerprint, especially the upper part where abundance of the heterolithic bedding might indicate tidal flat deposition (Fig. 5.48).



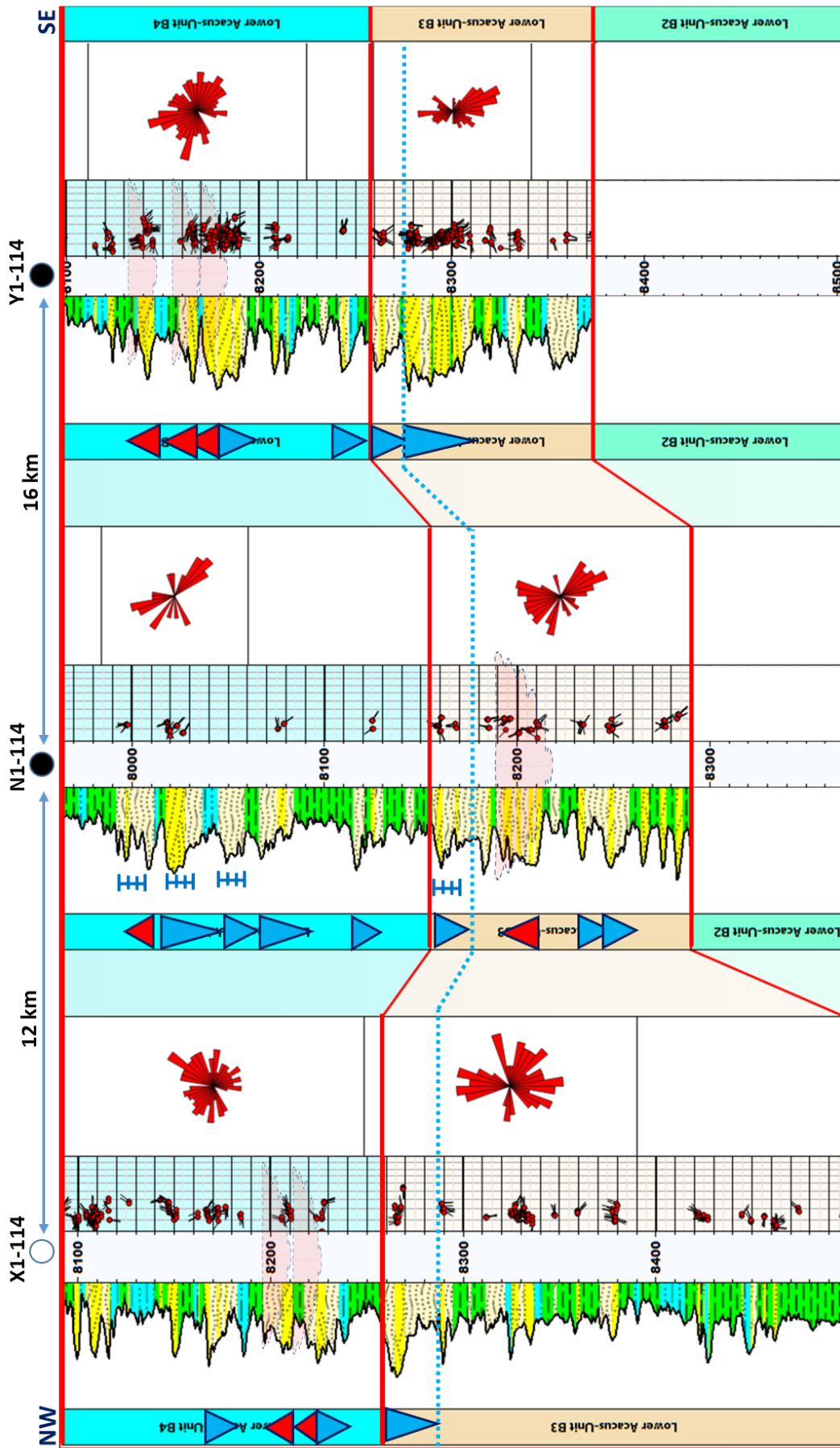


(Fig. 5.47) Detailed stratigraphic correlation of Unit B3 & Unit B4 among the studied wells.

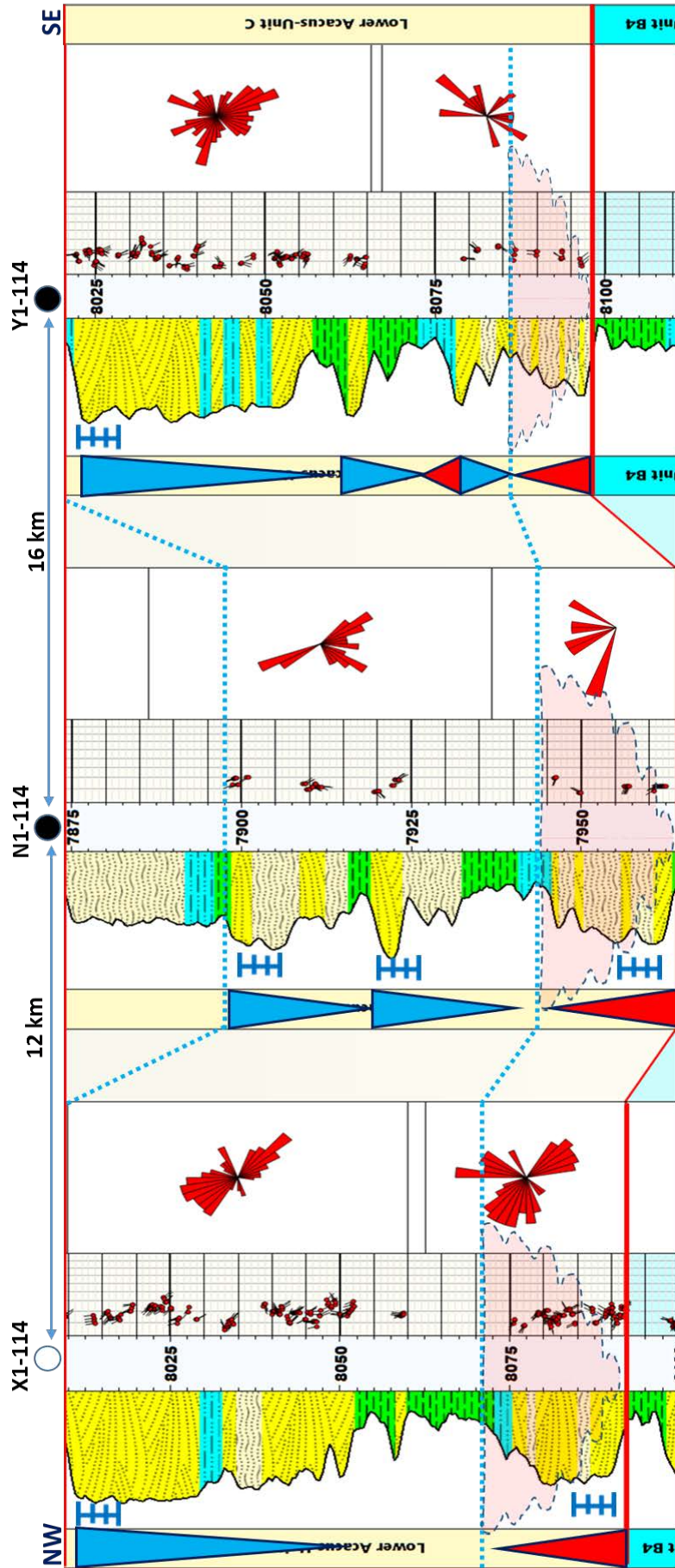


(Fig. 5.48) Detailed stratigraphic correlation of Unit C among the studied wells.



## 5.9. Considerations and Discussions

Previous regional studies indicated that the Silurian Lower Acacus reservoir was deposited in a transitional pattern from fluvial channel sandstone in the south, coastal deltaic sandstone and siltstone, to offshore marine siltstone in the north (Elfigih, 2000; and Hallett, 2002). The study area is located on the coastal deltaic dominated facies, with main trends toward NW-SE, showing good reservoir quality. Sediment supply of the Lower Acacus reservoir comes from three main sources (Qarqaf, Nafusah and Tihimboka arches); the contribution of each source depends on the geographic proximity (Hallett and Clark-Lewis, 2016). The study area is located closest to Nafusah Arch that could represent the main area of sand input. Y1-114 in the SE is located landwards, while X1-114 is located relatively seawards in the NW where marine processes influence the deposition. Therefore, the study area demonstrates clear tide influences on the deltaic sand-shale sequences, representing a mixture of depositional settings.

The mixed channel and tide-dominated delta is well known in the world, and Mahakam delta in Indonesia has long been viewed as one of the world's best examples of a mixed river-dominated and tide-dominated delta based on its morphology (Galloway 1975). Moreover, Salahuddin and Lambiase (2013) suggest that facies distributions are more evident indicators for such a complex setting than delta morphology-based classifications. The mixed setting could deposit clays in various forms and from different origins, which highly effected resistivity log measurements. As a result, many oil fields in Miocene Mahakam delta exhibit low-resistivity pay zones as in Attaka, Serang, Melahin, Kerindingan, and Sepinggan oil fields (Partono & Trevena, 2000). This is very similar to the case of Lower Acacus reservoir in Ghadames basin, NW Libya.

Therefore, facies analysis is important in depositional environment recognition (for example bioturbation indicate a period of energy loss), and in reservoir evaluations (bioturbation could generate a permeability heterogeneity by hindering the primary fabrics). The lateral development of these facies, as well as their internal direction, increase reservoir heterogeneities and inversely affect reservoir performance. This assures the stratigraphical control on the hydrocarbon entrapment even when promising structures are present. One clear example is X1-114 in the NW having a four-way closure and being a water saturated well, while a similar closure of Y1-114 in the NE is hydrocarbon saturated.

Actually, well X1-114 and well Y1-114 are laying at the same structural level providing a great comparison platform from which many facts could be inferred, such as that structural controls are not the only dominant controls on the presence and entrapment of hydrocarbons in the Ghadames Basin. Notably, most of the reservoir intervals in X1-114 are widely affected by bioturbation activity, hence reservoir internal texture might be affected creating a diagenetic barrier to the hydrocarbon movement since this well is found to be a water wet. Here stratigraphic controls had influenced the scenarios of oil presence with clearly devolved and accentuated structures.

It is worth to mention that hydrodynamic flushing may affect the mechanism of hydrocarbon entrapment as well. For example, an accumulated hydrocarbon within a relatively gentle-sided anticline, such in the case of well X1-114, might be pushed away by subsurface hydrodynamic flow; whereas steep-sided anticlines shall provide a stronger closure against hydrodynamic flushing such in the case of Y1-114. A better handle on the hydrodynamic regime in Ghadames Basin would aid to further clarify their effect on hydrocarbon entrapment mechanism.

## Conclusions

- Block-114 in Ghadames Basin is located on highly productive region in which Lower Acacus Member represents the main reservoir in the area.
- Five wells were used in this study for petrophysical evaluation and identification of different reservoir facies.
- Petrophysically, this reservoir is divided into three main units based on log characters these are (Unit A, B, and C) with Unit A at the bottom followed by B & C respectively.
- Unit A comprises 45ft of net pay in well M1-114 at the center of the study area. N1-114 exhibits around 35ft and Y1-114 accumulates about 27ft hydrocarbon filled interval. On the other hand, X1-114 and Z1-114 are water wet. The average porosity in this unit is (17 to 20%) within the clean sandstone intervals (VSH 17-26%).
- Unit B is considered to have the most potential for hydrocarbon exploration in the Lower Acacus reservoir. It encompasses around 101ft of net pay in N1-114 and 48ft in M1-114, while it is water wet in the other wells. This unit represents a heterogeneous inter-bedded of sand-shale sequences with less average porosity (14.5 to 19%) and possesses higher shale content  $V_{sh}$  (around 25% within the sandstone intervals), along with thicker shale intervals.
- Unit C at the very top of the reservoir has the thinnest net pay thickness with average 23ft among the analyzed wells (M1-114, N1-114, and Y1-114) and no hydrocarbon present in X1-114 and Z1-114 wells. This unit shows a relative range in VSH (11-28%) with average porosity 15%. Unit C within well N1-114 has shown the best Petrophysical characteristics and hydrocarbon accumulations.
- Some challenges have been faced during this study some of which are; the LRP (Low Resistivity Pay) and its effect on determining net pay. Although this phenomena exists, it is not the core interest of this study, due to lack of contributions of the latest well logs in this regard (ex. Dielectric Scanner, Rt-Scanner, Litho-scanner or NMR). Therefore, this study is highly dependent on the production data to modify the cutoffs and net pay calculations.

- Structurally, the study area shows a proportional increase in elevation towards the north with almost no effect on hydrocarbon entrapment mechanisms. Y1-114 is an oil-rich well located in the southern part of the area of interest at a lower depth, while Z1-114 is a dry well located on the highest portion of the area of interest.
- Stratigraphically, Lower Acacus reservoir exhibits a slight increase in thickness towards the north with lateral continuity of sand and shale horizons.
- For more detailed sedimentological characterization, FMI analysis aided in giving an idea about the effect of stratigraphic entrapment of hydrocarbon in the study area.
- Integration of core image and FMI analysis assisted in the recognition of four main facies within the Lower Acacus reservoir; these are heterolithic bedding, crossbedded sandstone, shaly-sand, and laminated shales.
- The associations of these facies along with the paleocurrent trend indicate a tidally influenced deltaic setting.
- Additionally, the paleocurrent direction measured from existing cross bedding shows a major trend towards NW-SE, which represents the trend of the delta geometry.
- Notably, most of the reservoir intervals in X1-114 are widely affected by bioturbation activity; hence, reservoir internal texture might be affected creating a diagenetic barrier since this well is water wet.
- Well X1-114 and well Y1-114 have provided a great comparison platform from which many facts could be inferred, such as that Structural controls are not the only dominant controls on the presence and entrapment of hydrocarbons in the Ghadames basin. Here stratigraphic controls had influenced the scenarios of oil presence with clearly devolved and accentuated structures.
- Unconventionally, understanding of hydrodynamic regime versus structural configuration of the entrapment is crucial in hydrocarbon exploration, for instance, a 4-way anticline with steep sides shall provide strong closure against the hydrodynamic flushing. In the undertaken study with the existing wells, vertical closure of the dry well X1-114 is half of the oil well Y1-114 closure, with similar anticline sizes.

## **Recommendations**

Future studies shall consider hydrodynamic flushing regimes, 3D seismic data, along with an expanded well dataset to better understand the depositional sequences of Lower Acacus reservoir. Thin section analysis will also be of great value to the research, especially with concern to the diagenetic influence on well log measurement as well as understanding the origin of the clay types (Authigenic or Allogenic). Special core analysis is recommended for better evaluation of Saturation Factors (m, n, and a) to be used in determining hydrocarbon saturation in a precise manner. Another important task will be classifying FMI dips into more detailed facies in order to better constrain the depositional setting of Lower Acacus reservoir.

## References

**Arabian Gulf Oil Company, (2009).** Intent To Drill (ITD) of X1-114, (AGOCO Internal Report) P150.

**Archie, G.E. (1942).** The electrical resistivity log as an aid in determining some reservoir characteristics. Transactions of the American Institute of Mining and Metallurgical Engineers, 146: P54–62.

**Arduini, M., Barassi, M., Golfetto, F., Orteni, A., Serafini, G., Tebaldi, E., Trincianti, E., and Visentin, C., (2003).** Silurian-Devonian sedimentary geology of the Libyan Ghadamis Basin: Example of an integrated approach to the Acacus Formation study; in Saleem, M. J., and Oun, M. K., eds; “The Geology of Northwest Libya” Volume II, p. 183 – 212.

**Bellini, E. and Massa, D., (1980).** A stratigraphic contribution to the Paleozoic of southern basins of Libya. In: Salem M. J. and Busrewil M. T (eds) The Geology of Libya. Academic press, London, I, P3-56.

**Boote, D. R. D., Clark-Lowes, D. D. & Traut, M. W., (1998).** Paleozoic petroleum systems of North Africa. In: MACGREGOR, D. S., MOODY, R. T. J. & CLARK-LOWES, D. D. (eds) Petroleum Geology of North Africa, Geological Society of London, Special Publication, P132,7-68.

**Bosnina, S., (2010).** Analysis of Microfaults and Fractures in Southern NC193 Concession, Zallah Trough, Sirt Basin. MS.c. theises, Garyounis University, Benghazi, Libya.

**Bracaccia, V., Carcano, C., and Drera, K., (1991).** Sedimentology of the Silurian-Devonian series in the southeastern part of the Ghadames basin. In: Salem M. J. and Belaid M. N (eds) The Geology of Libya. Academic press, London, V, 1727-1744.

**Clark-Lowes, D. D., (1985).** Aspects of Paleozoic cratonic sedimentation in southwest Libya and Saudi Arabia. Ph.D. Thesis University of London, UK.

- Cochran, M. D., and L. E. Petersen, (2001).** Hydrocarbon exploration in the Berkine Basin, Grand Erg Oriental, Algeria, in M. J. Downey, J. C. Threet, and W. A. Morgan, eds., *Petroleum geology of the twenty-first century: AAPG Memoir 74*, p. 531–557.
- Darling, H. L. & Sneider, R. M., (1992).** Production of low resistivity, low-contrast reservoirs, offshore Gulf of Mexico basin. *Transactions of the Gulf Coast Association of Geological Societies*, **42**, 73-88.
- Donselaar, M.E., Schmidt, J.M., (2005).** Integration of outcrop and borehole image logs for high-resolution facies interpretation: example from a fluvial fan in the Ebro Basin, Spain. *Sedimentology* 52, 1021e1042.
- Doveton, John, (2014).** *Principle of Mathematical Petrophysics*: United States, New York, Oxford University Press, P248.
- Echikh, K., (1998).** Geology and hydrocarbon occurrences in the Ghadames Basin, Algeria, Tunisia, and Libya, in Macgregor, D.S., Moody, R.T.J., and Clark-Lowes, D.D., eds., *Petroleum geology of North Africa: Geological Society, London, Special Publication 132*, p. 109–129.
- Elfigih, O. B., (1991).** The sedimentology and reservoir characteristics of the Lower Acacus Formation, NC2 Concession, Hamada Basin, NW Libya. MS.c. thesis, Memorial Univ., NFLD, Canada.
- Elfigih, O. B., (2000).** Regional Diagenesis and its relation to facies change in the Upper Silurian Lower Acacus Formation, Hamada (Ghadames) Basin NW Libya. Ph.D. thesis, Memorial Univ., NFLD, Canada.
- Ekstrom, M. P., Dahan, C. A., Chen, M., Lloyd, P. and Rossi, D., (1987).** Formation imaging with microelectrical scanning arrays. *Log Analyst*, 28, p.294-306.
- Folkestad, A., Veselovsky, Z., Roberts, P., (2011).** Utilizing borehole logs to interpret delta to estuarine: A case study of the subsurface Lower Jurassic Cook Formation in the Norwegian northern North Sea, *Marine and Petroleum Geology* 29 (2012), p. 255-275.

- Galloway, W.E., (1975).** Process framework for describing the morphologic and stratigraphic evolution of the deltaic depositional systems, in Broussard, M.L., ed., *Deltas, Models for Exploration*: Houston Geological Society, Houston, p. 87–98.
- Gaymard, R. and Poupon, A., (1968).** Response of neutron and formation density logs in hydrocarbon, bearing formation, p.3-12.
- Glover, P., (2012).** Petrophysics MSc Course Notes: Wire line logging, p.55-246.
- Hallett, Don, (2002).** *Petroleum geology of Libya*: Amsterdam, Elsevier Inc., 503 p.
- Hallett D., & D. Clark-Lowes, (2016).** *Petroleum geology of Libya*: Amsterdam, Elsevier, Second Edition, 392 p.
- Hammuda, O. S., (1980).** Geologic factors controlling fluid trapping and anomalous freshwater occurrence in the Tadrart Sandstone, Al Hamadah al Hamra area, Ghadames Basin. In: SALEM M. J. and BUSREWIL, M.T.(Eds) 2nd Symp. *The Geology of Libya*. Al-Fatah Univ., Fac. Sci., Tripoli, II, 501-507.
- Howllett, P., (2000).** Trapping styles in Ghadames Basin of Algeria, Libya and Tunisia, *The Geology of Northwest Libya Volume II*, Earth Science Society of Libya.
- Hrouda, M. S., Tyson, R. V. and Farrimond, P., (2002).** The hydrocarbon source potential of the Paleozoic rocks of the Ghadames Basin, NW Libya. *Ancient Biomolecules*, 4(3), 94.
- Knaust, D., (2013).** Classification of bioturbation-related reservoir quality in the Khuff Formation (Middle East): Towards a genetic approach, *in* M. Pöppelreiter (ed.), *Permo-Triassic Sequence of the Arabian Plate*: EAGE Publications, p. 247-267.
- Kreisa, R.D., Moiola, R.J., (1986).** Sigmoidal tidal bundles and other tide-generated sedimentary structures of the Curtis Formation, Utah. *Geological Society of America Bulletin* 97, 381e387.
- Krumbein, W. c. and Sloss, L. L., (1963).** *Stratigraphy and sedimentation*. Second Edition, Freeman, w. H. and Company, San Francisco, 660P.
- Krygowski, D. A., (2003).** *Guide to petrophysical interpretation*, Austin, Texas, USA, 136p.



- Letouzey, P., Reymond, A., Dartois, F., Debarre, R., Godart, Y., Elbakai, M., Miriheel, I., Rahuma, M., El-Harbi, A., Suliman, O, Kilani, M., (2005).** Petroleum Potential of the Ghadames Basin, Libya: A reevaluation leading to new play/prospect identification; AAPG International Conference and Exhibition-Paris 2005 Sep 11-14.
- Lisle, R.J., Brabham, P., and Barnes, J., (2011).** Basic Geological Mapping. Fifth Edition. John Wiley & Sons, Chichester, 105 pp.
- Lu'ning, S., J. Craig, D. K. Loydell, P. Storch, and B. Fitches, (2000).** Lower Silurian "hot shales" in North Africa: Regional distribution and depositional model: Earth Science Reviews, v. 49, p.121– 200.
- Maltman A., (1990).** Geological maps: an introduction. Van Nostrand, Reinhold, New York, 184 pp.
- McHardy W.J., Wilson M.J. & Tait J.M., (1982).** Electron microscope and X-ray diffraction studies of filamentous illitic clay from sandstones of the Magnus Field. Clay Minerals, **17**, 23–39.
- Meyer, B.L., and Nederlof, M. H., (1984).** Identification of Source Rocks on Wire line Logs by Density/Resistivity and Sonic Transit Time/Resistivity Crossplots, pp.121.
- Najem, A., M., (2011).** Integration Subsurface Structural Interpretation of the Ordovician Succession in the South-Central part of Concession NC186, Northern Murzuq Basin. MS.c. theises, Garyounis University, Benghazi, Libya.
- North, F.K., (1985).** Petroleum Geology. George Allen and Unwin Ltd. Sdney, Australia, 607p.
- Partono, Yoseph, J., and Trevena, Arthur, S., (2000).** Low-resistive reservoirs in the Miocene Mahakam Delta deposits in East Kalimantan (Abstract), AAPG International Conference and Exhibition, Bali, Indonesia.
- Potter, P.E., and Pettijohn, F.J., (1977).** Paleocurrents and Basin Analysis. 2nd Edition, Springer-Verlag, New York, 425 p.

- Ramadan, Z., J., (2008).** Structural and Sedimentological Analysis of the Middle Ordovician Successions Utilizing FMI Images and Openhole Logs, Murzuq Basin. MS.c. theises, Garyounis University, Benghazi, Libya.
- Reading, H. G., (1996).** Sedimentary Environments and Facies. Blackwell Scientific Publications.
- Rider, M., (1996).** The geological interpretation of well-logs, second edition. Whittles Publishing, Caithness.
- Rusk, D. C., (2001).** Libya: Petroleum potential of the underexplored basin centers—a twenty first-century challenge, in M.W. Downey, J. C. Threet, and W. A. Morgan, eds., Petroleum provinces of the twenty-first century: AAPG Memoir 74, p. 429–452.
- Salahuddin and Lambiase, J. J., (2013).** Sediment Dynamics and Depositional Systems of The Mahakam Delta, Indonesia: Ongoing Delta Abandonment on a Tide-Dominated Coast, Journal of Sedimentary Research, 503-521.
- Schlumberger, (1974).** Log Interpretation Manual / Applications: Houston, Schlumberger Well Service, Inc.V.2, 116p.
- Schlumberger, (1997).** Log Interpretation / Charts: Houston, Schlumberger Wire line and Testing, 139p.
- Schlumberger, (2002).** Borehole geology, geomechanics and 3D reservoir modeling, FMI, SMP-5822.
- Schlumberger, (2015).** Wireline Service Catalog, geomechanics and 3D reservoir modeling, FMI, SMP-5822.
- Serra, O., (1989).** Formation MicroScanner image interpretation. Schlumberger Educational Services, p. 117.
- Sinha, R. H. and Ben Rahuma, Milad M., (2000).** Preliminary Geological Appraisal of Ghadames Basin, Libya. Abstract presented on the Second Symposium of Sedimentary basin of Libya, Geology of Northwest Libya, Nov. 6-8 / 2000, Tripoli, Libya, G.S.P.L.A.J.

**Shrivastva C, Ganguly S, Khan Z., (2008).** Reconstructing Sedimentary Depositional Environment with Borehole Imaging and Core: A Case Study from Eastern Offshore India (IPTC-12253).

**Simandoux, P., (1963).** Dielectric measurements on porous media application to the measurement of water saturations: study of the behaviour of argillaceous formations. *Revue de l'Institut Français du Pétrole*, 18 (Suppl.): 193–215.

**Tiab, D., and Donaldson, E.C., (1996).** *Petrophysics, Theory and practice of Measuring Reservoir Rock and Fluid transport properties*: Huston, Texas. 706p.

**Tucker Maurice E., (2003).** *Sedimentary Rocks in the Field (Geological Field Guide)*, third edition. West Sussex, Chichester, England: John Wiley & Sons.

**Underdown, R., and Redfern, J., (2008).** Petroleum generation and migration in the Ghadames Basin, North Africa: A two-dimensional basin-modeling study, *AAPG Bulletin*, V. 92, No. 1, P. 53-76.

**Worthington, P. F., (1985).** The evaluation of shaly-sand concepts in reservoir evaluation: *The Log Analyst*, 26, 23–40.

## تقييم جوده المكنن و تفسير السرود التصورية لمكنن رمل الاكاكوس السفلى المختلط بالطفله فى المنطقه 114, شمال حوض غدامس

قدمت من قبل:

إبراهيم أحمد حسن المصلى

تحت إشراف:

الأستاذ الدكتور/ محمد بدر الدين عبد المالك

### المخلص

يشكل خزان أكاكوس السفلى فى الجزء الشمالى الشرقى من حوض غدامس (منطقه-114) نظاما دلتايا متأثرا بحركة المد والجزر. قد أظهرت المقاطع العرضية التركيبية والطبقية باستخدام برنامج Petrel (مسجل لشركة شلمبرجير) أن تكوين الخزان له سمك عام نحو الشمال والشمال الشرقى. بتروفيزيانيا تم تقسيم المكنن الى ثلاث وحدات رئيسية اعتماد على شكل السرود الكهربائية وهن (وحدة أ، ب، والوحدة ج) حيث الوحدة أ فى الاسفل متبوعة بالوحدة ب ثم ج. التحليل البتروفيزيائى باستخدام برنامج IP (مسجل لشركة لويد ريجيستر) بين أن خزان أكاكوس السفلى هو محمل هيدروكربونى فى منطقة الدراسة بمواصفات مكننيه جيدة جدا. متوسط حجم الطفلة حوالى 25 نسبة مئوية، المسامية تتراوح من 15 الى 20 من المئة ونسبة تشبع الماء حوالى 35 فى الابار النفطية. التحكم فى توزيع الهيدروكربون وطبقات الخزان تتم بشكل رئيسى من خلال توزيع السحنات الترسيبية وأقل مساهمة من التأثير التركيبى. وبناء على ذلك، تم إجراء تحليل للسرود الضوئية وصور العينات الاسطوانية باستخدام برنامج Techlog (مسجل لشركة شلمبرجير) لتحديد التراكيب الرسوبية الرئيسية المتواجدة فى منطقة الدراسة للابار المتوفرة. تم تجميع هذه التراكيب الرسوبية فى أربعة سحنات رئيسية من أجل رؤية التباين الرأسى والجانبى بين الآبار فى منطقة الدراسة. السحنات التى تم تحديدها هى السحنة الغير المتجانسة، التطبيق المتقاطع للصخر الرملى، صخور رملية مختلطة بالطفلة، وسحنات الطفلة رقيقة التطبيق. تواجد هذه السحنات مع بعضها تعكس تأثير المد والجزر على وضع دلتا مدعومه باتجاه التيارات القديمه. وبالإضافة إلى ذلك، فإن الاتجاه السائد التى تم قياسه من تقاطعات سحنات الحجر الرملى كان ثنائى الاتجاه نحو الشمال الغربى – الجنوب الشرقى، مع نماذج أقل متعددة وأحاديه الاتجاه.



**تقييم جوده المكنن و تفسير السرود التصويرية لمكنن  
رمل الاكاكوس السفلى المختلط بالطفله فى المنطقه  
114, شمال حوض غدامس**

قدمت من قبل:  
إبراهيم أحمد حسن المصلى

تحت إشراف:  
الأستاذ الدكتور/ محمد بدرالدين عبد المالك

قدمت هذه الرسالة استكمالاً لمتطلبات الحصول على درجة الماجستير في  
علوم الأرض

جامعة بنغازى  
كلية العلوم

أبريل 2018